

This item was submitted to Loughborough University as an MPhil thesis by the author and is made available in the Institutional Repository (<https://dspace.lboro.ac.uk/>) under the following Creative Commons Licence conditions.



For the full text of this licence, please go to:
<http://creativecommons.org/licenses/by-nc-nd/2.5/>

LOUGHBOROUGH
UNIVERSITY OF TECHNOLOGY
LIBRARY

AUTHOR/FILING TITLE

SAMUELS, U

ACCESSION/COPY NO.

040129377

VOL. NO.

CLASS MARK

LOAN COPY

0401293777



**FOCAL POSITION CONTROLLED PROCESSING HEAD
FOR A LASER PATTERN GENERATOR (LPG)
FOR FLEXIBLE MICROSTRUCTURING**

by

Dipl.-Ing. Uve Samuels

Master's Thesis

Submitted in the partial fulfilment of the requirements
for the award of
Master of Philosophy of the Loughborough University of Technology

December 1995

© Uve Samuels 1995

Loughborough University of Nottingham Library	
Date	June 96
Class	
Acc. No.	046129377

9/6451471

ACKNOWLEDGEMENTS

I would like to thank Professor Dr. Rob Parkin providing me with this interesting project for independent work. Furthermore, I am grateful to him for numerous stimulating discussions.

Also I would like to thank my co-supervisor Dr. Rowley.

For the encouraging support during planning and performing of the experimental work in the laboratories at the Fachhochschule Ostfriesland (FHO) in Emden, Germany, I would like to thank Professor Dr. Horst Kreitlow.

Equally, I would like thank the members of the research team at the Fachhochschule Ostfriesland for the interest come into being of this work. In particular I would like to thank Mr. Dipl.Ing. Jörn Miesner and Mr. Dipl.-Ing Arno Hinrichs for the fruitful discussions and the encouraging support of the experimental work.

I am also thankful to Dr. Steve Wright for the critical review of this report.

Last but not least I would like to thank to my family for the very kind atmosphere, which was the condition for this substantial work.

Uve Samuels

Loughborough / Emden, December 1995

ABSTRACT

FOCAL POSITION CONTROLLED PROCESSING HEAD FOR A LASER PATTERN GENERATOR (LPG) FOR FLEXIBLE MICROSTRUCTURING

By

Dipl.-Ing. Uve Samuels

In microstructuring processes a direct structuring of the substrate is, in most cases, not possible and therefore the profile is first obtained in photo resist and then, in a second step, transferred into the substrate. The resist structuring can be performed using the flexible characteristics of a laser pattern generator (LPG). In these processes, there is a beneficial relationship between the apparatus/equipment expense and the obtainable processing results. For a reproduceable processing result in all microstructuring tasks, good reproducibility of all process relevant parameters is required. In the application of a laser pattern generator, precise control of the focal position of the strongly focussed laser beam relative to the processing surface must be maintained.

For this reason, an optimised focal position controlled processing head concerning LPG microstructuring demands has been developed. This system is based on a distance sensor using a modified autofocus principle for the determination of the focal position, a piezo driven linear stage for the processing head movement relative to the processing surface and a digital controller for the required closed loop system. The optical, electronic, mechanical and computer elements of the general system were optimised concerning working range, resolution, reliability and miniaturisation.

The LPG with this system realised a good reproduceable processing result for microstructuring on different substrates. Several microstructures have been produced demonstrating both the flexibility and viability of the system.

CONTENTS

Page #

NOTATIONS/TERMINOLOGY	(vii)
LIST OF TABLES.....	(x)
LIST OF FIGURES	(xi)
1. INTRODUCTION	1
2. MANUFACTURE OF MICROSTRUCTURES	3
2.1. Serial procedures (maskless procedures)	5
2.2. Parallel procedures (mask procedures)	6
3. LASER PATTERN GENERATOR (LPG).....	9
3.1. Principle of the laser beam writer	9
3.2. Positioning system	10
3.3. Optical system.....	11
3.4. Control system.....	12
3.5. Focal positioning demands	12
4. FOCAL POSITION SENSOR	15
4.1. Tactile displacement measuring	15
4.2. Pressure distance sensors	15
4.3. Capacitive distance measuring	16
4.4. Acoustic echo-delay measurement.....	16
4.5. Laser triangulation	16
4.6. Autofocus principle.....	16
4.7. Selection and specification of the measurement principle	17

5.	SELECTION OF THE SENSOR COMPONENTS	19
5.1.	Selection of the measuring laser	20
5.2.	Selection of the focussing optic	21
5.3.	Selection of the beam splitter	21
5.4.	Beam manipulation.....	21
5.5.	Beam detection and beam analysis.....	22
6.	DETERMINATION AND OPTIMISATION OF THE PROCESSING HEAD CHARACTERISTICS	26
6.1.	Forming of the measuring beam.....	26
6.2.	Sensor model	30
6.2.1.	Analysis of the initial diameter D_0	32
6.2.2.	Analysis of the sensitivity constant K	33
6.2.3.	Sensor adjustment	37
6.3.	Beam manipulation and beam detection.....	39
6.4.	Experimental determination of the measuring characteristics of the sensor...	45
6.5.	Dimensioning of an optimised processing head	50
7.	SELECTION OF AN ACTUATOR.....	53
7.1.	Comparing the actuators	53
7.1.1.	Worm nut driven gearing.....	53
7.1.2.	Worm drive.....	54
7.1.3.	Plunger-coil motor	55
7.1.4.	Piezo translator	55
7.2.	Static behaviour of piezo translators.....	56
7.3.	Dynamic behaviour of piezo translators.....	57
7.3.1.	Mechanical system	57
7.3.2.	Electrical system	58
7.4.	Examination of the selected piezo translator	59

8.	DEVELOPMENT OF THE CONTROL SYSTEM.....	61
8.1.	Principle of the closed loop system.....	61
8.2.	Descripton of the control task	64
8.3.	Determination of the plant characteristics.....	65
8.3.1.	Step response.....	66
8.3.2.	Frequency domain transfer function.....	67
8.4.	Closed loop design.....	69
8.4.1.	Inflectional tangent method	69
8.4.2.	Frequency characteristic procedure.....	71
8.5.	Realisation of a digital controller device.....	72
8.6.	Determination of the controller device characteristics.....	74
8.7.	Closed loop system operation characteristics.....	77
9.	INTEGRATION OF THE PROCESSING HEAD INTO THE LPG	79
9.1.	Adjustment of the processing head	79
9.2.	Adjustment of the LPG	80
9.3.	System operation	80
9.4.	Examples for micro-structuring with the LPG	82
10.	DISCUSSION	87
11.	CONCLUSION	90
	REFERENCES	91

APPENDICES

Page #

A. OVERVIEW OF THE LPGA1

B. BLOCK DIAGRAM OF THE LPG.....B1

C. SOFTWARE CONCEPT OF THE LPG..... C1

D. PSD ANALYSING CIRCUIT.....D1-D4

E. RAY-TRACING MODEL OF THE MICROSCOPE OBJECTIVE E1-E5

F. RAY-TRACING MODEL OF THE TELESCOPE..... F1-F5

G. RAY-TRACING MODEL OF THE MEASURING LASERG1-G4

H. DERIVATION OF THE MATHEMATICAL SENSOR MODELH1-H8

I. RAY-TRACING MODEL OF THE SENSOR I1-I9

J. CONSTRUCTION OF THE EXPERIMENTAL SENSOR..... J1-J2

K. CONSTRUCTION OF THE SENSOR TRANSLATOR.....K1-K2

L. CONSTRUCTION OF THE SURFACE TILT SYSTEM L1-L2

M. CONSTRUCTION OF THE OPTIMISED PROCESSING HEAD M1-M11

N. CONSTRUCTION FOR THE SHIELDING OF THE PSD CIRCUITN1-N6

O. SIGNAL AMPLIFIER.....O1-O4

P. PIEZO DRIVER.....P1-P3

Q. CONTROLLER PARAMETER TABLE..... Q1

R. CONTROLLER PROGRAM FLOW CHART.....R1

S. CONTROLLER PROGRAM LISTINGS1-S7

T. OPTICAL CONSTRUCTION OF THE LPG..... T1-T3

U. CONSTRUCTION OF THE LPG POSITIONING SYSTEMU1-U3

V. PHOTOGRAPHSV1-V6

W. PUBLICATIONS..... W1-W40

NOTATIONS/TERMINOLOGY

A	-	First coordinate of the light spot on the PSD
A'	-	Reduced first coordinate for a real light spot on the PSD
$A/D-C$	-	Analogue/Digital Converter
AOM	-	Acousto optical modulator
A_R	-	Gain margin
a_n	-	Position of the beam waist on the input side of the lens n
a_n'	-	Position of the beam waist on the output side of the lens n
B	-	Second coordinate of the light spot on the PSD
B'	-	Reduced second coordinate for a real light spot on the PSD
B_W	-	Bandwidth
C	-	Capacity
C_T	-	Regidity
D	-	Diameter
D_0	-	Initial diameter
d	-	Displacement
$F(j\omega)$	-	Frequency transfer function
f	-	Frequency
f_g	-	Cut-off frequency
f_n	-	Focal length of lens n
f_0	-	Resonance frequency
f_0'	-	Reduced resonance frequency
H	-	Diameter of a real light spot on the PSD
h	-	Length of the PSD
I	-	Current
J	-	Controller adjustment parameter
K	-	Sensitivity constant
K_D	-	Derivative action parameter of the controller
K_I	-	Integral action parameter of the controller
K_P	-	Proportional action parameter of the controller
K_S	-	Transfer factor

\widetilde{K}	-	Auxillary parameter for controller design
LPG	-	Laser pattern generator
l	-	Length
m, M	-	Mass
m_{eff}	-	Effective mass
N	-	Step number
P	-	Power
PCB	-	Printed circuit board
PID	-	Controller characteristic
PIO	-	Parallel input/output
PSD	-	Position sensitive detector
R	-	Electrical resistor
RS-232	-	Serial computer interface
S	-	Signal
SIO	-	Serial input/output
SNR	-	Signal/noise ratio
T_A	-	Sampling time
T_g	-	Settling time
T_N	-	Reset time
T_R	-	Rise time
T_{RA}	-	Time for one controller loop
T_t	-	Dead time
T_U	-	Transfer lag
T_V	-	Derivative time
t	-	Time
U, v	-	Voltage
$v(t), v(k)$	-	Controller output voltage
$w(t), w(k)$	-	Set point
w_{on}	-	Beam waist of the input side of lens n
w'_{on}	-	Beam waist of the output side of lens n
$x(t), x(k)$	-	Controlled parameter
$x_a(j\omega), x_a(t)$	-	Output signal
$x_d(t); x_d(k)$	-	Negative derivation

$x_e(j\omega), x_e(t)$	-	Input signal
$y(t), y(k)$	-	Actuator output value
Z	-	Distance
Z_R	-	Rayleigh length
ΔZ	-	Distance difference
$\Delta\varphi$	-	Phase difference
φ	-	Phase
φ_R	-	Phase margin
λ	-	Wavelength
π	-	3.141592654.....
ω	-	Angular frequency

LIST OF TABLES

TABLE	DESCRIPTION	PAGE #
1	Characteristics of the linear axes	10
2	Characteristics of the rotary table	10
3	Characteristics of the processing laser	11
4	Characteristics of the microscope objective	11
5	Characteristics of the measuring laser	20
6	Characteristics of the expanding telescope	27
7	Characteristics of sensor setup I	45
8	Characteristics of sensor setup II	46
9	Surfaces used for sensor surveying	46
10	Characteristics of the optimised processing head	51

LIST OF FIGURES

FIGURE	DESCRIPTION	PAGE #
1	Profiles of the resist microstructures.....	3
2	Block diagram of microstructuring processes	4
3	Schematic representation of the multi mask procedure.....	7
4	Process flow of the multi mask procedure.	8
5	Principle of a laser beam writer	9
6	Optical system of the processing laser	12
7	Transformation of the gaussian beam	13
8	Block diagram of an autofocus sensor	19
9	Principles of beam manipulation	22
10	PSD element with a) ideal and b) real light spot.....	23
11	PSD analysing and evaluation circuit schematic.....	24
12	Optical system of the measuring laser	27
13	Transformation block of a lens	28
14	Transformation block of the general system.....	28
15	Optical system of the measuring laser beam using a ray-tracing program.....	29
16	Linearised setup of the sensor	31
17	Variation of l_1	34
18	Variation of l_2	35
19	Variation of f_1	36
20	Variation of f_2	37
21	Ray-tracing model of the sensor	38
22	Principles of knife edge and PSD adjustment	39
23	Simulation of PSD signals for different illuminations	42
24	Interdependence between PSD-signal form and light spot radius.....	43
25	Typical signal characteristics as a function of the measured value	44
26	Characteristic curves of the sensor based on setup I	47
27	Characteristic curves of the sensor based on setup II	48
28	Distance curve with different tilts of the measured surface.....	49
29	Principle of the optimised processing head	51

30	Characteristic curve of the optimised processing head	52
31	Principle of focus adjustment using a worm nut driven gearing	53
32	Principle of focus adjustment using a worm drive	54
33	Principle of focus adjustment using a plunger coil motor	55
34	Principle of focus adjustment using a piezo translator	56
35	Extension characteristic of a piezo translator	57
36	Extension of the piezo translator	59
37	Block diagram of a closed loop system.....	61
38	Signal flow diagram of a digital closed loop system	63
39	Principle setup of the focal position control system.....	64
40	Positive step response of the system to be controlled.....	66
41	Negative step response of the system to be controlled	67
42	Transformation of a sine wave signal by the system to be controlled .	68
43	Bode-diagram	69a
44	Step response for the determination of the system parameter	70
45	Signal for the dead time determination of the controller.....	75
46	Controller step response.....	76
47	Controlling characteristic with non optimal controller parameter	77
48	Controlling characteristic with optimal controller parameter	78
49	Segment of a line disk established without a correct focal position....	84
50	Segment of a line disk established with a correct focal position.....	84
51	Segment of a micro lens established without a correct focal position	85
52	Segment of a micro lens established with a correct focal position.....	86

1. INTRODUCTION

Microstructuring technology is concerned with the manufacture of optical, mechanical, or electronic structures with detail dimensions in the range of (sub)micrometers. The first two areas benefit from the technologically more mature microelectronics industry, where typically a semiconductor material (e.g. silicon or germanium) is microstructured for the generation of very compact electronic functions. The usual steps in the development of such structures for low cost single elements and, therefore, a broad application range are:

- development of small numbers of basic structures which can be combined to obtain a structuring of the geometrical shapes using lithography
- combination to produce a complex system
- high quality manufacturing with narrow tolerances

In all types of microstructuring the profile is first obtained in resist performed by lithographic manipulation via a light or particle source as the structuring tool. In a second step the structure is transferred to the required substrate.

The integration of microelectronics, mechanics, and optics is termed microsystem technology, the scope of which is broader than the mere miniaturisation of systems. Considering for example microelectronics, it should be amply clear that the results achieved to date would not have been possible by simply concentrating on producing large numbers of single transistors as cheaply as possible. Indeed, the integration of many components to component groups and these to systems has resulted in the rapid increase of the capability of the electronics and led to the great success of this branch of technology. Similarly, for the case of microsystem technology it is the intelligent symbiosis of many microstructures, which leads to systems that possess suitable capabilities to meet the needs of the applications in question.

Manifold applications of lithography exist in industrial manufacturing and expanding application fields have led to a continuous improvement of this technology. Furthermore, the research activity in nearly all disciplines forced by development potential has caused the improvement in lithographic technology as well and led to a steady maturing towards the high quality, low tolerance manufacturing capabilities available today.

In this work the laser pattern generator developed at the Fachhochschule Ostfriesland, Emden, Germany will be shortly presented to analyse the problem of precise focal position adjustment of the microstructuring processing head for reproduceable process results. As a result of this, the requirement of a control system to meet the focal position accuracy during the manufacturing process is demonstrated. Market research reveals that commercial devices do not exist that meet the demands in LPG application directly. Therefore, a computer based focal position control system for the processing head of the laser pattern generator presented here has been developed.

For this reason, a description and a classification of microstructuring technologies is performed in chapter 2 while in chapter 3 the laser pattern generator developed at the Fachhochschule Ostfriesland is presented.

After a comparison of different displacement sensor principles in chapter 4, in chapter 5 the components of the chosen autofocus sensor are investigated in detail.

Theoretical and experimental investigations of the sensor construction as well as the design of an optimised processing head are performed in chapter 6.

In chapter 7 different actuators for the positioning of the processing head are compared and the chosen piezo translator is investigated in detail.

The digital focal position control system for the processing head is presented and investigated in chapter 8.

The integration of the position controlled processing head into the LPG as well as microstructuring results are presented in chapter 9.

2. MANUFACTURE OF MICROSTRUCTURES

The manufacturing procedure to be described is a technique for the structuring of appropriate materials (hereafter denoted substrate) in the range of (sub)micrometers. Dependent on the application, different materials are employed. Examples of various application fields and the substrates used are listed below.

- **Micromechanics**

Generation of mechanical components (e.g. microturbines, gears, coils, cantilevers, rotors, motors, or drivetrains) typically in silicon [Menz93].

- **Microelectronics**

Manufacturing of electronic components (e.g. transistors, or diodes) in doped semiconductor material.

- **Micro-optics**

Generation of planar optics by modulation of the refractive index in glasses [Walk93] or the manufacturing of small structures for diffractive optics (e.g. gratings or fresnel lenses) as a three dimensional structure in polymethylmethacrylate (PMMA), glass, resist, or silicon [Broc91][Find85][Lens92b].

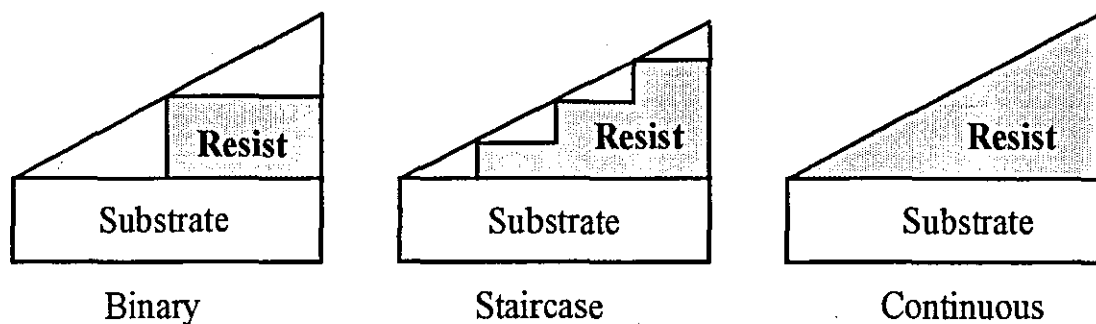


Fig. 1: Profiles of the resist microstructures

The above list shows that the structure is only rarely required in the resist itself as the end product. In most cases the structure is required in a special substrate dependent on the application. A direct structuring of the substrate is, in most cases, not possible with the required precision and, therefore, the profile is at first obtained in resist and then, in a second

step, transferred into the substrate. Therefore, the resist substrate will be exposed with an appropriate light or particle beam source, such that this resist may be removed at the exposed positions in a subsequent process (development). This leads to a structure that can have a binary, staircase, or continuous profile (compare figure 1).

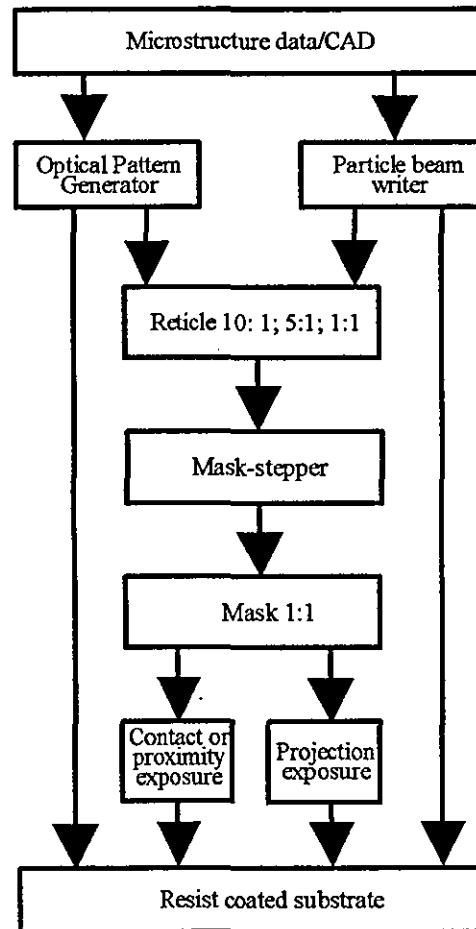


Fig. 2: Block diagram of microstructuring processes

The resist structuring procedures can be separated into two main categories: serial and parallel manufacturing which will be explained in the chapter. Figure 2 depicts this separation graphically.

A CAD-programme designed for this special application generates the microstructure data in a file which is then transferred to the light or particle writer. The data can be written in original size into a resist coated substrate or as a reticle in a magnified size into a light sensitive

material as a film for example. For further processing, these reticles are reduced to the original size using a mask stepper and transferred by contact, proximity or projection procedures into the resist coated substrate. The direct writing of the structures is called the serial process, while the use of masks is called the parallel process. Following resist structuring, an additional processing step is required. This is the actual manufacturing, which is performed in a so called batch process affecting, in a cost effective manner, the whole surface. These processes can be very different for the different materials and the different profiles and are not subjected to attention here.

2.1. Serial procedures (maskless procedures)

In order to write the appropriate structure in the serial method, the (laser) light [Golt90] [Herz92][Jäge89][Yata91] or (electron or ion) particle beam [Aoya90][Arno85][Frey92] is guided over the surface of the substrate, whereby the intensity of the beam is varied quickly. The microstructuring apparatus is controlled by a computer. Serial devices with a light or particle beam may be grouped as:

- Writers: the object to be manipulated is moved under the focussed beam using a positioning system.
- Scanner: deflection units steer the laser, electron, or ion beam over the object.

Also, combinations of these procedures may be employed in a single device[Hase92].

The advantage of the use of such a system is the possibility of manufacturing continuous, staircase and binary resist structures without the need for complex intermediate steps. As a result of the serial techniques, these procedures are very time consuming and, therefore, very expensive and in series production only useful under special conditions. The main application of these devices is to be found in the manufacture of prototypes and/or single units of masks for the parallel series manufacture.

From the point of view of resolution, the ion beam scanner followed by the electron beam scanner delivers the best results. However, the relatively high purchase price and process costs, the more expensive resist as well as the required vacuum system make this system unattractive in comparison to the laser devices (laser beam scanner and writer). These laser beam devices deliver the characteristic of focal spots with diameters in the range of the wavelength of the

laser light used. Furthermore, the laser beam devices have the advantage that there is a much greater pool of photo resist experience available to be drawn upon.

2.2. Parallel procedures (mask procedures)

The lateral structures which are stored on the mask are transferred onto the resist coated substrate via a lithographic process. In the principle setup for the parallel procedure, the mask which carries the geometry of the structure is illuminated by a beam source. Dependent on the local mask transparency, the resist coated substrate behind the mask is exposed and subsequently structured. These procedures can be used to transfer a complete mask structure in a parallel way and are, therefore, very effective methods. In general, the minimum structure sizes are larger than those obtainable from serial procedures. For different minimum structures which are to be transferred, different regions of the electromagnetic spectrum are used. The smaller the wavelength, the smaller is the minimum structure which is possible, owing to diffraction effects.

Developed parallel procedures can be grouped as:

- multi mask procedures [d'Aur72][Pole91] and
- single mask procedures [Ande90][Jäge92]

Here the use of these procedures for the manufacture of continuous and staircase profiles will be briefly investigated. Binary structures are special cases of these techniques.

In multi mask procedures, the masks carrying the desired structures are exposed one after the other onto the resist. The required processing steps are depicted in figure. 3.

In line a.) the process flow for the manufacture of a staircase resist profile is shown. Mask manufacture, substrate preparation, resist coating, the successive exposure of the masks into the prepared resist and the development of the resist leads to the structure. If required, this profile can be transferred into the substrate using etching techniques. In line b.) the manufacture of a staircase substrate profile is demonstrated. After every exposure, the resist is developed and the substrate selectively etched. After every exposure, development and etching, a new resist layer is coated on the substrate and each of the remaining masks is exposed in turn.

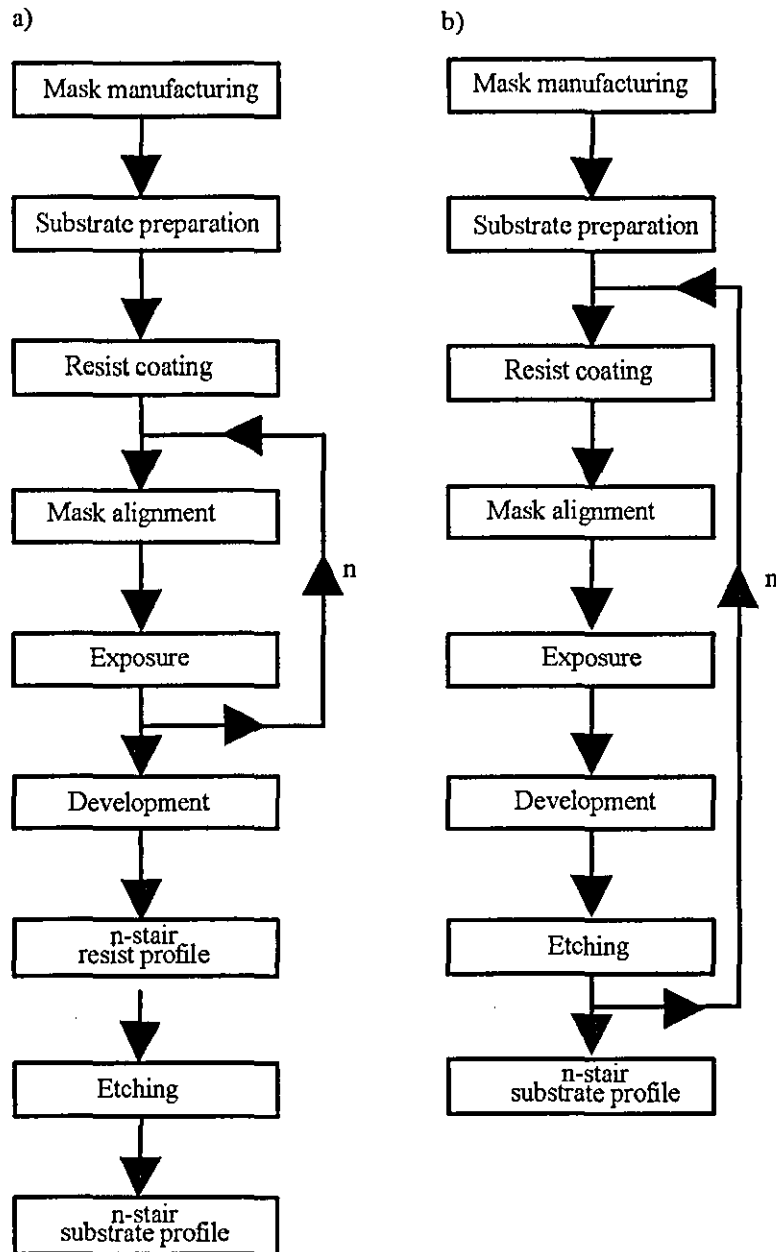


Fig. 3: Schematic representation of the multi mask procedure

Structures obtained via the above procedures approach an ideal continuous profile with larger numbers of masks. Using N masks, 2^N stairs can be generated [Dome91]. For this procedure, before transferring a new mask onto the resist, this mask must be aligned to the previous exposed/etched structures. Achievable accuracy with commercial devices is typically in the range of $5\mu\text{m}$. For this reason, the mask positioning is the most expensive part of these

processes [Jäge92]. Figure 4 shows the principal steps of these procedures and the achieved structure.

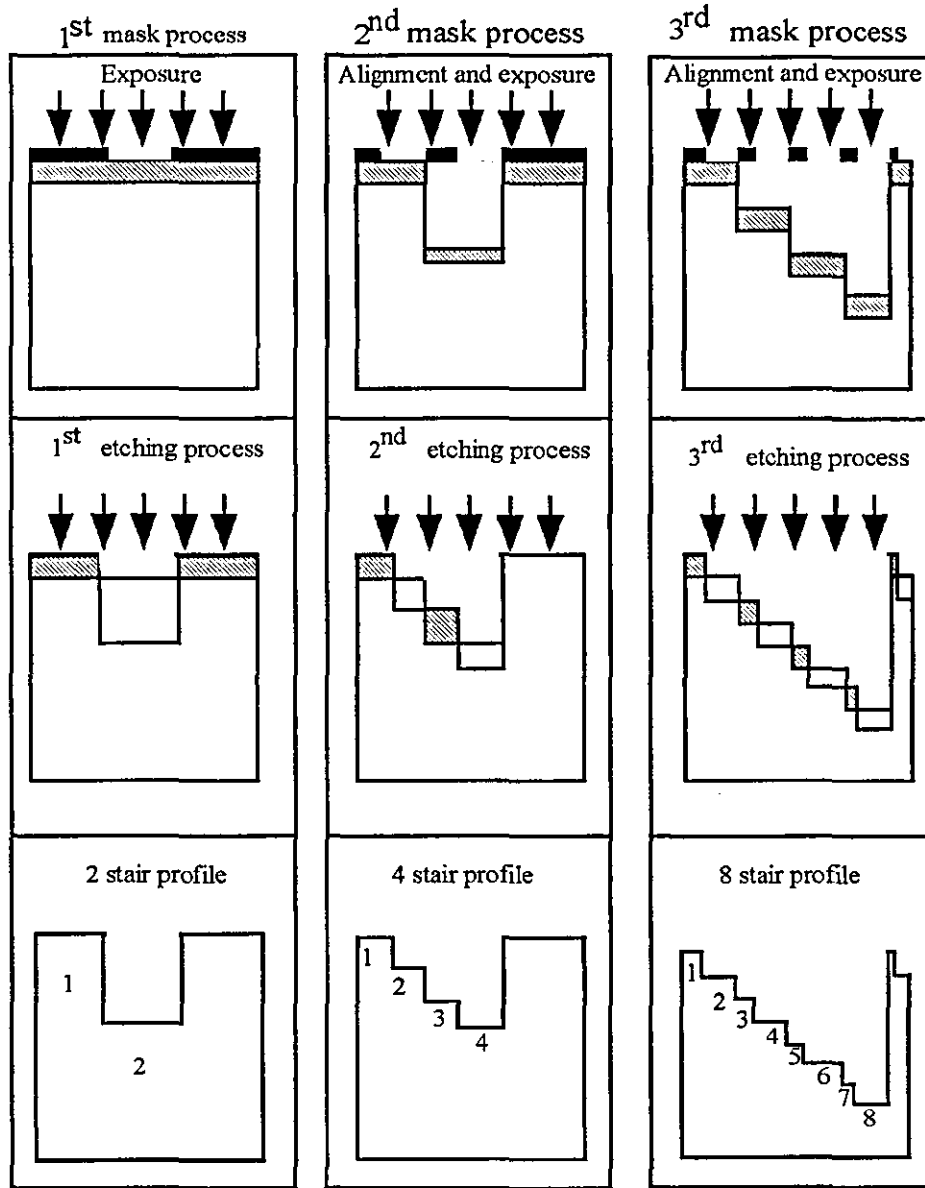


Fig. 4: Process flow of the multi mask procedure

Continuous and staircase profiles can also be manufactured using a single mask [Jäge92]. The mask structure will be transferred in one process cycle. Compared to the multi mask procedure, no expensive alignment procedure is required. A linear proportionality between the exposure and the resist removal is only given between narrow boundaries (linear portion of the resist characteristic) [Bart77] [Gamb91] [Lens92a] [Step82]. Therefore, there are higher demands on the control of the process parameter as compared to the multi mask procedures.

3. LASER PATTERN GENERATOR (LPG)

This chapter presents the principle and the characteristics of the system developed at the Fachhochschule Ostfriesland paying special attention to the demands of maximum flexibility.

3.1. Principle of a laser beam writer

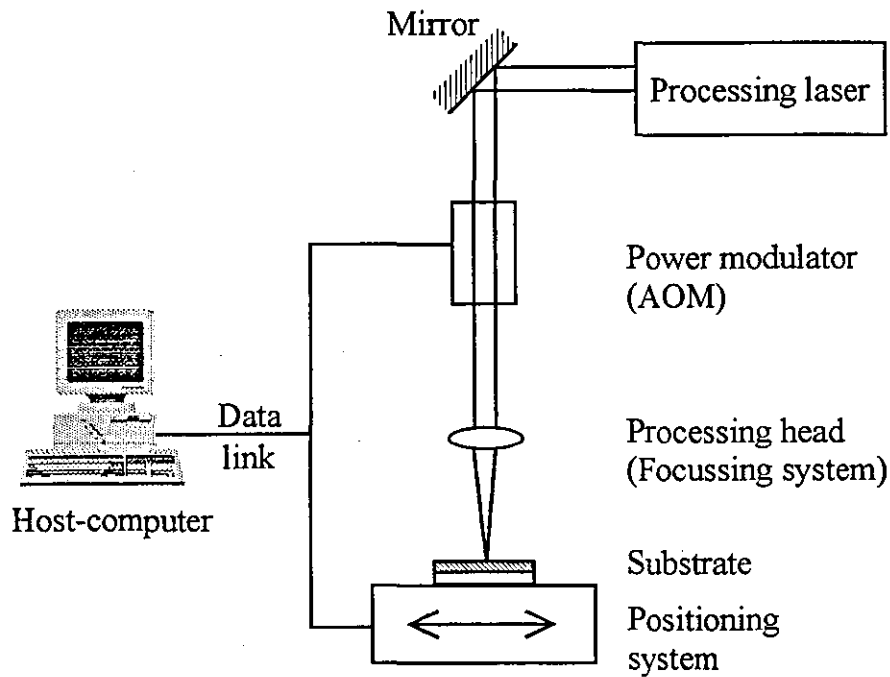


Fig. 5: Principle of a laser beam writer

The principle of a laser beam writer (see figure 5) is based on a positioning system which moves the resist coated substrate under the focussed laser beam. The positioning resolution and the beam geometry affect the smallest manufacturable structure while the maximum object size is a function of the travel range of the positioning system. For very small structures the laser beam has to be strongly focussed. Distortions of the exposure are a result of positioning errors of the positioning system and are minimised by high precision positioning systems in combination with a high resolution positioning encoder and/or laser interferometer for positioning control. An acousto-optic modulator (AOM, or Bragg cell) provides the analogue and digital beam modulation for accurate exposure. The complete system is controlled by a computer system (host-computer) which exchanges data with all the components of the laser beam writer.

3.2. Positioning system

For the manufacture of universal structures possessing various degrees of symmetry, two linear axes and one rotary table were chosen and implemented. These were mechanically combined with the centres of the linear axes in line with the rotary axis. Thus, it was possible to realise cartesian coordinates by two linear axes as well as polar coordinates by one linear axis together with the rotary axis. A host computer organises and controls actions of the stages via a controller.

The linear axes are comprised of crossed stages of a PM500-1L system from Newport corporation. The PM500 controller has a link to the host computer via a RS-232 port. The movements of the linear axes are measured using a direct axis interface (DAI) [Newp93] and a laser interferometer with a resolution of 16nm. The characteristics of the system are:

Resolution	25nm
Travel range	1" (=25.4mm)
Speed	0.01 μ /s - 50mm/s
Acceleration/Deceleration	0-2500mm/s ²

Table 1: Characteristics of the linear axes

Resolution	1/1000°(= 1count)
Smallest step size	3/1000°
Travel range	no limitation
Radial runout	16 μ m
Speed	up to 10°/s

Table 2: Characteristics of the rotary table

The rotary axis is the model M-495A in controlled by the controller MM2000 and a driver unit, all from Newport corporation. The characteristic parameters of the rotary table are given in table 2.

3.3. Optical system

A He-Cd laser (Omnichrome) provides a beam with a wavelength in the sensitivity range of the resist.

Model	4074-P-43
Laser-mode	TEM ₀₀
Beam output semi-diameter	0.5mm
Waist position	5mm behind* the output window
Wavelength	441.6nm
Rayleigh length	1.82m
Polarisation	linear (1:500)
Divergence angle	0.57mrad

Table 3: Characteristics of the processing laser

For digital and analogue power modulation of the laser beam, an external acousto-optic modulator (AOM) with a bandwidth of 20MHz (3dB) is employed. The AOM (model QZM-8-2) in combination with the RF-Driver (FFA-80, both from Brimrose) are controlled by the host computer, while the beam intensity is measured using a photodetector. For the purpose of microstructuring, the required small focal area is achieved via a microscope objective (Newport corporation). This microscope objective in combination with an adjustment system for the z-axis form the processing head of the LPG.

Type	M-60X
Focal length	2.9mm
Clear aperture	5mm
Numerical aperture	0.85
Working distance	0.3mm

Table 4: Characteristics of the microscope objective

* see figure 6

3.4. Control system

The host computer is a personal computer based on an IBM-compatible system with a 80386-33 processor from Intel. A hard disc is used for the storage of the programmes and data, and a floppy drive is available for data exchange with the environment. For the application as a host computer, the system is equipped with four different interfaces, in addition to the serial and parallel ports.

- A 12 bit A/D and D/A converter DAQ-1212A functions as the host computer port to analogue input and output signals
- The rotary table is controlled via the MM2000 controller
- A PIO interface provides the link to the direct axis interface (DAI)
- A 24 bit counter is used to evaluate the signals from the laser interferometer quadrature signals

The linear axis controller PM500 is connected via the serial RS-232 interface. An overview of the LPG is given in Appendix A, while the block diagram of the LPG is in Appendix B and a diagram of the software concept is in Appendix C.

3.5. Focal positioning demands

The beam of the He-Cd-laser is focussed as described above using a microscope objective with a short focal length in order to obtain a focal diameter in the range of $1\mu\text{m}$. Here, the resulting beam geometry at the processing location will be investigated. For the manufacture of microstructures, the following optical system was designed.

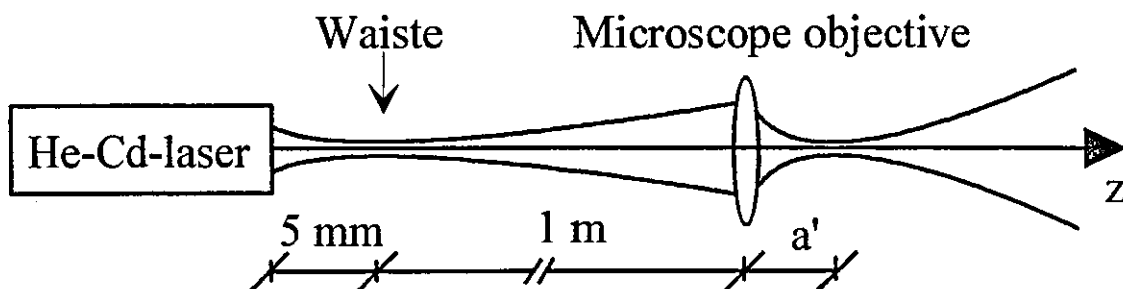


Fig. 6: Optical system of the processing laser

For the investigation of beam geometry of the optical system, the transformation of a Gaussian beam as affected by a lens, as sketched in figure 7 will be investigated, under consideration of the laser, the microscope objective, and the construction geometry employed.

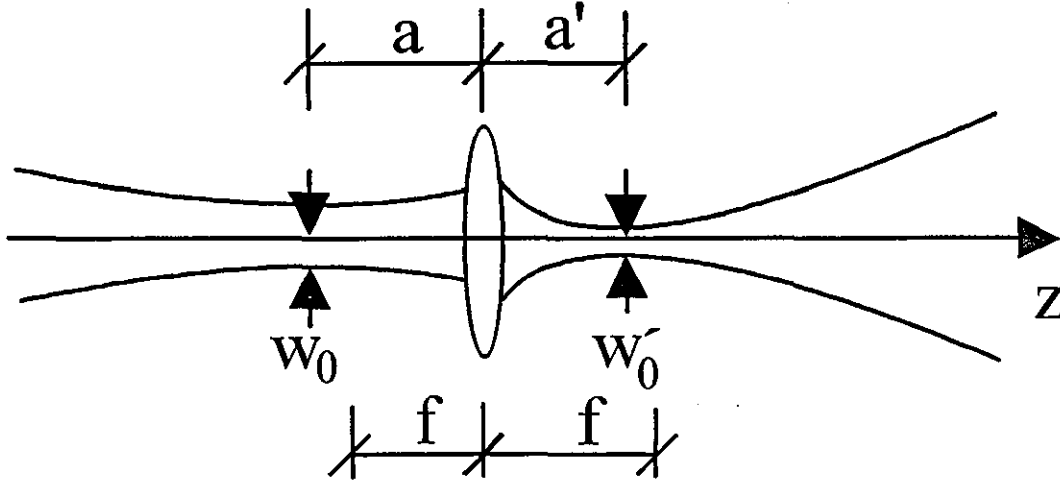


Fig. 7: Transformation of a Gaussian beam

Consider a beam waist w_0 of the laser output at a distance a on the left hand side of the lens. On the other side of the lens with the focal length f a new beam waist w_0' at the distance a' is formed. New parameters as a result of the self transformation characteristics of the gaussian beam may be calculated [Eich91]. The new position of the beam waist is given by the following equation:

$$a' = -f + \frac{f^2(f - a)}{(f - a)^2 + Z_R} \quad (1)$$

The new beam waist w_0' following the lens is given by equation (2).

$$w_0' = \frac{fw_0}{\sqrt{(a - f)^2 + Z_R}} \quad (2)$$

with

$$Z_R = \frac{\pi w_0^2}{\lambda} \quad (3)$$

where λ is the laser wavelength and Z_R is the so-called Rayleigh length. This parameter is defined as the distance from the beam waist at which the beam area is double that of the beam waist and describes therefore, the beam divergence.

According to equation (2), for minimal focal diameter in micro processing, the input Rayleigh length has to be as large as possible and, therefore, according to equation (3) the input beam waist w_0 as large as possible as well. The maximum beam waist w_0 is limited by the clear aperture of the microscope objective.

Also, according to equation (2) the distance a between the laser output waist and the microscope objective has to be as large as possible.

For the construction geometry from figure 6, and the characteristics of the laser (table 3) and the microscope objective (table 4), the beam waist can be determined according to equation (2):

$$w_0' = 0.7 \mu m \quad (4)$$

The waist location can be determined according to equation (1)

$$a' = 2.9025 mm \quad (5)$$

According to equation (3) the Rayleigh length at the laser focus point can be calculated as:

$$Z_R' = 3.5 \mu m \quad (6)$$

In order to obtain reproduceable process results with the LPG in spite of the enormous beam divergence behind the microscope objective, it is necessary to adjust the focal position precisely. For flexible manufacturing processes with variable focal positions in the manufacturing process, a control system is required. A position accuracy of at least $Z_R'/2$ should lead to satisfactory results. This accuracy criterion should be achieved in the development of the autofocus system. The catch range or working range of the closed loop system should be of the order of several Rayleigh lengths.

4. FOCAL POSITION SENSOR

It is the task of the displacement sensor to measure the distance between the processing head of the LPG and the prepared surface of the substrate (or resist), so that from this the accurate focal position of the processing laser in relation to the prepared surface can be determined. In connection with laser material processing, capacitive and tactile displacement sensors have been developed [Topk88], whereas in the area of lithography for the employment of laser beam and electron beam writers, signals for automatic focussing are provided for by pressure distance sensors [Töns93]. These systems, however, do not have the degree of resolution required for the LPG. Other types of displacement sensors available on the market cannot be employed in the LPG without major reconstruction and adjustment efforts. Therefore, the sensor comparison in this chapter focusses on the selection of a measurement principle employable in the LPG which should, in addition to resolution and measurement range, distinguish itself by good dynamic behaviour.

4.1. Tactile displacement measuring

In most cases, a diamond stylus is linked to a displacement measurement system which converts the displacement into an electrical quantity. Suitable devices are inductive or optical displacement measurement systems working on an incremental or absolute basis. The measurement range is some μm . A great advantage of these sensors is the dynamic range of the measurement process, i.e. profile changes of the work piece can be followed quickly. Furthermore, this technology is well known and of high operational security. The disadvantage of tactile measurements is the physical contact with the measurement object or work piece. This can cause damage to the surface, e.g. at a resist. In addition, the focus is determined only indirectly, i.e. the Rayleigh range of the system must be known. An example for this measurement system is the Linear Variable Differential Transformer (LVDT).

4.2. Pressure distance sensors

The objective is encapsulated above the exposure area and pressure is generated in a chamber by means of supplying inert gas. From the pressure of the gas streaming out, which varies with the distance between the processing head and the surface being structured, the displacement can be determined [Töns93]. The advantage of a relatively wide measurement range is detracted from a relatively low resolution.

4.3. Capacitive distance measuring

The distance d can be determined through measurement of the capacitance of the head/work piece system. One capacitor plate is generated by coating the lens with a metallic layer, which in addition is light-transmissive. The opposite capacitor plate is the electrically conductive work piece. The capacitance changes with changing distance between the two plates. The advantage of this measurement principle is the relatively simple analysis and evaluation circuit; the main disadvantages are the environmental conditions influencing the measurement signal. The air around the measurement point serves as the dielectric of the capacitor, and for high precision distance measurements it must not be subjected to unknown changes [Topk88].

4.4. Acoustic echo-delay measurement

An acoustic transmitter positioned within the sensor transmits a signal which is reflected from the measurement surface and then detected by a receiver, which is also built into the sensor. From the echo-delay, the distance can be subsequently determined.

4.5. Laser triangulation

A laser beam is diffusely reflected from the surface to be measured and subsequently imaged onto a detector. The location of the light point on the detector is a function of the distance between the laser head and measurement surface. Standard components do not provide the required resolution. The resolution of this system can only be increased by minituarisation of the physical construction [Krei93].

4.6. Autofocus principle

The principle of automated focussing (autofocus) has been long known and is employed in photography to enable cameras to focus on objects at essentially every distance desired. Sensors used for autofocussing are optimised for distance measurement and provide the highest resolutions. They are also distinguished by outstanding lateral and vertical resolution and show good results on highly reflecting as well as on scattering surfaces [Göpe93].

4.7. Selection and specification of the measurement principle

Due to the special characteristics of the objects (resist), tactile distance measurement is not feasible and only contactless principles may be considered. The principles of pressure distance measurement, capacitive distance measurement, and acoustic echo delay measurements will not be considered, as their resolution is too low for microprocessing. Both of the light-optical sensors (triangulation and autofocus) have the advantage that the measurement beam and the evaluation beam can be optically coupled utilising a measurement laser. However, due to the desired sensor resolution - the optical system of the triangulation sensor would require positioning very close to the focus location which is impractical. Regarding the autofocus sensor, there is the possibility that the beam reflected from the measurement surface can be separated from the optical system and then analysed and evaluated relatively far away from the focus location. The high number of measureable surface classes as well as the relatively good relation between measurement range and resolution constitute additional advantages of this sensor principle. Therefore, the displacement sensor to be employed should work according to the autofocus principle.

The functionality of the autofocus sensor concerning special applications depends mainly on the surface characteristics of the object to be measured, for the classification of which, various parameters have to be observed [Töns93]:

- reflectivity
- absorbtivity
- transmittivity
- surface angle relative to the incoming light
- surface roughness

For correct measurements, it is crucial, that a sufficient portion of the beam scattered from the object to be measured is collected by the sensor. This condition is fulfilled by highly reflecting surfaces with roughness smaller than the wavelength of the laser and is classified as directed reflections, as long as the reflected beam re-enters the lens system.

Surfaces of high roughness with diffuse reflection of the laser light can be measured nearly independently from the angle between surface and sensor axis. In this case, it is essential that the degree of absorbtion by the surface is as small as possible. Very often, surfaces are characterised by mixed reflections, i.e. the incoming laser beam is reflected diffusely into preferred directions. These types of surfaces are very suitable for measurements with an autofocus sensor [Over92].

For the classification of different surfaces according to their reflection characteristics, five different classes were described [Töns93]:

- Class 1 : diffusely reflecting
- Class 2 : mainly diffusely reflecting
- Class 3 : mixed reflecting
- Class 4 : reflecting mainly in a preferred direction line
- Class 5 : reflecting in a preferred direction line

5. SELECTION OF THE SENSOR COMPONENTS

Market research reveals, that the autofocus sensors commercially offered are especially designed for employment in surface quality assurance. Not a single device has proven itself to be directly usable for coupling of an additional processing (exposure) laser from outside without major reconstruction efforts. The simultaneous use of a single laser beam as an exposure and measuring beam is not possible with an LPG. The exposure beam does not allow for displacement measurements due to the modulation necessary for structuring during the switch off phases.

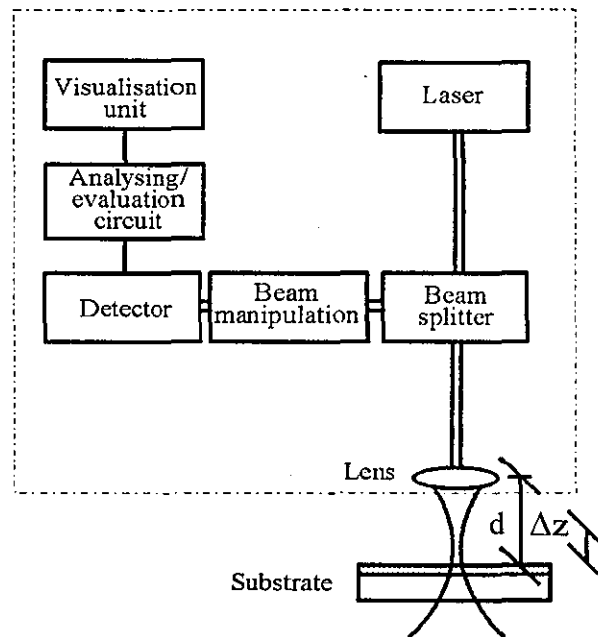


Fig. 8: Block diagram of an autofocus sensor

All autofocus methods are based on the following construction (compare figure 8) known from CD players. The light emitted from a laser is strongly focussed by a lens of short focal length and reflected from the measurement surface back into the optical system beam line. The measurement surface is separated from the sensor at distance d and in a distance Δz to the focus position, which is to be determined. The reflexion is separated from the beam, then manipulated and registered by special photo detectors, so that the displacement can be determined by an analysing and evaluation unit and visualised on a display. This type of sensor was developed resulting in different characteristics of measurement range and resolution as well as employment characteristics [Brod87][Brod89][Brod90][Brei92][Cass90][Over92][Töns93].

Wide measurement ranges were realised by the combination of the autofocus sensor with a high precision motion device and a secondary sensor. Thereby the sensor is permanently held at a defined distance to the measurement surface by means of the autofocus signal. The amount of displacement is registered by a sensor connected to the motion device.

For the employment of a displacement measuring system on the basis of autofocussing for the determination of the focal position within an LPG, the various components of the autofocus sensor will now be investigated and the components selected in order to achieve the development of a sensor of optimal flexibility and with the advantage of a linear measurement characteristic of the control system.

5.1. Selection of the measuring laser

The measurement process should not influence the exposure process negatively and, therefore, must employ a wavelength larger than that of the yellow spectral range because of the resist's spectral sensitivity. For flexible application, the laser power should be simple to modulate via an electronic signal. For a compact sensor design, the laser has to be small in size leading to the choice of a semiconductor laser with a wavelength near the infrared region. Stability of the mode, wavelength, and power are additional criteria for the selection. A product from the company Spindler&Hoyer was chosen having the following characteristics:

Type	DS670
Wavelength λ	670 \pm 10nm
Power P	0.5..1mW
Power stability	\pm 5%
Radiation characteristics	multimode
Beam shape	circular
Beam divergence	0.5 mrad
Polarisation	linear (1:60)

Table 5: Characteristics of the measuring laser

5.2. Selection of the focussing optic

Owing to the desire to couple measuring and processing beams, the microscope used for forming the processing beam is also used for focussing of the measuring beam. In the application of the sensor in the LPG, both beams pass the focussing optic simultaneously. The data are given in table 4.

5.3. Selection of the beam splitter

To separate the beam reflected from the measuring surface, a beam splitter cube was chosen. In comparison to a beam splitter plate, the cube has the advantage that there is no displacement between the incoming and outgoing beam and that ghost images are avoided.

5.4. Beam manipulation

Following the separation of the laser beam reflected from the measurement surface, it must be manipulated for the subsequent generation of the optoelectronic signal. To this end, three different methods are utilised:

- partial beam shadowing by a knife edge (Foucault's Principle)
- beam shaping by a cylindric lens
- beam separation by a wedge prism

Figure 9 shows the characteristics of the images on the detector plane generated by these methods and in dependence on the focus position. With all methods, the image of the beam profile on the detector plane for the focal position $\Delta Z = 0$ is, in case of the Gaussian beam used, a circular light spot. With the partial beam shadowing method both the intra-focal ($\Delta Z < 0$) and the extra-focal positions ($\Delta Z > 0$) result in a fade-out of one half of the beam and the size of the visible semi circle changes depending on the measurement value ΔZ . With the cylindrical lens method for the measurement surface at extra-focal position or the intra-focal position, the initially circular shape is distorted to an ellipse. The relation between the extensions of the two principal ellipse axes is a function of ΔZ . With intensity distribution achieved by wedge prism amplitude separation and with the measurement surface in focal position ($\Delta Z = 0$), a circular image appears on the detector plane for either part of the beam. For a displacement of the measurement surface, either the inner or the outer half of the full circle are faded out, and the displacement can thus be determined.



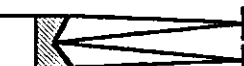











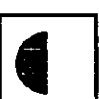
		Beam manipulation			
		 Knife edge	 Cylindrical lens	 Wedge prism	
Processing surface position	intra focal $\Delta Z < 0$				
	focal $\Delta Z = 0$				
	extra focal $\Delta Z > 0$				

Fig. 9: Principles of beam manipulation [Töns93]

A comparison of the different methods reveals, that the partial beam shadowing-, the cylindrical lens, and the wedge prism methods are especially suitable for continuous displacement measurements. For the first two methods mentioned, the efforts for adjustments and cost are normally lower than those for the prism method. Therefore, the partial beam shadowing principle was chosen for the construction of autofocus sensors, which is a well known principle for optical displacement measurements.

5.5. Beam detection and beam analysis

Depending on the beam manipulation system, the intensity distribution on the detector plane is characteristic of the measurement value. The intensity must be registered by an opto-electronic sensor which is adapted to the measurement method employed, and then, by means of a signal analysing and evaluation circuit, converted to a signal indicative of the displacement.

The photodetectors to be employed can detect the intensity either with a small active area at some place of interest for the beam manipulation or, with large area sensors, by integration of a line or an area. The first group includes detectors on the basis of small photo diodes which can, for special application conditions, be connected as diode pairs or as four-quadrant diodes and are operationally linked with an analysis and evaluation circuit [Naum92].

The detection of intensity distribution by means of large area sensors in connection with the utilisation of CCD elements allows for cross-sectional surveys with different scan rates and resolutions due to the intensity detection in every pixel of the CCD element [Naum92]. Thus, various methods of signal analysis can be used. The line or area camera must be linked to an analysis computer via an interface. The relatively high machine effort is, therefore, the main disadvantage of this procedure.

In addition to the CCD line and area camera, the second group includes the one-dimensional or two-dimensional position sensitive detectors (PSD). While CCD-elements allow pixel-wise analysis, the PSD provides in the case of one-dimensional measurement ranges, two characteristic currents I_A and I_B for the position of a light spot, which although ideally very small, under real condition may be somewhat larger (see figure 10).

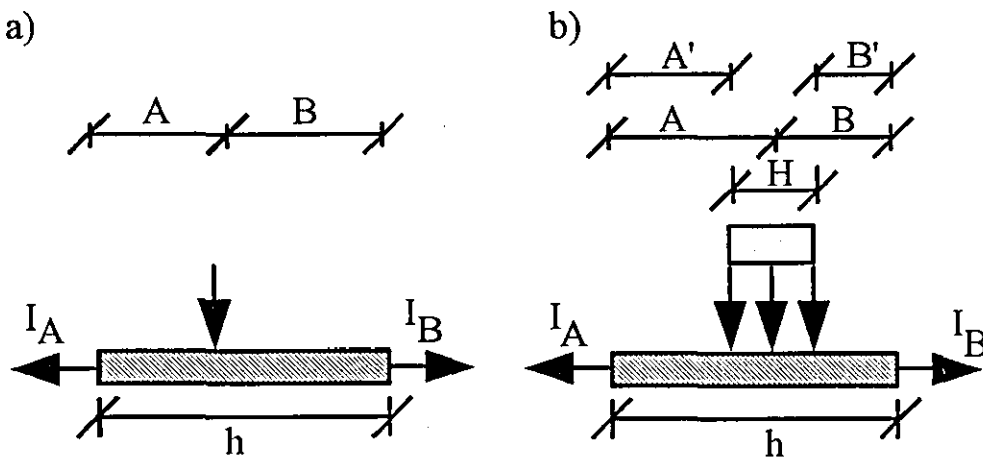


Fig 10: PSD element with a) ideal and b) real light spot

PSDs work like large area PIN-photo-diodes with two output channels. The relation between the output currents gives information on the light spot size and its position. The PSD in combination with an electronic analysing and evaluation circuit operates nearly independent on the intensity of the light spot. In PSD analysis, the schematic analysing and evaluation circuit shown in figure 11 below can be used for the generation of a signal corresponding to the position and size of the light spot.

The currents generated by the PSD element are converted via a transimpedance amplifier into two voltages proportional to the currents and subsequently linked to an adder and subtractor. The output signals of the adder and subtractor are combined by a divider so that the output signal S of the circuit depending on the geometries for an ideal light spot shown in figure 10a, can be determined.

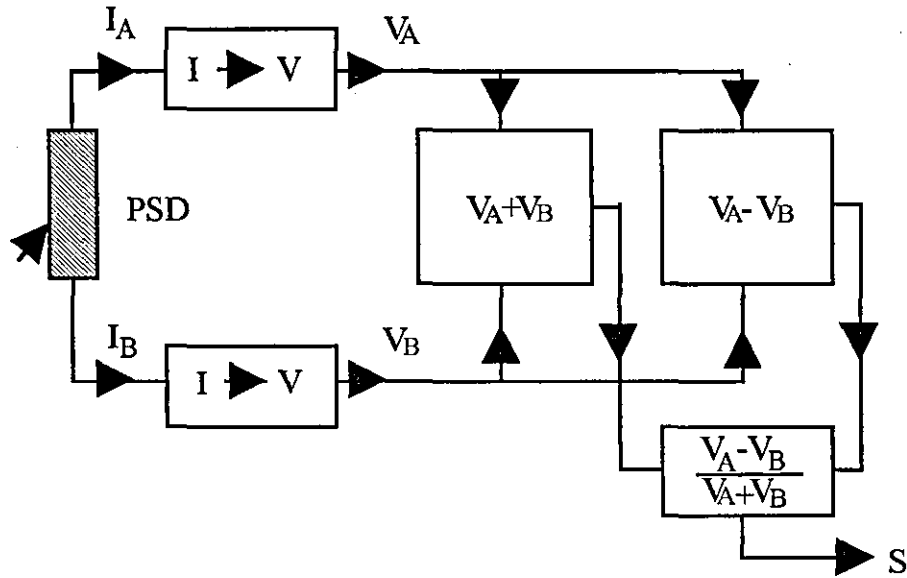


Fig. 11: PSD analysing and evaluation circuit schematic [Sike95]

Equation (7) describes the relation between the two currents I_A and I_B according to the position of the light spot on the PSD, where h is the length of the PSD and A and B are the coordinates of the light spot on the detector surface. Equation (8) describes the output signal $S(A, h)$ of the circuit for this illumination.

$$\frac{I_A}{I_B} = \frac{B}{A} = \frac{h-A}{A} \quad (7)$$

$$S(A, h) = \frac{I_A - I_B}{I_A + I_B} = 1 - \frac{2A}{h} \quad (8)$$

For a real light spot (compare figure 10b) with finite diameter H , the relation between the PSD currents I_A and I_B is given by the reduced coordinates A' and B' described by equation (9), whereas equation (10) describes the output signal $S(A, h, H)$ for this illumination.

$$\frac{I_A}{I_B} = \frac{B'}{A'} = \frac{B - \frac{H}{2}}{A - \frac{H}{2}} \quad (9)$$

$$S_{(A, h, H)} = \frac{I_A - I_B}{I_A + I_B} = \frac{h - 2A}{h - H} \quad (10)$$

For the intensity analysis in the detector plane, the PSD S3931 from Hamamatsu Company was chosen. It has an active area of 1 x 6 mm and is sensitive in the red wavelength range. For signal analysis and evaluation, a circuit was constructed and applied as recommended by the PSD manufacturer (see Appendix D).

6. Determination and optimisation of the processing head characteristics

Since the measuring principle and the components have been selected, the design of the sensor is to be optimised for use in the LPG. In order to adjust the measuring range of the autofocus sensor symmetrically around the focal position of the processing laser and to detect misalignment of the processing laser on the processed surface in both directions with the same proportional part, attention has to be paid to the possibility of a flexible and adjustable beam coupling between measurement and exposure beams. Also, a mathematical model will be introduced to adjust the sensor and to allow a directed adjustment of its measuring range and resolution as well to prove the linear operating mode of the sensor principle. It is further the intention to determine the optimum position of knife edge and PSD in the beam guidance system of the sensor with respect to the linear signal flow which is dependent upon the measured variable d or ΔZ respectively. In order to design, realise, and test a processing head which will be optimised to be used in a laser beam writer, two flexible and modularly constructed sensor prototypes will determine the measuring characteristics of the sensor on an experimental basis.

6.1. Forming of the measuring beam

A beam splitter/combiner will be introduced to couple the beam of the measuring laser with the optical axis of the processing laser. In order to enable both beams to pass through the lenses of the microscope used for focussing, the beam splitter is adjusted to align them. In this way the processing laser will be used for the resist structuring and the measuring laser will control the distance between the lenses of the microscope and the surface to be processed. Forming of the measuring beam will result in coupling the beams of the measuring laser with the processing laser in a geometric manner. In this way, the focussing of both lasers will come to one point and will introduce a measurement range which is symmetrically adjusted around the focal position of the processing laser. This allows measuring of focal positions in equal parts beneath and above the surface to be processed, i.e. the measurement range of the sensor is distributed around the focal point of the processing laser in a concentric way. The objective in forming the measuring beam is the course of its beam caustic, which influences its deviation and by this the resolution of the sensor. All this leads to the choice of a Keplerian telescope from Newport Corporation, which will be introduced in the semiconductor laser beam in front of the microscope.

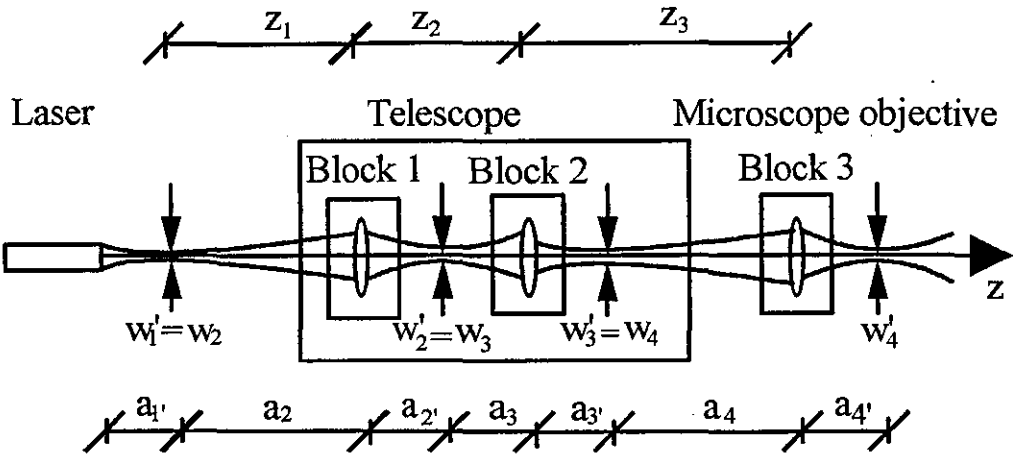


Fig. 12: Optical system of the measuring laser

Type	T81-3X
Expansion ratio	3x
Entrance aperture	3.0mm
Exit aperture	6.0mm
Input beam diameter	1.0mm
Focal range	1m to infinity
Wavefront distortion	$\lambda/4$ on axis
Transmission	>95%

Table 6: Characteristics of the expanding telescope

The position of the telescope and its optimum adjustment will be determined by the investigation of the beam of the measuring laser.

The optical system of the measuring laser consisting of the laser itself, two lenses of the telescope, and the lenses of the microscope, is arranged as shown in figure 12. In order to describe the context of the beam forming as shown in chapter 3.5 the beam of the laser has to be transformed by each lens positioned in the system. The transformation done in this way leads to a beam caustic at the measuring position behind the lens of the microscope which not only depends on the displacements Z_1 , Z_2 , and Z_3 between the components and to the focal distances f_2 , f_3 , and f_4 of the lenses, but also upon the wavelength λ and beam profile of the semiconductor laser. This general system can be decomposed in subsystems which execute the transformation of the beam waist position according to equation (1) and the beam waist radius w according to equation (2). Such a transformation block is shown in figure 13.

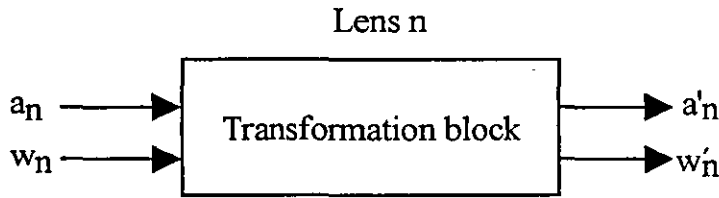


Fig. 13: Transformation block of a lens

As shown in figure 12, the laser and its beam characteristics are the input variables for the first lens (block 1). When the system components have been selected, the separation of the lenses represents the degree of freedom of the general system in adjusting the desired beam geometry at the measuring position. In this case, this general system is represented by the transformation block shown in figure 14.

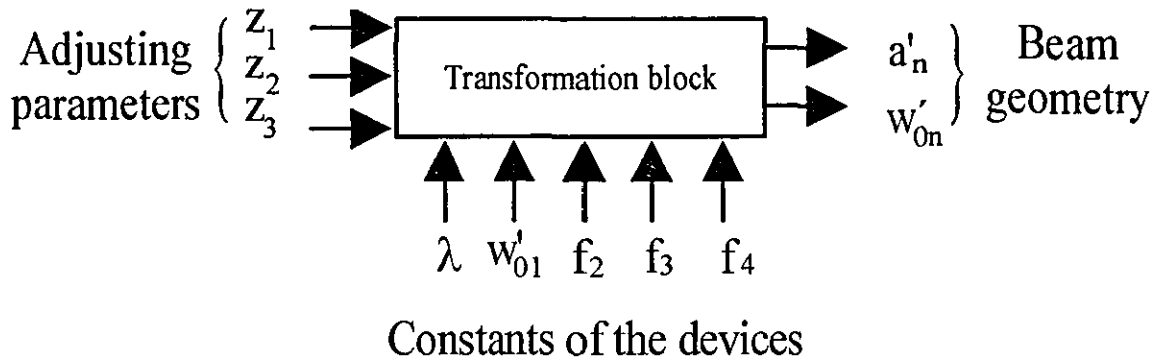


Fig. 14: Transformation block of the general system

The input variables of this transformation block are the component displacements Z_1 , Z_2 , and Z_3 . The system parameters λ and w_0' of the laser as well as f_2 , f_3 , and f_4 of the lenses are system constants. A particular adjustment of these parameters at the input of the transformation block will lead to a particular beam geometry at the measuring position determined solely by radius w_{04}' and position a_4' of the focus.

The analytical description of equation (2) representing the beam radius w_{04}' and equation (1) representing the focus position a_4' requires combination of all transformation blocks, beginning at the lenses of the microscope and ending at the laser, which expresses the position of the beam waists by using the distances between the lenses. This task can be performed by ray-

tracing programs. Using the laws of geometric and Gaussian optics determined by equations (1) and (2), the programme “Zemax”, for instance, can simulate the beam expansion at each position along the optical axis.

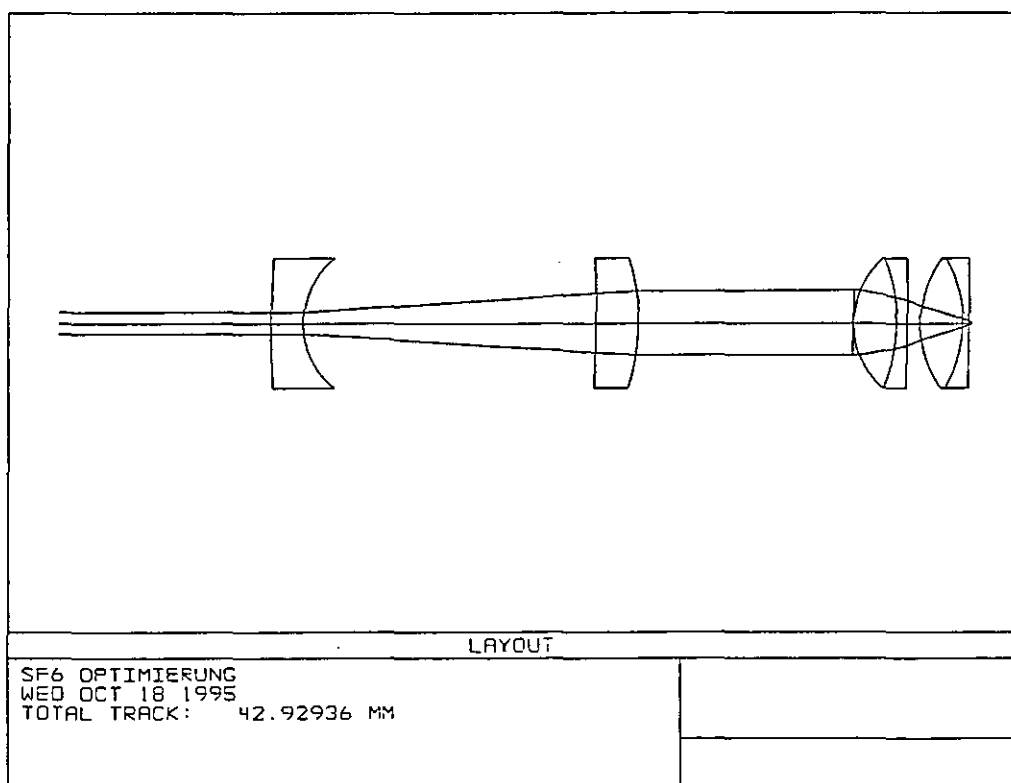


Fig. 15: Optical design of the measuring laser beam using a ray-tracing program

Figure 15 shows a laser beam coming from the left expanded by the telescope and strongly focussed by the microscope. The ray-tracing application simulates a general system (Appendix E, F, and G) including the optical components using manufacturers specifications, thus enabling the investigation of the beam parameters at the output area (measuring area) just behind the microscope. A certain radius, w , and position of a focus, a , was introduced to an optimisation routine which is part of the Zemax application. This leads to the advantage that no discrete components had to be changed, but rather only variations of the distances of the lenses are necessary to fulfil the adjustment task. The focal position of the processing laser was determined in chapter 3.5 and the focal position of the measuring laser was matched to this position. In order to reach a relatively high measuring sensitivity the beam divergence of the measuring laser was adjusted to twice that of the processing beam. Optimising the beam path in this manner leads to the following displacements between laser and lenses (see figure 12):

- $Z_1=40\text{mm}$
- $Z_2=14\text{mm}$
- $Z_3=700\text{mm}$

The measuring laser is multimode and, therefore, all calculations in accordance with the rules of Gaussian optics will lead to approximations only. In case the calculated focal positions of measuring and processing beam within this beam path do not match or the beam divergence of the measuring laser needed for necessary sensor resolution is not large enough, the focal adjustment at the telescope (displacement variation of Z_2) will have to be corrected experimentally.

6.2. Sensor model

The function of the autofocus sensor is established by splitting, manipulating and detecting the beam of the measuring laser reflected at the measured surface from the beam path of the processing laser by means of a beam splitting cube, focussing lens and knife edge, and PSD located in the detector plane. The test signal is generated in a post-connected electronic circuit (see also chapter 5). In optimising this setup for an adjusted measuring range and resolution needed for a particular measurement task, a mathematical model will have to be developed. To do this the beam path of the complete system has to be linearised (setup without beam splitting cube) in accordance with the rules of geometric optics.

The input beam of the measuring laser with its radius w and parallel boundary rays is collected by the lenses of the microscope in the focal plane f_1 . Depending on the distance ΔZ of the measured surface to the focal plane f_1 of the microscope, the reflected boundary rays pass on different tracks through the system which consists of microscope objective, sensor lens separated by a distance l_1 , and the detector plane displaced with respect to the sensor lenses by a distance l_2 .

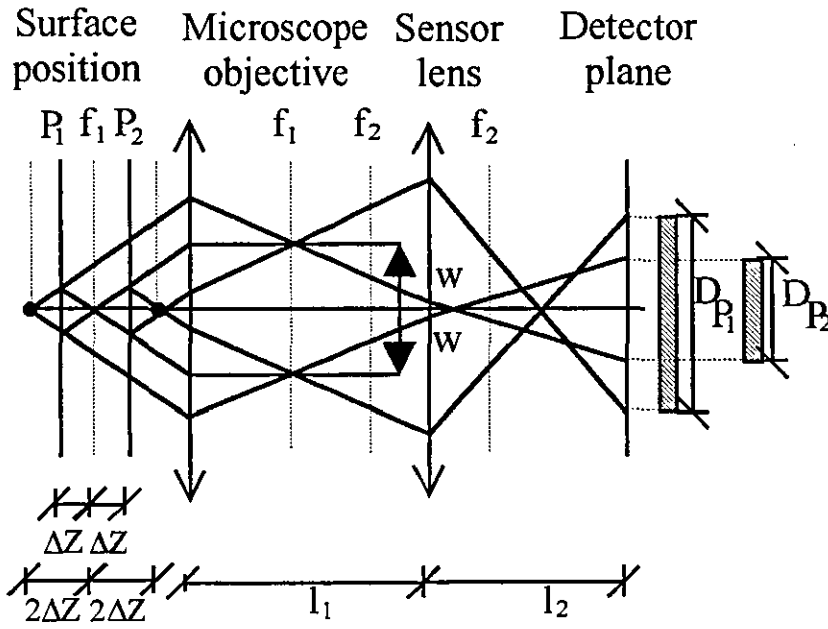


Fig. 16: Linearised setup of the sensor

In the detector plane a spot is reproduced whose diameter D is determined by the distance ΔZ of the measuring surface. This spot is detected by the PSD.

The development of a mathematical model has the purpose to describe the diameter D of the spot as a function of the distance ΔZ for a setup determined by the distances l_1 and l_2 as well as the focal distances f_1 and f_2 of the lenses. This is done by establishing the functional context of the sensor (equation (11)) using the optical image equation. This context and its meaning for the sensor principle will now be discussed (see Appendix H for complete derivation).

$$D = D_0 + K\Delta Z \quad (11)$$

with

$$D_0 = 2w \frac{(l_2 - f_2)}{f_2} \quad (12)$$

and

$$K = 4w \frac{(f_1 l_2 - f_1 f_2 - l_1 l_2 + l_1 f_2 - l_2 f_2)}{f_1^2 f_2} \quad (13)$$

In accordance to equation (11), the diameter D of the spot is composed of the initial diameter D_0 which is subject to the setup and an element $K\Delta Z$ which is subject to the measured variable in a linear manner. The factor K which is part of the second term represents the sensitivity of changing of diameter with respect to the measured variable ΔZ and determines the sensitivity of the measurement setup. The context described by equation (11) is valid only considering paraxial rays and assuming infinitely large lenses. Practical limitations of this model calculation are given by the geometry of the object used in this setup. The operation of the measuring system must not allow screening of the rays caused by small lens apertures.

In the following chapters, the model for the spot adjustment according to equation (11) will be discussed considering the initial diameter D_0 of equation (12) and the factor K of equation (13) as the sensitivity of the diameter changes.

6.2.1. Analysis of the initial diameter D_0

According to equation (12), the initial diameter D_0 of the spot is completely independent of the focal distance f_1 of the microscope objective used for focussing. It is only influenced by the focal distance f_2 of the sensor lens and the distance l_2 between the sensor lens and the detector plane as well as the radius w of the beam. Considering the resulting characteristics, one has to consider three cases:

Case a1: $l_2 = f_2$, the detector plane is located at the focal plane of the sensor lens.

Case a2: $l_2 < f_2$, the detector plane is located in front of the focal plane of the sensor lens.

Case a3: $l_2 > f_2$, the detector plane is located behind the focal plane of the sensor lens.

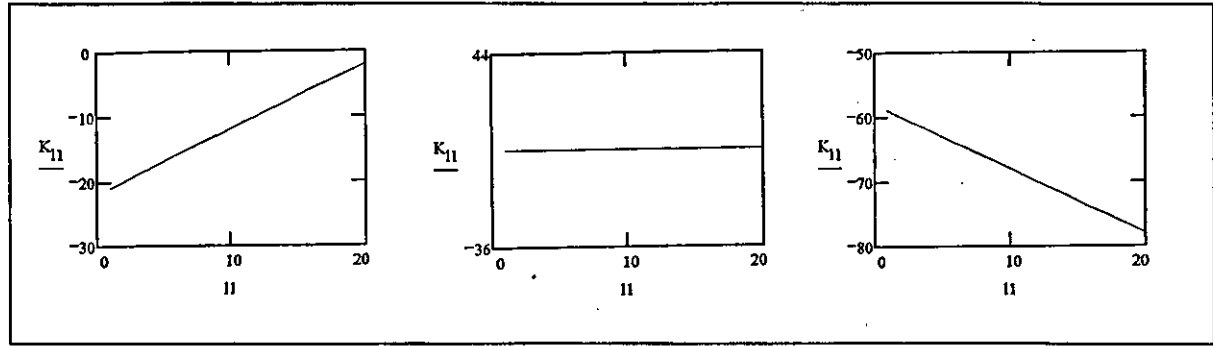
In case a1 the initial diameter $D_0 = 0$, whereas in cases a2 and a3, and using equal displacements ΔZ in front of and behind the focal plane of the sensor lens, the initial diameter has the same value and is symmetrically placed around its focal plane.

6.2.2. Analysis of the sensitivity constant K

According to equation (11) the sensitivity constant K determines the change in diameter for given values of ΔZ given by $K\Delta Z$. The enormous number of influencing arguments leads, according to equation (13), to equal values of the sensitivity constant K using different settings of focal distances, beam radii, and distances. The resulting sensor adjustment, with all its variation possibilities and their practical meaning, will be investigated by modelling equation (13) in a mathematical manner and systematically varying all parameters in meaningful physical limits (see case b1 to b4). The sign of the sensitivity constant K has no meaning and is a question of definition whether diameter D increases or decreases in changing the displacement direction of ΔZ .

Case b1: Variation of l_1

In this case, simulation series with varying l_1 will be conducted for two different values of f_1 . In the first case of both simulation series (see figure 18a) and 18d)), the focal distance f_2 is larger than the distance l_2 between sensor lens and detector plane, for the cases 17b) and 17e) f_2 equals l_2 and for the two remaining cases of both simulation series (17c) and 17d)) f_2 is smaller than l_2 .



a)

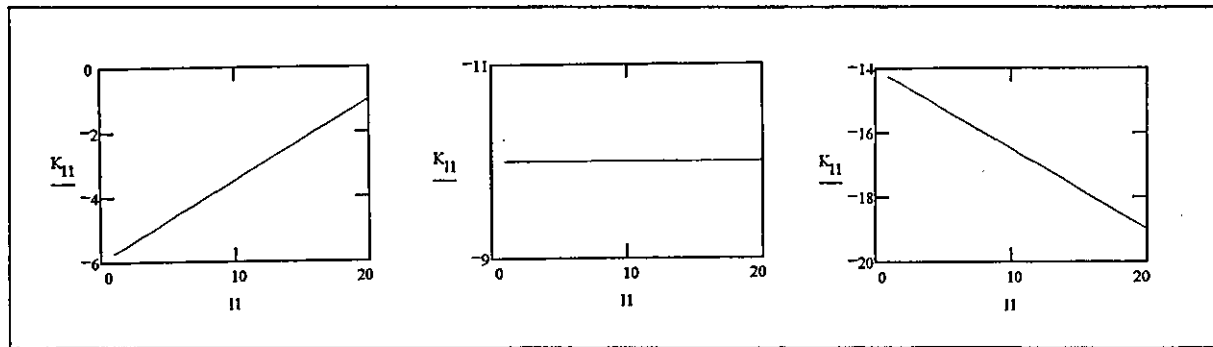
$l_1 = 1..20mm$
 $l_2 = 10mm$
 $f_1 = 2mm$
 $f_2 = 20mm$
 $w = 2mm$

b)

$l_1 = 1..20mm$
 $l_2 = 20mm$
 $f_1 = 2mm$
 $f_2 = 20mm$
 $w = 2mm$

c)

$l_1 = 1..20mm$
 $l_2 = 30mm$
 $f_1 = 2mm$
 $f_2 = 20mm$
 $w = 2mm$



d)

$l_1 = 1..20mm$
 $l_2 = 10mm$
 $f_1 = 4mm$
 $f_2 = 20mm$
 $w = 2mm$

e)

$l_1 = 1..20mm$
 $l_2 = 20mm$
 $f_1 = 4mm$
 $f_2 = 20mm$
 $w = 2mm$

f)

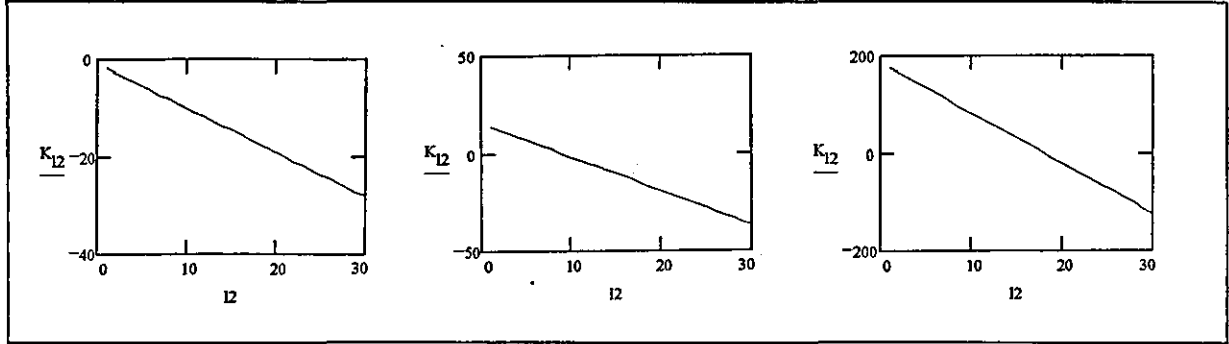
$l_1 = 1..20mm$
 $l_2 = 30mm$
 $f_1 = 4mm$
 $f_2 = 20mm$
 $w = 2mm$

Fig. 17: Variation of l_1

It can be seen from this simulation series that l_1 can occupy values which prove a linear dependence. In case $l_2 = f_2$, K remains constant while l_2 is changing and comparing both simulation series K and f_1 are interdependent. The values of K increase, while values of f_1 decrease (comparing figure 17b) and 17e)). In cases where f_2 is unequal to l_2 , one will find a positive slope for $f_2 > l_2$ and a negative slope for $f_2 < l_2$. In both cases the range of K values depends on f_1 and rises with increasing values of f_1 .

Case b2: Variation of l_2

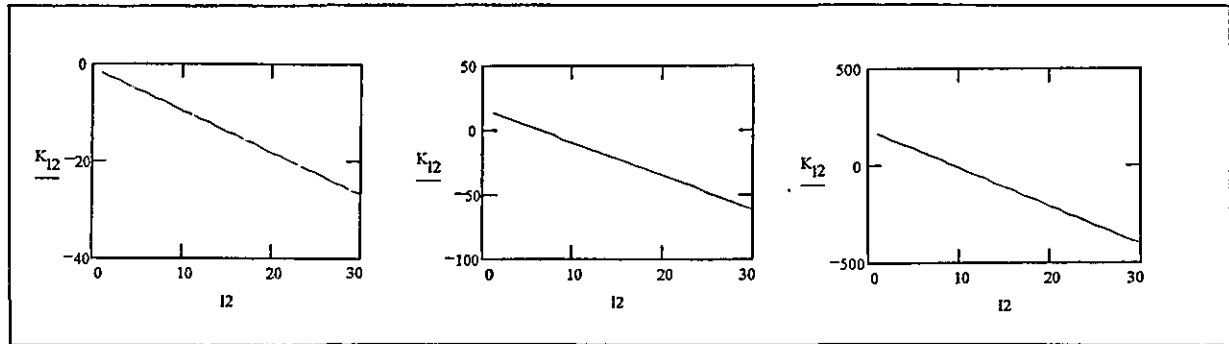
Simulation series with varying l_2 will be conducted for two different values of f_2 . In the first case of both simulation series (see figure 18a) and 18d)), the distance between the microscope objective and the sensor lens are smaller than the focal distance f_1 of the microscope lens, while in both remaining cases of both simulation series, l_1 is larger than the focal distance f_1 .



a)
 $l_1 = 2\text{mm}$
 $l_2 = 1..30\text{mm}$
 $f_1 = 2.9\text{mm}$
 $f_2 = 20\text{mm}$
 $w = 2\text{mm}$

b)
 $l_1 = 20\text{mm}$
 $l_2 = 1..30\text{mm}$
 $f_1 = 2.9\text{mm}$
 $f_2 = 20\text{mm}$
 $w = 2\text{mm}$

c)
 $l_1 = 200\text{mm}$
 $l_2 = 1..30\text{mm}$
 $f_1 = 2.9\text{mm}$
 $f_2 = 20\text{mm}$
 $w = 2\text{mm}$



d)
 $l_1 = 2\text{mm}$
 $l_2 = 1..30\text{mm}$
 $f_1 = 2.9\text{mm}$
 $f_2 = 10\text{mm}$
 $w = 2\text{mm}$

e)
 $l_1 = 20\text{mm}$
 $l_2 = 1..30\text{mm}$
 $f_1 = 2.9\text{mm}$
 $f_2 = 10\text{mm}$
 $w = 2\text{mm}$

f)
 $l_1 = 200\text{mm}$
 $l_2 = 1..30\text{mm}$
 $f_1 = 2.9\text{mm}$
 $f_2 = 10\text{mm}$
 $w = 2\text{mm}$

Fig. 18: Variation of l_2

It can be seen that in all six cases the characteristic curve shows the linear relationship between sensitivity constant K and l_2 . Graphs 18a) and 18d) do not cross the zero axis, while all other graphs cross the zero axis in the range of $0 < l_2 < f_2$. It also can be seen that in each simulation series with f_2 remaining constant K occupies the same value where $l_2 = f_2$. This proves K is independent of l_1 , however, comparing both simulation series, K and f_2 are interdependent. At this point, larger values of f_2 lead to larger values of K . It also proves within the complete range of l_2 larger values of l_1 and smaller values of f_2 result in a larger range of K values.

Case b3: Variation of f_1

While analysing f_1 , this parameter was varied for different values of l_1 . In the first case l_1 equals f_2 and in the remaining two cases l_1 is larger than f_2 .

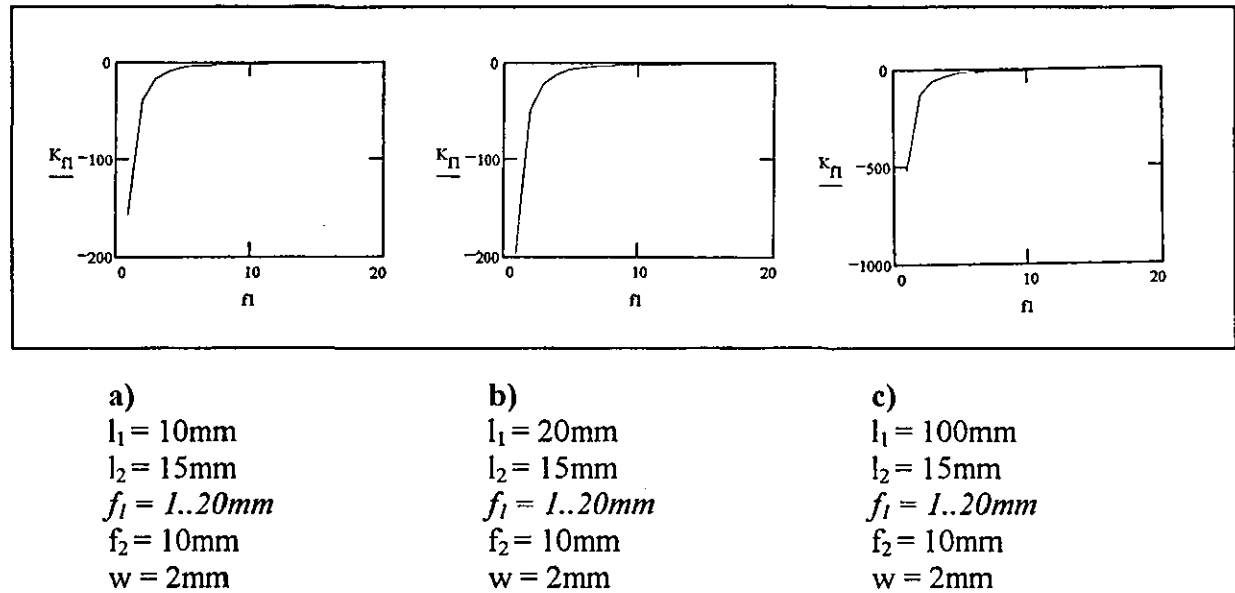


Fig. 19: Variation of f_1

One sees that increasing values of f_1 force the sensitivity constant K asymptotically to zero, while increasing values of l_1 widen the range of K values.

Case b4: Variation of f_2

While analysing f_2 , this parameter was kept variable for different values of l_2 . In all cases l_2 lies within the range of f_2 and increases its value from 20a) over 20b) to 20c).

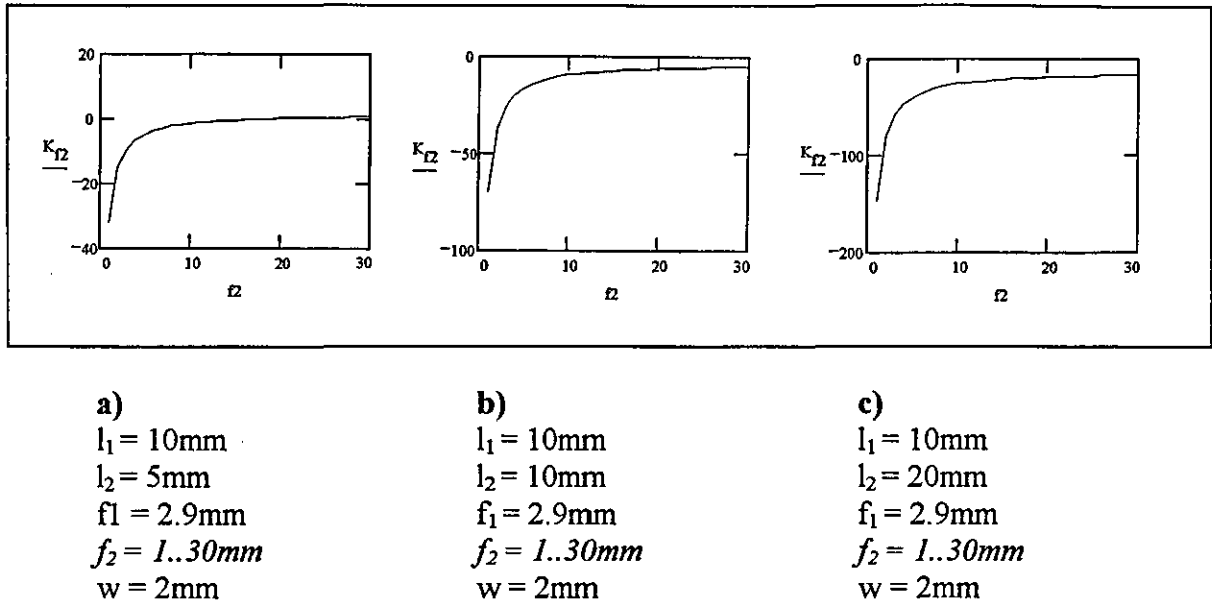


Fig. 20: Variation of f_2

One sees that increasing values of f_2 force the sensitivity constant K asymptotically to a limiting value. The range of K -values increases with increasing values of l_2 . It also can be seen that graph 20a) crosses zero while graphs 20b) and 20c) do not reach zero.

Case b5: Analysis of w

The interdependence between sensitivity constant K and radius w of the laser beam is a linear function.

6.2.3. Sensor adjustment

The systematic analysis of equation (11) allows the following conclusions in dimensioning the sensor considering cases a1 to a3 for its first term derived from equation (12) and considering cases b1 to b5 for its second term derived from equation (13):

- The adjustment of the initial diameter D_0 is determined by the ratio of the distance l_2 and the focal distance f_2 . For all l_2 , which are smaller than $2f_2$, the symmetric beam path permits a compact setup in placing the detector plane in front of the focal plane of the sensor lens.

- In order to increase the sensitivity constant K as much as possible, the focal distances f_1 and f_2 need to be kept as small as possible and the distances l_1 and l_2 as large as possible. The influence of the focal distances f_1 and f_2 on the sensitivity constant K is not linear over the whole range, while the influence of the distances l_1 and l_2 is absolutely linear.
- Certain different combinations of l_1 , l_2 , f_1 , and f_2 result in a sensitivity constant K which is zero. In this case, the principle of the sensor is abolished and, therefore, changing the measurable variable ΔZ will not result in a changed diameter D of the spot. Setups without sensor characteristics can be avoided using equation (13) in testing the sensitivity.
- The sensor installation and its required measuring range should lead to a setup, which is adapted to the detecting characteristics and aims for a signal with linear interdependency between itself and the measurable variable (see next chapter). A coarse preset of the K -value using equation (13) with the focal distances f_1 and f_2 of the lenses could be found, which in turn can be adjusted changing the distances l_1 and l_2 between the lenses and changing the beam radius w by means of an iris aperture. In order to keep the setup as compact as possible, the distances should be kept as short as possible.

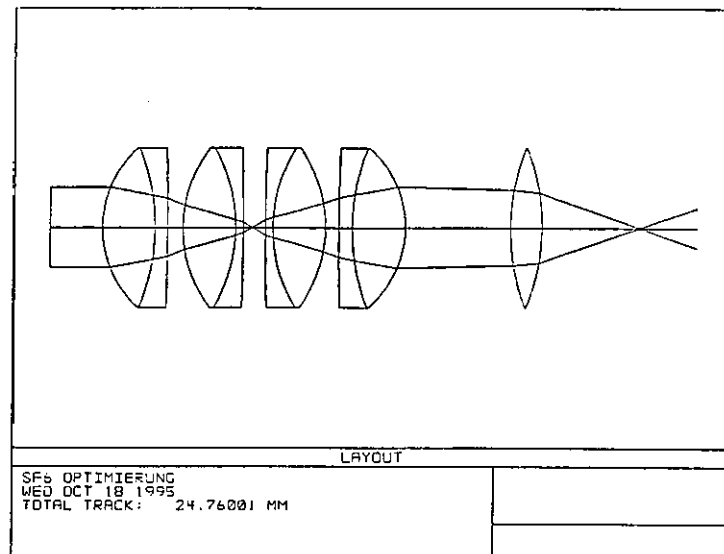


Fig. 21: Ray-tracing model of the sensor

Checking of the calculations and of the sensor characteristics was done by simulating the sensor in a computerised raytracing model (see Appendix I for details).

Mirroring the microscope lenses at the measuring surface with its displacement d results in a programmable forward-configuration of the sensor. In this way, the measurable variable ΔZ can be easily simulated with the displacement d between the microscope objectives. This model enables one to consider the diameter of the spot in the detector plane, which results as an outcome of a certain setup. Skillful adjustment of the distances will result in an optimised sensor characteristic.

6.3. Beam manipulation and beam detection

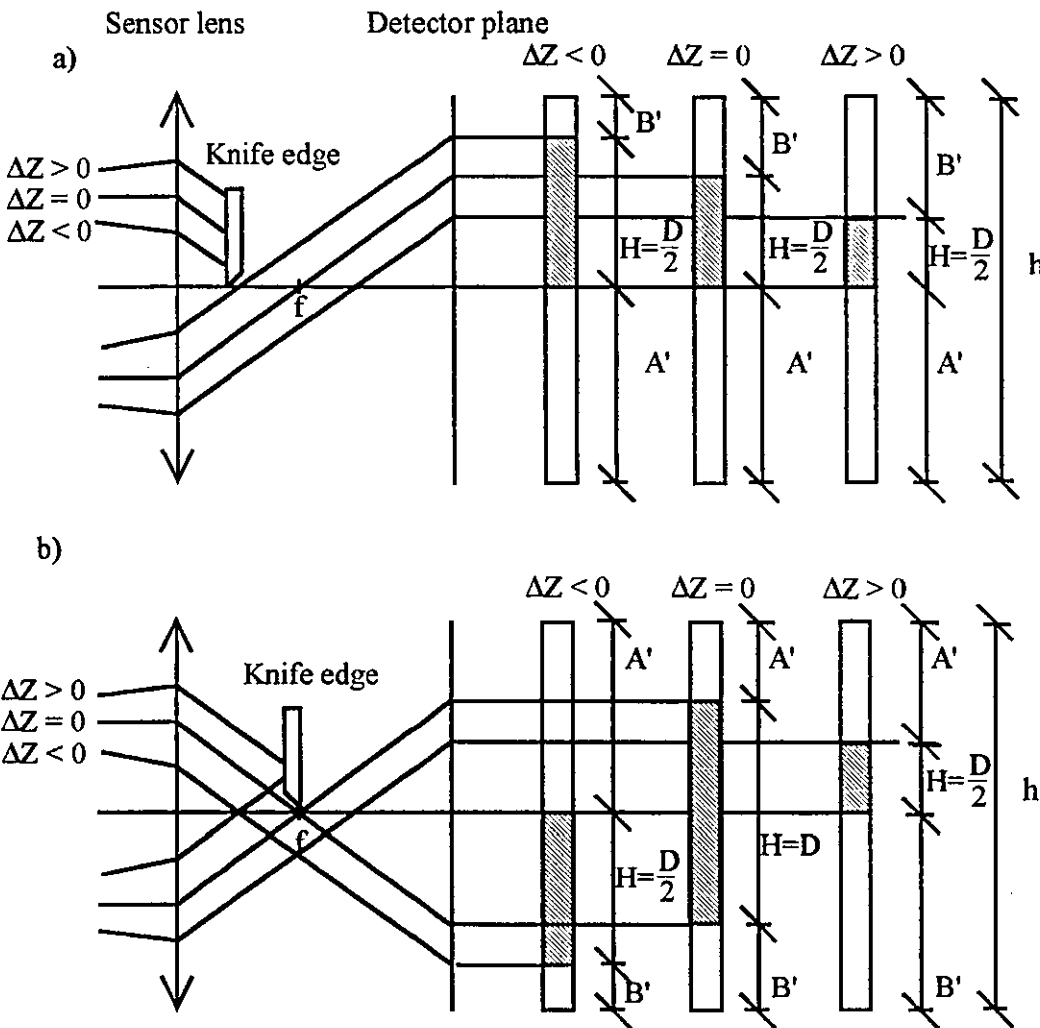


Fig. 22: Principles of knife edge and PSD adjustment

In order to fulfill the requirement of the sensor that the signal course stays linear over the complete measuring range, not only the diameter D of the light spot needs to prove its linear interdependence to the measurable variable, but also the resulting PSD-signal has to follow this linearity. To test this, the functional interdependence between different knife edge- and PSD-positions with PSD-signals resulting from the illumination have to be examined and the setup needs to be optimised to result in a steep but linear signal curve. Positioning knife edge and PSD follows two principle setups (see figure 22).

In both setups the intersection point of the boundary rays with the optical axis (focal point) located between sensor lens and detector plane varies with different values of the measurable variable ΔZ or d . In the middle of the measuring range ($\Delta Z = 0$) the boundary rays intersect with the optical axis in the focal plane of the sensor lens. In changing the measurable variable ΔZ , the position of the intersection point moves and results in a changed diameter of the light spot when no knife edge is present. The knife edge masks half of the light spot and only a semi-circle can be observed in the detector plane.

The difference in both setups is as follows: in case a) the knife edge is positioned to the optical axis in such a way that the intersection point of the boundary rays with this axis never touches the knife edge. In this case, one can always observe a semi-circle in the detector plane while changing ΔZ within the measuring range ($\Delta Z > 0$ and $\Delta Z < 0$). In case b) the knife edge is positioned within the moving range of the intersection point between boundary rays and optical axis and in case the intersection is just above the beam stop ($\Delta Z = 0$) one can observe the total light spot while in all other cases only the upper ($\Delta Z < 0$) or lower ($\Delta Z > 0$) semi-circle can be seen.

The signal form, resulting in both setups from the illumination of the PSD and its connected evaluation circuit will now have to be analysed. In this process, one will assume a homogeneous illumination over the total beam cross-section and a very much broader diameter of the light spot than the PSD-input. In this case, the total or half a light spot corresponds to a real PSD illumination with the height H (see figure 10b) and leads to equation (10) which describes the real light spot but, with the above assumptions, also the signal form S .

Analysis of the signal form for setup from figure 22a)

In a first step, the characteristic signal form $S = f(A, h, H)$ of equation (10) is subject to the analysis for the setup shown in figure 22a). In this case, over the total length h of the PSD one will find an unilluminated length A' , an illuminated length H , and another unilluminated length B' . The ratio of the PSD-currents resulting from this illumination is determined according to equation (9):

$$\frac{I_A}{I_B} = \frac{B'}{A'} \quad (14)$$

Introducing the illumination shown in figure 22a). and a length h of the PSD, the current I_A can be expressed as a function of I_B .

$$I_A = I_B \frac{h - A' - H}{A'} \quad (15)$$

The analysing circuit connected to the PSD performs signal forming, for an illumination with a real light spot according to equation (10). This leads by substituting equation (15) to the following signal:

$$S(A', h, H) = \frac{h - 2A' - H}{h - H} \quad (16)$$

As a function of an illumination with a height $H = D/2$, one will find the signal forms shown in figure 23 when the PSD-length is normalised to $h = 1$ and different selected lengths of A' will be chosen.

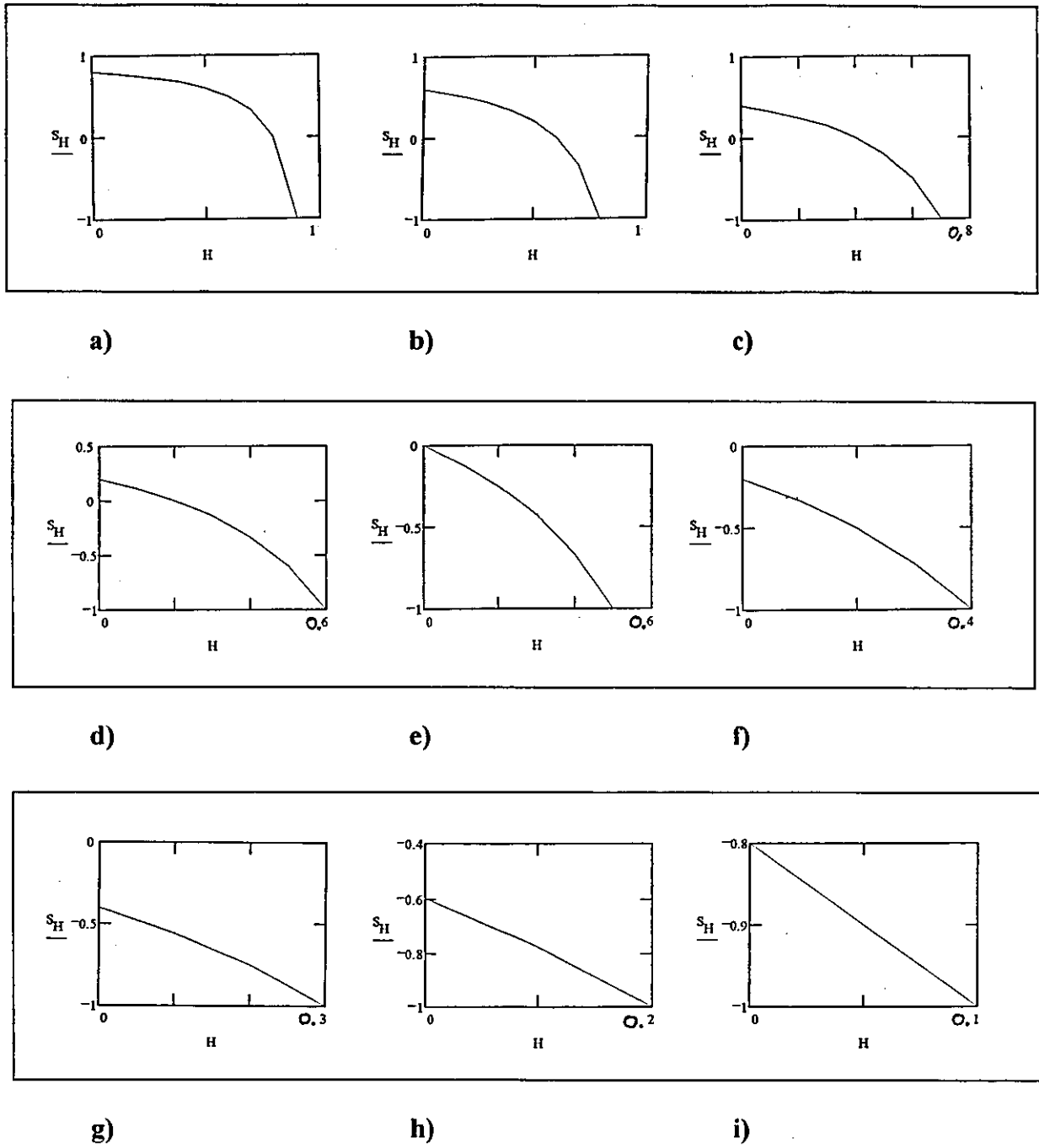


Fig. 23: Simulation of PSD-signals for different illuminations

Figure 23 proves when the values of A' are increased, the defined range of H also increases by the same amount. The range of values for $S(H)$ will decrease with increasing values of A' . At the same time, the linearity improves, so that in practice the actual adjustment on one hand will be a compromise between $S(H)$ with a range of value as large as possible and H with a defined range also as large as possible or, on the other hand one is selecting an operating range with a portion of the characteristic curve where the signal level swing can be considered to be linear.

Analysis of the signal form for setup from figure 22b)

The PSD with its length h is positioned symmetrically to the optical axis to assure a symmetric illumination ($A = B = h/2$). The illumination of the upper half of the PSD with $H = D/2$ leads to the following current ratio:

$$\frac{I_A}{I_B} = \frac{B}{A-H} = \frac{h/2}{h/2-H} \quad (17)$$

The illumination of the lower half leads to this current ratio:

$$\frac{I_A}{I_B} = \frac{B-H}{A} = \frac{h/2-H}{h/2} \quad (18)$$

Introducing these relations into the function which describes the signal formed by the evaluation circuit (equation (10)) results in a signal form $S(h,H)$ described by equation (19).

$$S(h,H) = -\frac{H}{h-H} \quad (19)$$

The interdependence between light spot and signal form $S(H)$ for a normalised length $h = 1$ of the PSD is shown in figure 24.

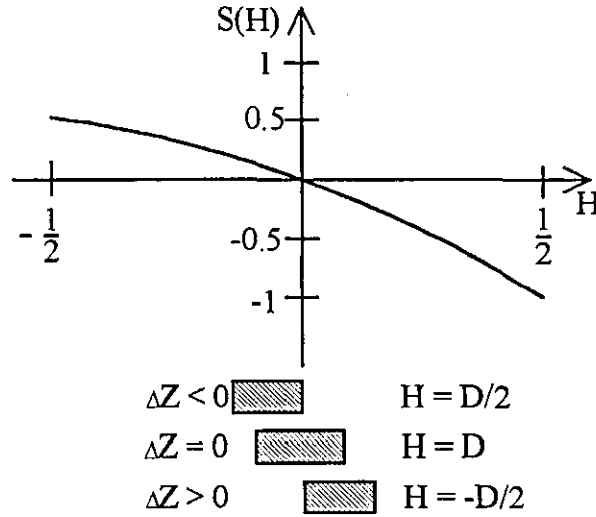


Fig: 24: Interdependence between PSD signal form $S(H)$ and light spot

This function intersects the origin of the coordinate system when the distance ΔZ equals zero. Positive x -values result in value ranges with negative sign of function $S(H)$ which are twice as much as those of negative x -values with positive sign, indicating a significant nonlinear response in both directions. Also the characteristic of the illumination of the PSD is sketched resulting to the measurement characteristics shown in figure 25.

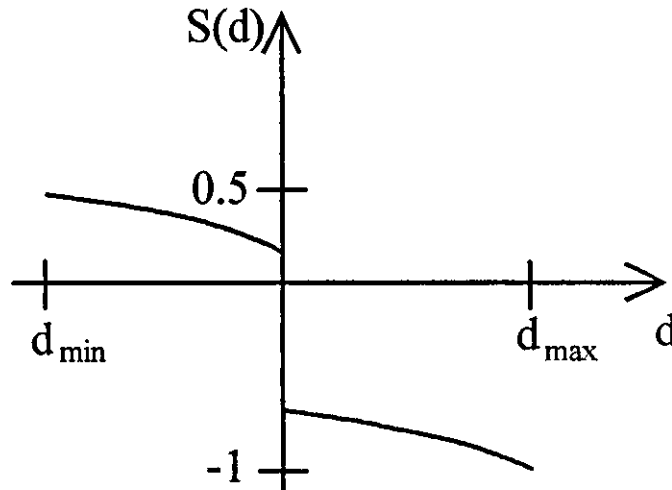


Fig. 25: Typical signal characteristics as a function of the measured value

The actual signal form depends upon the actual illumination and geometry (as shown in figure 24 and figure 22b). The positioning of the beam spot in this setup is in the middle of the measurement range ($\Delta Z = 0$) and results in an illumination of the PSD which is centred on the optical axis (see figure 22b) with a light spot $H = D$ and according to equation (10) a signal value which is zero. Small deviations from this position ($\Delta Z \neq 0$) result in a light spot where the upper or lower half is screened and only the alternate half of the PSD is illuminated with $H = D/2$. The resulting sensor curve shows a discontinuity at this position.

In summary it can be said that the positioning of the beam spot and the PSD as introduced in 22a) allows the installation of a distance sensor with nearly linear characteristics, while the installation introduced with solution 22b) is, due to the jump in the curve characteristics, not practicable. However, this solution can be used for a very sensitive detection of a zero, or for recognising the direction of displacements.

6.4. Experimental determination of the measuring characteristics of the sensor

In order to establish the experimental determination of the measuring characteristics of the sensor, modules of the "Micro-Bench" type from Spindler & Hoyer corporation were used (Appendix J). This enables adjustment of all degrees of freedom of the sensor by changing components and flexible adjustment of their distance. Two different setups were examined in the following manner:

Setup I

Microscope objective (Spindler&Hoyer)	
Focal length f_1	2.93mm
Numerical aperture NA	0.85
Entrance aperture	5mm
Achromatically corrected	
Sensor lens (Spindler&Hoyer)	
Focal length f_2	20mm
Type	singlet
Setup geometry, distances	
Microscope objective to the Sensor lens l_1	70mm
Sensor lens to the knife edge	40mm
Knife edge to the PSD	25mm
Adjustment parameter	
Beam diameter is adjustable by a variable aperture	3mm, 4mm, 5mm, 6mm

Table 7: Characteristics of sensor setup I

Setup II

Microscope objective (Olympus)	
Type	DPlanApo100UV
Focal length f_1	1.69mm
Numerical aperture	0.75 to 1.3 adjustable
Entrance aperture	4.4mm
Achromatically corrected	
Sensor lens (Spindler&Hoyer)	
Focal length f_2	20mm
Type	singlet
Setup geometry, distances	
Beam waist w	1.5mm
Microscope objective to the sensor lens l_1	70mm
Sensor lens to the knife edge	40mm
Knife edge to the PSD	22mm
Adjustment parameter	
Numerical aperture of the microscope objective is used	minimum and maximum NA will be adjusted

Table 8: Characteristics of sensor setup II

The adjustment of the sensors was performed by placing a frosted plate into the detector plane at first and by displacing the component a measuring range of some micron was preadjusted. Secondly, the frosted plate was exchanged with the PSD and in using its fine adjustment device, the PSD and knife edge were positioned to reflect a nearly linear curve characteristic.

Four different surfaces with different characteristics were examined to determine the measuring characteristics:

Surface 1:	mirror (class 5)
Surface 2:	copper (class 4)
Surface 3:	white card board (class 2)
Surface 4:	resist coated glass (class ?)

Table 9: Surfaces used for sensor surveying

The active principle of autofocussing is based on the light reflected from the surface of the object. Scattered radiation caused by rough surfaces does affect the functioning of the sensor. Scattered radiation can only be useful when it is very much directed and contains no misinformation.

The characteristic curves for setup I shown in figure 26 have been determined by displacing the surface with a precisely adjustable linear axis (Appendix I).

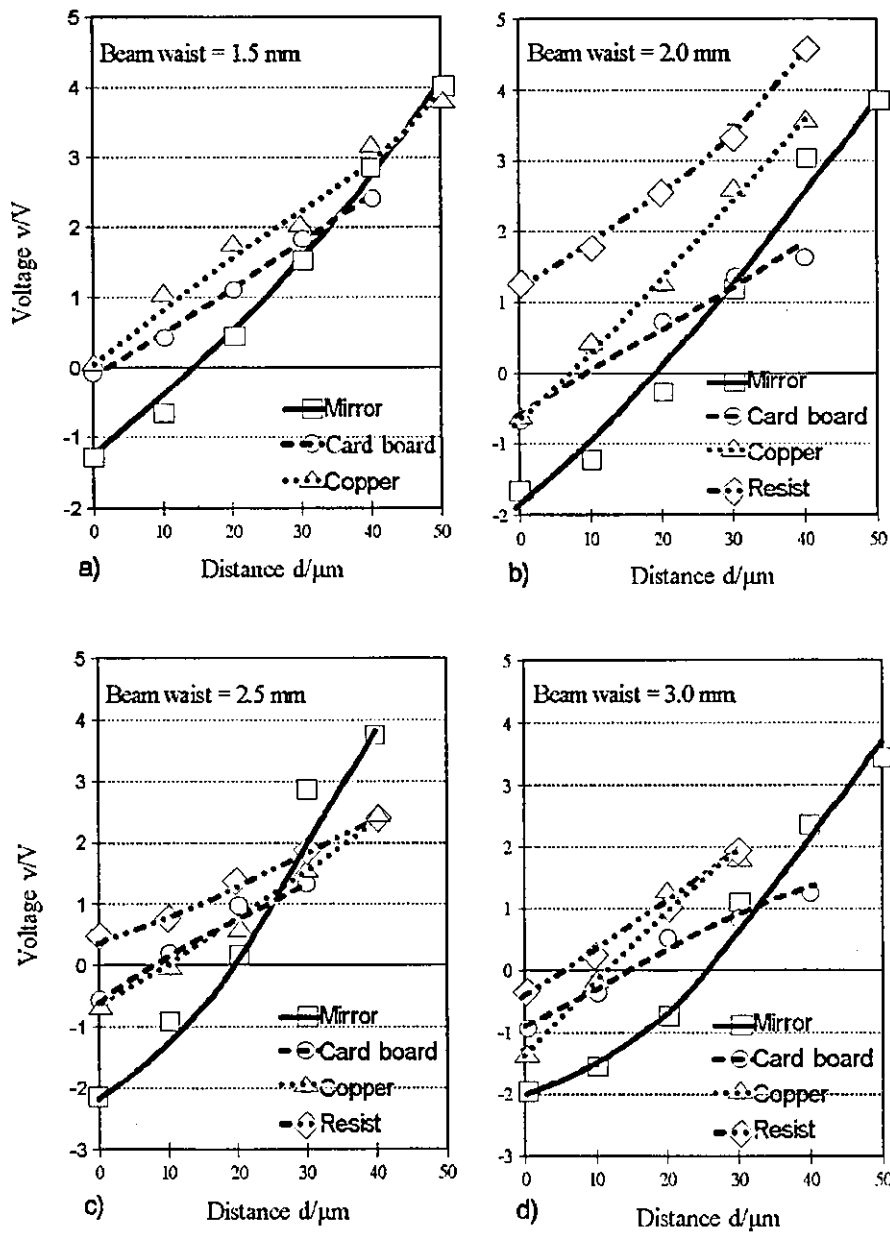


Fig: 26: Characteristic curves of the sensor based on setup I

The characteristic curves shown in figure 26a) to 26d) illustrate the displacement curves recorded from four different surfaces mentioned above and having used four different beam radii with the values $w = 1.5\text{mm}$, $w = 2\text{mm}$, $w = 2.5\text{mm}$ and $w = 3\text{mm}$. For this illustration, the beginning of the measuring range coincides with the origin of the coordinate system so the curve illustration is without reference.

Figures 26a) to 26d) illustrates that different surfaces will lead to characteristic curves of similar kind which have almost linear form over a measuring range of about $40\mu\text{m}$. However, their slope and, therefore, also their value range differs. Card board and resist substrate almost have a nearly identical slope while the slope of copper is steeper and finally the slope of the mirror is the steepest. In the beginning of the measuring range different surfaces lead to different starting voltages which are nearly identical considering card board and copper. The highest value was found for the resist substrate and the lowest for the mirror. It cannot be seen that the beam radius w significantly influences the measuring range and the slope of the characteristic curves, however the curves will be moved downwards when the beam radius w is increased. It must be noted that in case of the resist substrate, the beam with a radius of $w = 1.5\text{mm}$ will allow no measurement which is due to its poor reflection.

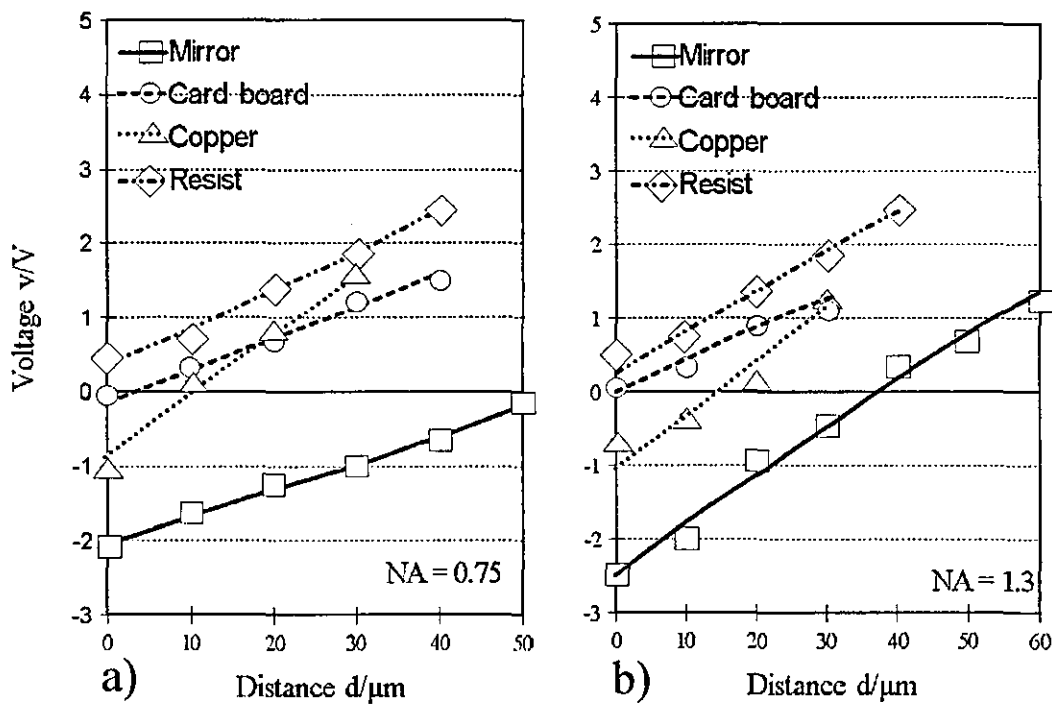


Fig. 27: Characteristic curves of the sensor based on setup II

Figure 27 illustrates the characteristic curves based on setup II. These curves were generated by varying the distance to the surface using the linear axis while the numerical aperture of the microscope lens was adjusted to the smallest and to the largest possible value.

Figures 27a) and 27b) illustrate that both numerical apertures result in an identical characteristic and almost linear form of the curves when using identical surfaces. The slope of the curve for card board and resist substrate show similar values, while the slope for the mirror is steeper and copper shows the steepest slope. All surfaces with both numerical apertures ($NA = 0.75$ and $NA = 1.3$) result in a measuring range of about $30\mu m$ and only the mirror leads to significantly larger values. Considering copper and the mirror the slope of the curves is increasing when the numerical aperture increases while it remains almost constant considering card board and the resist substrate.

Considering the examination of the curve dependence on orientation between the surface and the sensor axis it has to be noted that if a limiting angle between surface and sensor axis is exceeded insufficient light intensity will be coupled into the sensor. Scanning a surface of structured shape with this type of sensor this state can be reached easily, however the signal depends on the structure of the surface. To prove the functional dependence between measured result and orientation, the measured surface was tilted relative to the sensor axis by a defined angle (see Appendix L for setup). Setup I with a beam radius of $w = 1.5mm$ was used for this examination.

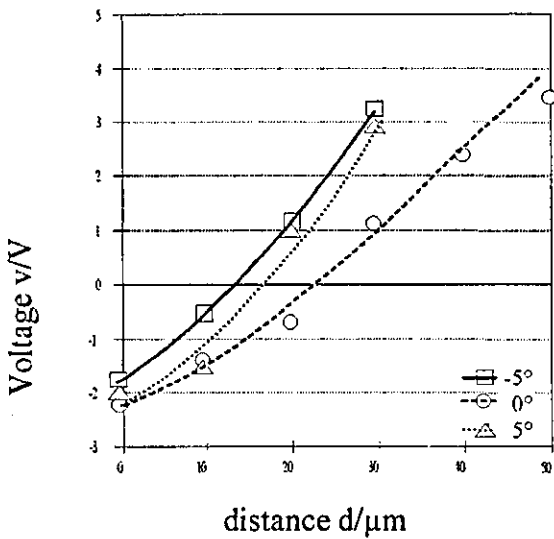


Fig. 28: Distance curve with different tilts of the measured surface

In tilting the surface more than 5 degrees, it was only possible to find a meaningful context between the distance to be measured and the sensor signal. From figure 28 it can be seen that for tilts of 5 degrees the measuring range will be upset in both directions while the measuring sensitivity increases.

To summarise for the experimental determination of the sensor characteristic, it can be stated that the sensor has nearly linear characteristic curves for surfaces of various kinds. This is also true for the surface of a mirror which is difficult to survey with other setups [Brei92], but leads to good and reproducible test results in this case. Surfaces of various kinds deliver a different measurement range, different origin of the measuring range, and a different sensitivity. In both sensor setups I and II, the measurement ranges are similar. The use of a microscope lens with very short focal distance increases the measurement sensitivity in setup II, however compared with setup I this was compensated by changing the setup geometry (reduction of l_2). In comparing the setups, it also can be seen that the highest measurement sensitivity of each setup is provided by a different surface, which was the mirror in setup I and copper in setup II. Increasing the tilt of the measured surface leads to mutilated test results or non functioning of the measuring principle and should be avoided. Finally, it can be stated that the sensor needs to be calibrated every time the measured surface is changed. An absolute measurement can only be done by using a reference point.

6.5. Dimensioning of an optimised processing head

In operating the autofocus sensor in the LPG, its processing head was optimised to be small and compact in its mechanical design and, however, to stay adjustable over a wide range (see Appendix M). Also, all optical components can easily be exchanged in order to match the processing head to be used in environments of various kinds. The laser will be coupled to this setup and provides simultaneous coupling of the measuring and processing laser. An optical filter separates the processing laser from the PSD analysing circuit. Using a conducting housing for the processing head provides its electrical shielding by connecting this housing to ground.

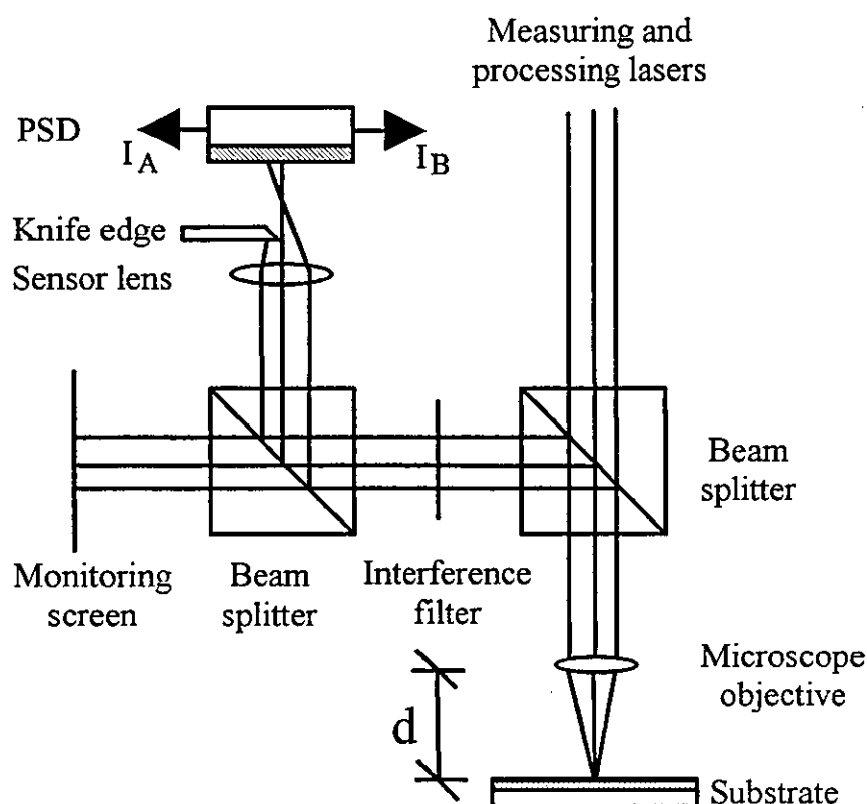


Fig. 29: Principle of the optimised processing head

Figure 29 illustrates the beam path of the sensor which is using a second beam splitter cube. The characteristic data of the optimised processing head are given in table 10.

Microscope objective (Newport) (compare chapter 3.3.)	
Focal length f_1	2.9mm
Numerical aperture NA	0.85
Entrance aperture	5mm
Achromatically corrected	
Sensor lens (Spindler&Hoyer)	
Focal length f_2	10mm
Type	singlet
Setup geometry, distances	
Microscope objective to the sensor lens	30mm
Sensor lens to the knife edge	5mm
Knife edge to the PSD	10mm

Table 10: Characteristics of the optimised processing head

The second beam splitter cube enables a manual preset of the processing head while monitoring a reflected portion of the measuring beam on a screen (frosted plate). Different

displacements between measured surface and processing head will result in light spots with different diameters to be monitored on the screen. One else can adjust an object placed on the positioning system by monitoring its image on the screen. The total electronic evaluation circuit was shielded by placing it into a conducting housing (Appendix N). All signal lines are shielded and kept as short as possible. In order to prevent the influence of the PSD signals via signal lines, the electronic evaluation circuit was placed as close as possible to the PSD. Matching of the signal level and reducing the noise influence will be provided by an amplifier (Appendix O) using an optional low pass filter. In determining the working characteristic, the characteristic curve shown in figure 30 was established by manually moving the sensor across a resist surface.

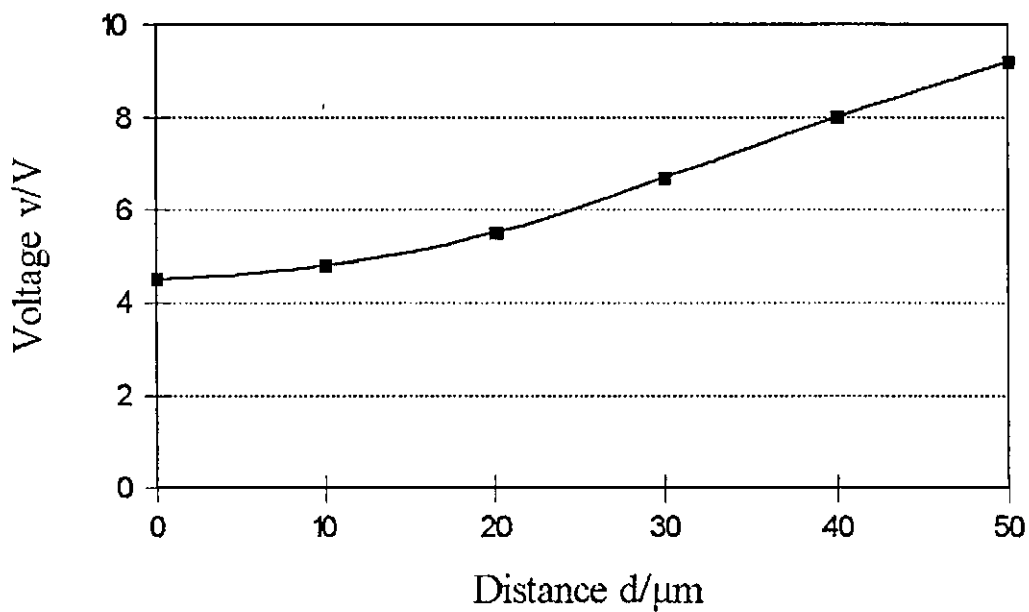


Fig. 30: Characteristic curve of the optimised processing head

Figure 30 illustrates a measuring range of the sensor adjusted to about $50\mu\text{m}$ which can be considered linear over a range of $30\mu\text{m}$. The related resulting signal level swing of 3.45V has superimposed a stochastic noise of $U_{pp}=50\text{mV}$. The resolution of the sensor is better than $0.5\mu\text{m}$ and was determined by moving the measuring head within the linear range using a piezo translator. Defined displacements of this size could be separately recorded using a digitised voltmeter.

7. SELECTION OF AN ACTUATOR

In developing a position controlled processing head for the LPG the associated actuator is, after the sensor, the second most important system component. The actuator is needed to position the processing head and its laser beam focus to the correct distance from the processing surface. On one hand, the actuator must be capable of positioning the focusing lens with a very high accuracy and, on the other it needs to have a high dynamic range. Besides those requirements, the actuators control range and vibrational insensitivity is important too. In order to establish a general view for the selection, different actuator systems will be compared. The selected piezo translator will be examined in depth with respect to its static and dynamic operation and after this, its specific characteristics for this purpose will be determined.

7.1. Comparing the actuators

7.1.1. Worm nut driven gearing

The positioning of the focal position and, therefore, the required movement of the whole sensor or the microscope lens can be done with a worm nut driven gearing.

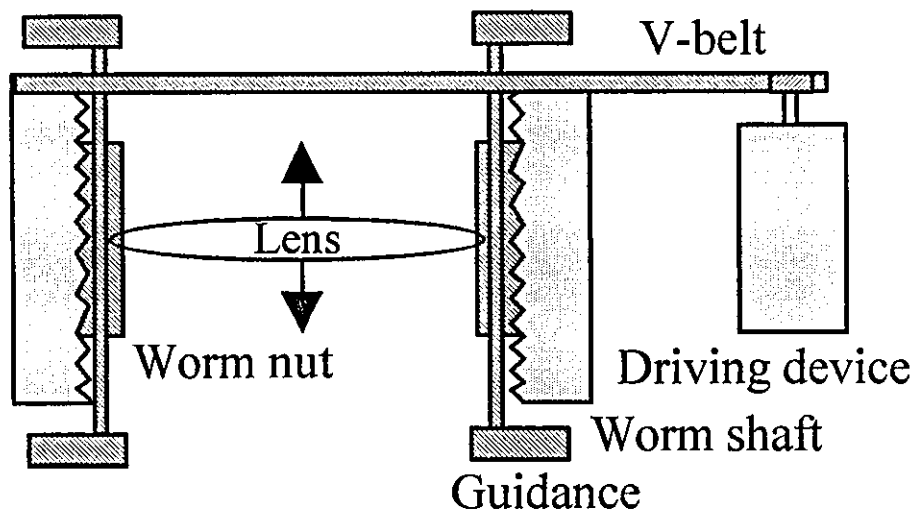


Fig. 31: Principle of focus adjustment using a worm nut driven gearing

A motor and a suitable drive drives the worm nut. A worm shaft is guided only in the vertical plane and converts the turning of the worm nut into a linear movement of the focusing lens.

Depending on the slope of the worm shaft, the positioning accuracy may be different. An advantage of this system is its large linear movement range. In order to prevent negative interference of oscillations, a very accurate guidance is needed.

7.1.2. Worm drive

Another possibility to move the focal position by using a worm drive is illustrated in figure 32.

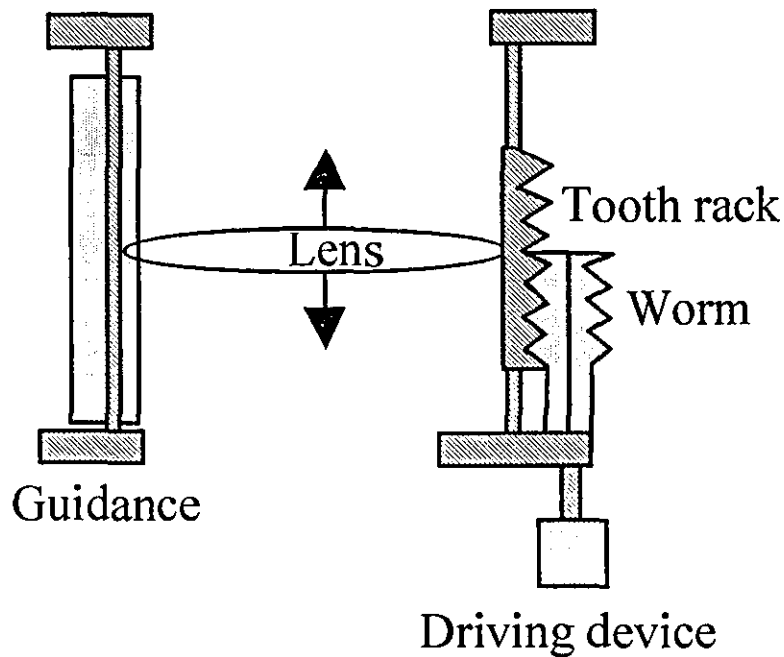


Fig. 32: Principle of focus adjustment using a worm drive

This is a purely mechanical drive. With very carefully dimensioned components, position accuracies within the micron range are possible. The drive can be done using step or servo motors. The movement of stepper motors results in discrete steps only. Servo motors do need a more complex closed-loop-system. The advantage of the system lies in its insensitivity to oscillations. Its disadvantage is its relatively long control time.

7.1.3. Plunger-coil motor

The principle of a plunger-coil is similar to the principle of a loud speaker (voice-coil).

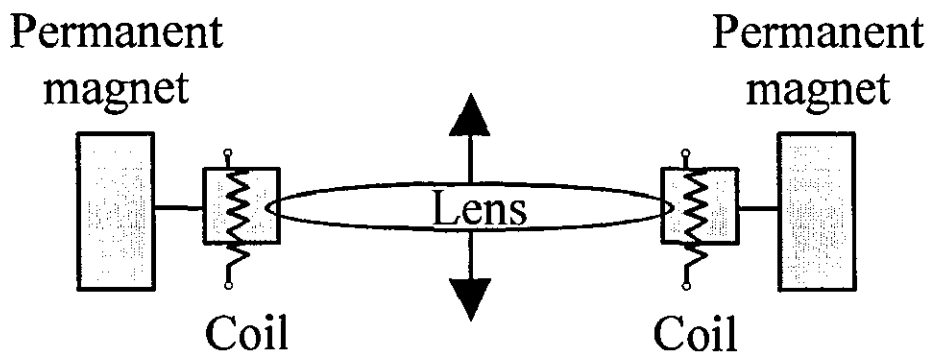


Fig. 33: Principle of focus adjustment using a plunger-coil motor

The sensor lens is fastened to a coil, which in turn, is mechanically connected to a permanent magnet via a ligament. As soon as direct current passes through the coil, it moves the lens up- or downwards depending upon the direction of the current. A positioning device of very high accuracy, the system precisely positions the lens. It has to be noted that this system is very sensitive to oscillation (low damping). A suitable attenuation against oscillation, perhaps an eddy-current brake, should be used.

7.1.4. Piezo translator

A piezo translator is suitable to adjust the sensor as well. The voltage proportional movement of a piezo translator permits very sensitive changes of the positioning in the (sub)micrometer range. The slightest change of the operating voltage will result in a smooth and almost linear motion. There are no threshold voltages which could affect the continuous motion. The piezo translator does not use a geared or rotating shaft. Its extension is purely based upon solid distortion and does not show ageing. Compared to other control elements, piezo translators are characterized by a very high controlling speed, whereas its controlling range is relatively small, i.e. in the area of some microns.

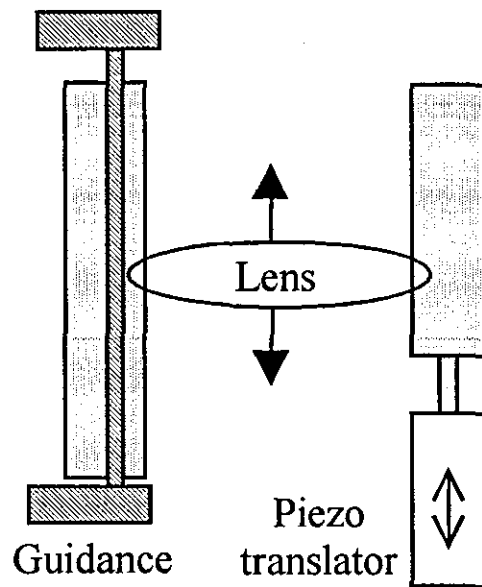


Fig. 34: Principle of focus adjustment using a piezo translator

Comparing all control elements, it needs to be noted that the piezo translator is, with respect to the dynamic range as well as its resolution, the best solution. However a simple drive necessarily needs a linear control characteristic which only can be realised approximately. The controlling range of only some microns is sufficient considering the adjustment of the Rayleigh length which also needs only some microns, in the course of which piezo translators can be assisted by a manual controlling element. Another advantage of piezo translators can be seen in their relatively simple drive control.

7.2. Static behaviour of piezo translators [Phys94]

A piezo electric device is an electrically controlled element which functions upon the piezoelectric effect. In piezoelectric translators, the inverse piezoelectric effect is used. The geometric distortion of the crystal is directly proportional to value and sign of an applied voltage. The small extension of the piezo element will be overcome by stacking several piezo elements and/or applying a lever mechanism to achieve larger controlling ranges.

The extension of the piezo translator is not exactly proportional to the applied electrical field strength. In a voltage/extension diagram (see figure 35) its nonlinear behaviour will be illustrated by a hysteresis loop. The extension range depends whether a lower or higher voltage had previously been applied. The maximum range of the hysteresis loop be up to 15% of the range passed.

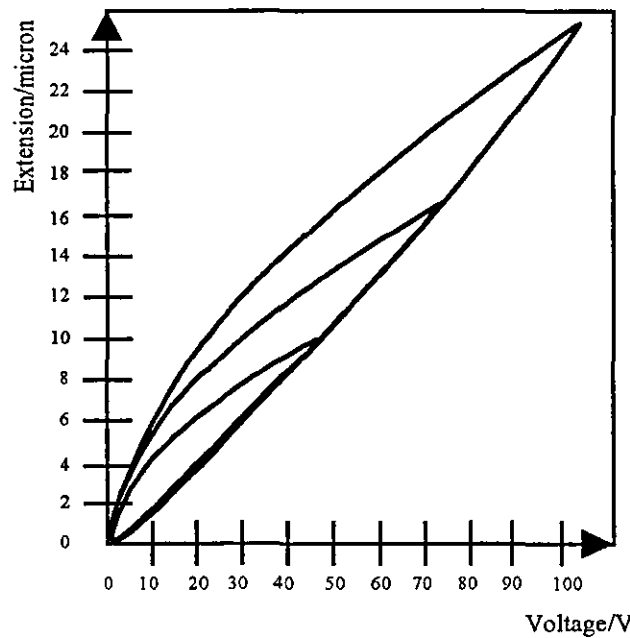


Fig. 35: Extension characteristic of a piezo translator

7.3. Dynamic behaviour of piezo translators [Phys94]

The closed-loop-process and its control element must position the processing head precisely and quickly and sets particular requirements on the piezo translator. The piezo translator must be able to follow fast changing control signals virtually instantaneously. In course of this the amplitude form of the extension must be coincident with the input signal to the extension possible. The transient response can not be guaranteed up to high frequencies, however it will be determined by the resonant frequency f_0 of the translator and the output power P of the amplifier. From there, the mechanical characteristics of the moving part and electrical characteristic of the control device shall be examined.

7.3.1. Mechanical system

The mechanical response of the clamped and unloaded piezo translator, which is the oscillation response will be described by its elastic characteristic called rigidity C_T and its effective mass m_{eff} which is half of the mass m of the piezo translator. In this case the resonant frequency will amount to:

$$f_0 = \frac{1}{2\pi} \sqrt{\frac{C_T}{m_{eff}}} \quad (20)$$

Clamping an external mass M , compared with the resonant frequency f_0 of equation (20) a reduced resonant frequency f_0' :

$$f_0' = f_0 \sqrt{\frac{m}{m + 2M}} \quad (21)$$

As a first estimate, one can state that a usable dynamic control will be established up to a frequency f_g which is about 60..70% of the resonant frequency f_0' of the total system described in equation (21). This statement aims at the resonant frequency of a free piezo translator with external additional mass.

$$f_g \approx 0.6..0.7 f_0' \quad (22)$$

7.3.2. Electrical system

The controlling electronic circuit and its possible maximum cut-off frequency f_g for a sine wave operation of the piezo translator depends on the available maximum output power of the amplifier. This cut-off frequency f_g can be determined using equation (23):

$$f_g = \frac{P}{U_0^2 C} \quad (23)$$

In this equation U_0 is the nominal voltage and C is the capacitance of the piezo translator.

In an operational environment with two switched positions the piezo translator responds analogously to a capacitor. The applied voltage follows equation (24).

$$U_C(t) = U_0 \left(1 - e^{-\frac{t}{RC}} \right) \quad (24)$$

The voltage raises and lowers in an exponential manner determined by the time constant RC . Static conditions will lead to an expansion proportional to the Voltage $U_C(t)$, however in a dynamic environment, the actual mechanical characteristics needs to be considered. The mass of the piezo translator and its elastic characteristics determine its capability to oscillate. The switching process generates resonant oscillation which superimposes the voltage form in time and leads to transients. In a sense, the piezo translator can be considered as a spring-mass system.

7.4. Examination of the selected piezo translator

The piezo translator Piezomike P-854-00 (low voltage PZT), based on Lead-Zirconate-Titanate (PZT) from Physik Instrumente (PI) and a single channel low voltage amplifier P-860-00, which drives the linear positioner M-105.00 were selected. The piezo translator allows a cross movement of $30\mu\text{m}$. From where the controlling range of $30\mu\text{m}$ allows a maximum extension of the hysteresis loop using the clamped Piezomike of about $4.5\mu\text{m}$ maximum. To examine the hysteresis response and, in the course of this, the resulting piezo positioning of the sensor the piezo translator was controlled by a triangular signal of low frequency in a linear range of its characteristic curve.

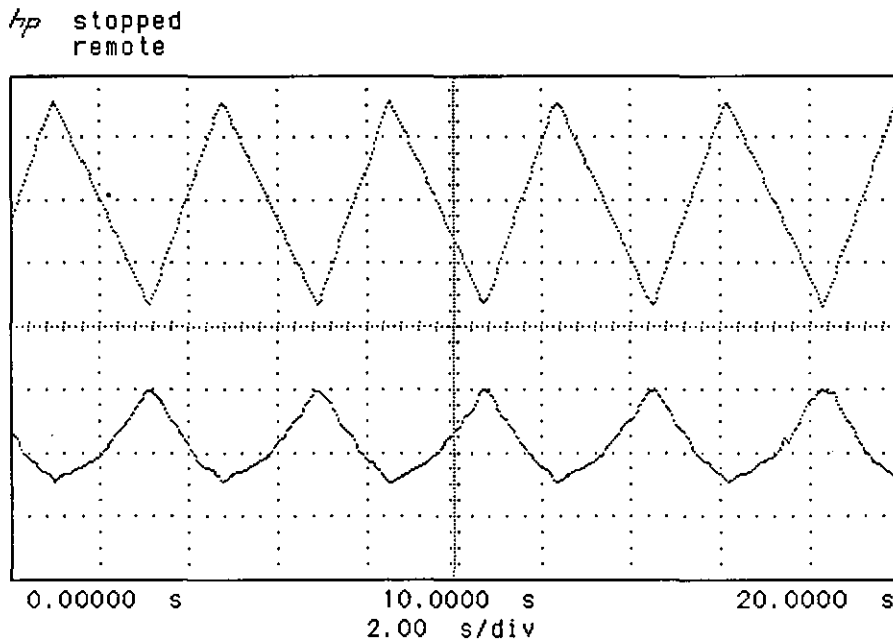


Fig. 36: Extension of the piezo translator

In the upper part of figure 36, the control voltage for the piezo translator is illustrated. For a period length of only 4 seconds the quasi static response, which is the almost undelayed response of the translator to the applied electrical signal is examined. The distorted triangular signal generated by the sensor reflects the hysteresis characteristic of the piezo translator.

The analytical examination of the dynamic characteristics of the translator starts with the calculation of the resonant frequency f_0 of the unloaded translator. This will be done by introducing an effective mass of the piezo translator of $m_{\text{eff}} = 1.8\text{g}$ and a rigidity $C_T = 1.5\text{N}/\mu\text{m}$ into equation (20).

$$f_0 = 4.6\text{kHz} \quad (25)$$

For motion of the processing head of about $M = 1\text{kg}$, equation (21) provides the reduced resonant frequency f_0' ,

$$f_0' = 195\text{Hz} \quad (26)$$

which permits a sinusoidal motion of the complete processing head with a cut-off frequency f_g of

$$f_g \approx 0.6 \cdot 0.7 \cdot 195\text{Hz} \approx 110\text{Hz} \quad (27)$$

The cut-off frequency f_g for the electric control will be calculated using equation (23) and in introducing a voltage $U_0 = 100\text{V}$, power $P = 1\text{W}$, and a capacitance $C = 2\mu\text{F}$.

$$f_g = \frac{1W}{10^4 V^2 2 \cdot 10^{-6} F} = 50\text{Hz} \quad (28)$$

This frequency lies very much below the cut-off frequency determined by the mechanical characteristics. From there, the control electronics represent the limiting element for the dynamic positioning. A control with a higher speed leads to an amplifier with increased output power, however critical frequencies from up to 50Hz used in the LPG should be considered to be the upper limits of the requirements. Controlling of the piezo translator will be done via a control circuit (Appendix P) which is connected to the host computer of the LPG.

8. DEVELOPMENT OF THE CONTROL SYSTEM

For automated adjustment of the focal position to a predefined value in LPG applications a closed loop system is required which uses the optical displacement sensor for displacement determination of the processing head relative to the processing surface and the piezo translator to adjust the processing head as required. For this reason, the displacement sensor is mounted on the piezo translator in order to obtain the focal position adjustment system relative to the processing surface.

For the closed loop system design, the characteristic of the control system (processing head) will be determined in this chapter in order to optimise the closed loop system for demands in the LPG application.

8.1. Principle of the closed loop system

In a closed loop system, a predefined value of a physical parameter will be achieved as a result of the continuous measurement and control of this parameter.

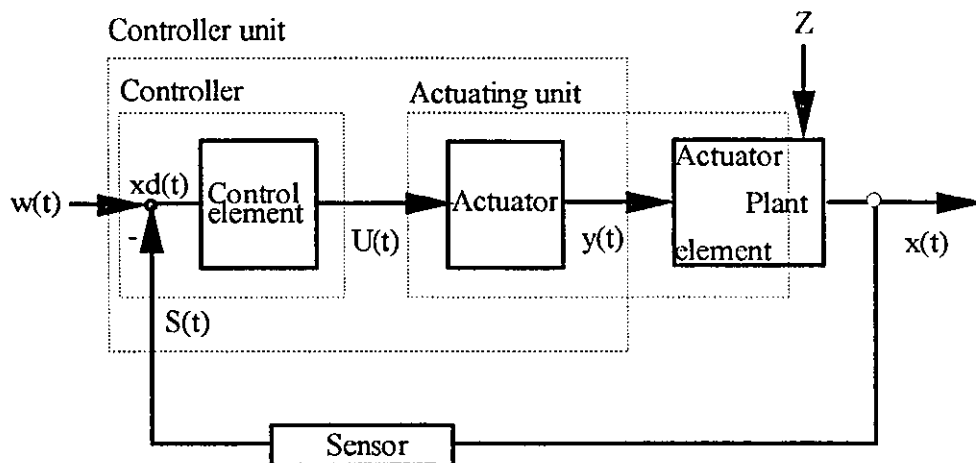


Fig. 37: Block diagram of a closed loop system [Leon70]

The principle of a closed loop system will be explained by use of the block diagram sketched in figure 37. The comparator in the controller compares the set point $w(t)$ with the sensor signal $S(t)$ obtained by the measurement of the control parameter $x(t)$. A determined negative deviation $xd(t)$ will be transferred to the control element. The controller output value $U(t)$ is linked to the actuator in the actuating unit that delivers the actuator output value $y(t)$ to the

actuating element that affected the control parameter $x(t)$. The changes of $x(t)$ as a result of $y(t)$ are registered by the sensor and transferred to the comparator in order to obtain a closed loop system. Disturbances Z influence the closed loop system at every point mentioned above and are in most cases observed at the system to be controlled (plant).

For the assessment of the designed closed loop system, in general the following characteristics are of interest:

- The dynamic behaviour of the controlled parameter $x(t)$ for changes of the set point. This is called the follow-up characteristic.
- The dynamic reaction of the controlled parameter to disturbances. This is called the disturbance characteristic.

In the ideal case the parameter $x(t)$ to be controlled should be equal to the set point $w(t)$ and every disturbance z should be compensated immediately so that there is no influence to the controlled parameter $x(t)$.

Both demands can not be realised. In order to achieve the best disturbance and follow-up characteristics possible, the controller has to deliver an optimised output value $U(t)$ for negative deviation $x_d(t)$. For this reason there are high accuracy demands on the controller unit. The actuator output value $y(t)$ of the controller unit can be adjusted by the following parameters:

- K_P :Factor for the term proportional to the negative deviation $x_d(t)$.
- K_I :Factor for the integration term of negative deviation $x_d(t)$.
- K_D :Factor for the derivative term of the negative deviation $x_d(t)$.

For optimising a closed loop control system for the demands in different applications, different weighted combinations of the factors K_P , K_I , and K_D can be combined. The actuator output value $y(t)$ of the so called PID-characteristic for the elimination of a negative deviation $x_d(t)$ can be calculated using equation (29) [Reut90]:

$$y(t) = K_P x_d(t) + K_I \int x_d(t) dt + K_D \frac{dx_d(t)}{dt} \quad (29)$$

or in conjunction with the parameter for the reset time $T_N = K_P/K_I$ and the derivative time $T_V = K_D/K_P$

$$y(t) = K_P \left[xd(t) + \frac{1}{T_N} \int xd(t) dt + T_V \frac{dxd(t)}{dt} \right] \quad (30)$$

In controller applications, the K_P parameter determines the speed of control following a step response proportionally to the negative deviation $xd(t)$, while the K_I -parameter cares for the elimination of the typically permanent existing negative deviation of the P-characteristics. A D-controller does not exist, but the D-characteristic in combination of the other parameters cares for an additional acceleration of the closed loop system. The price for increased controlling speed is a perhaps more oscillatory behaviour of the closed loop system caused by the derivative of negative deviations [Reut90].

Today, the controller is seldom realised as an analogue electronic system and, in most cases is implemented as a sampling (digital) controller. Figure 38 shows the signal flow diagram of such a single value controller.

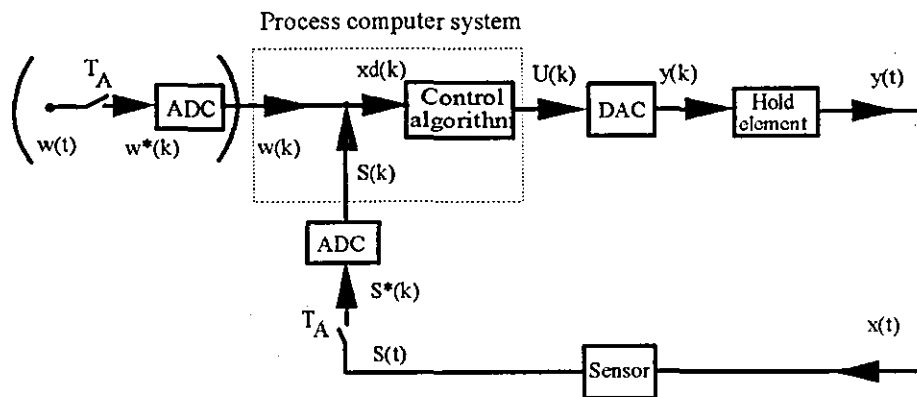


Fig. 38: Signal flow diagram of a digital closed loop system

The controlled parameter $x(t)$ is measured by the sensor that delivers the signal $S(t)$. This signal $S(t)$ as well as the current set point $w(t)$ are sampled synchronously with the sampling time T_A and are then converted into the numerical values $S(k)$ and $w(k)$. In a different variation, the set point $w(t)$ can be delivered by the programme of the processing computer system. After the processing computer has determined the negative deviation $xd(k)$ the controller algorithm calculates the sequence of the the controller output voltages $U(k)$ which are D/A converted and fixed by a hold element representing the actuator output $y(k)$. The controller algorithm is based on a time discrete description of the continuous behaviour of equation (29).

For the desired transfer characteristic of an analogue controller, an operational amplifier is connected to an input and feedback network. These networks are based on simple RC-elements which influence the characteristic of the controller.

8.2. Description of the control task

For the design of the focal position control system, the demands on the accuracy and speed of the controller have to be investigated and determined.

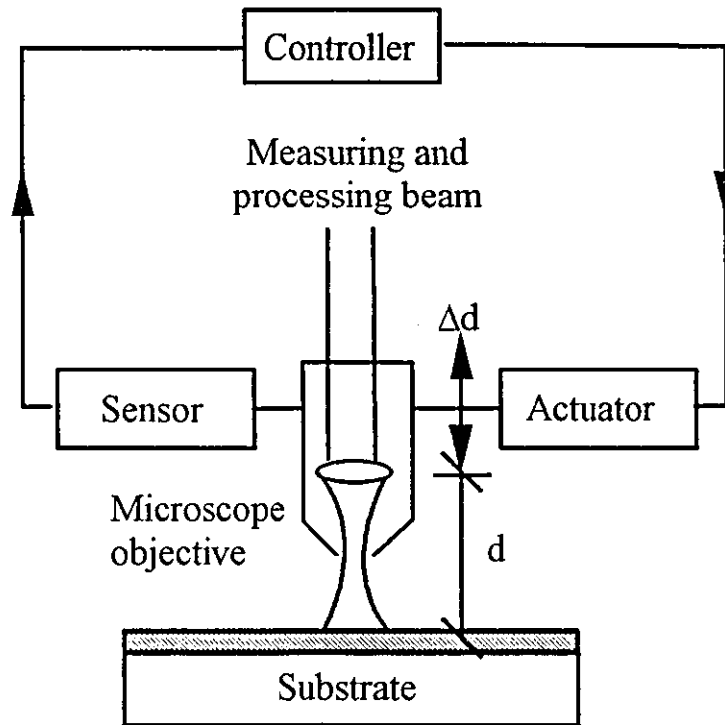


Fig. 39: Principle setup of the focal position control system

The technical arrangement of the system to be controlled is based on the sensor (chapter 5) and the actuator (chapter 7) which for data exchange are linked to the controller as sketched in figure 39. The distance d between the processing surface and the processing head is the parameter to be controlled and measured by the sensor. The sensor signal S is transferred to the controller in order to determine the appropriate actuator output value $y(t)$ for any possible negative deviation in order to influence the distance d between the processing head and the processing surface.

For a reproduceable processing result, an accuracy criterium of half the Rayleigh length of the processing focal position has been presented in chapter 2. As a result of the Rayleigh length of $3\mu\text{m}$ of the LPG processing beam (compare chapter 3.5.) the focal position has to have an accuracy of $\pm 1.5\mu\text{m}$ and, therefore, the sensor signal according to the linear portion of the characteristic curve shown in figure 29 an accuracy of $\pm 0.17\text{V}$. This means that the control system has to ensure that the sensor signal does not deviate from the set point by more than 0.17V . The accuracy of the signal generation has, therefore, a major influence on the accuracy of the complete system. For this reason the signal noise was reduced to a peak to peak value of $U_{pp} = 50\text{mV}$ (with stochastic characteristics) by using a low-pass filter and sensor shielding. As a result of the good signal to noise ratio (SNR) the sensor meets the requirements as one part of the development. In controller design, as the second part of the closed loop system design, special attention must be paid to the SNR as well in order to eliminate any negative influence due to large noise levels of the component.

In dynamic behaviour of the closed loop system two different demands have to be considered:

- the follow-up characteristic of the system: the distance between the processing head and the processing surface has to be adjustable in order to have additional freedom for more flexible processing.
- disturbance characteristics of the system: changes of the controlled parameter as a result of substrate defects, bend and/or tilt of surfaces. These different surface profiles should not have any influence on the processing result.

In most of the processing tasks in micro manufacturing there is only a slow controlling speed required because the quality of the substrate surfaces is very good. Furthermore the writing process is only performed in a small area on the substrate surface so that distance changes between the processing head and the substrate due to bent or tilted surfaces have normally no influence. Therefore, in the closed loop design a compromise between a good follow characteristic and a good disturbance characteristic has to be considered.

8.3. Determination of the plant characteristics

In this chapter the dynamic properties of the system based on the sensor and the actuator will be investigated and determined because they are required for the selection of the correct type of controller and the optimum controller parameters. Therefore, the sensor is mounted on the piezo translator and set perpendicular to a resist coated glass substrate in the vertical position as sketched in figure 39. While the piezo translator is driven by two special signal types, the

sensor signal is observed. For these experiments, the linear portion of the sensor characteristic in figure 30 is used.

8.3.1. Step response

First of all, the sensor output signal for a piezo input signal $x_e(t)$ that changes the level in theoretically infinitely short time will be registered. Mathematically, this ideal input signal is described by the following equations:

$$x_{e(t)} = 0 \quad \text{for } t < 0 \quad (31)$$

$$x_{e(t)} = \hat{x}_e \quad \text{for } t > 0 \quad (32)$$

where \hat{x}_e is the level of the input signal.

Figure 40 shows in the upper part the positive input step of 3.5V and, in the lower part, the resulting output signal. Figure 41 shows the same behaviour for a negative input step of -3.5V.

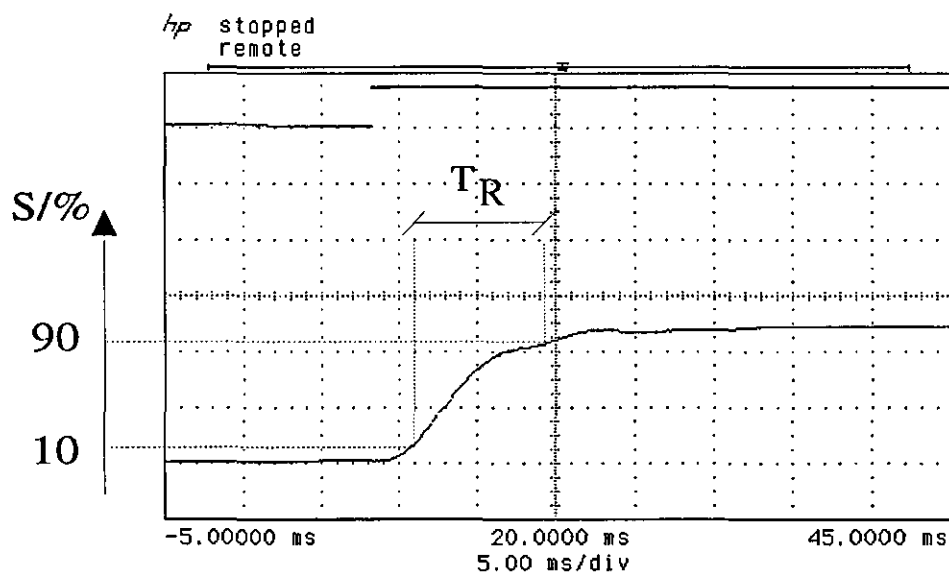


Fig. 40: Positive step response of the system to be controlled

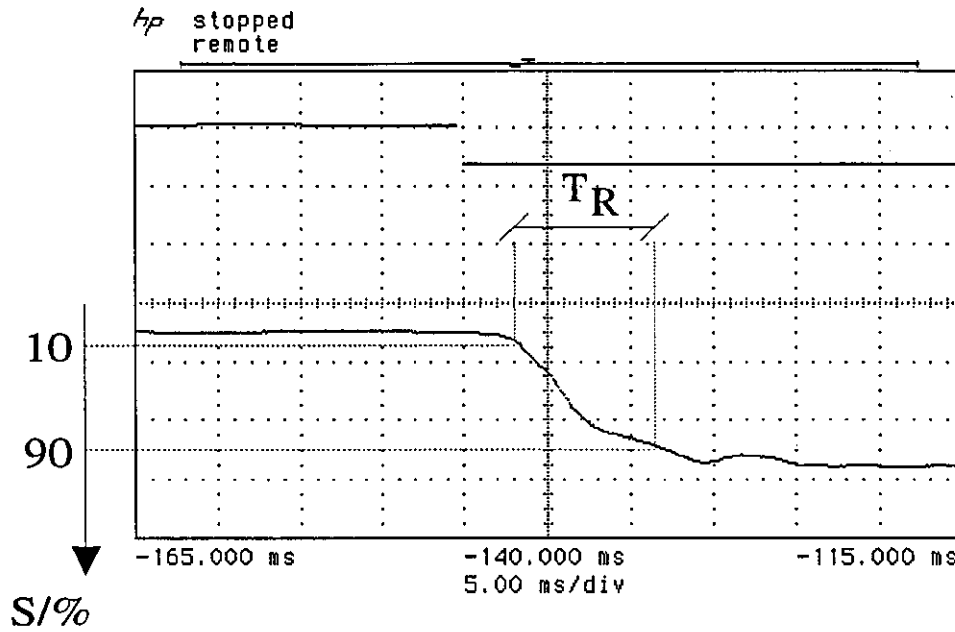


Fig. 41: Negative step response of the system to be controlled

For both step responses to steps of the same level but opposite sign, the same s-profile characteristic of the response is observed where both responses have the same signal levels and nearly the same time dependence. This s-profile characteristic indicates a delayed system of higher order.

The cut-off frequency of the system can be approximately determined by the following known relation [Bühl95]

$$B_w T_R \approx 0.35 \quad (33)$$

where B_w is the bandwidth and T_R the rise time of the signal, that is, the time required to rise from 10% to 90% of the maximum value. In figure 40 and figure 41, the rise time can be determined to $T_R \approx 8\text{ms}$ so the cut-off frequency which is equal to the bandwidth of the system can be nearly determined according to equation (33) with $f_g \approx 43\text{Hz}$ (see equation 28).

8.3.2. Frequency domain transfer function

In addition to the investigation of the step response of the closed loop system elements, the investigation of the response to a sine wave input signals plays a major role. The input signal $x_e(t)$ has the following time dependent characteristic

$$xe(t) = \hat{x}e \sin(\omega t) \quad (34)$$

Where $\hat{x}e$ is the input amplitude and $\omega = 2\pi f$ the angular frequency and f the frequency.

For a linear transfer function of an element, the output signal will be a sine wave signal as well. As a function of the frequency f , the amplitude x_a and the phase difference $\Delta\phi = \phi_e - \phi_a$ between the input signal and the output signal have different values. This behaviour can be described by the frequency transfer function. This can be expressed in a complex form [Reut90]:

$$F(j\omega) = \frac{x_a(j\omega)}{x_e(j\omega)} \quad (35)$$

where j indicates the complex behaviour.

As an example figure 42 shows in the upper part the input sine wave signal with a frequency $f = 100\text{Hz}$ and in the lower part the output signal of the sensor with the same frequency. Also the amplitudes and the phase difference of both signals are indicated. By measurement of this characteristic at different frequencies the frequency transfer function was determined.

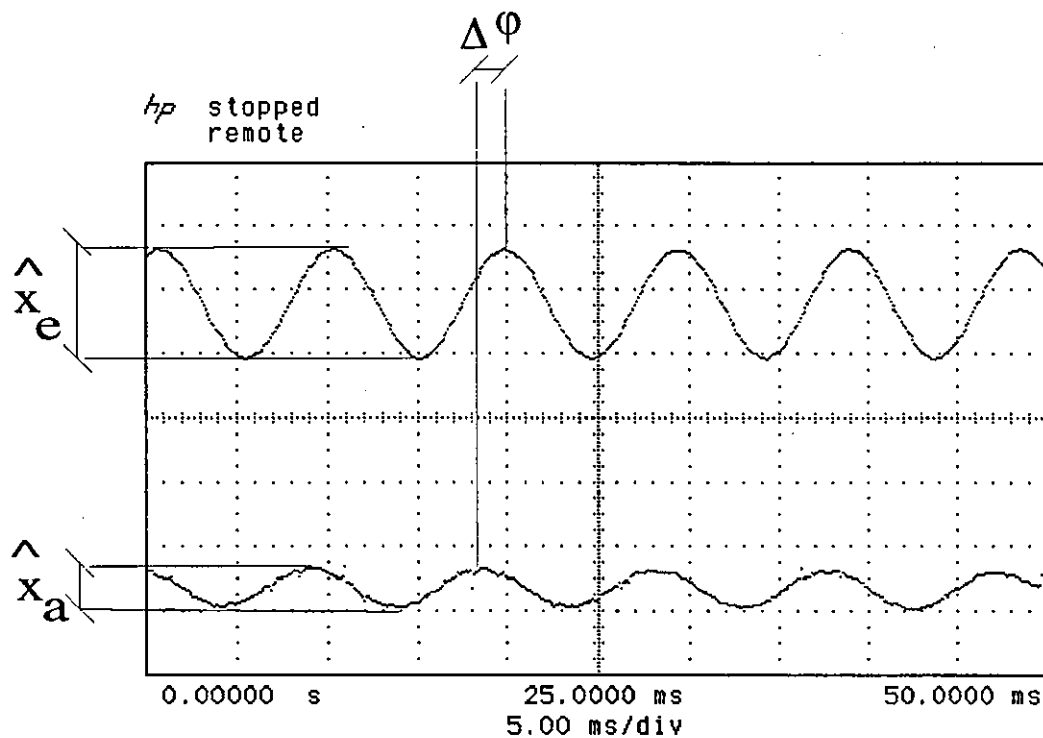


Fig. 42: Transformation of a sine wave signal by the system to be controlled

The amplitude of the frequency transfer function $|F(j\omega)|$ is defined as the output signal amplitude \hat{x}_a divided by the input signal amplitude \hat{x}_e , whereby the phase difference $\Delta\phi$ can be determined by the delay of the output signal compared to the input signal. Figure 43 shows the frequency transfer function of the system to be controlled as a Bode-diagram. For the determination of the cut-off frequency, the point where the amplitude is decreased by 3dB has to be found. In this system the angular frequency at this point has a value of $\omega_g = 240/s$ where the amplitude value drops from 1.6dB to -1.4dB and therefore the cut-off frequency is determined by $f_g = 38\text{Hz}$ (compare equation (28)).

8.4. Closed loop design

After the description of the closed loop system demands and the determination of the characteristics of the system to be controlled in this chapter, the correct controller type will be selected and the optimum controller parameters will be determined. The first assumption for the closed loop system design is that the controller has no characteristic delay time that has to be taken into account. Therefore, the complete system delays are only a result of the system to be controlled. The selection of the controller type is not critical in comparison to the selection of the controller parameter. In closed loop system applications with controlled systems having a dead time or transfer lag, the controller parameters have to be adjusted correctly because they influence the stability of the system enormously. In the LPG, a quiescent positioning control of the processing head is desired so that a controller without a D-characteristic will be designed.

8.4.1. Inflectional tangent method [Chie55]

Out of the s-profile step response characteristic for systems of higher order with transfer lag, the parameters

- T_U : Transfer lag
- T_g : Settling time
- K_S : Transfer factor

can be determined graphically.

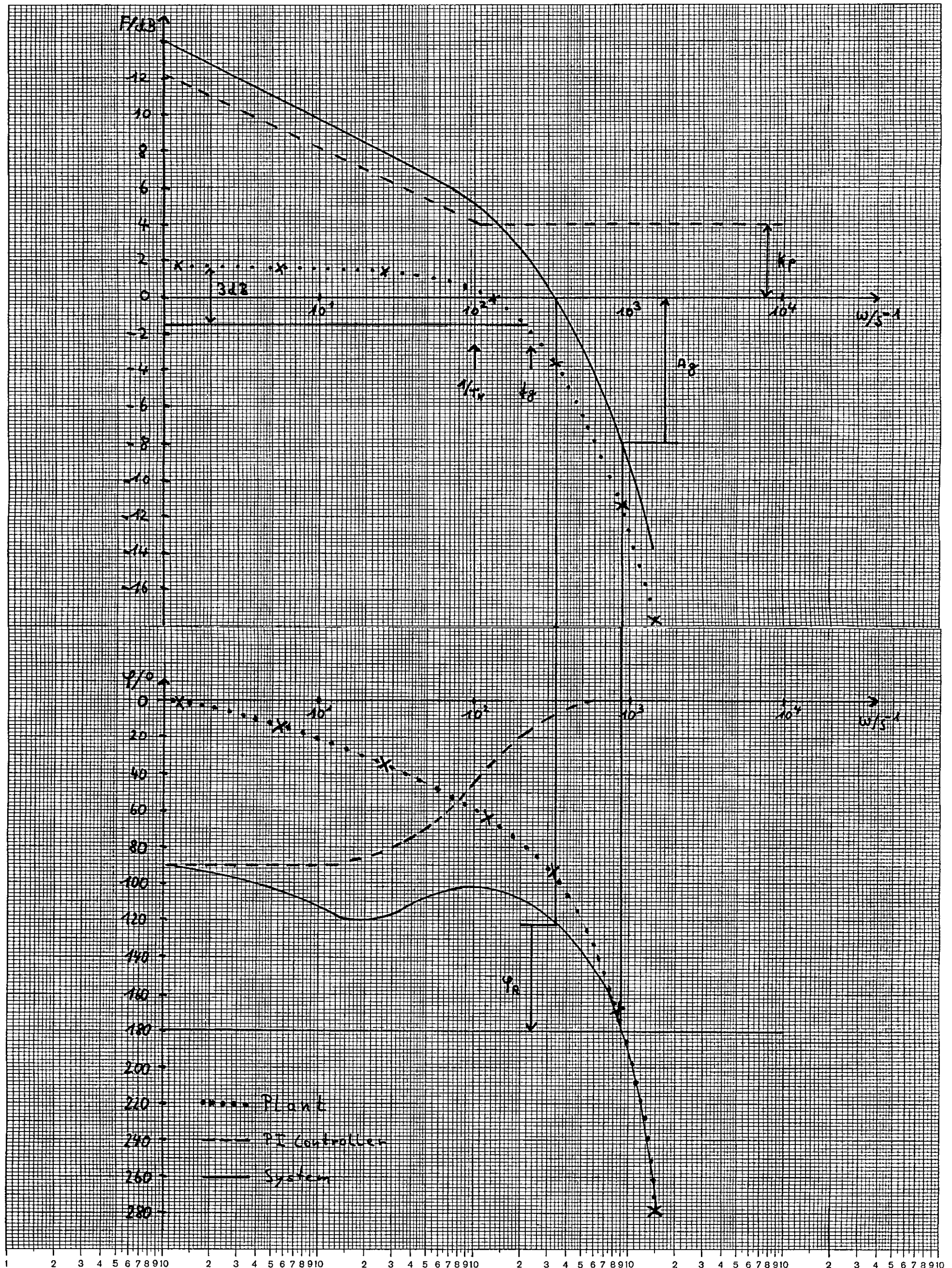


Fig. 43: Bode-Diagram

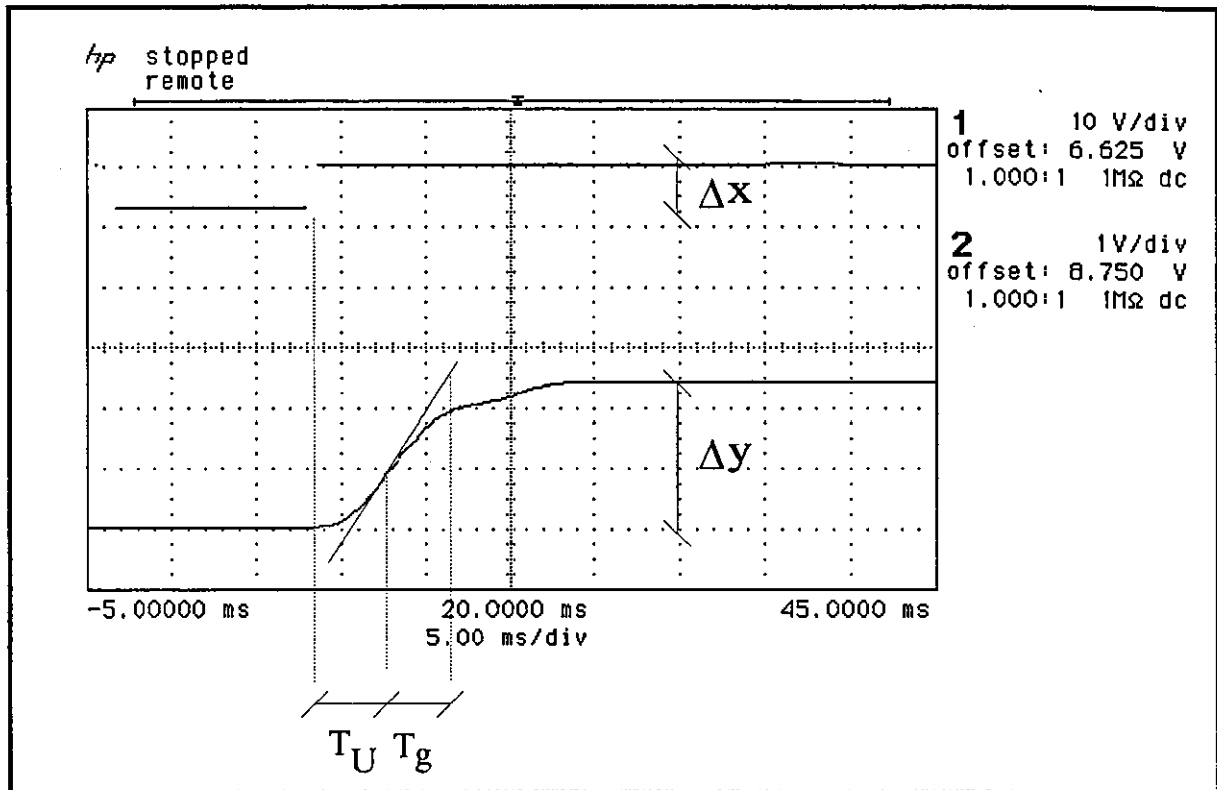


Fig. 44: Step response for the determination of the system parameter

Figure 44 shows the positive step response of the system to be controlled with the sketched inflectional tangent which can be used to determine the time parameters T_U and T_g of the system. The transfer factor K_S is defined as the output signal change Δy divided by the input signal change Δx . The following parameters can be determined from the step response:

- $T_U = 4\text{ms}$
- $T_g = 4\text{ms}$
- $K_S = 0.345$

For the determination of the controller parameters using the rule from Chien, Hrones and Reswick an auxiliary parameter may be calculated:

$$\tilde{k} = \frac{T_g}{T_U K_S} = 2,9 \quad (36)$$

Using this parameter and the table from Chien, Hrones and Reswick (see Appendix Q), the parameters of the selected controller with the desired characteristic can be read. For the PI-controller with a compromise between a good disturbance characteristic and a good follow-up characteristic, the following parameters can be determined:

$$K_P = 0.34\tilde{k}..0.6\tilde{k} = 1.1.7 \approx 1.4 \quad (37)$$

$$T_N = 1.2T_g..4T_U = 6ms..16ms \approx 10ms \quad (38)$$

8.4.2. Frequency characteristic procedure

For the interconnection of the system and controller, a resulting frequency transfer response will be achieved. For the determination of the resulting frequency transfer response of the open system, the Bode-diagram can be used. The resulting Bode-diagram of the open system can be achieved by superpositioning of the amplitude and phase transfer function of the characteristic curves for the system and the controller. The stability of the closed loop system can be determined reading the gain margin A_R in the amplitude transfer function and the phase margin φ_R in the phase transfer function. The gain margin is defined as the distance of the amplitude value to the 0dB line in the amplitude transfer function at the angular frequency where the phase transfer function contacts the 180° line while the phase margin is defined as the distance of the phase value to the 180° line in the phase transfer function at the angular frequency where the amplitude transfer function contacts the 0dB line (see figure 43). This is a modified expression of the Nyquist criterion [Bühl95].

This relationship can not only be used for closed loop analysis, but also for the synthesis of a closed loop system. For different values of the amplitude and the phase margin different characteristics of the closed loop system can be achieved. For a good follow-up characteristic the gain margin has to be in the range

$$12 \text{ dB} < A_R < 20 \text{ dB}$$

while the phase margin has to be in the range

$$50^\circ < \varphi_R < 80^\circ$$

and for a good disturbance characteristic

$$4 \text{ dB} < A_R < 12 \text{ dB}$$

$$20^\circ < \varphi_R < 60^\circ$$

For the desired compromise between a good follow-up and disturbance characteristic, a gain margin in the range of 12dB and a phase margin of 55° must be tuned.

Use of this behaviour for the closed loop design is performed in the Bode diagramme (see figure 43) where the amplitude transfer function and the phase transfer function of both the system and the controller are overlaid. The parameters used for the PI-controller are the parameters determined by the inflectional tangent method having the values $K_p = 1.4$ and $T_N = 10\text{ms}$. It can be read from the Bode-diagram that a phase margin of $\varphi_R = 55^\circ$ and a gain margin of $A_R = 8\text{dB}$ will be achieved that leads, in accordance with the above explained criteria, to an appropriate compromise between a good follow-up and disturbance characteristic.

8.5. Realisation of a digital controller device

Because of the possibility of most flexible operation, a digital controller will be implemented in the host computer of the LPG (see chapter 3.4.). A 12 bit A/D and D/A converter is the controller interface. This device can read analogue data with a clock rate up to 100kHz (given by the manufacturer). A computer programme (see Appendix R and S) using a PID-software algorithm performed the reading of the sensor signal, the comparison of the controlled parameter with the set point, determination of the controller output value, and output of the analogue signal to the piezo translator. The controller programme has been implemented for the possibility of flexible controller strategies. To this end, the controller can be activated and interrupted dependent upon defined conditions. The control programme is called by the control part of the main programme of the LPG.

To explain the functioning of a digital controller, the digital PID algorithm will be presented which is a time discrete model of the ideal transfer function of the PID-controller [Sont91] (compare equation (29)).

$$y(t) = K_p \left[x_d(t) + \frac{1}{T_N} \int x_d(t) dt + T_v \frac{dx_d(t)}{dt} \right] \quad (39)$$

In equation (39) the integral of $x_d(t)$ as well as the derivative from $x_d(t)$ have to be approximated.

$$\int_0^t xd(t)dt \Rightarrow \sum_{i=0}^{k-1} xd(i)T_A \quad (40)$$

$$\frac{dxd(t)}{dt} \Rightarrow \frac{xd(k) - xd(k-1)}{T_A} \quad (41)$$

where T_A is the sampling time and k the number of samples of the digital controller (compare chapter 8.1.). This relation can be used to determine the controller output voltage as:

$$U_{(k)} = K_P \left[xd(k) + \frac{T_A}{T_N} \sum_{i=0}^{k-1} xd(i) + \frac{T_V}{T_A} \{xd(k) - xd(k-1)\} \right] \quad (42)$$

For the computer modelling of the controller characteristic this equation will be written again for the point of time $(k-1)$.

$$U_{(k-1)} = K_P \left[xd(k-1) + \frac{T_A}{T_N} \sum_{i=0}^{k-2} xd(i) + \frac{T_V}{T_A} \{xd(k-1) - xd(k-2)\} \right] \quad (43)$$

The difference of equation (43) and (42) leads to the so called PID- positioning algorithm.

$$U_{(k)} = U_{(k-1)} + J_0 xd(k) + J_1 xd(k-1) + J_2 xd(k-2) \quad (44)$$

with the following parameters:

$$J_0 = K_P \left[1 + \frac{T_V}{T_A} \right] \quad (45)$$

$$J_1 = K_P \left[-1 + \frac{T_A}{T_N} - \frac{2T_V}{T_A} \right] \quad (46)$$

$$J_2 = K_P \frac{T_V}{T_A} \quad (47)$$

If there is an integrating element (e.g. a stepper motor) connected to the digital controller element that performed the task of the holding element, the definition

$$\Delta U_{(k)} = U_{(k)} - U_{(k-1)} \quad (48)$$

can be used to define the so called PID speed algorithm as given by equation (49)

$$\Delta U_{(k)} = J_0 x d_{(k)} + J_1 x d_{(k-1)} - J_2 x d_{(k-2)} \quad (49)$$

8.6. Determination of the controller device characteristics

For a fast and a stable controlling system characteristic, a short but in every case constant dead time of the controller is required [Bühl95]. Therefore, the dead time of the digital controller has to be taken into account. This is influenced by the time for one run through the controller algorithm and the sampling time of the program.

For the determination of the controller dead time, the controller programme has to be manipulated so that the beginning and the end of the control process of the open system can be observed on an oscilloscope connected to the controller output port. For this, the sensor signal will be read in and stored as the current set point. After this, the output signal at the open controller output port will be increased by 0.5V. Then the controller starts to work. Since a negative deviation does not exist, the controller gives out the initial voltage. The same procedure with an output signal 0.5V more negative than the initial level will follow. Figure 45 shows the signal of the controller output at the open system.

The signal in figure 45 with the duration of $T_1 = 2\text{ms}$ represents the time required for the measurement of the current sensor signal and storage of this value as the current set point as well as the calculation and output of the signal 0.5 V higher or lower voltage on the analogue output port.

The signal in figure 45 with the duration of $T_2 = 6\text{ms}$ represents the time required for the measurement of the sensor signal the following comparison of the set point and the current value, storage of the negative deviation as well as one controller loop and the output of the controller output voltage.

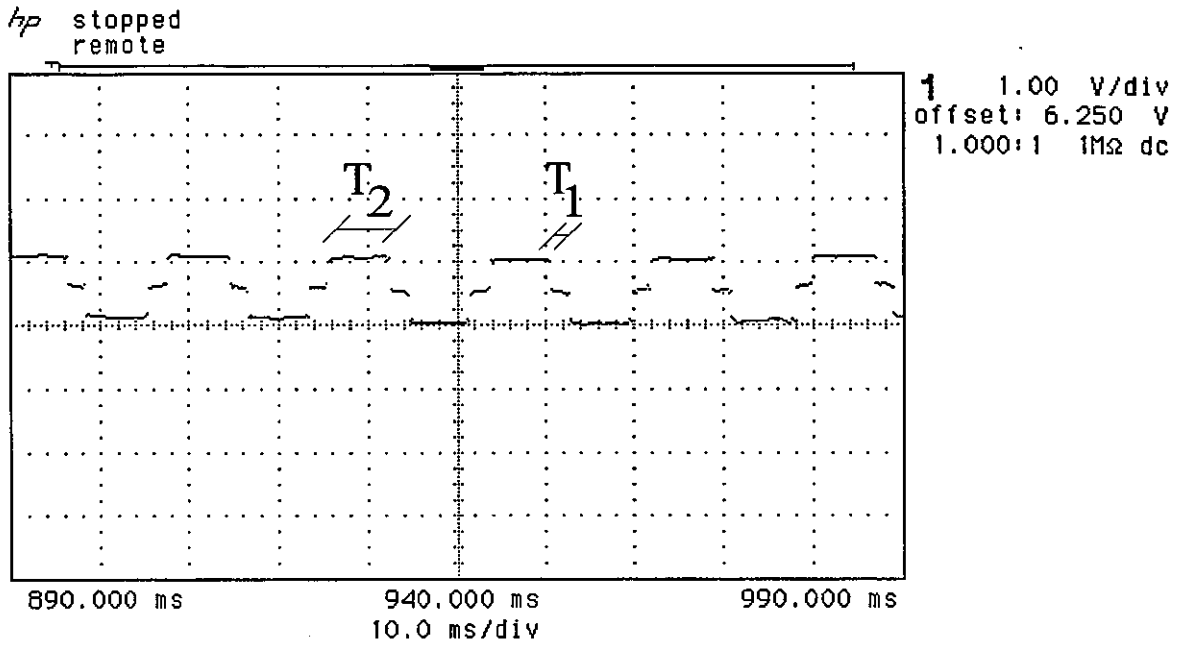


Fig. 45: Signal for the dead time determination of the controller

The difference of the durations $T_2 - T_1$ gives approximately the time for one controller loop, while the sampling time of the discrete controller is given by T_2 . The controller dead time T_t may now be calculated [Bühl95]:

$$T_t = \frac{T_A}{2} + T_{RA} = \frac{6ms}{2} + 4ms = 7ms \quad (50)$$

For the determination of the controller parameter in closed loop system design for the system based on the system to be controlled and the digital controller, this additional time has to be taken into account. For this reason, the transfer lag T_U of the step response sketched in figure 44 has to be extended by the dead time T_t of the digital controller. Therefore the new system parameters are:

- $T_U = 11ms$
- $T_g = 4ms$
- $K_S = 0.345$

Using equation (36) for the auxiliary parameter according to Chien, Hrones and Reswick

$$\tilde{k} = \frac{T_g}{T_U K_S} = 1.1 \quad (51)$$

the new PI-controller parameter according to the equations (37) and (38) are:

$$K_P = 0.34\tilde{k}..0.6\tilde{k} = 0.37..0.66 \approx 0.5 \quad (52)$$

$$T_N = 1.2T_g..4T_U = 4.8ms..44ms \approx 30ms \quad (53)$$

For the determination of the open controller behaviour, the step response for a step given from an external signal source will be recorded and investigated.

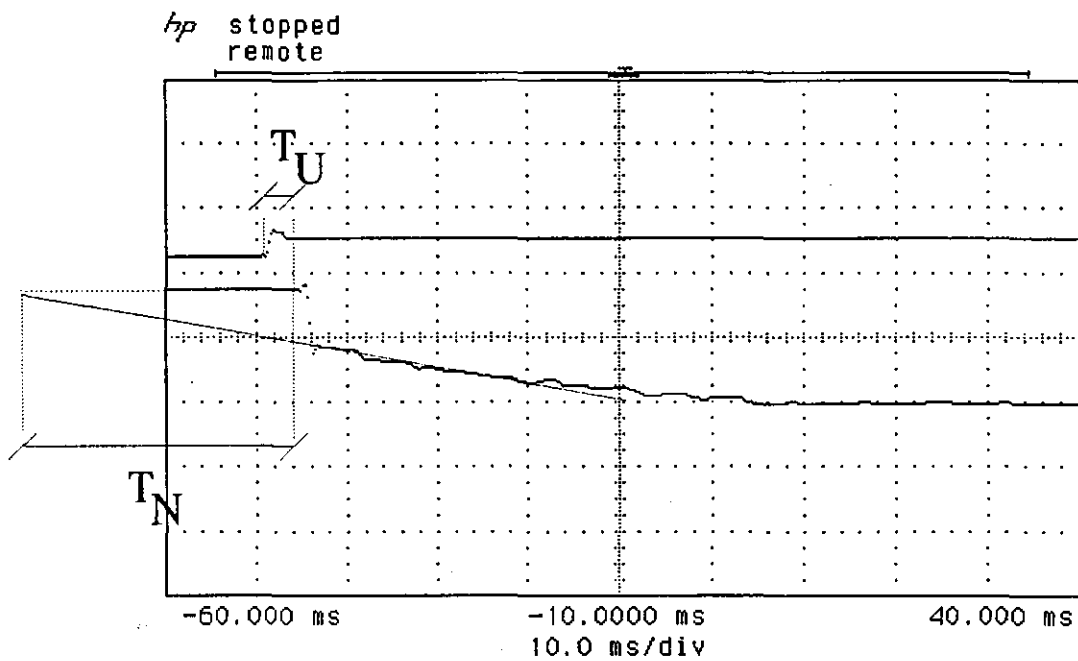


Fig. 46: Controller step response

Figure 46 illustrates in the upper part the signal that represents the step of the external signal source given to the controller input channel while the signal in the lower part of the figure represents the output signal of the controller as the reaction to the step input signal. The typical characteristic of a PI controller, i.e. a step caused by the K_P parameter and a continuous increase of the output signal until a maximum value is reached may be recognised. Also illustrated are the reset time $T_N \approx 30ms$ and the transfer lag $T_U \approx 7ms$ of the controller.

8.7. Closed loop system operation characteristics

In order to demonstrate the working characteristic of the closed loop system, the reaction of the developed closed loop system to a step of the set point parameter will be investigated. For this reason the controller program has been manipulated so that after reaching a stationary controlled parameter value a new set point will be defined.

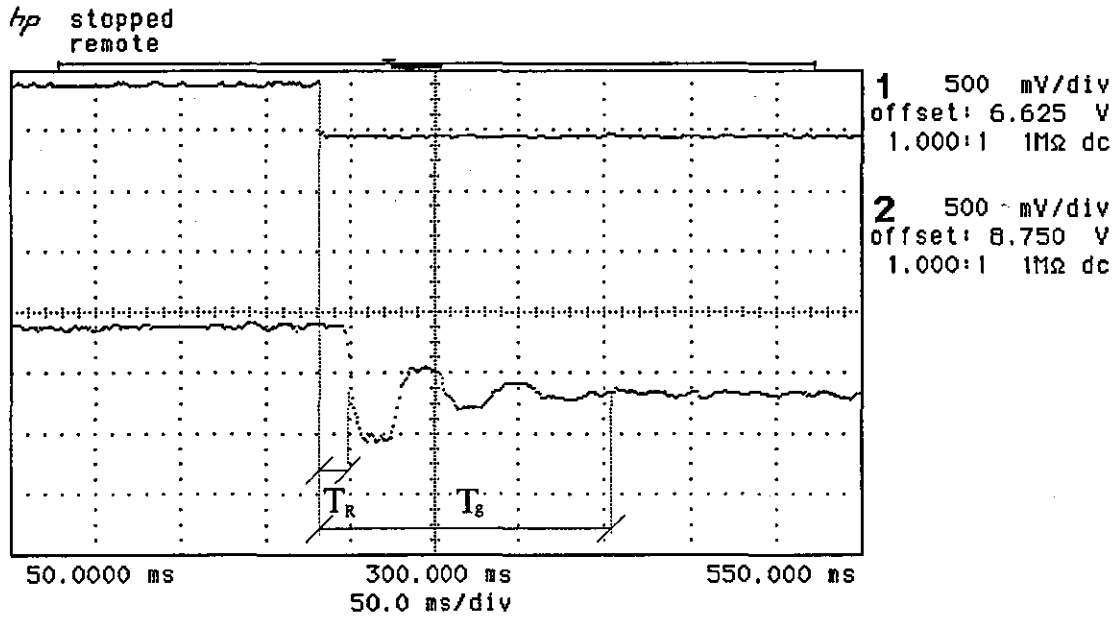


Fig. 47: Controlling characteristic with non optimal controller parameters

In the upper part of figure 47 is seen the step of the set point that affects the controlled parameter behaviour shown in the lower part of the figure. A large overshoot of the controlled parameter that is a result of non optimal controller parameters may be observed. The rise time T_R is determined as nearly 20ms, while the settling time T_g is nearly 170ms, after which all values of the controlled parameter are in a range that can be tolerated. This non optimum oscillating starting characteristic was obtained with the parameter theoretically determined in the last chapter. Experimental optimisation of these initial values leads to the controlling behaviour shown in figure 48.

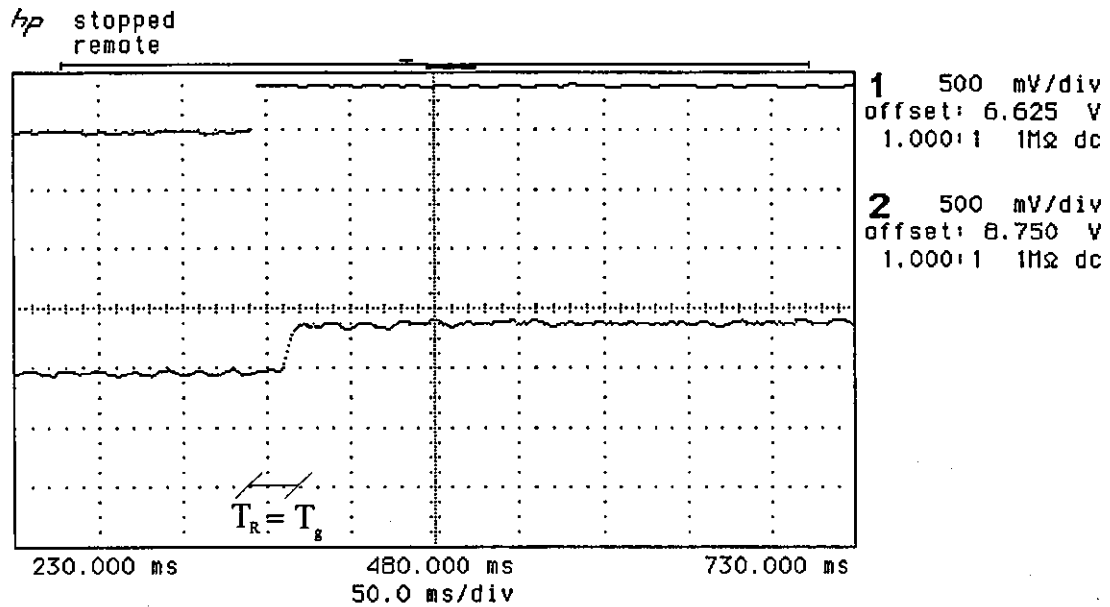


Fig. 48: Controlling characteristic with optimal controller parameters

Figure 48 shows that nearly 30ms after the new set point is activated, the controlled parameter reached the desired value. Also, it can be seen that the rise time T_R and settling time T_g have nearly the same value in the range of 30ms. This result was obtained with the following parameters:

- $K_P = 0.35$
- $T_N = 7\text{ms}$

The figures 47 and 48 indicate that for both controller parameter adjustments, the controlled parameter that corresponds to the distance d between the processing head and the processing surface is stable. The controlled parameter in both cases has a superimposed noise signal with a peak to peak amplitude of nearly $U_{pp} = 60\text{mV}$. The required signal accuracy of $\pm 0.17\text{V}$ for the focal position accuracy of $\pm 1.5\mu\text{m}$ is achieved and is not influenced negatively by this noise. Also, the speed of the controlling system which allows control of the distance with a correction time of nearly 30ms is suitable for the desired processing tasks of the LPG to date.

9. INTEGRATION OF THE PROCESSING HEAD INTO THE LPG

Adjustment and installation of the processing head into the vertical z-axis of the laser beam writer requires optical and mechanical adjustments. On the one hand, it is a question of coupling between processing beam and measuring beam and, on the other, it is a question of adjusting the processing head relative to the surface and to the defined center of the positioning unit. The operation of computer aided digital closed-loop controlled focal positioning permits the exposure of micro-structures on various substrate forms using different exposure strategies. From there, different exposure tasks set different requirements for the closed-loop control. The requirements shall be fulfilled by using different strategies for the operation of the closed-loop control. Furthermore, first results of the exposures using the LPG and the position controlled processing head are presented and discussed.

9.1. Adjustment of the processing head

The installation of the processing head into the LPG requires some adjustments, which are necessary to align the beam path of the measuring laser beam. The processing laser of the laser beam writer will be adjusted to a beam diameter necessary to build up structures of required width and results in a defined beam geometry behind the microscope lens. The measurement range of the distance sensor shall be adjusted to place its center on the position of the focus of the processing laser. By adjusting the caustic of the measuring beam, the resolution of the sensor can be adjusted (see chapter 6.1). By installing a telescope with adjustable focus range into the optical path of the measuring laser (Appendix T) it is made possible to set the measuring laser to different beam geometries. Starting values for the necessary adjustments were found by the examinations done in chapter 6.1. For the optimum adjustment of the measuring beam, a series of exposures were executed to determine measuring range and exposure results as a function of the telescope adjustment. The sensor setting found in this way is only valid for a certain surface (in this case resist); for other surfaces new settings will have to be found.

9.2. Adjustment of the LPG

Prior to starting the exposure, the LPG needs to be adjusted. This can be done by using the second beam splitter cube installed in the processing head (see figure 29) to monitor the reflexion of the measuring laser on the screen (frosted plate) and manually positioning the surface to be processed into the capture range of the sensor by operating the displacement unit which is coupled to the piezo translator. For a more accurate preadjustment the sensor voltage can be monitored with a digital voltmeter.

The alignment of the positioning system (Appendix U) beneath the optical axis can also be done by using the second beam splitter cube of the processing head. An object placed on the positioning system can be imaged on a screen by the microscope. For example, to position the center of the rotational axis directly underneath the microscope lens a cross grating can be imaged, whilst being turned by the positioning system. An improper alignment of the axes to one another results in an optical axis intersected by grating rays and on the imaging plane fast travelling stripes which rotate around a central point when the alignment is achieved. Monitoring the image and displacing the position of the rotation axis by linear movement of the axis allows the adjustment of the axis for very small rotationally symmetric structures.

9.3. System operation

For the exposure of relatively large structures with a relatively small focus, different procedures for writing strategies have been developed. In principle two fundamental procedures are available [Menz93]:

- raster-scan-procedure
- vector-scan-procedure

In the raster-scan-procedure the exposing beam is guided in form of a meander and with constant distance over the total surface, which can be covered by the beam. In the process of this and using an acousto-optic modulator (AOM) the beam will be switched on for those positions to be exposed and it remains switched off for the other positions.

The vector-scan-procedure uses the fact that wide ranges of most objects do not have to be addressed. Instead of moving the beam over the total surface, it is only addressed to those

areas which need to be considered. While jumping from one area to another the beam, of course, remains switched off.

In using this procedure, one has to differentiate between exposures which need a constant focal position and procedures where the focal position will be kept variable in order to get different exposure results.

Besides the adjustment of the focal position and the possibility to control the focal position via the piezo translator for both procedures, the applicability of the closed-loop controlled focal positioning, which, depending on the surface substrate has different requirements in controlling the adjustment of the focal positioning, shall be examined. One can expect that only those substrates shall be structured, which do not show microscopic surface defects (scratches in the resist). Unsuitable substrates need to be eliminated by quality control prior to exposure.

Surfaces subject to exposure are allowed to have a planar or other profile. These types of profile can be created by substrates with a desired profile (spherical surfaces) or deviation in layer thickness resulting from the manufacturing of the substrate, or coated surfaces with resist.

Depending on the combination of the exposure strategy, how the default set value is introduced, and the surface form used, different closed-loop controls can be advantageously applied.

Small changes of displacement between substrate surface und processing head can be neglected for planar surfaces, which shall be described using a small object.

The changes which might result for steeper slopes and/or larger objects cannot be neglected in all cases. In these cases one has to stop motion after a certain line of path and within a tolerable height difference, which depends on the slope and the size of the object and do a stationary readjustment of the focal positioning. In determining the displacements between the maximum line of paths of the readjustments, it is, for example, possible to determine the slope of the surface using the measurements of three different positions. In this manner, one is able to determine the displacements for the required accuracy of the focal positioning and the size of the object for which a readjustment is necessary. This means using the raster-scan- or the

vector-scan-procedure to do a readjustment of the focal positioning after ten paths. This procedure has the disadvantage of an elongated processing time and therefore should not be used where short processing time is important, such as in series production.

Using formed surfaces one has to do a readjustment of the focal positioning depending on its required accuracy and the form and height of the profile. In order to aim for short working time, the readjustment should be done in parallel to the writing of the laser writer. In doing this, the operation of the closed-loop should only be started if preset limits are exceeded, which results in a smoother operation of the system.

The above statements apply without restrictions for structures with variable distance between processing head and substrate surface (controlling variable of the closed-loop is variable itself), however, an adjustment of the focal position is also necessary when a new focal positioning is required because of different exposures.

9.4. Examples for micro-structuring with the LPG

Each discrete step in a manufacturing process of micro-structuring has a fundamental influence on its result and, from this, an accurate determination of each discrete process parameter of the total process is required. The readjustment and accurate control of all parameters is one of the conditions necessary for the reproducibility of the manufacturing results. For example the correct preparation of the substrate by keeping to the parameters for cleaning and resist coating is as important as keeping to the parameters when exposing and processing photosensitive materials.

Successful operation of the LPG used for micro-structuring depends on the stability of the following beam parameters: laser intensity, beam profile and polarisation. Furthermore, a correct and rapid laser modulation as well as the exact velocity and position control of the displacement units are necessary.

As in all manufacturing procedures using light, in this special process the characteristic curve needs to be determined, which reflects the result of each single step of the process in accordance with the radiant exposure.

In order to achieve the necessary reproducibility, the parameters adjusted for the particular processing have to be determined and reproduced for the next process.

The LPG has following degrees of freedom:

- Position : Position at which an exposure will be done
- Focal position : Position of the minimum focal spot relative to the substrate surface
- Radiant exposure : Duration and intensity of the laser beam on one position

In structuring the resist, laser exposures will result in changes of the height profiles which are proportional to the amount of exposure taking into account various boundary conditions [Lens92a]. Using a Gaussian profile and having the possibility to keep the focal position variable, results in diverse structuring possibilities. Two differing strategies:

- static exposure and
- dynamic exposure

and the resulting micro-structures using the LPG and its integrated position controlled processing head will be discussed.

Static exposure

Using a binary coded barcode plate, it will be shown how to generate approximately continuous lines from a combination of discrete exposure points, selecting the correct parameters for exposure and positioning. This will be done by addressing the positioning unit to the desired position, adjusting the processing head to the required focal position, and exposing the resist with a defined intensity and duration.

Figure 49 shows a segment of a line disk established with this strategy. This was done by applying a bit pattern over the radius, which corresponds to a certain angle position out of 10000 incremental angle positions for the total circuit. In comparison to figure 49 the pattern in figure 50 shows a much higher quality that is a result of a correct focal position during the structuring process achieved by the processing head. With this exposure technique, lines with a thickness of $1\mu\text{m}$ and of $4\mu\text{m}$ length representing a logic null and of $20\mu\text{m}$ representing a logic one were introduced. The discrete exposure points have a displacement to one another of $0.7\mu\text{m}$, in this they overlap and result in approximately continuous lines.

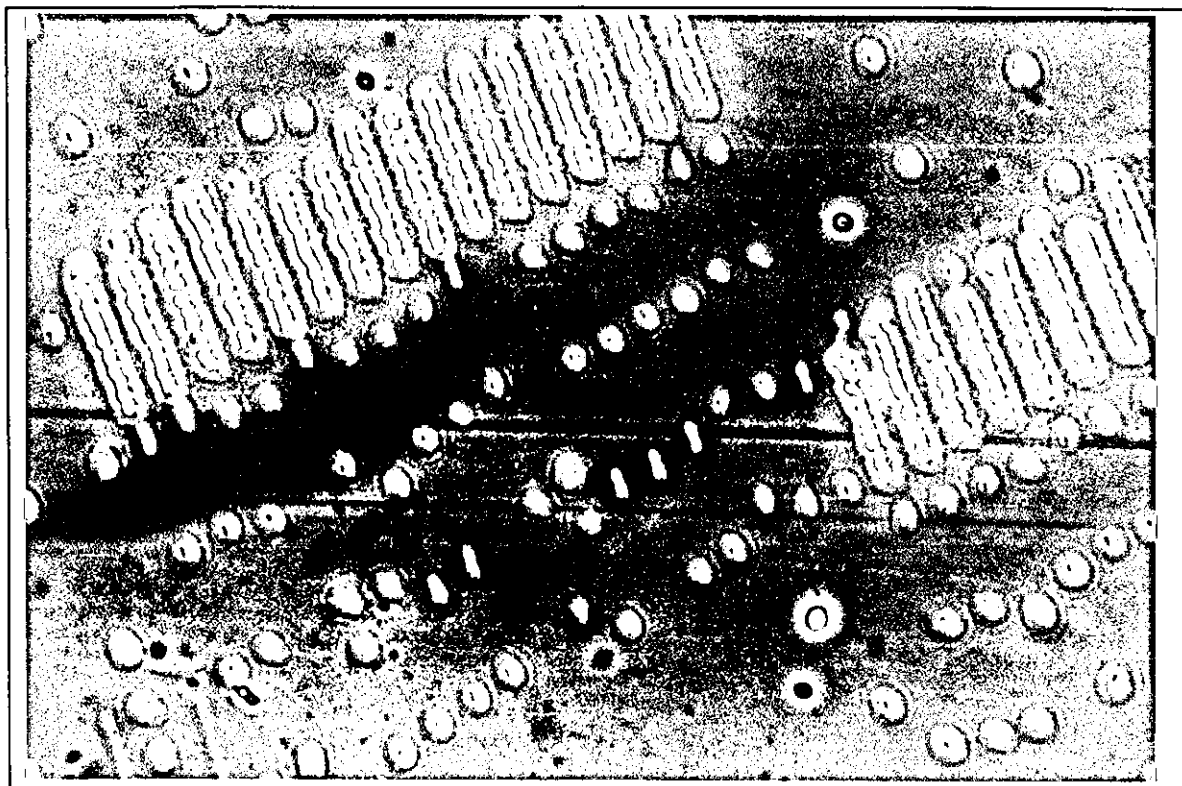


Fig. 49: Segment of a line disk established without a correct focal position

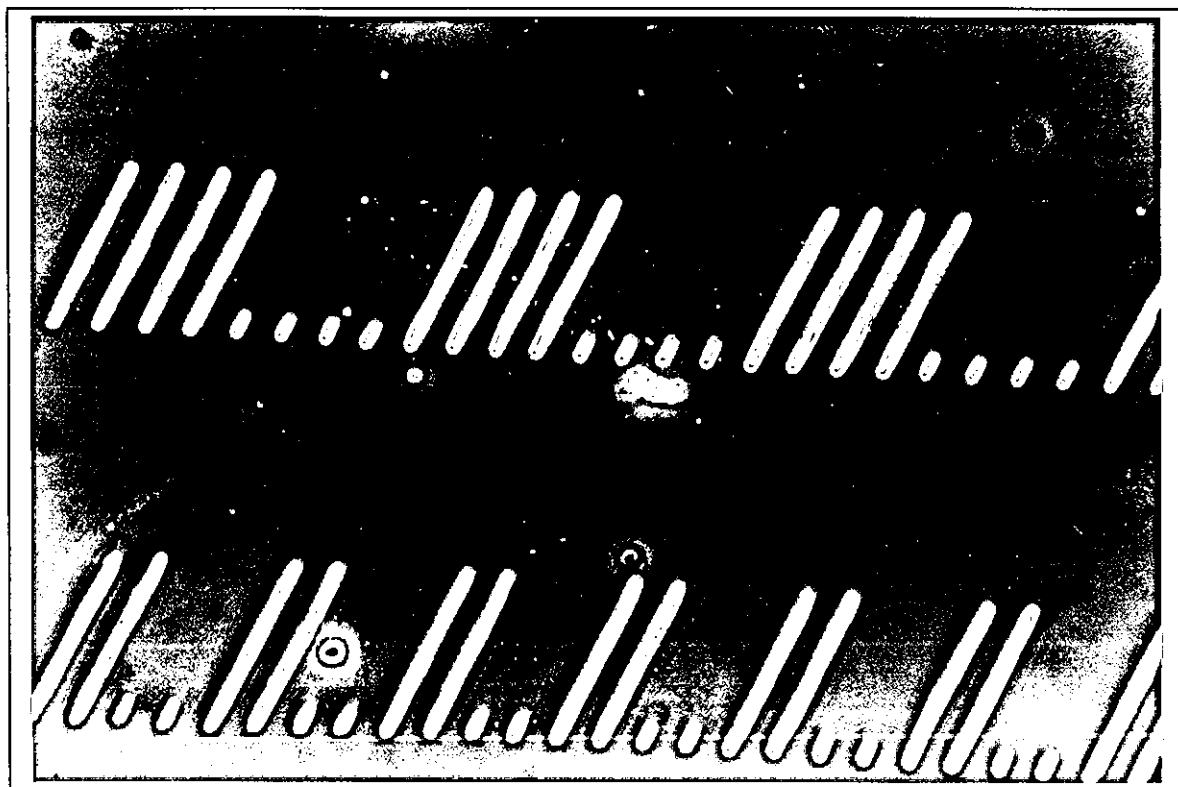


Fig. 50: Segment of a line disk established with a correct focal position

Dynamic exposure

The substrate is moved by the positioning unit under a continuously radiating laser beam in such a manner, that the desired structure is established by the subsequent processing. In doing this, the velocity of the positioning unit needs to be matched to the desired exposure and during the total motion process the focal position must be kept to the required distance by the closed-loop control.

Figures 51 and 52 illustrate a micro lens established with this strategy, whereby in figure 51 the focal position is not correct installed and in figure 52 a high quality resist pattern indicates correct focal position. The rotating unit applies the velocity matched to the radius and by this enables the establishment of structures with a width smaller than $1\mu\text{m}$



Fig. 51: Segment of a micro lens established without a correct focal position



Fig. 52: Segment of a micro lens established with a correct focal position

For the structures illustrated in figure 50 and figure 52, the resulting structure width stays within the order of magnitude of the smallest structures which can theoretically be established with these strategies (see also chapter 3.3). The closed-loop controlled focal positioning of the processing head ensures the correct focal positioning while exposing large objects.

Finally, for the assessment of the position controlled processing head, it can be stated that the LPG is capable of reproducible processing of planar substrates. However, the exposure of curved surfaces, with or without variable focal position, still needs to be examined in further studies.

10. DISCUSSION

This study introduces different microstructure manufacturing technologies and separates the technologies into serial and parallel procedures.

The laser beam writer developed with all the mechanical, optical, opto-electronic, and computer components has been described. The characteristics of the focal positioning adjustment were analysed and, in order to establish the required accuracy of the focal positioning, a criterion of $Z_R'/2$ was introduced. In order to meet this focal position accuracy during the structuring process, a closed loop system consisting of a distance sensor, an actuator and a digital controller is required.

For choosing the best distance sensor, different sensor principles have been investigated which lead to an autofocus principle as the best sensor with regards to the LPG demands.

A market survey has demonstrated that there is no autofocus sensor available which can be employed in the LPG without major reconstruction and adjustment efforts. For this reason different autofocus sensor principles were investigated leading to a setup using a semiconductor laser as the light source, a microscope objective for the beam focussing, a beam splitter tube for beam separation, a lens and a knife edge for beam manipulation and a PSD as the detector.

Furthermore, a raytracing model for the beam forming system was developed in order to know how to couple both the processing and the measuring laser beam in the LPG application. Also a mathematical model for the optical part of the sensor has been developed which enables specific sensor construction meeting the measurement demands in different applications. This model also shows the linear working characteristics of the sensor principle. Additionally, the sensor has been investigated in a raytracing model leading to the same measurement characteristics as the mathematical model. Based on the simulation results, the sensor output signal as a function of the measured distance for different positions of the knife edge and the PSD are mathematically simulated in order to optimise the sensor setup for a nearly linear signal characteristic. With the help of two prototype sensors, the applicability and the linear measurement characteristics of the sensor for distance determination on different surfaces has been demonstrated. Based on the described theoretical and experimental investigations, an

optimised sensor has been designed, constructed, and tested. This sensor has been adjusted in such a manner that a good linear measurement range of $30\mu\text{m}$ with a resolution of better than $0.5\mu\text{m}$ for distances to a resist layer has been achieved. This autofocus sensor is characterised not only by its flexible and adjustable measurement and resolution range and its good linear characteristic curve, but also by a relatively low price which results from use of several standard components. Furthermore, this sensor has the advantage of a large dynamic range described by a high cut-off frequency, which is the result of a sensor principle without any moving parts.

A sensor optimised to fulfil a special task may need fewer degrees of freedom for adjustment, or can work without adjustable elements when more accurate manufacturing techniques are established. Further optimisation of the measurement head can be established when specially selected optical components are introduced. In this way, it might be possible to combine beam splitting, focussing, forming, and screening (shadowing) in one component, which will result in less volume, weight, and adjustment effort. Multi-function optical elements of this kind can be established by placing so-called diffractive optical elements [Herz92] onto the surface of the beam splitter cube. Using these kinds of optical elements, it might also be possible to minimise or even eliminate the interdependence between the measurement signal and the tilt of the measured surface to the sensor axis.

Furthermore, miniaturisation may result in setups of lower weight and sensitivity which can open new application fields even in vibration influenced environments. With a computer controlled positioning system consisting of linear and rotating axes, one can realise a cylindrical coordinate system or, using two linear axes, a measuring system with cartesian coordinates, permitting an automatic survey of micro-structures (Reverse Engineering) [Over92]. From there, the LPG can be used not only to expose, but also to survey micro-structures. A conceivable online survey in exposing resist cannot be realised since the result of the exposure is only measureable after the process of development.

For the required processing head positioning, different actuators have been compared. The chosen piezo translator with a travel range of $30\mu\text{m}$ has been investigated theoretically in order to determine the static and the dynamic behaviour of the actuator. The cut-off frequency was theoretically determined with a value of 50Hz restricted by the electronic driver circuit. If larger correcting displacements and faster position changes of the processing head are

required, other piezo translators having a larger positioning range and a piezo driver with more output power may be preferable.

For the required adjustment of the focal position, the sensor has been mounted on the piezo translator, obtaining a system that has been implemented and analysed for control system design. The cut-off frequency was experimentally determined in the range of 40Hz. For this system, a digital controller has been realised on the host computer of the LPG and optimised to meet the requirements in focus position accuracy of $Z_R'/2$ in the application of the LPG. The working characteristic of the control system was analysed showing a settling time of 30ms which is suitable for the applications considered. If faster settling times are required, a faster digital controller (DSP) or an analogue controller circuit has to be developed.

For the integration of the processing head into the LPG, the adjustment of the processing head and of the complete LPG was described. For the manufacture of different structures different exposure and working strategies of the processing head were analysed. With two different controlling strategies, which were tailored to the exposure strategies and operation characteristics of the LPG, the operation of the focal position control was successfully demonstrated and the focal position accuracy criterion was proven through the successful manufacture of two typical micro-structures with the LPG. The operation of the position controlled processing head in the LPG gives reproduceable and good exposure of planar objects. Structuring of non-planar substrates needs to be examined in further studies.

11. CONCLUSION

For a reproduceable manufacturing result of microstructures using a laser beam writer the focal position accuracy of the strongly focussed laser beam is a major demand. For this reason a focal position controlled processing head for the laser pattern generator designed and constructed at the Fachhochschule Ostfriesland has been developed.

This system is based on a modified autofocus sensor for focal position determination that can be adjusted for different application demands, a flexible digital controller in the host computer of the LPG for the closed loop system and a piezo driven linear axis for the required focal position adjustment. After the analysis of each of these three components, they were first independently optimised and then combined and tuned to an optimised, complete system.

Using different application strategies of the system the reproducibility of the processing result, which is caused by the exact focal position during the structuring process, has been demonstrated by the manufacture of several microstructures.

References

- [Ande90] Anderson, H., et.al., Single photomask multilevel kinoforms in quartz and photoresist: manufacture and evaluation, *applied optics*, Vol. 29, No. 28, pp.4259-4267, (1990)
- [Aoya90] Aoyama S., Horie, N. Yamashita, T., Micro Fresnel Lens Fabricated by Electron-Beam Lithography, *Proc. SPIE*, vol.1211, pp. 175-183, (1990)
- [Arno85] Arnold, S., Electron beam fabrication of computer generated holograms, *Optical Engineering*, Vol. 24(5), pp. 803-807, (1985)
- [Bart77] Bartolini, R.A., *Holographic Recording Materials* (edited by Smith, H.M.), *Topics in Applied Physics*, Vol. 20, Springer Verlag, pp. 209-227, (1977)
- [Brei92] Breitmeier, U., *Lasermesstechnik zur Oberflächen-Qualitätskontrolle*, *Laser und Optoelektronik*, 2/1992
- [Broc91] Brock, P.J., et.al., Fabrication of Grooved Glass Substrates by Phase Mask Lithography, *SPIE*, Vol. 1463, pp. 87-100, (1991)
- [Brod87] Brodmann, R., Ein neuer optischer Feintaster und seine Anwendungen, *Technische Rundschau* Nr. 39/1987
- [Brod89] Brodmann, R., Messen in CD-Qualität, *Laser* 3/1989
- [Brod90] Brodmann, R. in Treiber, H., *Der Laser in der industriellen Fertigungstechnik*, Hoppenstedt Technik Verlag, Darmstadt (1990)
- [Bühl95] Bühler, E., *Script zur Vorlesung Regelungstechnik*, FB E+I, Fachhochschule Ostfriesland, 1995
- [Cass90] Cassjens, H.-G., Entwicklung und Erprobung eines berührungslos messenden Laser-Rauhheitssensors mit dynamischer Fokussierung und einem Interface zu einem Datenerfassungs- und -auswertesystems, Final year project at Fachhochschule Ostfriesland, Supervisor: Prof. Dr. H. Kreitlow, Emden, Germany, (1990)
- [Chie52] Chien, K.L., Hrones, J.A., Reswick, J.B., On the Automatic Control of Generalized Passive Systems, *Trans of the ASME* 74 (1952)
- [d'Aur72] d'Auria, L., Huignard, J.P., Roy, A.M., Spitz, E., Photolithographic fabrication of thin film lenses, *Optics Communications*, Vol. 5(4), pp. 232-235, (1972)
- [Dome91] Domes, M.P., Dowling, R.J., McKee, P., Wood, D., Efficient optical elements generate intensity wheight spot arrays; design and fabrication, *Applied Optics* 31, Vol. 30, No. 19
- [Eich91] Eichler, J., Eichler, H.-J., *Laser*, Springer Verlag, Berlin (1991)

- [Find85] Findalky, Glas waveguides by ion exchange: a review, Opt.Eng., Vol.24, No.2, p244, (1985)
- [Frey92] Frey, H., Ionenstrahlgestützte Halbleitertechnologie, VDI-Verlag, Düsseldorf, (1992)
- [Gale92] Gale, M.T., Rossi, M., Schütz, H., Fabrication of 2-dimensional continuous-relief diffractive optical elements, Proc. SPIE, vol.1732, pp. 58-65, (1992)
- [Gamb91] Gambog, W., et.al., Holographic transmission elements using improved photopolymer films, SPIE Vol.1555, pp. 256-267, (1991)
- [Golt90] Goltzos, W., Liu, S., Polar Coordinate Laser Writer for Binary Optics Fabrication, Proc. SPIE, vol.1211, pp.137-149,(1990)
- [Göpe93] Göpel, W., Sensors, Optical sensor (volume 6), VCH Verlag, Weinheim, 1993
- [Gros94] Grosser, L., Prinzipien der Autofokussierung, Internal report, Fachhochschule Ostfriesland, Supervisor: Prof.Dr. Horst Kreitlow, Emden, Germany, (1994)
- [Hase92] Haselbeck, S, et. al., Synthetic phase holograms written by laser lithography, Proc. SPIE, vol. 1718, pp. 117-128, (1992)
- [Herz92] Herzig, H.P., Dändliker, R., Design and fabrication of diffractive optical elements for beam shaping and imaging, Proc. SPIE, vol. 1718, pp. 130-137, (1992)
- [Jäge89] Jäger, E., Hoßfeld, J., Tang, Q., Tschudi, T., Design of a laser scanner for kinoform fabrication. Proc. SPIE, vol. 1136, pp.228-235, (1989)
- [Jäge92] Jäger, E., Computergenerierte Holografisch Optische Elemente, Ph.D. Thesis, Tschudi, T., Lauterborn, W., Universität Darmstadt, (1992)
- [Krei93] Kreitlow, H., Probian, D., Lippert, P., Lensch, G., Micro engineered displacement sensor, Proceedings Laser '93, München 1993
- [Lens92a] Lensch, G., Kreitlow, H., Lippert, P., Budzinski, Ch., Interferometrische Herstellung von tiefen diffraktiven Strukturen in Fotoresist, Jahrestagung der DGaO, Friedrichsroda 1992
- [Lens92b] Lensch, G., Lippert, P., Kreitlow, H., Budzinski, Ch., Optimized Replication of Interferometrically Generated Deep Diffraction Structures by Embossing into Thermoplastics, SPIE No. 1780-27, (1992)
- [Leon70] Leonhard, W., Einführung in die Regelungstechnik, Verlag Vieweg, Braunschweig 1970
- [Menz93] Menz, W., Bley, P., Mikrosystemtechnik für Ingenieure, VCH Verlag, Weinheim, (1993)

- [Naum92] Naumann, H., Schröder, G., Bauelemente der Optik, Carl Hanser Verlag, München, (1992)
- [Newp93] Newport Catalogue (1993)
- [Over92] Overmeyer, L., Dickmann, K., Dynamischer Autofokussensor zur dreidimensionalen Mikrostrukturierung, *tm Technisches Messen* 59/1992
- [Phys94] Physic Instruments Catalogue 1994
- [Pole91] Poleshuk, A.G., Fabrication of phase structures with continuous and multilevel profile for diffractive optics, *SPIE*, Vol. 1574, 89-100, (1991)
- [Reut90] Reuter, M., Regelungstechnik für Ingenieure, Vieweg Verlag, Braunschweig 1990
- [Schre84] Schreier, D., Synthetische Holografie, Physik Verlag, Leipzig, (1984)
- [Sike95] Data sheet PSD, SiTek electro optics
- [Sont91] Sontheim, B., Graf, G., Analoge und digitale Regelkreise auf dem PC simuliert, *Elektronik* 22/1991
- [Step82] Steppan, H., Buhr, G., Vollmann, H., The resist Technique - A Chemical Contribution to Electronics, *Angew. Chem. Int. Ed. Engl.*, 21 (1982)
- [Stre92] Streibl, N., et. al., Laser Beam Writing of Computer generated Diffractive Optical Components, *Proc. SPIE*, vol. 1732, pp. 67-74, (1992)
- [Topk88] Topkaya, A., Schmall, K.H., Majoli, R., Non contact capacitive clearance control system for laser cutting machines, *Proc. of the SPIE*, Volume 1024, 1988
- [Töns93] Tönshoff, H.K., Heekenjann, P.B., Overmeyer, L., Autofocus sensor for micro-machining, *Laser und Optoelectronik*, 25(6), (1993)
- [Walk93] Walker, S.J., Design and fabrication of high efficiency beam splitters and beam deflectors for integrated planar micro-optic systems, *Applied Optics*, Vol. 32, No. 14, pp.2494-2501, (1993)
- [Yata91] Yatagai, T., et. al., CAD system for CGHs and laser beam lithography, *Proc. SPIE*, vol. 1555, pp. 8-12, (1991)

APPENDICES

Page #

A. OVERVIEW OF THE LPGA1

B. BLOCK DIAGRAM OF THE LPG.....B1

C. SOFTWARE CONCEPT OF THE LPG.....C1

D. PSD ANALYSING CIRCUIT.....D1-D4

E. RAY-TRACING MODEL OF THE MICROSCOPE OBJECTIVE..... E1-E5

F. RAY-TRACING MODEL OF THE TELESCOPE..... F1-F5

G. RAY-TRACING MODEL OF THE MEASURING LASERG1-G4

H. DERIVATION OF THE MATHEMATICAL SENSOR MODELH1-H8

I. RAY-TRACING MODEL OF THE SENSOR I1-I9

J. CONSTRUCTION OF THE EXPERIMENTAL SENSOR..... J1-J2

K. CONSTRUCTION OF THE SENSOR TRANSLATORK1-K2

L. CONSTRUCTION OF THE SURFACE TILT SYSTEM L1-L2

M. CONSTRUCTION OF THE OPTIMISED PROCESSING HEAD M1-M11

N. CONSTRUCTION FOR THE SHIELDING OF THE PSD CIRCUITN1-N6

O. SIGNAL AMPLIFIERO1-O4

P. PIEZO DRIVER.....P1-P3

Q. CONTROLLER PARAMETER TABLE.....Q1

R. CONTROLLER PROGRAM FLOW CHART.....R1

S. CONTROLLER PROGRAM LISTINGS1-S7

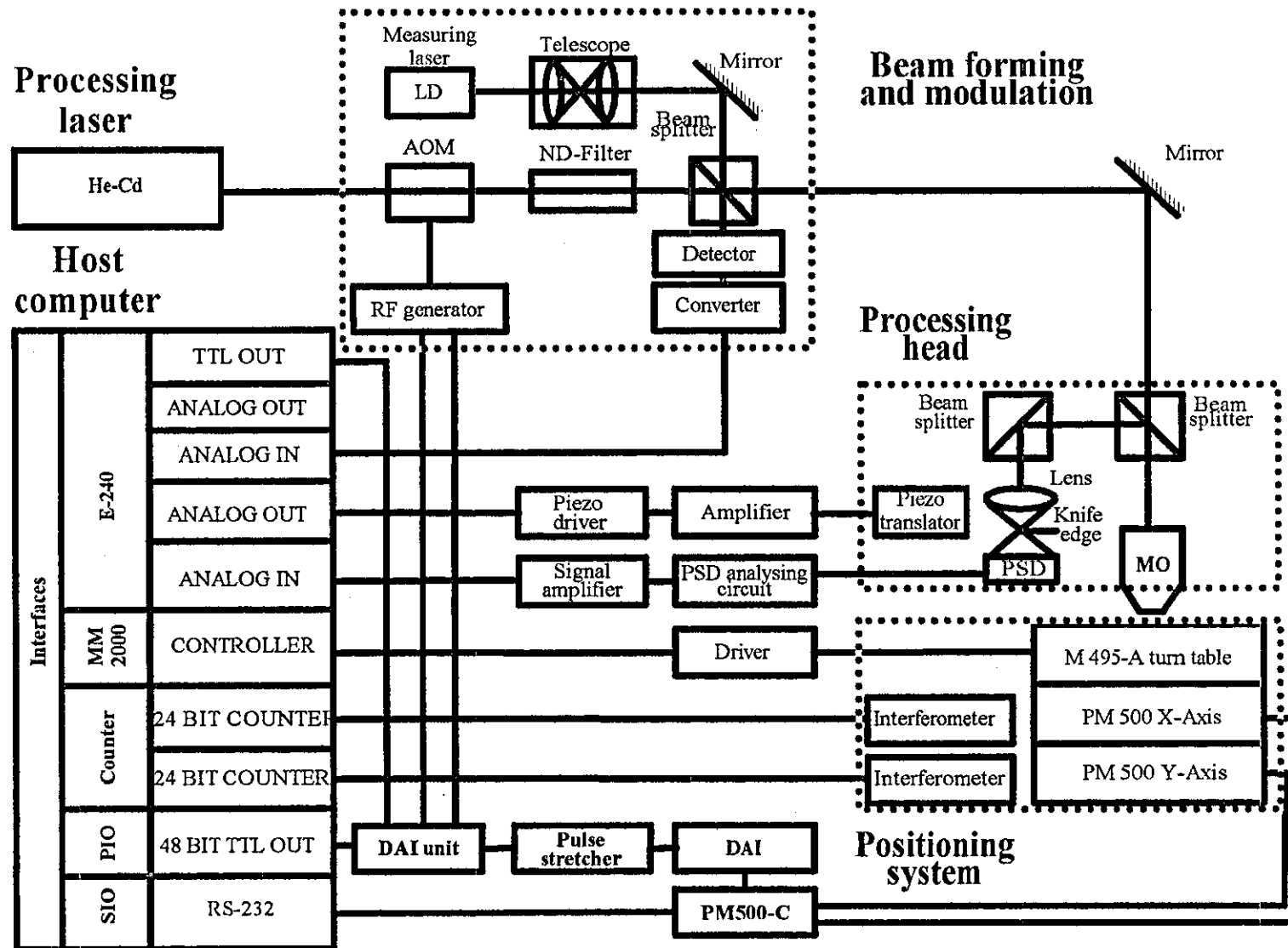
T. OPTICAL CONSTRUCTION OF THE LPG..... T1-T3

U. CONSTRUCTION OF THE LPG POSITIONING SYSTEMU1-U3

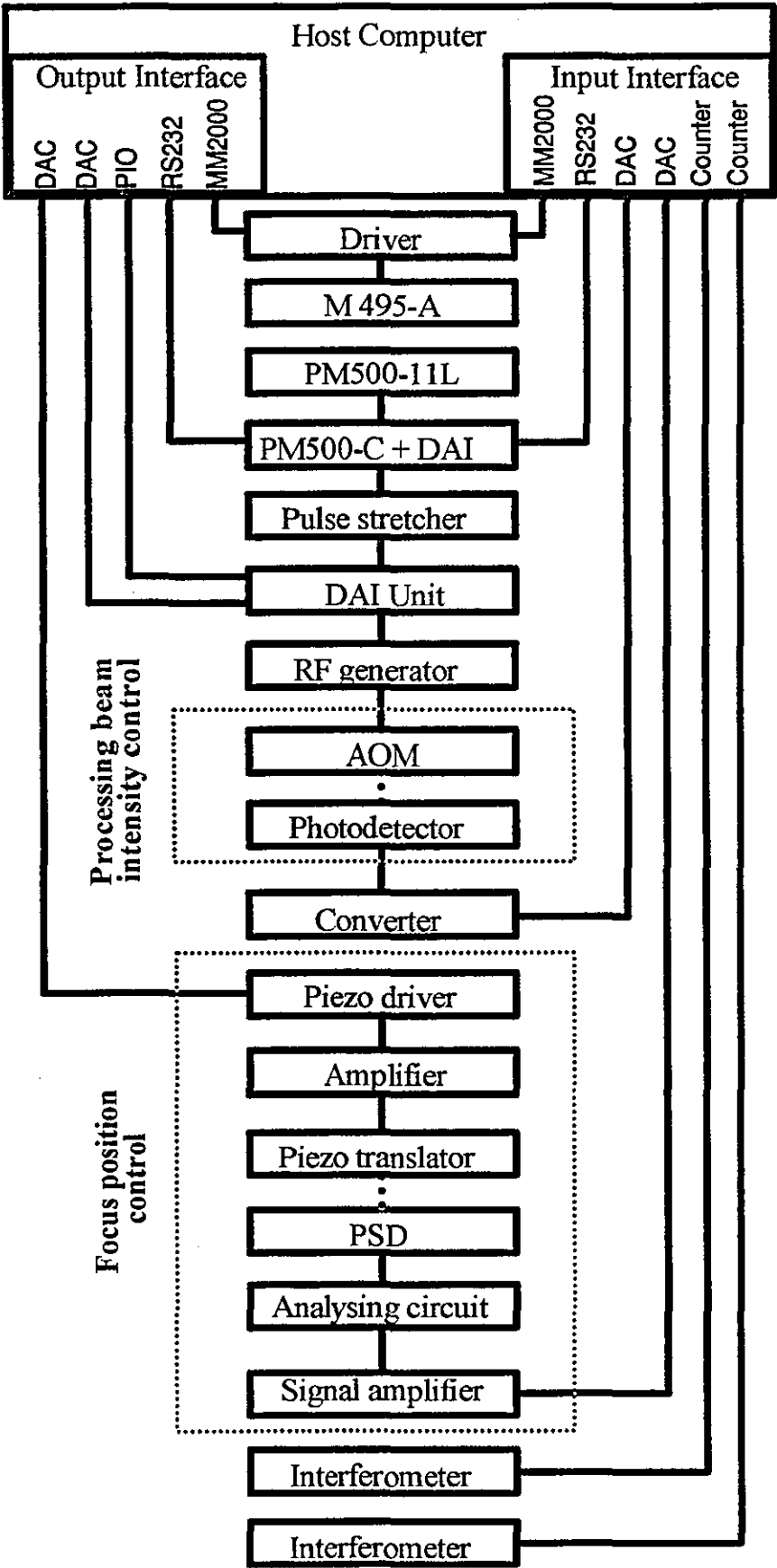
V. PHOTOGRAPHSV1-V6

W. PUBLICATIONS..... W1-W40

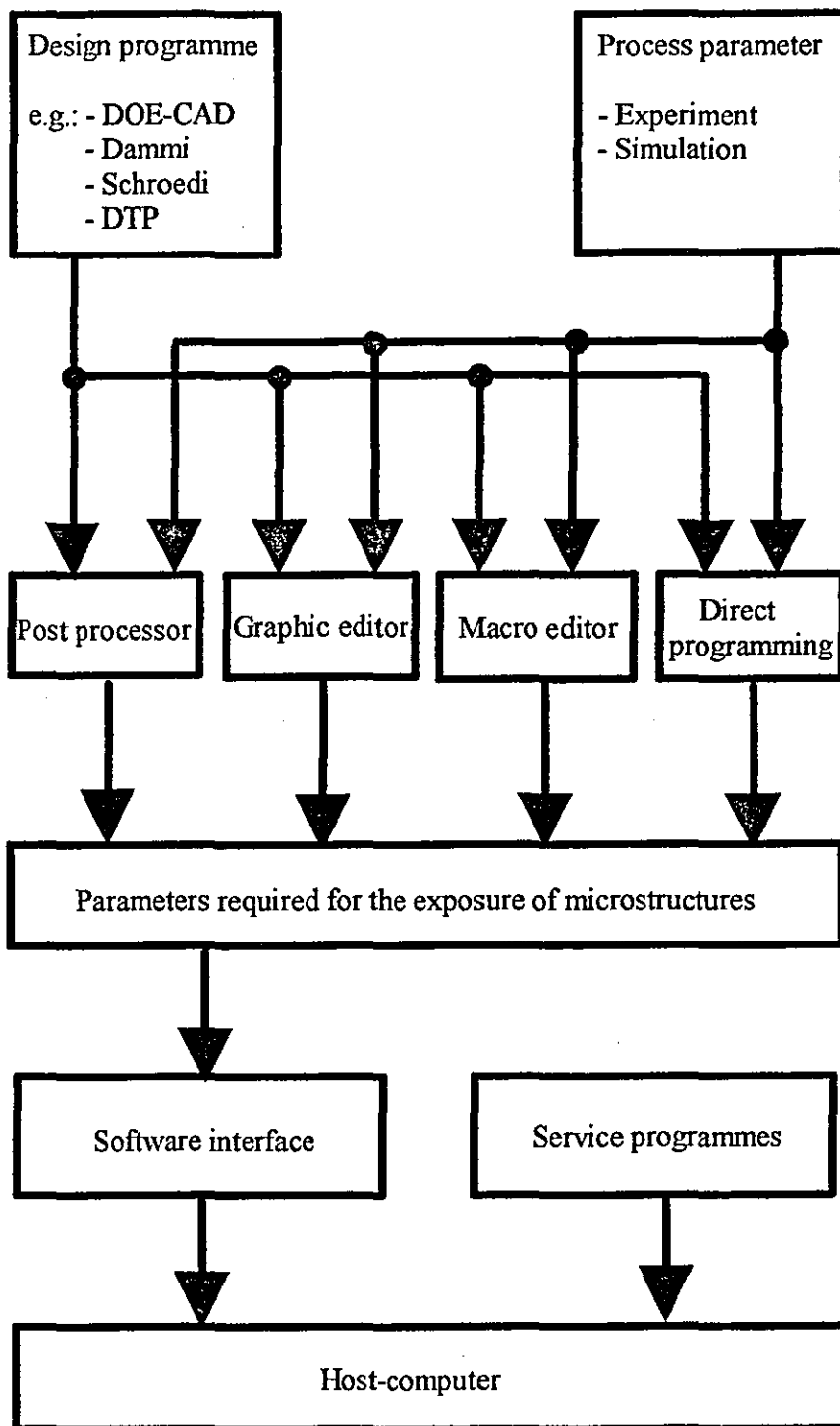
OVERVIEW OF THE LPG



BLOCK DIAGRAM OF THE LPG

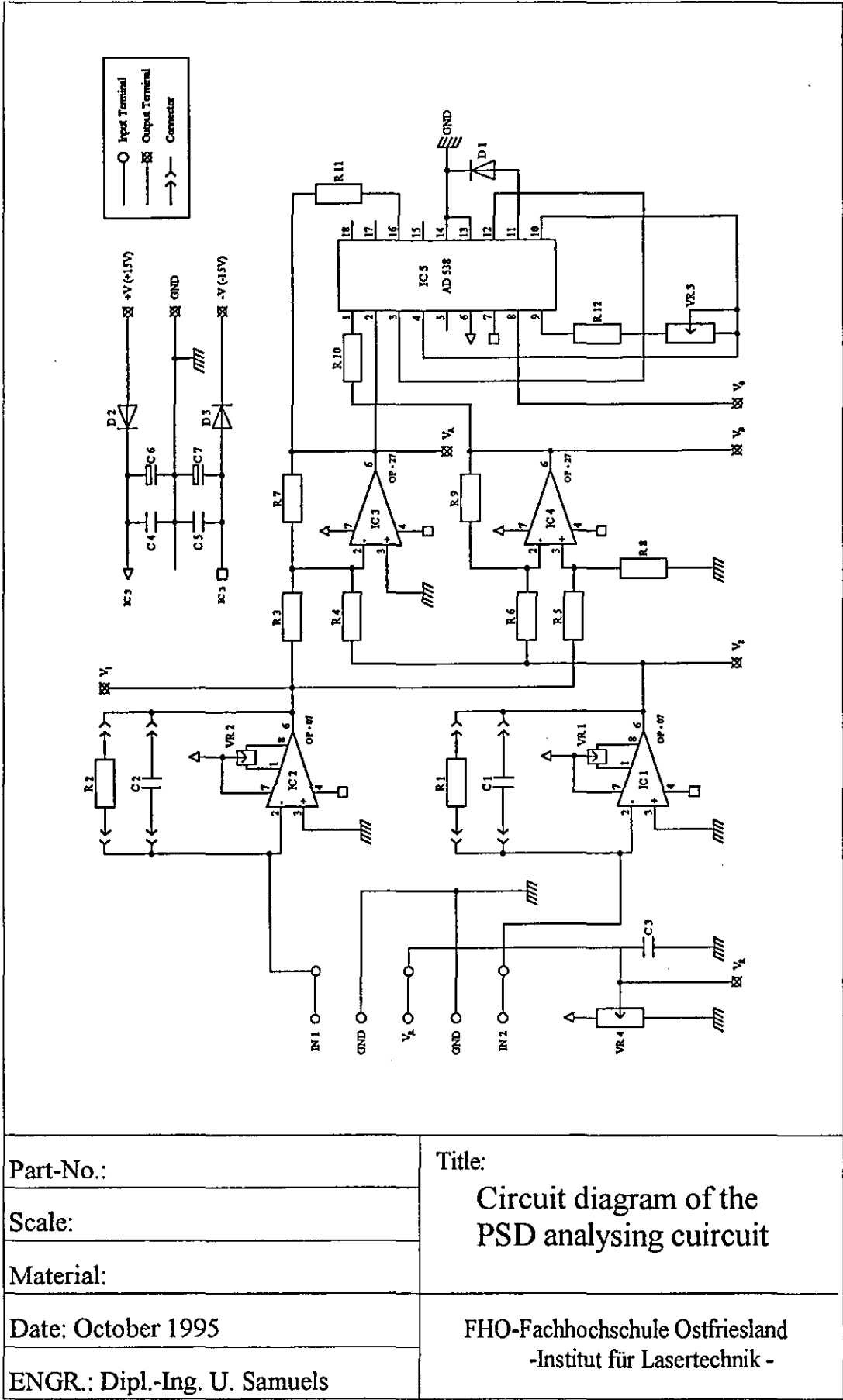


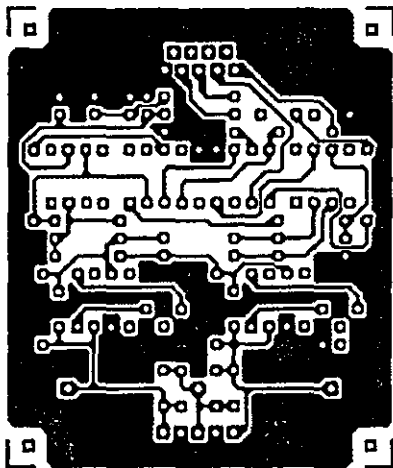
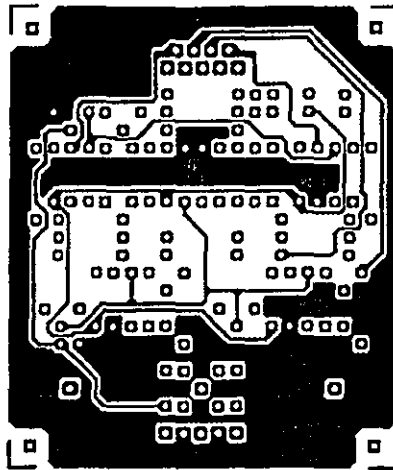
SOFTWARE CONCEPT OF THE LPG



PSD ANALYSING CIRCUIT

CONTENTS	PAGE #
1. Circuit diagram	D1
2. PCB layout	D2
3. Input terminal	D3
4. Output terminal	D4
5. Parts list	D5





Part-No.:	Title: PCB of the PSD analysing circuit
Scale:	
Material:	
Date: October 1995	FHO-Fachhochschule Ostfriesland -Institut für Lasertechnik -
ENGR: Dipl.-Ing. U. Samuels	

3. Input terminal

Pin #	Description	Colour
1	IN 1	blue
2	GND	black
3	V _R	red
4	GND	black
5	IN 2	blue
6		
7		
8		
9		

Table D1: PSD - Analysing - circuit → Input terminal (Sub-D)

4. Output terminal

Pin #	Description	-
1	Bias voltage output (V _R)	
2	Analog divider output (V ₀)	V_B / V_A (at $V_A > 0$)
3	- V (- 15V)	
4	+ V (+ 15V)	
5	GND	
6	Difference signal output (V _B)	$V_1 - V_2$
7	Head amplifier output (V ₁)	
8	Head amplifier output (V ₂)	
9	Sum signal output (V _A)	$V_1 + V_2$

Table D2: PSD - Analysing - circuit → Output terminal (Sub-D)

5. Parts list

<u>Part No.</u>	<u>Description</u>
C1	1nF Foil
C2	1nF Foil
C3	100nF Ceramic
C4	100nF Ceramic
C5	100nF Ceramic
C6	10 μ F Elco 25V
C7	10 μ F Elco 25V
D1	1N4148
D2	1N4148
D3	1N4148
IC1	OP-07CN
IC2	OP-07CN
IC3	OP-27CN
IC4	OP-27CN
IC5	AD538
R1	100k Ω
R2	100k Ω
R3	10k Ω
R4	10k Ω
R5	10k Ω
R6	10k Ω
R7	10k Ω
R8	10k Ω
R9	10k Ω
R10	36k Ω
R11	36k Ω
R12	10k Ω
VR1	20k Ω
VR2	20k Ω
VR3	20k Ω
VR4	20k Ω

RAY-TRACING MODEL OF THE MICROSCOPE OBJECTIVE

CONTENTS	PAGE #
1. Surface data summary	E1
2. System data	E1
3. 2D-Layout	E2
4. 3D-Layout	E3
5. Through focus spot diagram	E4
6. Gaussian beam parameters	E5

1. Surface data summary

SURFACE DATA SUMMARY:

Surf	Type	Radius	Thickness	Glass	Diameter	Conic
OBJ	STANDARD	Infinity	Infinity		0	0
STO	STANDARD	Infinity	20.00013		0	0
2	STANDARD	3.99995	1.999971	SF6	6.000037	0
3	STANDARD	-8.000001	0.5000016	BK7	6.000037	0
4	STANDARD	-99.99967	0.599999		6.000037	0
5	STANDARD	5.000001	1.999995	SF6	6.000037	0
6	STANDARD	-5.999984	0.3	BK7	6.000037	0
7	STANDARD	-100.0012	0.1494		6.000037	0
IMA	STANDARD	Infinity	0		0	0

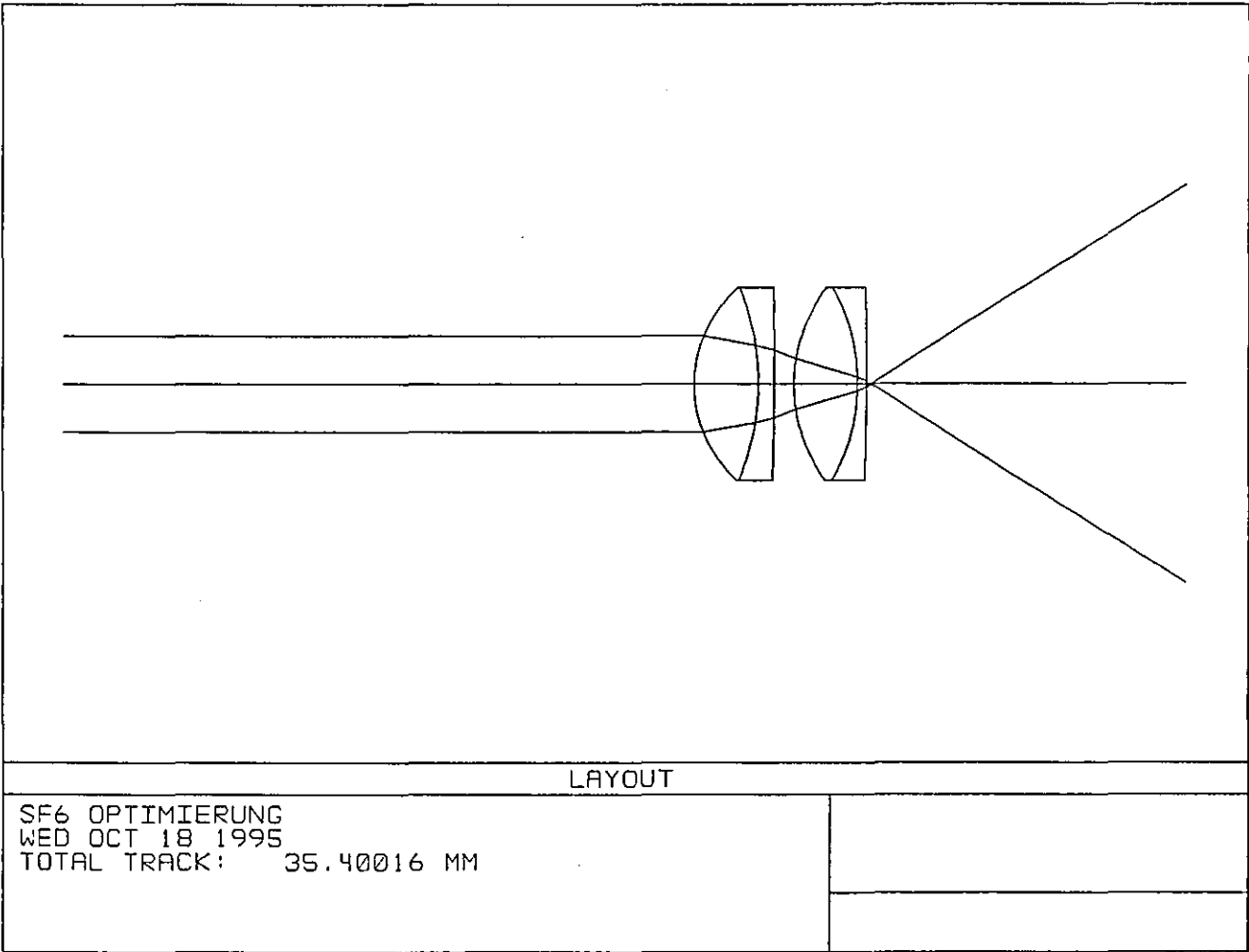
2. System data

```

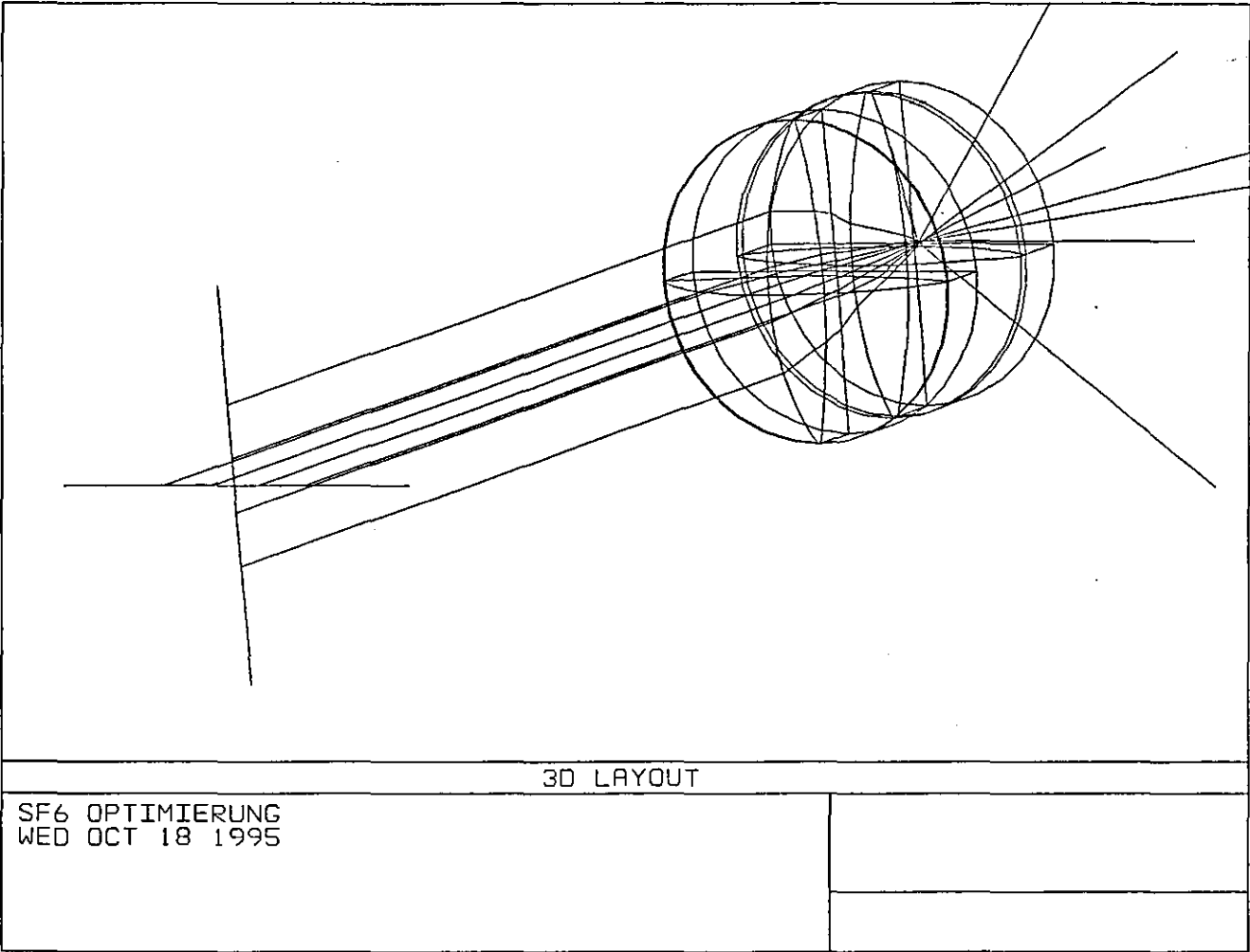
File : C:\UVE\MO.ZMX
Title: SF6 OPTIMIERUNG
System Aperture : Entrance Pupil Diameter
Eff. Focal Len. : 2.87722
Total Track : 25.5495
Image Space F/# : 0.959073
Working F/# : 0.939214
Obj. Space N.A. : 1.5e-010
Stop Radius : 1.5
Parax. Ima. Hgt.: 0
Parax. Mag. : 0
Entr. Pup. Dia. : 3
Entr. Pup. Pos. : 0
Exit Pupil Dia. : 0.462364
Exit Pupil Pos. : 0.611641
Maximum Field : 0
Primary Wave : 0.441000
Lens Units : Millimeters
Angular Mag. : 0
Active Config : 1 of 1

```

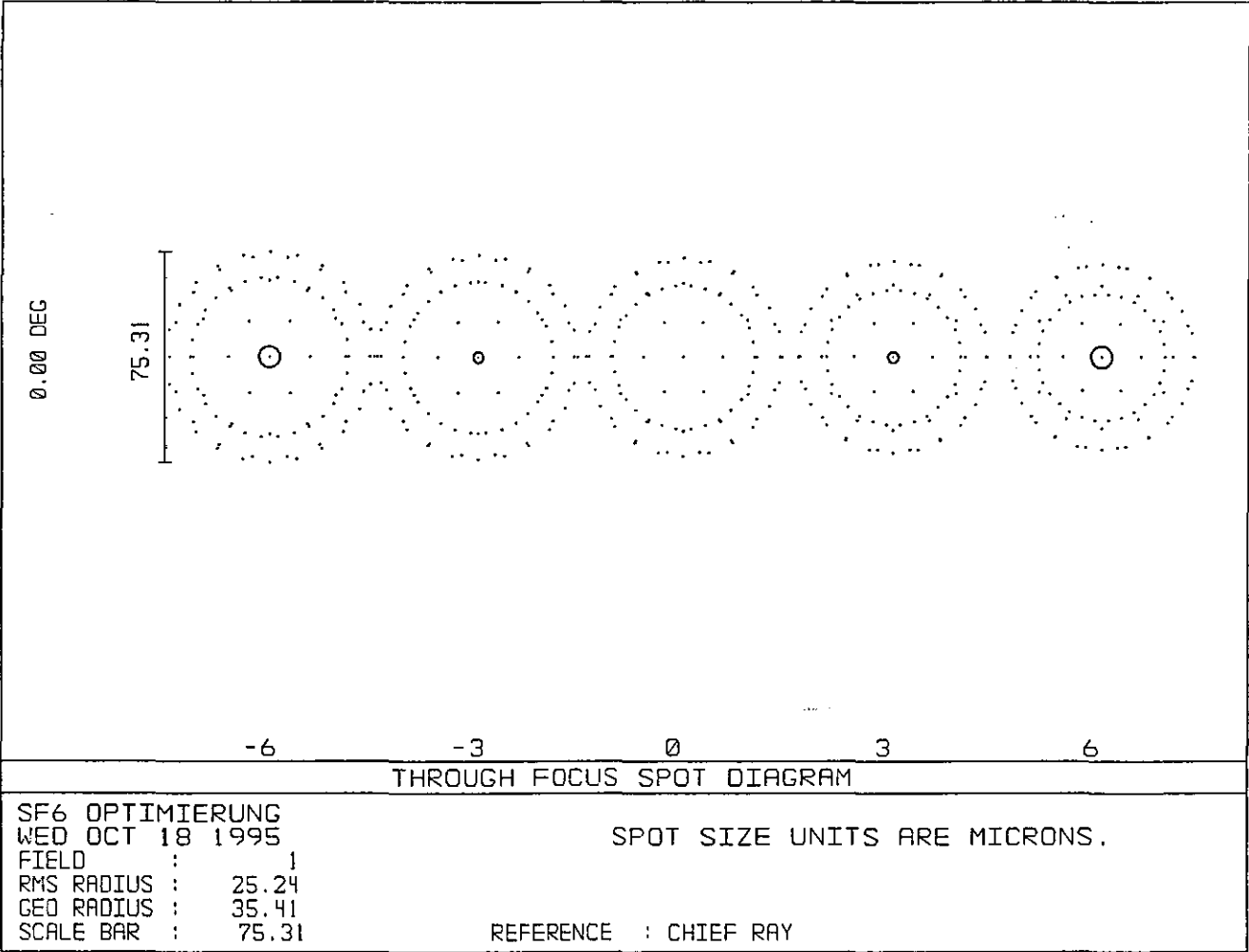
3. 2D-Layout



4. 3D-Layout



5. Through focus spot diagram



6. Gaussian beam parameters

Gaussian Beam Parameters

SF6 OPTIMIERUNG

Wed Oct 18 1995

Data for 0.4410 microns.

Units for waist, size, and waist-z distance are Millimeters.

Units for divergence semi-angle are radians.

Sur	Waist	Size	Waist Z	Divergence
OBJ	9.35831E+005	1.50000E+000	1.00000E+010	9.35831E-005
STO	1.50000E+000	1.50000E+000	0.00000E+000	9.35831E-005
2	1.50000E+000	4.43160E-004	-8.73542E+000	3.06760E-001
3	1.15658E+000	3.86914E-004	-4.86522E+000	3.48038E-001
4	1.03771E+000	3.81177E-004	-2.81784E+000	3.52854E-001
5	8.16755E-001	2.77286E-004	-2.97613E+000	4.68631E-001
6	2.67886E-001	2.69710E-004	-7.85525E-001	4.79886E-001
7	1.65578E-001	2.69259E-004	-3.17601E-001	4.80571E-001
IMA	3.40217E-004	2.69259E-004	3.98898E-004	4.80571E-001

RAY-TRACING MODEL OF THE TELESCOPE

CONTENTS	PAGE #
1. Surface data summary	F1
2. System data	F1
3. 2D-Layout	F2
4. 3D-Layout	F3
5. Through focus spot diagram (input plane)	F4
6. Through focus spot diagram (output plane)	F5

1. Surface data summary

SURFACE DATA SUMMARY:

Surf	Type	Radius	Thickness	Glass	Diameter	Conic
OBJ	STANDARD	Infinity	Infinity		0	0
STO	STANDARD	Infinity	10		0	0
2	STANDARD	45.67	1.5	BK7	6	0
3	STANDARD	3.8	13.88		6	0
4	STANDARD	-50.63	2	BK7	6	0
5	STANDARD	-10.17	10		6	0
IMA	STANDARD	Infinity	0		0	0

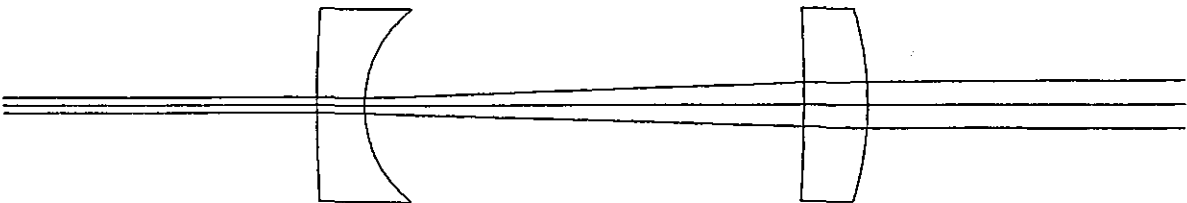
2. System data

```

File : C:\UVE\TELE.ZMX
Title: SF6 OPTIMIERUNG
System Aperture : Entrance Pupil Diameter
Eff. Focal Len. : -470.241
Total Track : 37.38
Image Space F/# : 470.241
Working F/# : 441.617
Obj. Space N.A. : 5e-011
Stop Radius : 0.5
Parax. Ima. Hgt. : 0
Parax. Mag. : 0
Entr. Pup. Dia. : 1
Entr. Pup. Pos. : 0
Exit Pupil Dia. : 2.66013
Exit Pupil Pos. : -137.081
Maximum Field : 0
Primary Wave : 0.441000
Lens Units : Millimeters
Angular Mag. : 0
Active Config : 1 of 1

```

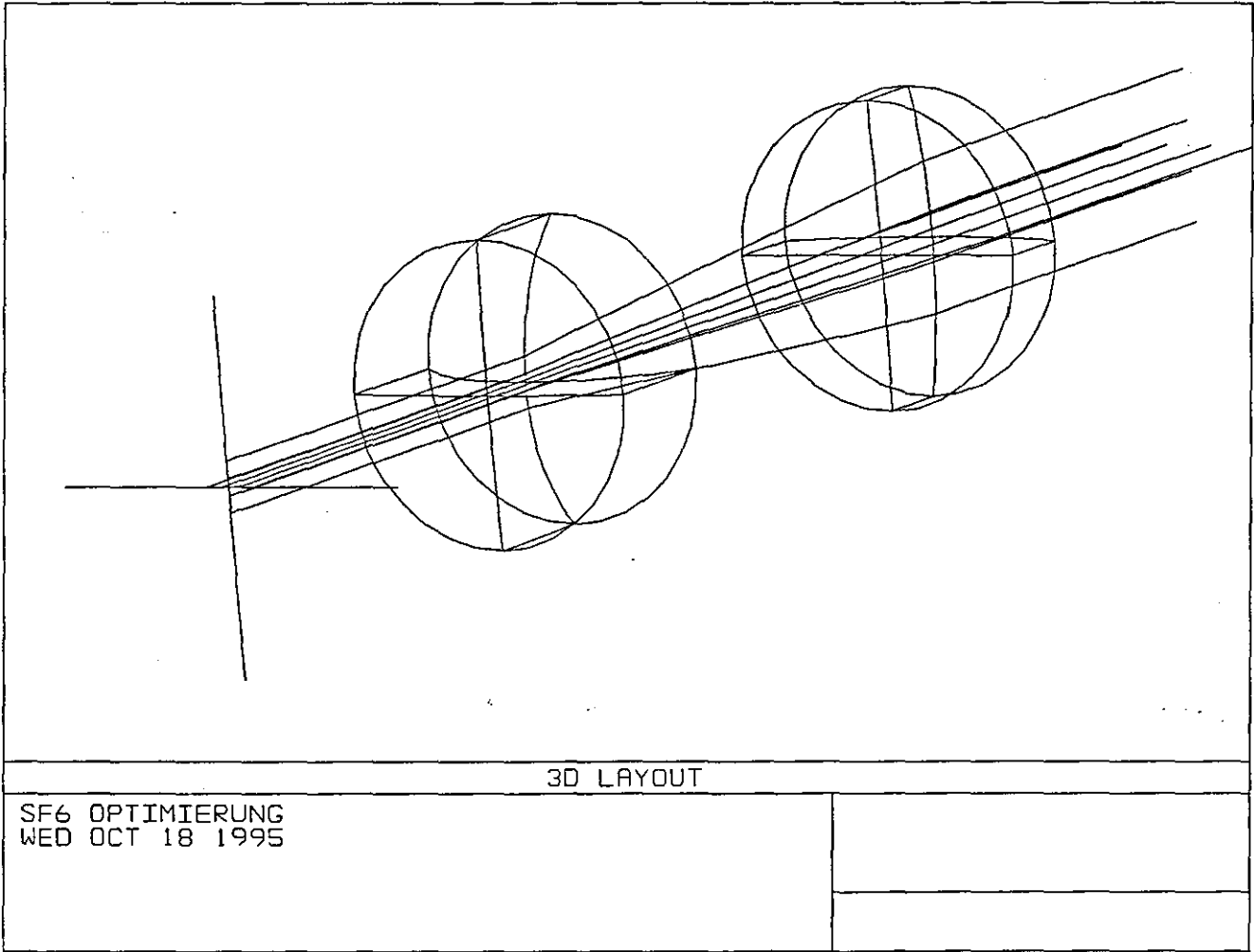
3. 2D-Layout



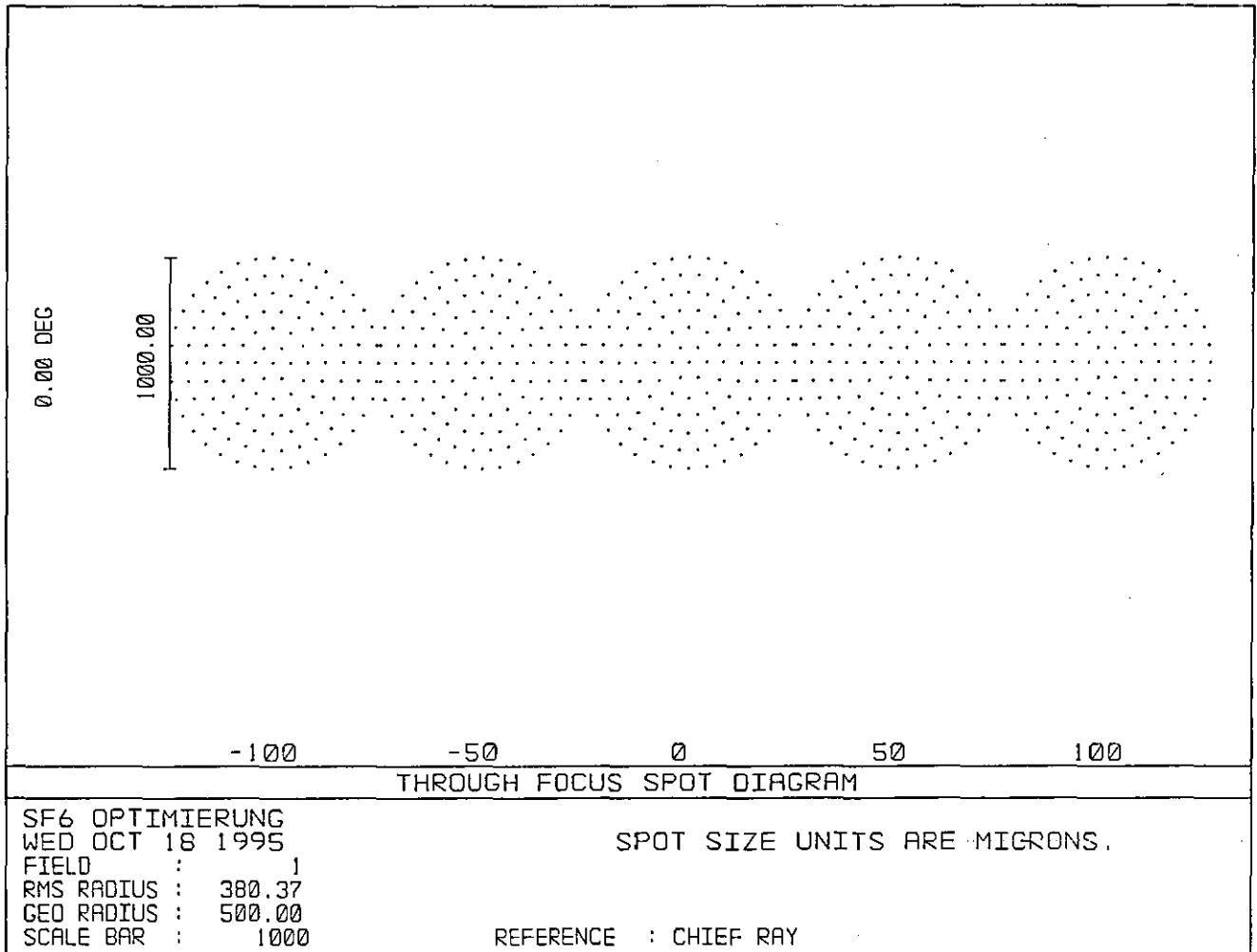
LAYOUT

SF6 OPTIMIERUNG
WED OCT 18 1995
TOTAL TRACK: 37.38000 MM

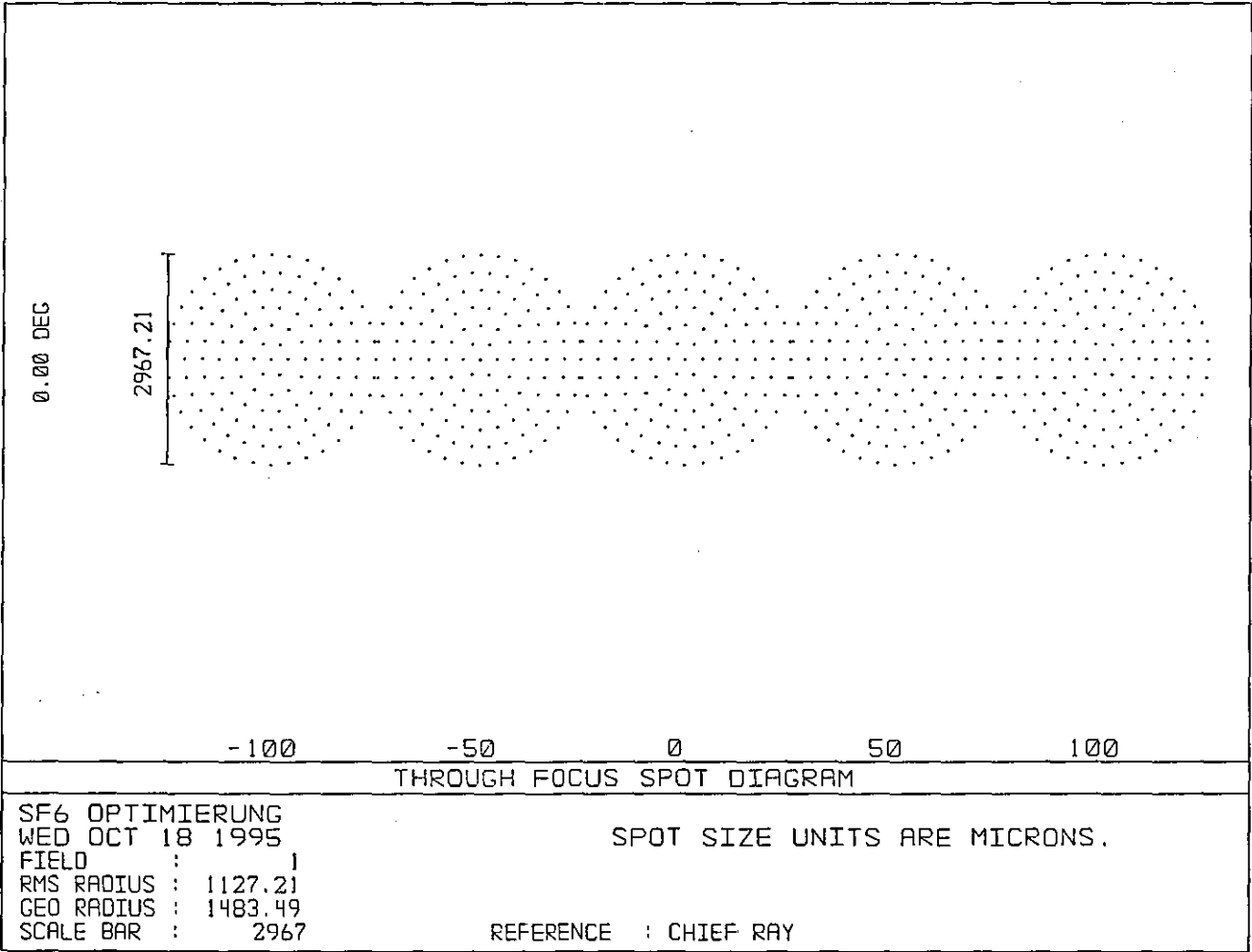
4. 3D-Layout



5. Through focus spot diagram (input plane)



6. Through focus spot diagram (output plane)



RAY-TRACING MODEL OF THE MEASURING LASER

CONTENTS	PAGE #
1. Surface data summary	G1
2. System data	G1
3. 2D-Layout (original)	G2
4. 2D-Layout (principle)	G3
5. 3D-Layout (principle)	G4

1. Surface data summary

SURFACE DATA SUMMARY:

Surf	Type	Radius	Thickness	Glass	Diameter	Conic
OBJ	STANDARD	Infinity	Infinity		0	0
STO	STANDARD	Infinity	40		0	0
2	STANDARD	45.67	1.5	BK7	6	0
3	STANDARD	3.8	14		6	0
4	STANDARD	-50.63	2	BK7	6	0
5	STANDARD	-10.17	700		6	0
6	STANDARD	Infinity	0		4.084543	0
7	STANDARD	Infinity	0		4.084543	0
8	STANDARD	3.99995	1.5	SF6	6.000037	0
9	STANDARD	-8.000001	0.5000016	BK7	6.000037	0
10	STANDARD	-99.99967	0.599999		6.000037	0
11	STANDARD	5.000001	1.999995	SF6	6.000037	0
12	STANDARD	-5.999984	0.3	BK7	6.000037	0
13	STANDARD	-100.0012	0.1494		6.000037	0
IMA	STANDARD	Infinity	0		0	0

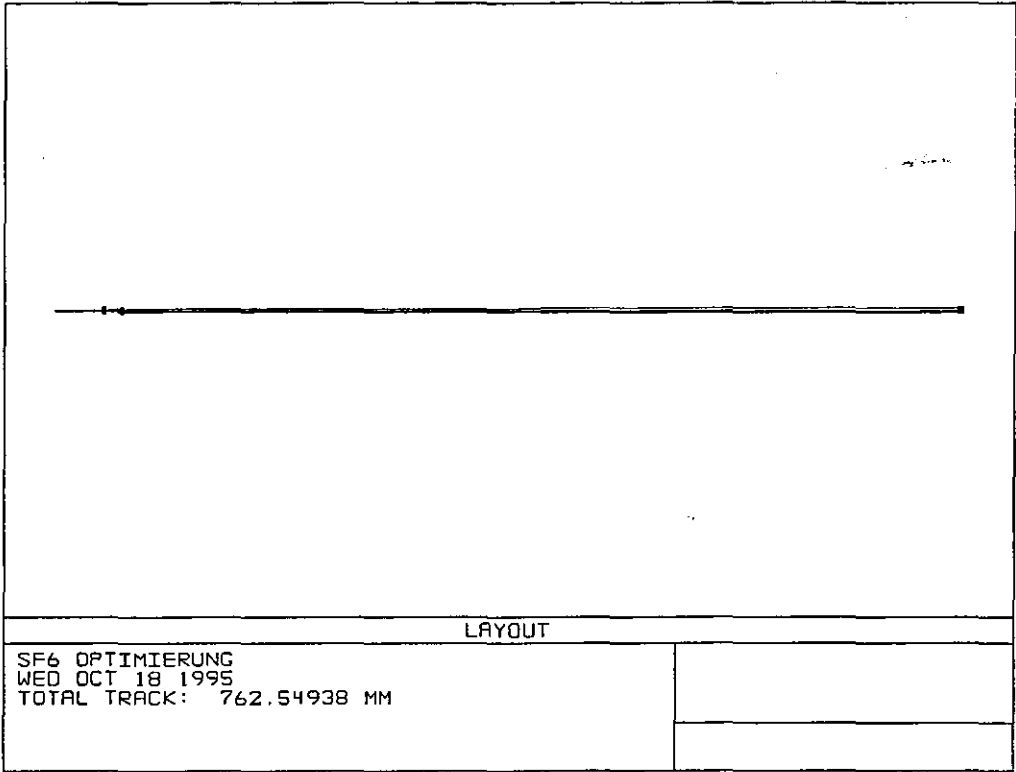
2. System data

```

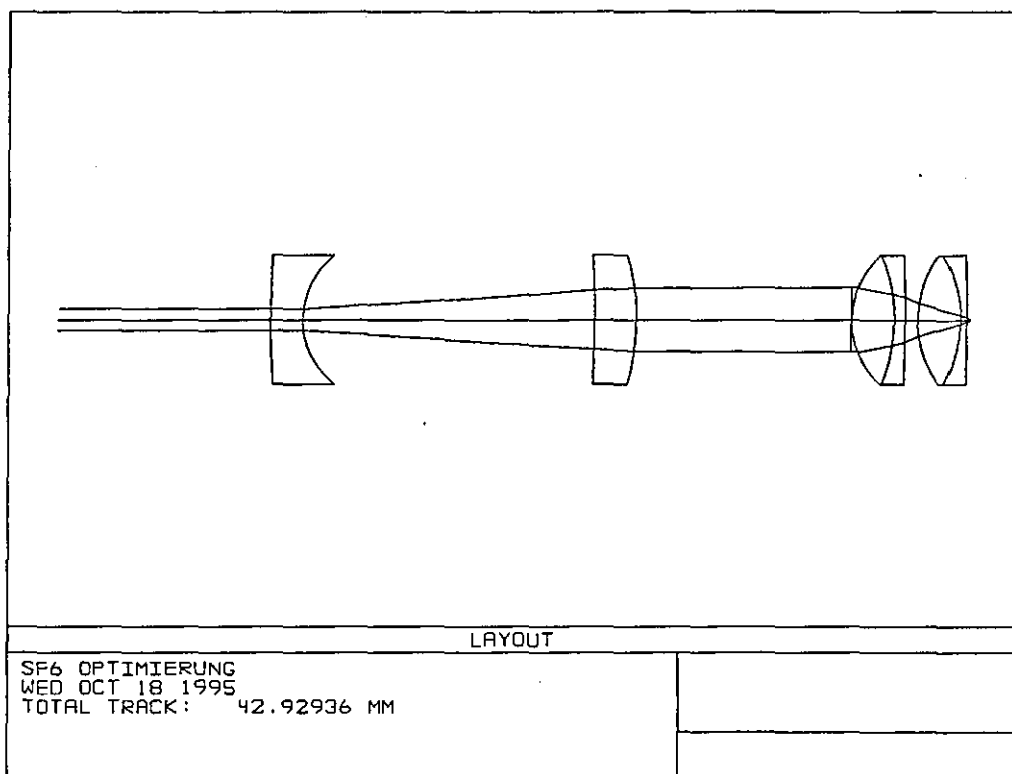
File : C:\UVE\RAYTRACE.ZMX
Title: SF6 OPTIMIERUNG
System Aperture : Entrance Pupil Diameter
Eff. Focal Len. : 0.692755
Total Track : 762.549
Image Space F/# : 0.692755
Working F/# : 0.651675
Obj. Space N.A. : 5e-011
Stop Radius : 0.5
Parax. Ima. Hgt.: 0
Parax. Mag. : 0
Entr. Pup. Dia. : 1
Entr. Pup. Pos. : 0
Exit Pupil Dia. : 0.00655005
Exit Pupil Pos. : 0.271701
Maximum Field : 0
Primary Wave : 0.441000
Lens Units : Millimeters
Angular Mag. : 0
Active Config : 1 of 1

```

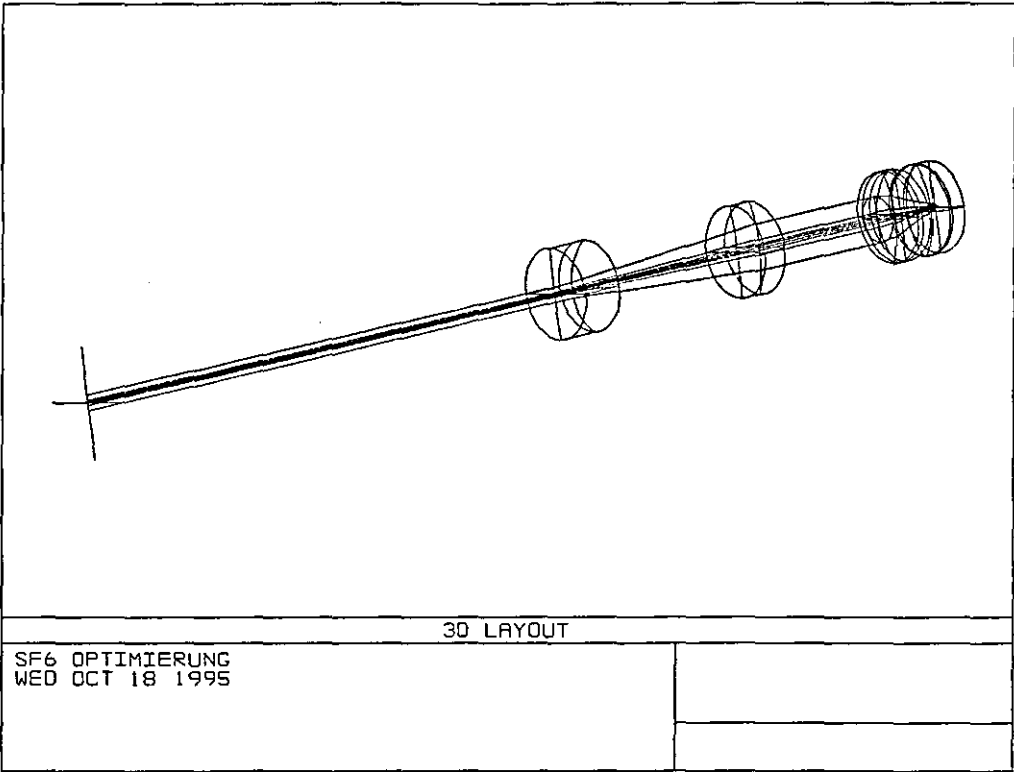
3. 2D-Layout (original)



4. 2D-Layout (principle)



5. 3D-Layout (principle)



**DERIVATION OF THE
MATHEMATICAL SENSOR MODEL**

CONTENTS	PAGE #
1. Derivation schematic	H1 - H2
2. Derivation	H3 - H8

1. Derivation schematic

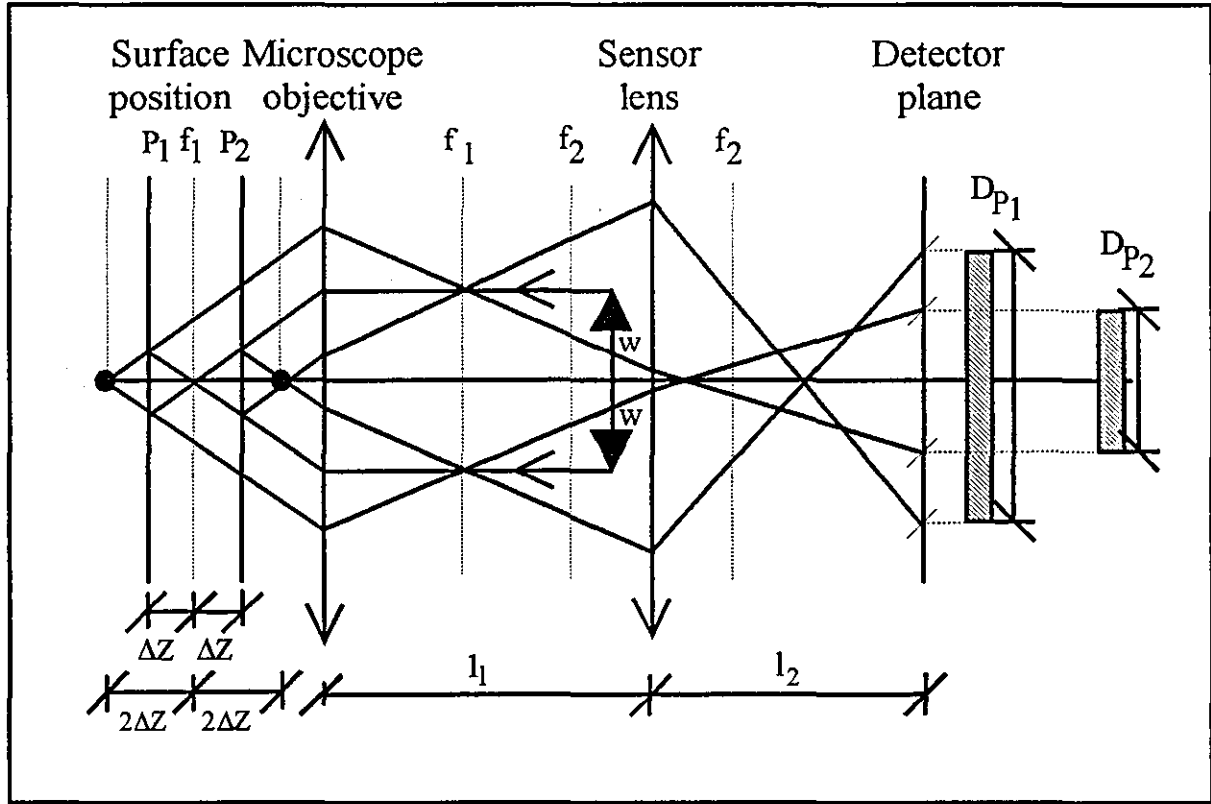


Fig.H1: Principal of the beam guiding system of the sensor

A surface in distance ΔZ to the focal plane f_1 of the microscope objective results in a light spot with the diameter D in the detector plane.

The mathematical description of the sensor will be investigated in three principal steps.

a.) For the description of the complete system, the influence of the focal length f_1 of the microscope objective and the distance l_1 between the microscope objective and the sensor lens will be investigated. They both affect the height h in which and the angle α under which the principle beams will contacts the sensor lens as a function of the ΔZ and the laser beam semi-diameter w . Therefore the following principle relations are required:

$$h = f(w, f_1, l_1, \Delta Z) \quad (\text{H1})$$

$$\alpha = f(w, f_1, l_1, \Delta Z) \quad (\text{H2})$$

b.) Then the influence of the parameter h and α in conjunction with the focal length f_2 of the sensor lens and the distance l_2 between the sensor lens and the detector plane to the light spot diameter D will be investigated. Therefore the following fundamental relation is required:

$$D = f(h, \alpha, f_1, l_2) \quad (\text{H3})$$

c.) Following the above investigation, the results of the investigations under a.) and b.) will be combined to the mathematical sensor model leading to the following relation:

$$D = f(w, f_1, f_2, l_1, l_2, \Delta Z) \quad (\text{H4})$$

2. Derivation

a.) Determination of the transformation characteristic of the microscope objective

A surface in the distance ΔZ to the focal plane f_1 of the microscope objective has the result that the microscope objective images a point whose apparent location is at the position

$$a_1 = f_1 + 2\Delta Z \quad (H5)$$

This point will be imaged so that the image location can be found using the lens equation

$$\frac{1}{f} = \frac{1}{a} + \frac{1}{a'} \quad (H6)$$

where f is the focal length, a the distance of the object to the lens and a' is the distance of the image to the lens. Using equation (H6) the position of the image is

$$a_1' = \frac{f_1(f_1 + 2\Delta Z)}{f_1 + 2\Delta Z - f_1} = f_1 \frac{(f_1 + 2\Delta Z)}{2\Delta Z} \quad (H7)$$

As a result of the location of a_2 and the fact that every beam has a diameter w of the input beam at the back focal plane of the microscope objective, the principle beam propagation between the lenses can be drawn as seen in the following figure.

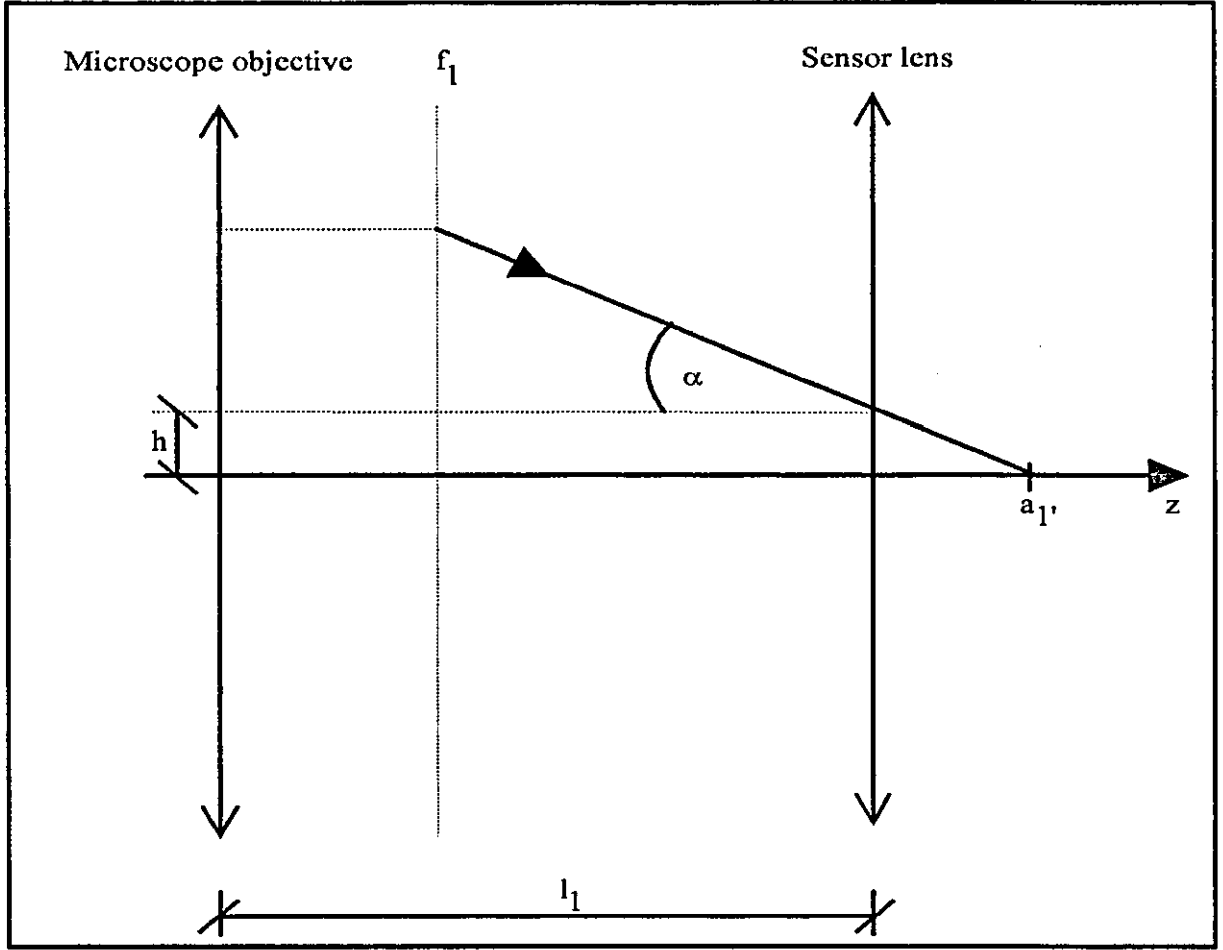


Fig. H2: Geometry of the beam propagation between the lenses

Using the information of figure H2 and the trigonometric law, the following expression can be found:

$$\tan(\alpha) = \frac{w}{a_1' - f_1} \quad (\text{H8})$$

Using this equation and equation (H7), the angle between the incident beam and the lens plane can be found:

$$\alpha = \arctan \left(\frac{w}{f_1 \frac{(f_1 + 2\Delta z)}{2\Delta z} - f_1} \right) \quad (\text{H9})$$

Also, information about the height h at which the principal beams contact the lens can be found using the law of similar triangles for the geometry sketched in the above figure

$$\frac{h}{a_1' - l_1} = \frac{w}{a_1' - f_1} \quad (\text{H10})$$

This expression can be used to determine the height h by combination with equation (H7)

$$h = \frac{w(f_1 \frac{(f_1 + 2\Delta Z)}{2\Delta Z} - l_1)}{f_1 \frac{(f_1 + 2\Delta Z)}{2\Delta Z} - f_1} \quad (\text{H11})$$

b.) Determination of the transformation characteristic of the sensor lens

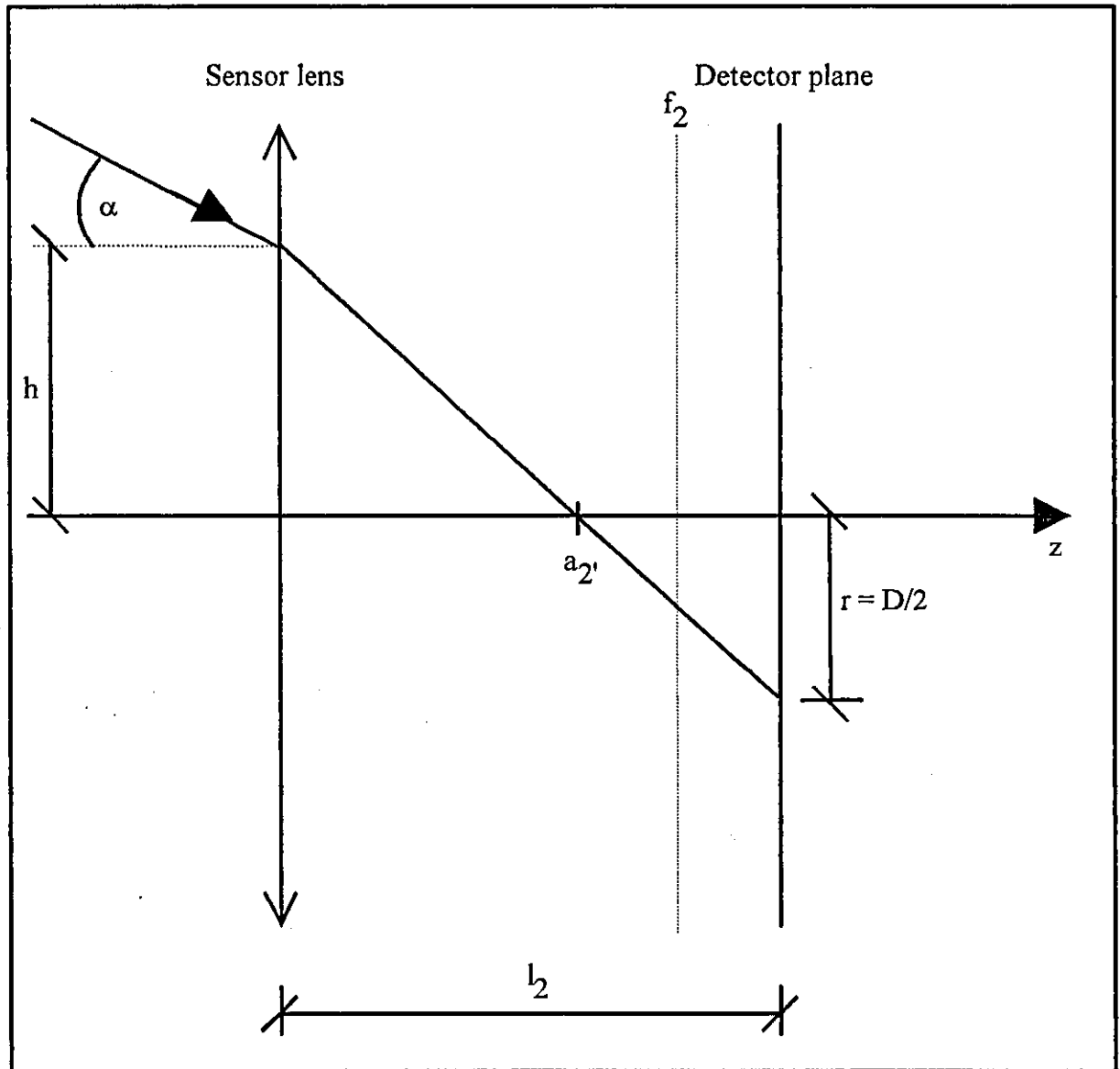


Fig.H3: Geometry of the beam propagation between the sensor lens and the detector plane

Using geometrical laws, the following equation can be found:

$$\frac{r}{l_2 - a_2'} = \frac{h}{a_2'} \quad (\text{H12})$$

where r indicates the semi-diameter of the light spot at the focal plane.

As illustrated in the above figure H3, the incident beam contacts the surface of the sensor lens at the height h and under the angle α so that the point that will be imaged by the lens is apparently located at

$$a_2 = \frac{h}{\tan(\alpha)} \quad (\text{H13})$$

To find the location of the image of this point, equation (H6) can be used

$$a_2' = \frac{a_2 f_2}{a_2 - f_2} \quad (\text{H14})$$

Putting equation (H14) into equation (H12), the expression for the semi-diameter of the light spot is found.

$$r = \frac{h(l_2 - \frac{a_2 f_2}{a_2 - f_2})}{\frac{a_2 f_2}{a_2 - f_2}} \quad (\text{H15})$$

$$r = \frac{h(l_2 a_2 - l_2 f_2 - a_2 f_2)}{a_2 f_2} \quad (\text{H16})$$

Putting equation (H13) into this expression, the desired function is found

$$r = \frac{h(l_2 \frac{h}{\tan(\alpha)} - l_2 f_2 - f_2 \frac{h}{\tan(\alpha)}) \tan(\alpha)}{h f_2} \quad (\text{H17})$$

$$r = \frac{h(l_2 - f_2)}{f_2} - l_2 \tan(\alpha) \quad (\text{H18})$$

c.) Combination of the results of the investigations und a.) and b.)

The equations (H9) and (H11) have to be put into the equation (H18) in order to combine the results of the investigations under a.) and b.).

$$r = \frac{w(f_1 \frac{(f_1 + 2\Delta Z)}{2\Delta Z} - l_1)(l_2 - f_2)}{f_2(f_1 \frac{(f_1 + 2\Delta Z)}{2\Delta Z} - f_1)} - \frac{l_2 w f_2}{f_2(f_1 \frac{(f_1 + 2\Delta Z)}{2\Delta Z} - f_1)} \quad (H19)$$

which reduces to

$$r = w \left\{ \frac{l_2 - f_2}{f_2} + 2 \frac{(f_1 l_2 - f_1 f_2 - l_1 l_2 + l_1 f_2 - l_2 f_2)}{f_1^2 f_2} \Delta Z \right\} \quad (H20)$$

This leads to the diameter of the light spot

$$D = 2r = D_0 + K\Delta Z \quad (H21)$$

with the initial diameter

$$D_0 = 2w \frac{(l_2 - f_2)}{f_2} \quad (H22)$$

and the sensitivity constant given by

$$K = 4w \frac{(f_1 l_2 - f_1 f_2 - l_1 l_2 + l_1 f_2 - l_2 f_2)}{f_1^2 f_2} \quad (H23)$$

RAY-TRACING MODEL OF THE SENSOR

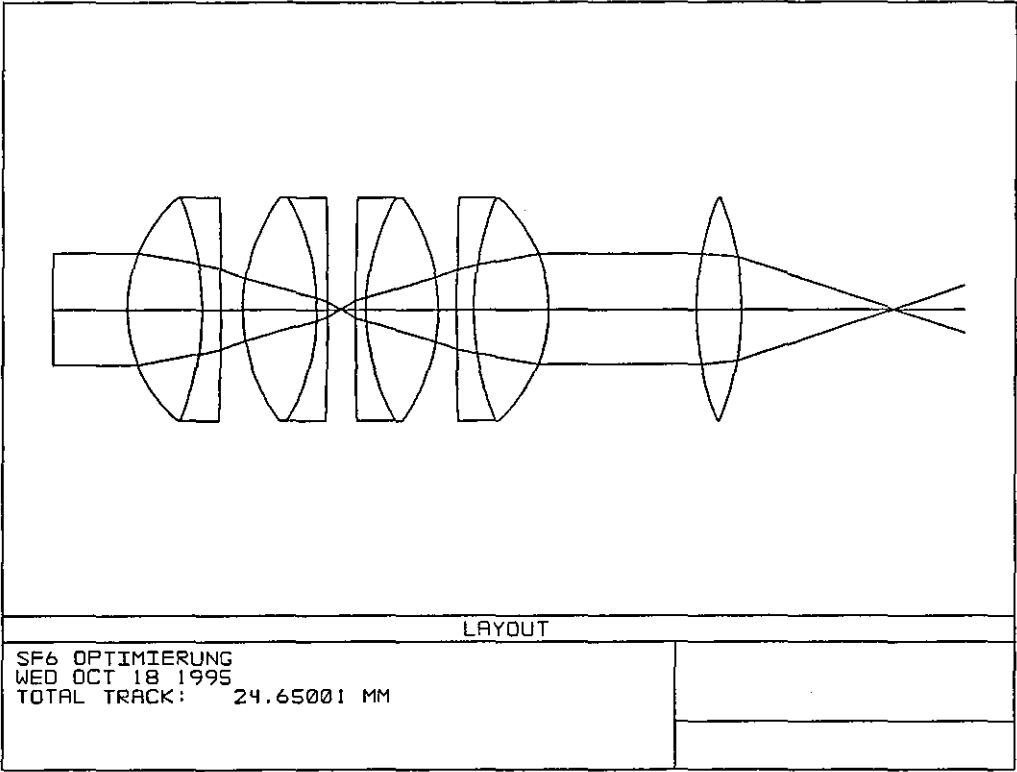
CONTENTS	PAGE #
1. Surface data summary ($\Delta Z = 0$)	I1
2. System data ($\Delta Z = 0$)	I2
3. Spot diagram ($\Delta Z = 0$)	I3
4. Surface data summary ($\Delta Z = -100$)	I4
5. System data ($\Delta Z = -100$)	I5
6. Spot diagram ($\Delta Z = -100$)	I6
7. Surface data summary ($\Delta Z = 100$)	I7
8. System data ($\Delta Z = 100$)	I8
9. Spot diagram ($\Delta Z = 100$)	I9

1. Surface data summary ($\Delta z = 0$)

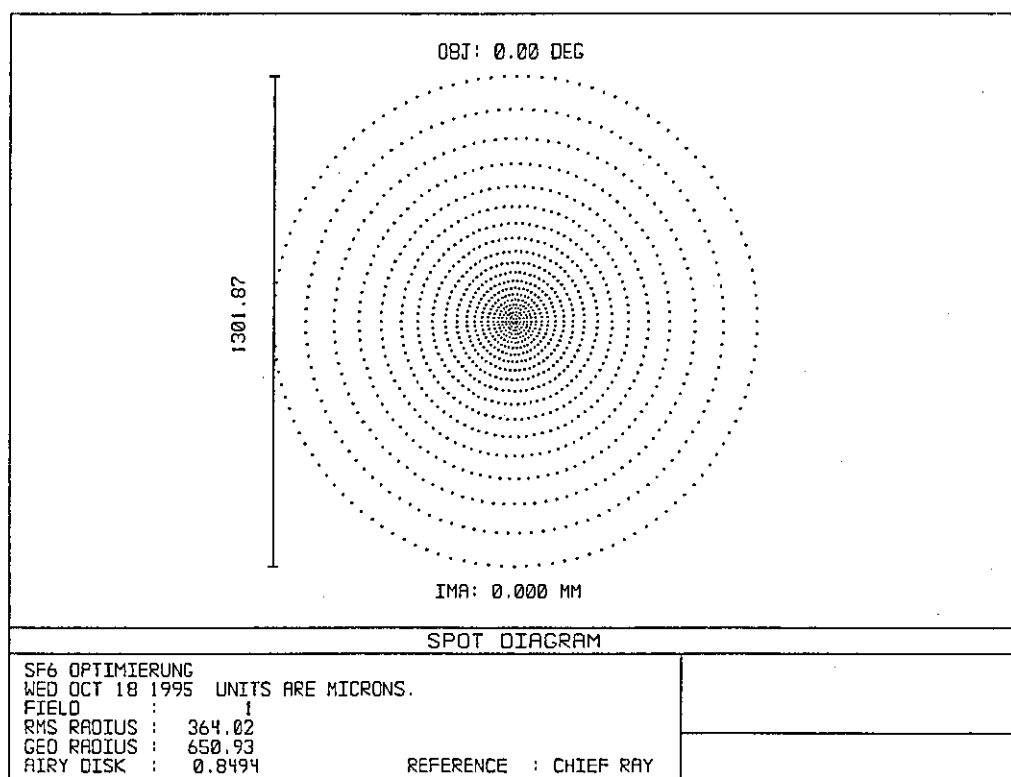
SURFACE DATA SUMMARY:

Surf	Type	Radius	Thickness	Glass	Diameter	Conic
OBJ	STANDARD	Infinity	Infinity		0	0
STO	STANDARD	Infinity	2		3	0
2	STANDARD	4	2	SF6	6	0
3	STANDARD	-8	0.5	SF1	6	0
4	STANDARD	-99	0.6		6	0
5	STANDARD	5	2	SF6	6	0
6	STANDARD	-6	0.3000048	SF1	6	0
7	STANDARD	-100	0.76		6	0
8	STANDARD	100	0.3	SF1	6	0
9	STANDARD	6	2	SF6	6	0
10	STANDARD	-5	0.5		6	0
11	STANDARD	100	0.5	SF1	6	0
12	STANDARD	8	2	SF6	6	0
13	STANDARD	-4	4		6	0
14	STANDARD	8	1.2	SF6	6	0
15	STANDARD	-8	6		6	0
IMA	STANDARD	Infinity	0		0	0

2. 2D-Layout ($\Delta z = 0$)



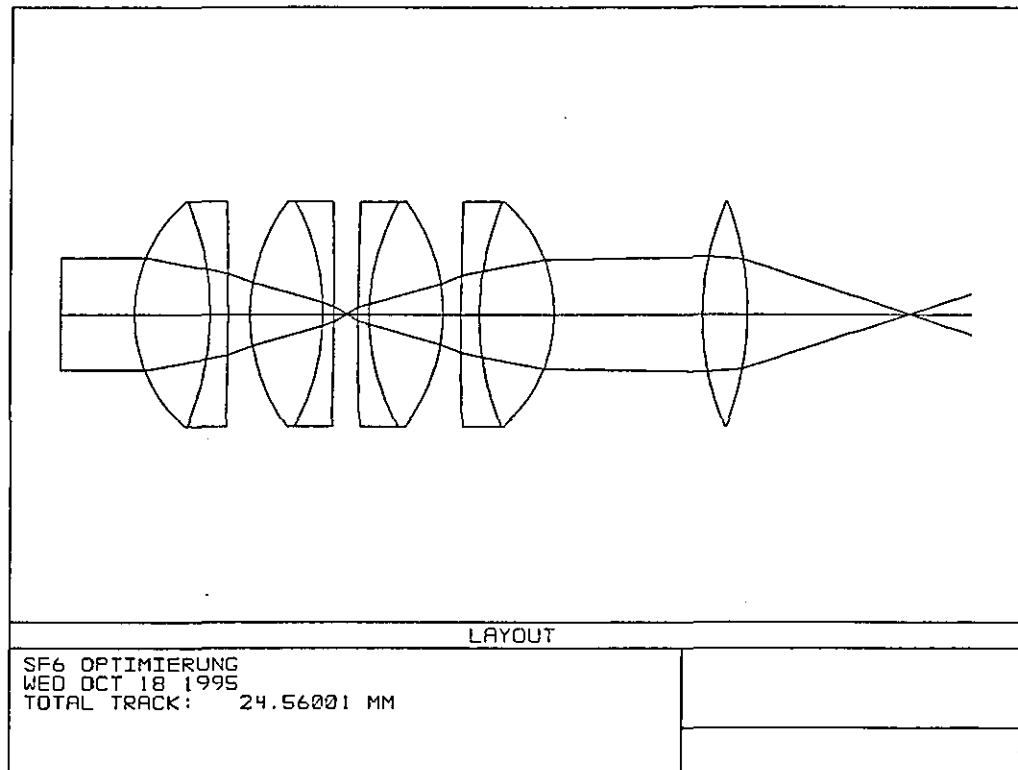
3. Spot diagram ($\Delta z = 0$)

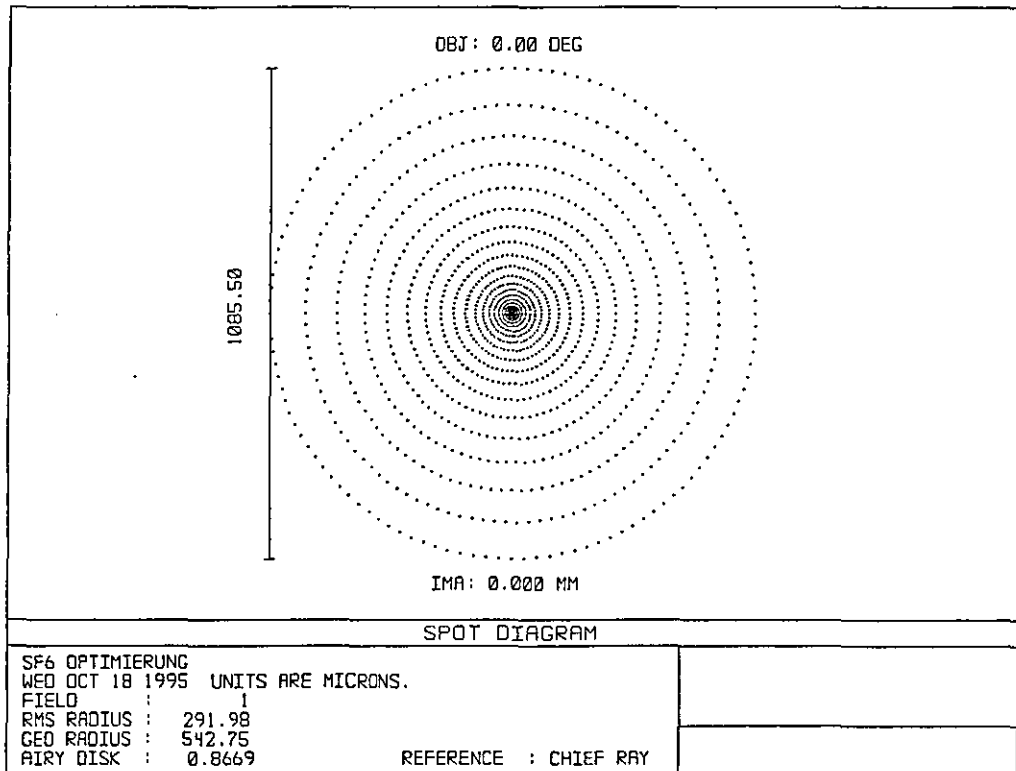


4. Surface data summary ($\Delta z = -100\mu\text{m}$)

SURFACE DATA SUMMARY:

Surf	Type	Radius	Thickness	Glass	Diameter	Conic
OBJ	STANDARD	Infinity	Infinity		0	0
STO	STANDARD	Infinity	2		3	0
2	STANDARD	4	2	SF6	6	0
3	STANDARD	-8	0.5	SF1	6	0
4	STANDARD	-99	0.6		6	0
5	STANDARD	5	2	SF6	6	0
6	STANDARD	-6	0.3000048	SF1	6	0
7	STANDARD	-100	0.66		6	0
8	STANDARD	100	0.3	SF1	6	0
9	STANDARD	6	2	SF6	6	0
10	STANDARD	-5	0.5		6	0
11	STANDARD	100	0.5	SF1	6	0
12	STANDARD	8	2	SF6	6	0
13	STANDARD	-4	4		6	0
14	STANDARD	8	1.2	SF6	6	0
15	STANDARD	-8	6		6	0
IMA	STANDARD	Infinity	0		0	0

5. 2D-Layout ($\Delta z = -100\mu\text{m}$)

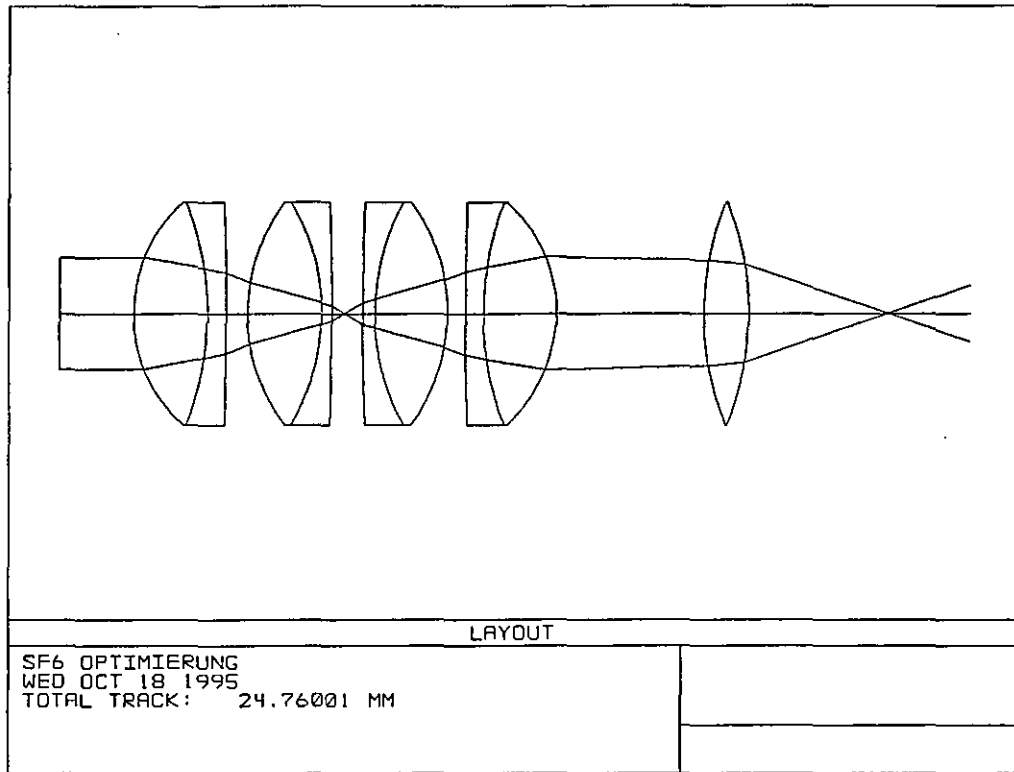
6. Spot diagram ($\Delta z = -100\mu\text{m}$)

7. Surface data summary ($\Delta z = 100\mu\text{m}$)

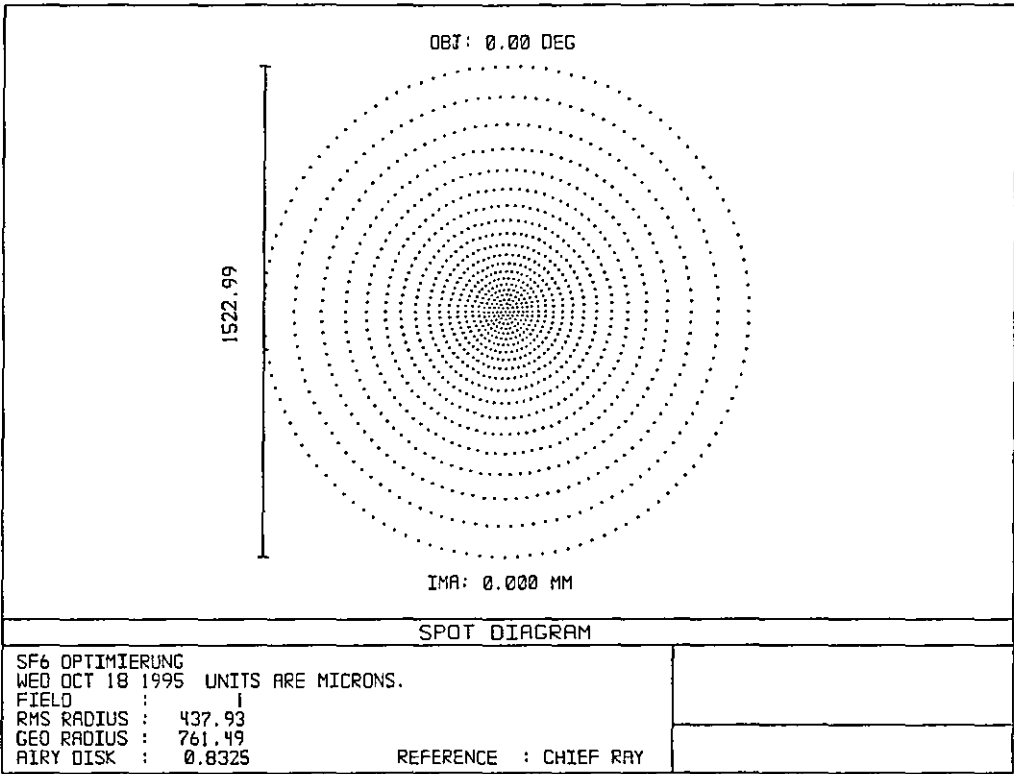
SURFACE DATA SUMMARY:

Surf	Type	Radius	Thickness	Glass	Diameter	Conic
OBJ	STANDARD	Infinity	Infinity		0	0
STO	STANDARD	Infinity	2		3	0
2	STANDARD	4	2	SF6	6	0
3	STANDARD	-8	0.5	SF1	6	0
4	STANDARD	-99	0.6		6	0
5	STANDARD	5	2	SF6	6	0
6	STANDARD	-6	0.3000048	SF1	6	0
7	STANDARD	-100	0.86		6	0
8	STANDARD	100	0.3	SF1	6	0
9	STANDARD	6	2	SF6	6	0
10	STANDARD	-5	0.5		6	0
11	STANDARD	100	0.5	SF1	6	0
12	STANDARD	8	2	SF6	6	0
13	STANDARD	-4	4		6	0
14	STANDARD	8	1.2	SF6	6	0
15	STANDARD	-8	6		6	0
IMA	STANDARD	Infinity	0		0	0

8. 2D-Layout ($\Delta z = 100\mu\text{m}$)

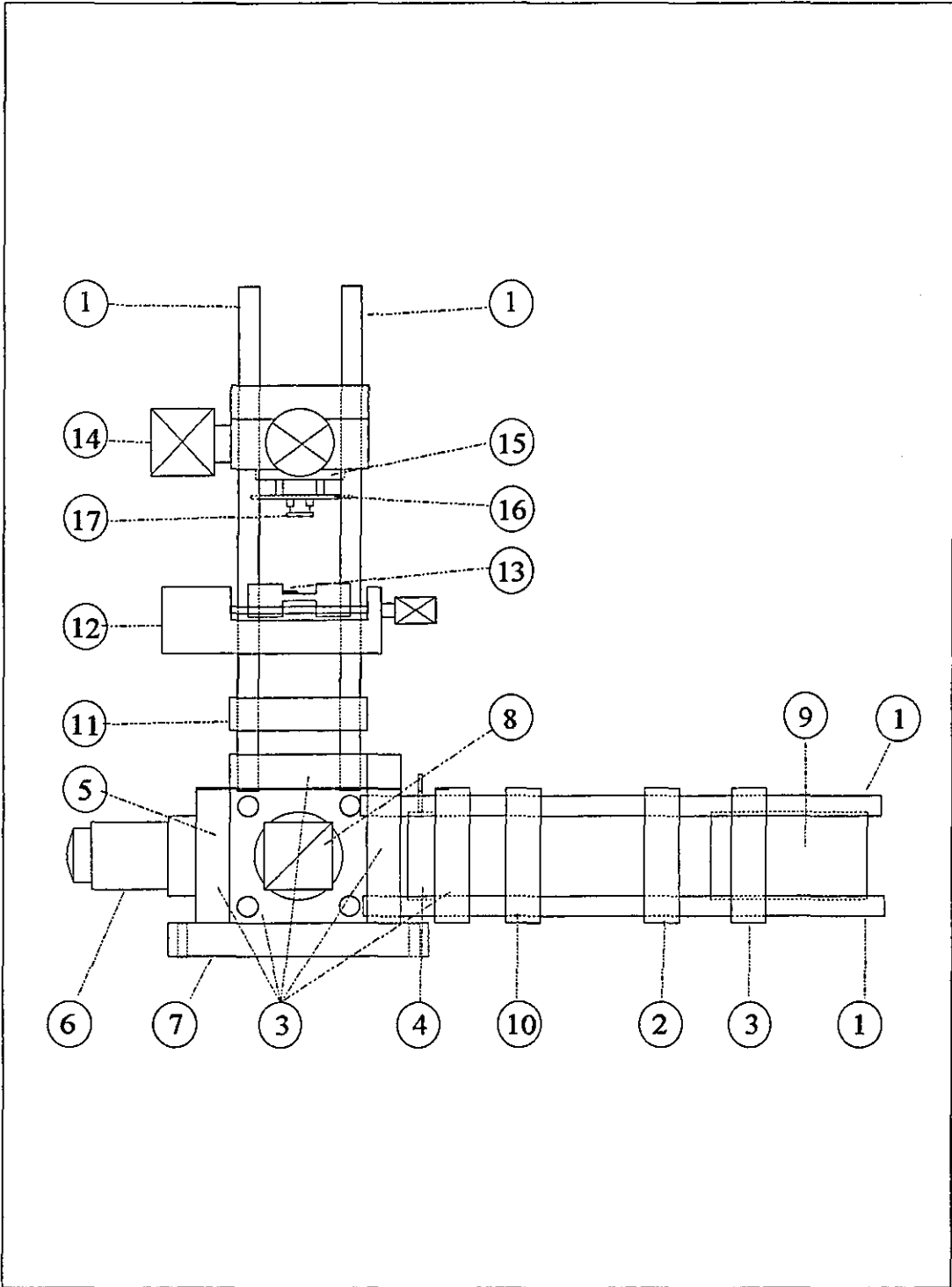


9. Spot diagram ($\Delta z = 100\mu\text{m}$)



**CONSTRUCTION OF THE
EXPERIMENTAL SENSOR**

CONTENTS	PAGE #
1. Assembly schematic	J1
2. Parts list	J2



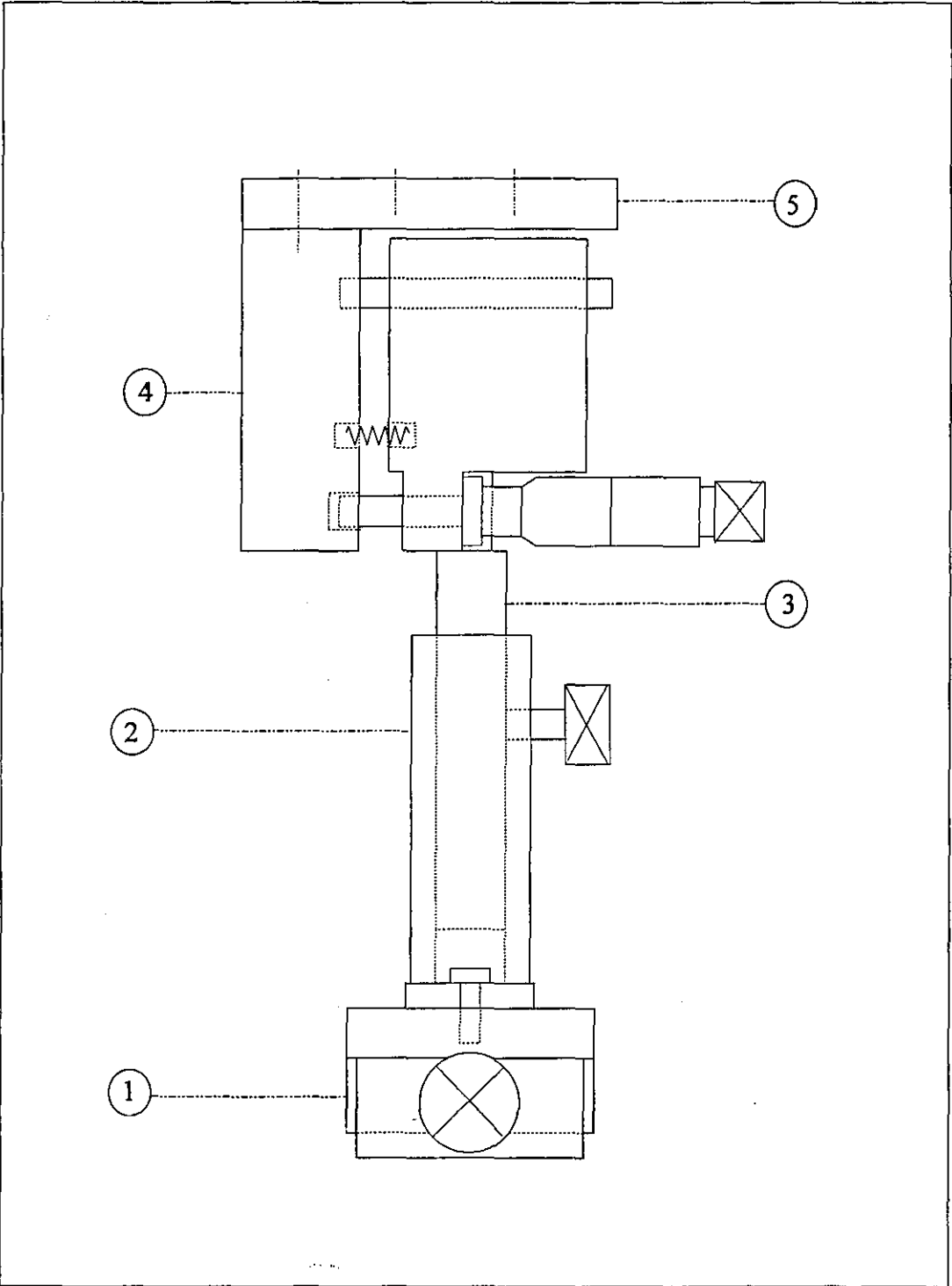
Part-No.:	Title: Assembly schematic of the experimental sensor
Scale:Arbitrary	
Material:	
Date: October 1995	FHO-Fachhochschule Ostfriesland -Institut für Lasertechnik -
ENGR.: Dipl.-Ing. U. Samuels	

2. Parts list

<u>Part No.</u>	<u>Description</u>
1	Precision rods
2	Lens mount with lens $f = -20\text{mm}$
3	Mount
4	Iris
5	Microscope objective adapter
6	Microscope objective
7	Sensor base plate
8	Beam splitter cube
9	Semiconductor laser
10	Lens mount with lens $f = 50\text{mm}$
11	Lens mount with lens $f = 20\text{mm}$
12	Single axis alignment system
13	Knife edge
14	Dual axis alignment system
15	PSD mount
16	PCB for the PSD
17	PSD

CONSTRUCTION OF THE SENSOR TRANSLATOR

CONTENTS	PAGE #
1. Assembly schematic	K1
2. Parts list	K2



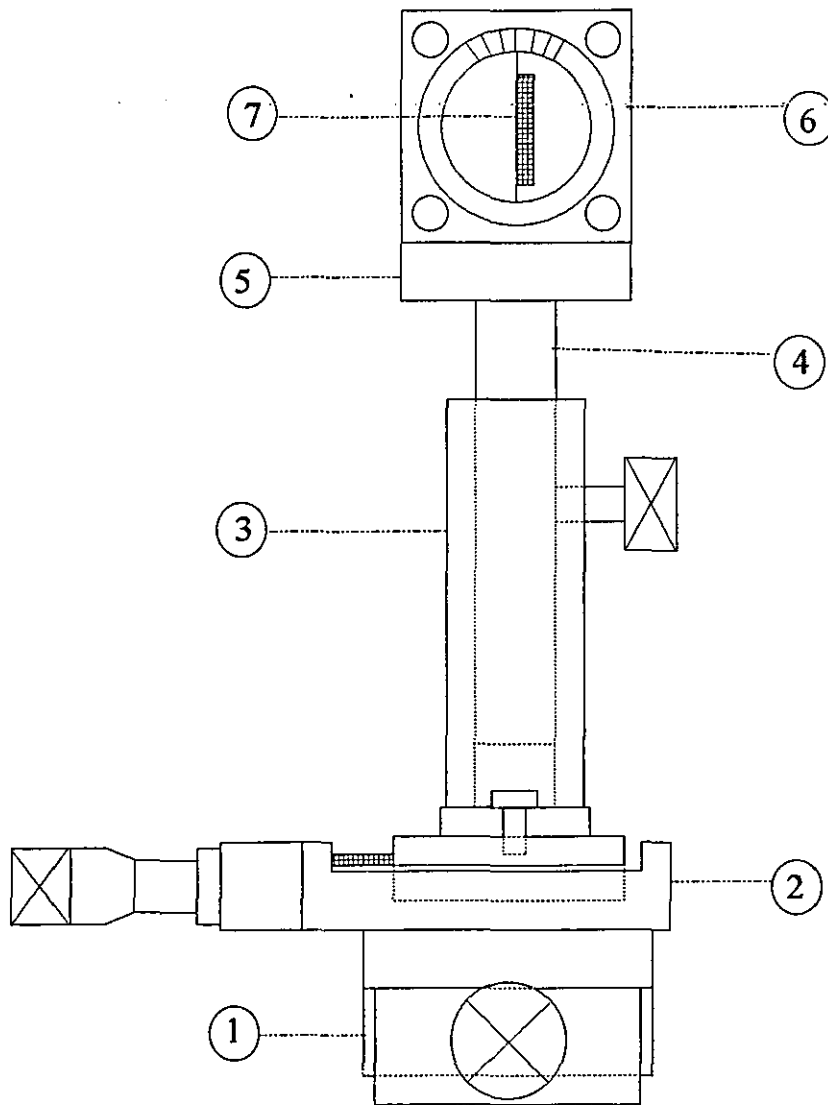
Part-No.:	Title: Assembly schematic of the sensor translator
Scale: Arbitrary	
Material:	
Date: October 1995	FHO-Fachhochschule Ostfriesland -Institut für Lasertechnik -
ENGR.: Dipl.-Ing. U. Samuels	

2. Parts list

<u>Part No.</u>	<u>Description</u>
1	Carriage
2	Post
3	Post holder
4	Linear axis
5	Sensor base plate

CONSTRUCTION OF THE SURFACE TILT SYSTEM

CONTENTS	PAGE #
1. Assembly schematic	L1
2. Parts list	L2



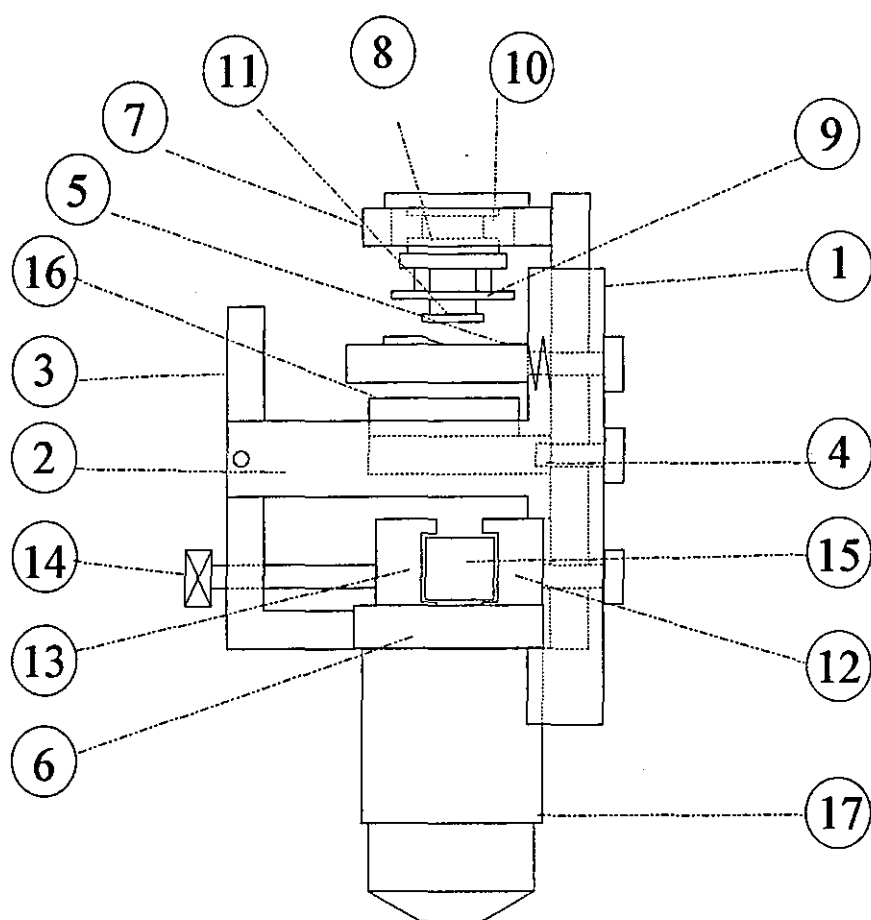
Part-No.:	Title: Assembly schematic of the surface tilt system
Scale: Arbitrary	
Material:	
Date: October 1995	FHO-Fachhochschule Ostfriesland -Institut für Lasertechnik -
ENGR.: Dipl.-Ing. U. Samuels	

2. Parts list

<u>Part No.</u>	<u>Description</u>
1	Carriage
2	Linear axis
3	Post
4	Post holder
5	Adapter
6	Micro rotation stage
7	Substrate

CONSTRUCTION OF THE OPTIMISED PROCESSING HEAD

CONTENTS	PAGE #
1. Assembly schematic	M1
2. Parts list	M2
3. Blue prints	
M/1 Base plate	M3
M/2 Connection plate	M4
M/3 Adapter for the piezo translator	M5
M/4 Lens mount	M6
M/5 Knife edge mount	M7
M/6 Microscope objective mount	M8
M/7 PSD adjustment unit	M9
M/8 PSD mount	M10
M/12, M/13 Beam splitter mount a and b	M11



Part-No.:

Scale: Arbitrary

Material:

Date: October 1995

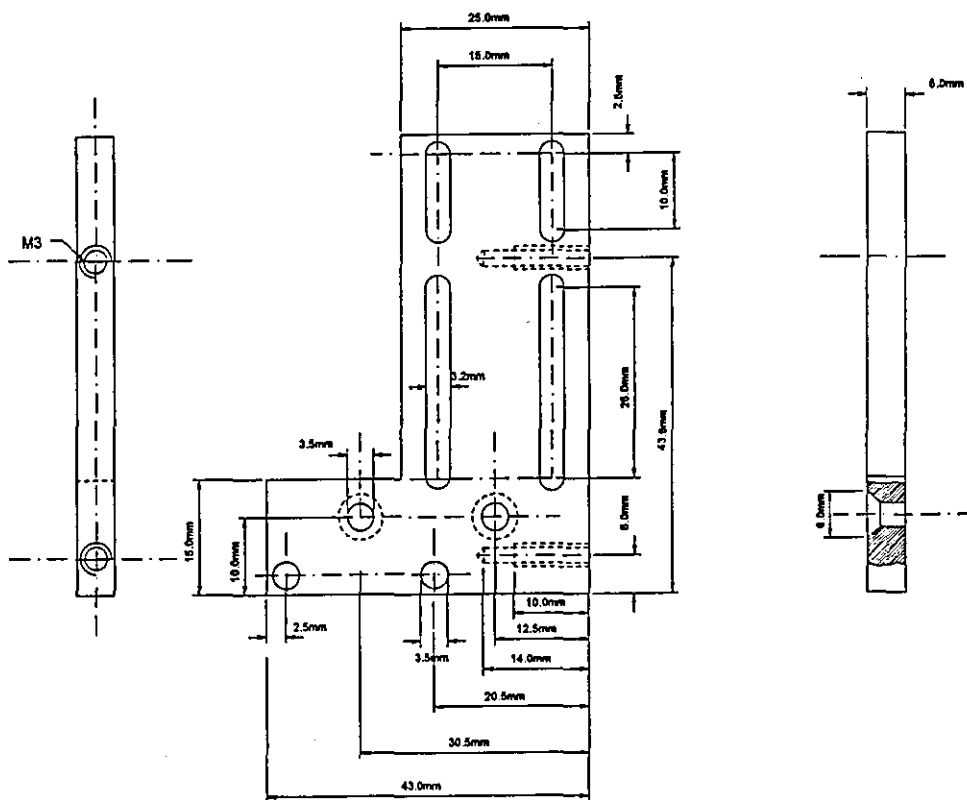
ENGR.: Dipl.-Ing. U. Samuels

Title:

Assembly schematic of the
optimised processing headFHO-Fachhochschule Ostfriesland
-Institut für Lasertechnik -

2. Parts list

<u>Part No.</u>	<u>Description</u>
1	Base plate
2	Connection plate
3	Adapter for the piezo translator
4	Lens mount with lens $f = 20\text{mm}$
5	Beam stop mount with beam stop
6	Microscope objective mount
7	PSD adjustment unit
8	PSD mount
9	PCB for the PSD
10	Leaf spring
11	PSD
12	Beam splitter holder a
13	Beam splitter holder b
14	Threaded rod
15	Beam splitter
16	Interference filter
17	Microscope objective



Part-No.: M/1

Scale: 1:1

Material: Aluminium

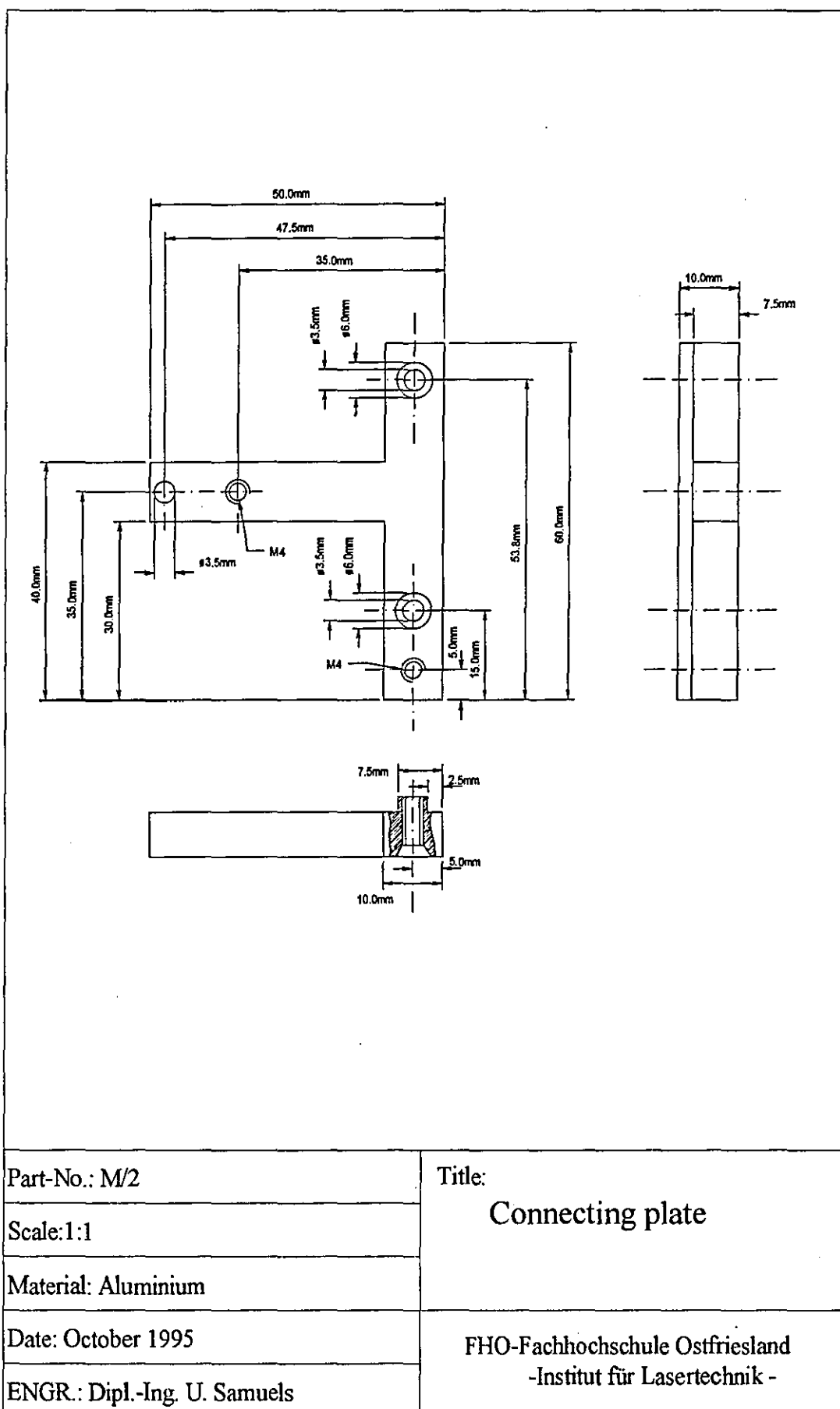
Date: October 1995

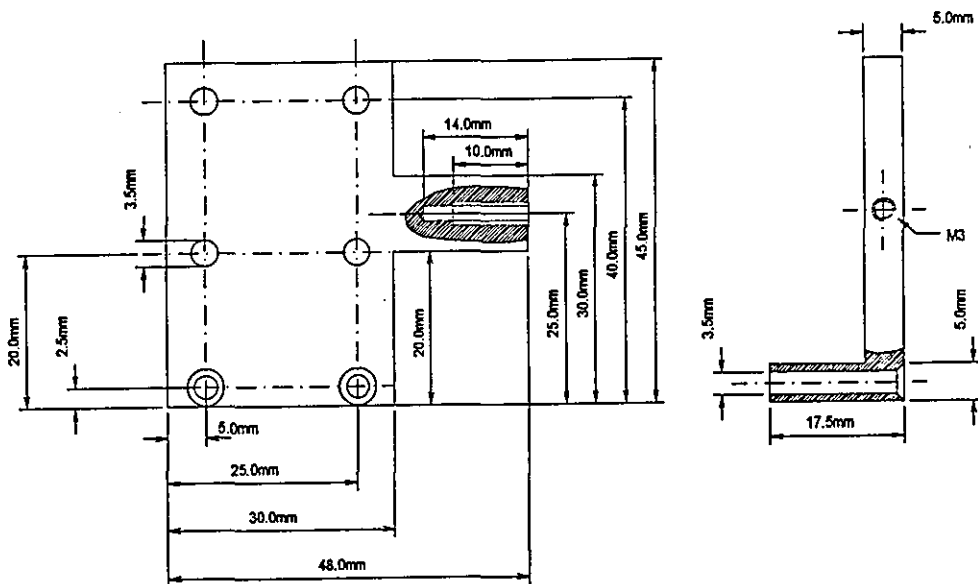
ENGR.: Dipl.-Ing. U. Samuels

Title:

Base plate

FHO-Fachhochschule Ostfriesland
-Institut für Lasertechnik -





Part-No.: M/3

Scale: 1:1

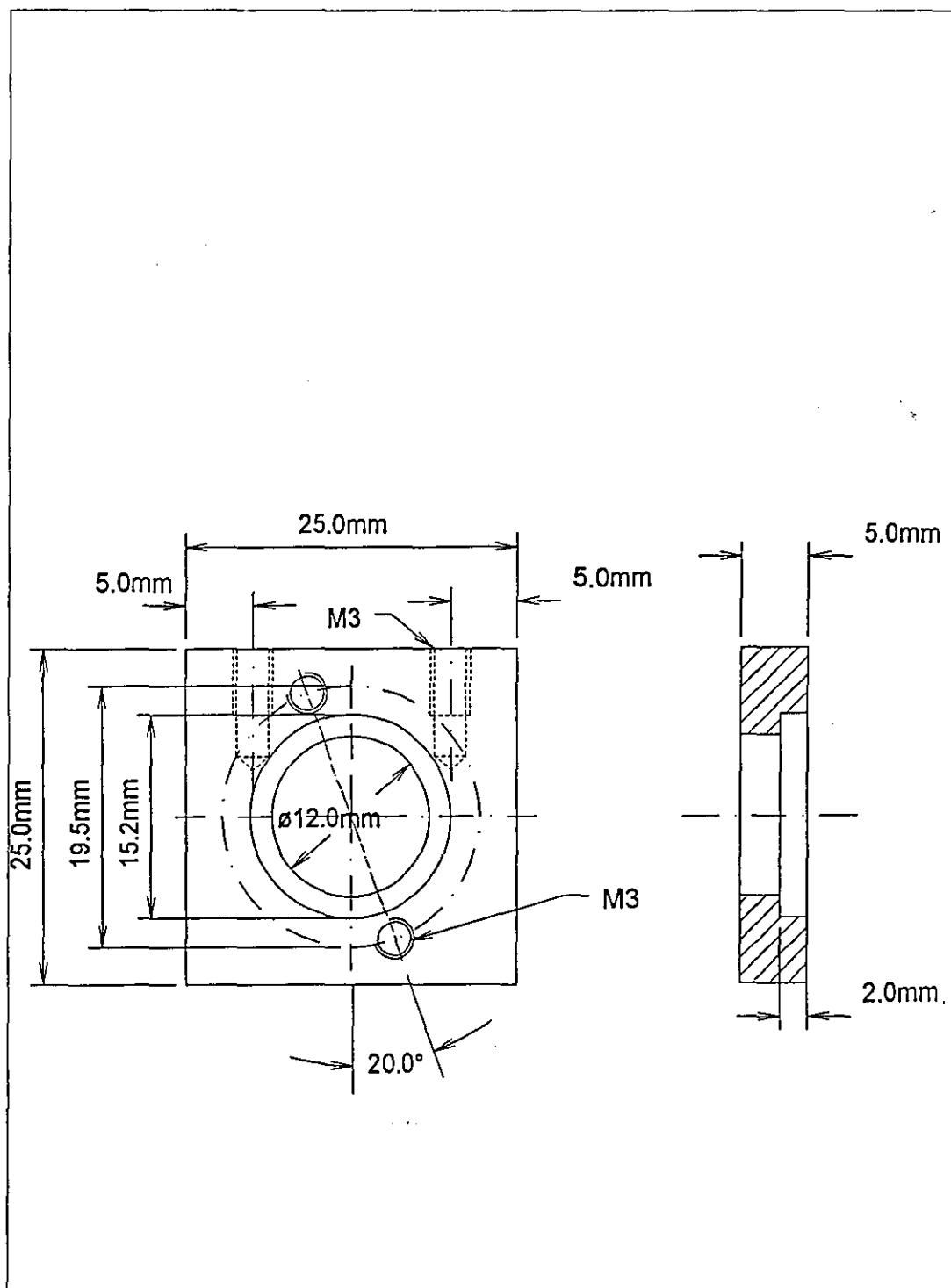
Material: Aluminium

Date: October 1995

ENGR.: Dipl.-Ing. U. Samuels

Title:

Adapter for the
piezo translatorFHO-Fachhochschule Ostfriesland
-Institut für Lasertechnik -



Part-No.: M/4

Scale: 2:1

Material: Aluminium

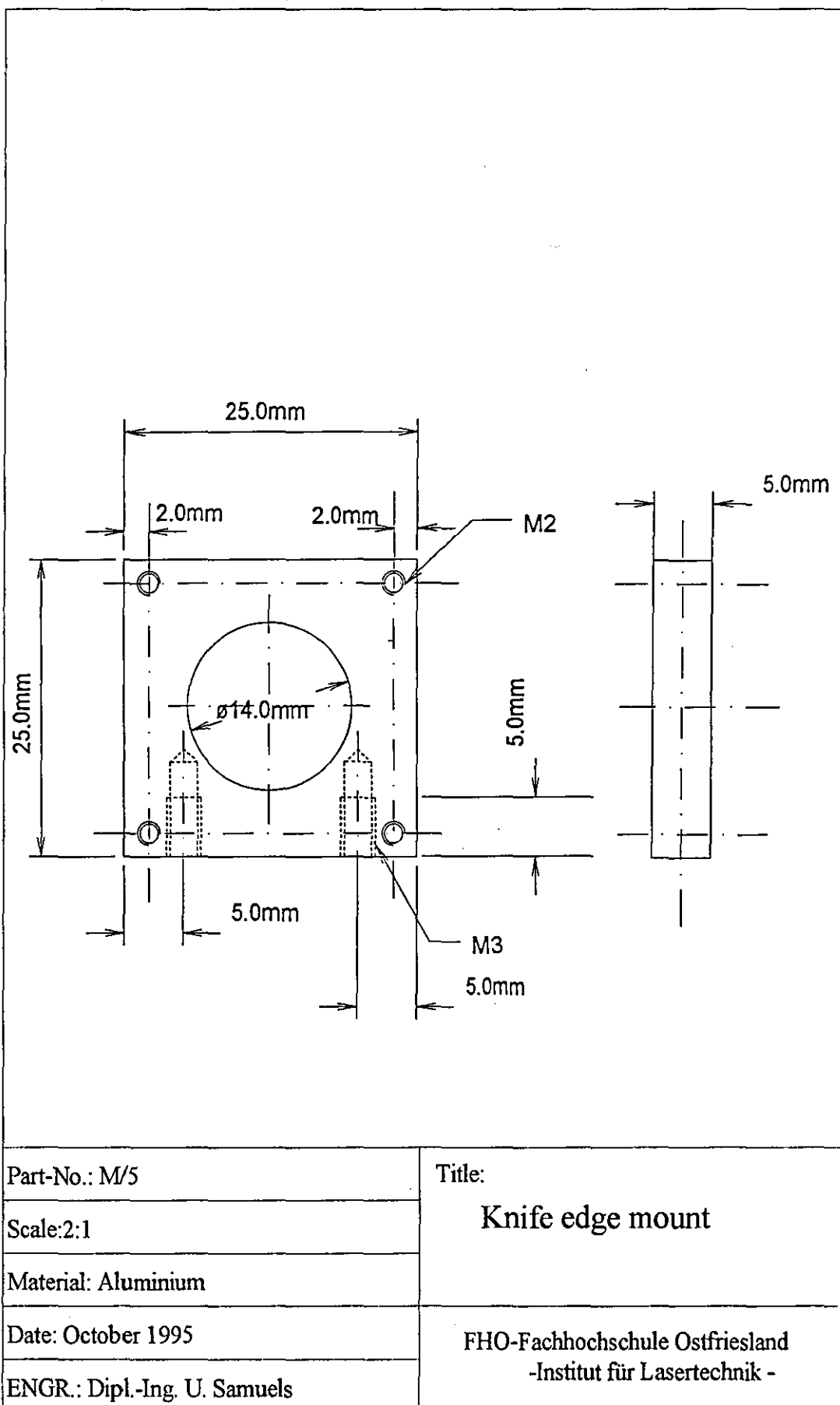
Date: October 1995

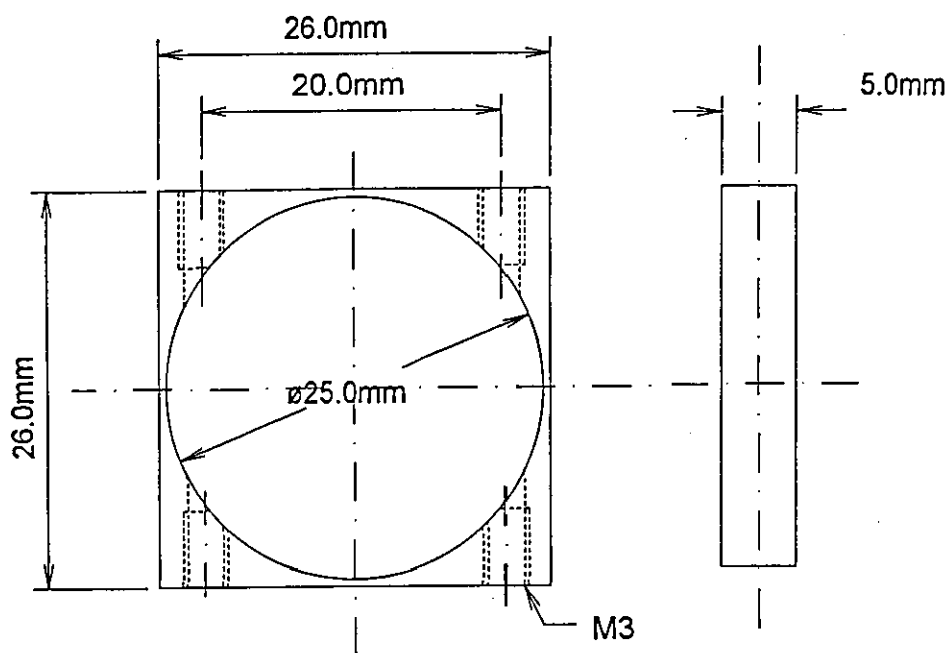
ENGR.: Dipl.-Ing. U. Samuels

Title:

Lens mount

FHO-Fachhochschule Ostfriesland
-Institut für Lasertechnik -





Part-No.: M/6

Scale: 2:1

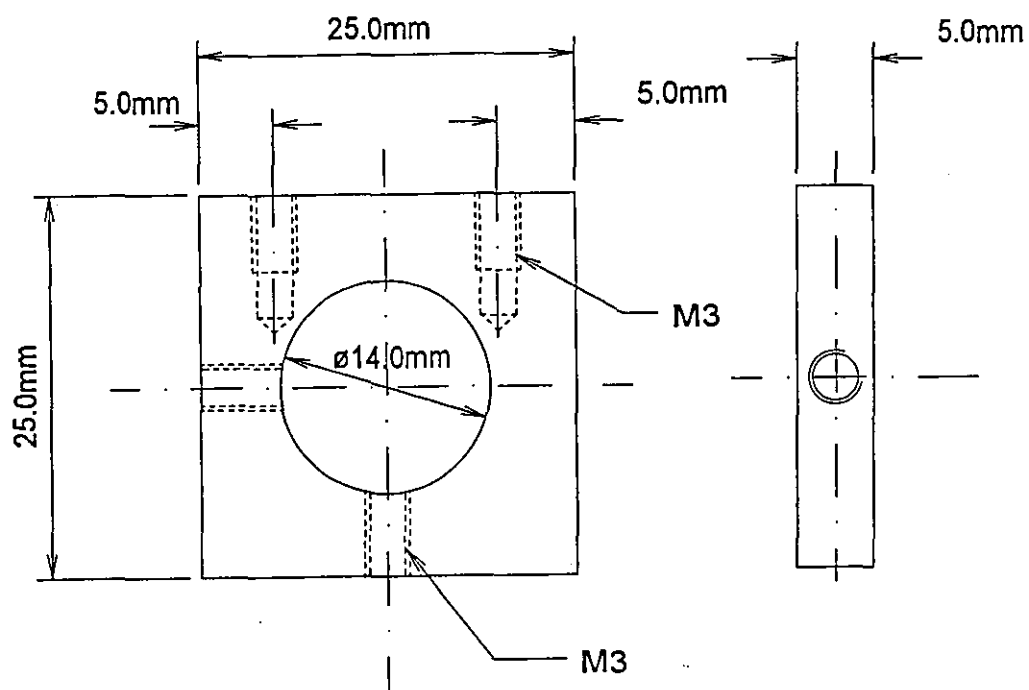
Material: Aluminium

Date: October 1995

ENGR.: Dipl.-Ing. U. Samuels

Title:

Microscope objective
mountFHO-Fachhochschule Ostfriesland
-Institut für Lasertechnik -



Part-No.: M/7

Scale: 2:1

Material: Aluminium

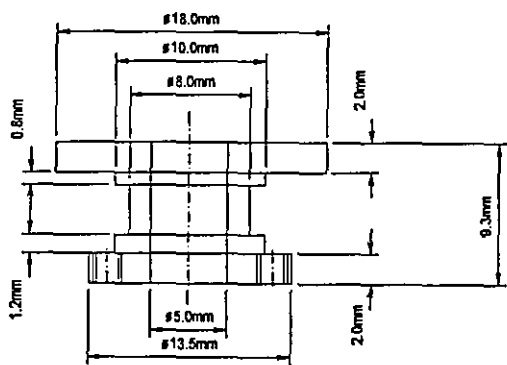
Date: October 1995

ENGR.: Dipl.-Ing. U. Samuels

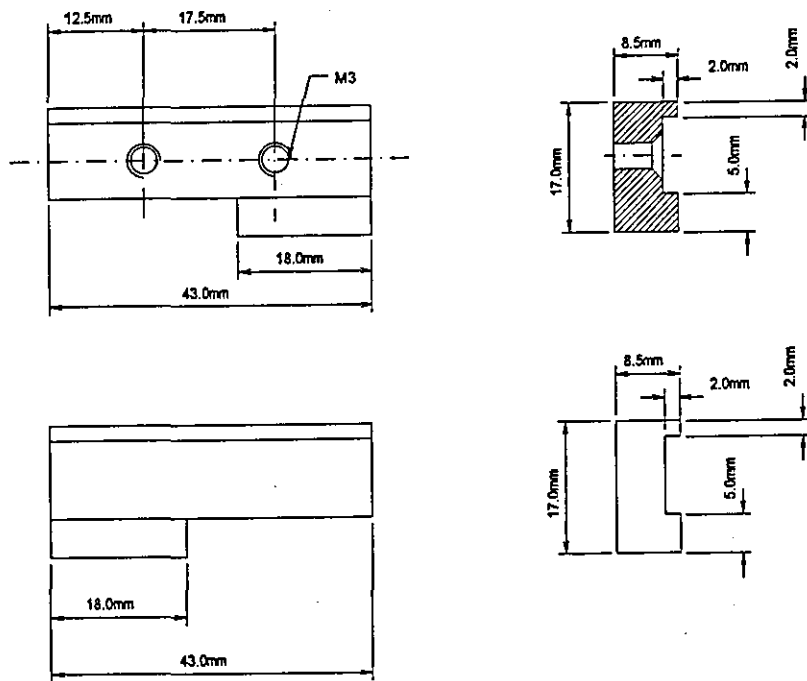
Title:

PSD adjustment unit

FHO-Fachhochschule Ostfriesland
-Institut für Lasertechnik -



Part-No.: M/8	Title: PSD mount
Scale: 2:1	
Material: Aluminium	
Date: October 1995	FHO-Fachhochschule Ostfriesland -Institut für Lasertechnik -
ENGR.: Dipl.-Ing. U. Samuels	



Part-No.: M/12 and M/13

Scale: 1:1

Material: Aluminium

Date: October 1995

ENGR.: Dipl.-Ing. U. Samuels

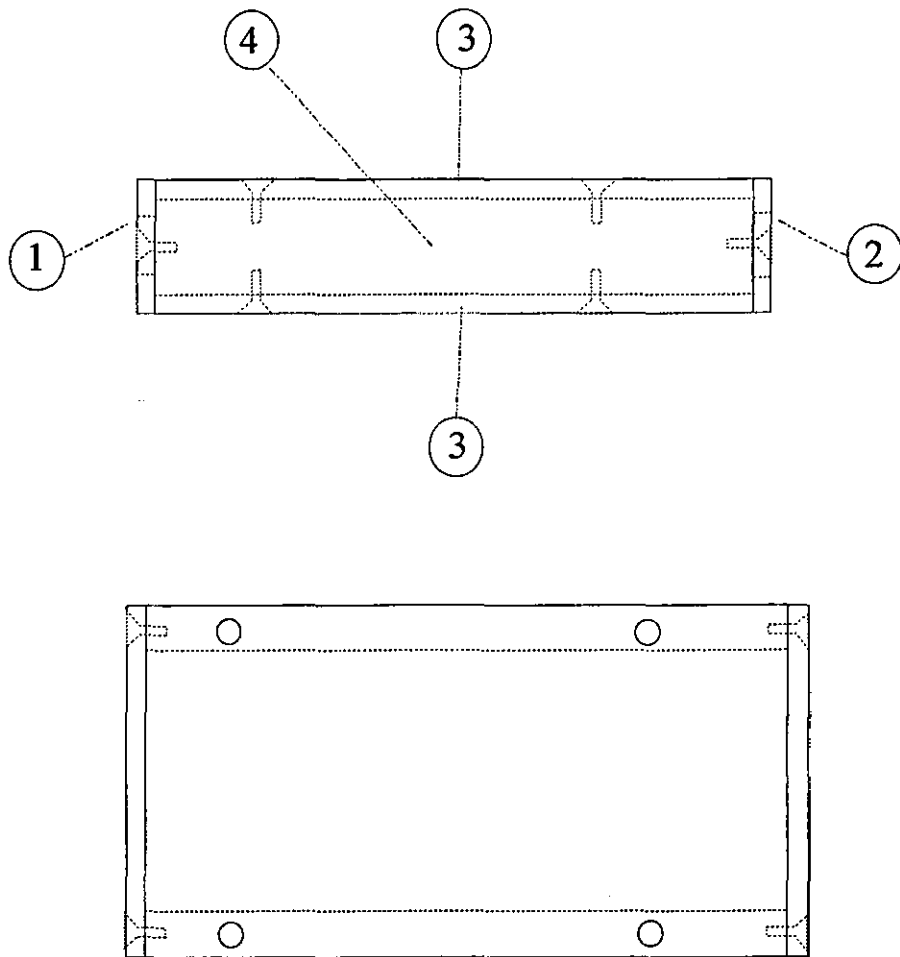
Title:

Beam splitter mount

FHO-Fachhochschule Ostfriesland
-Institut für Lasertechnik -

CONSTRUCTION OF THE SHIELDING OF THE PSD ANALYSING CIRCUIT

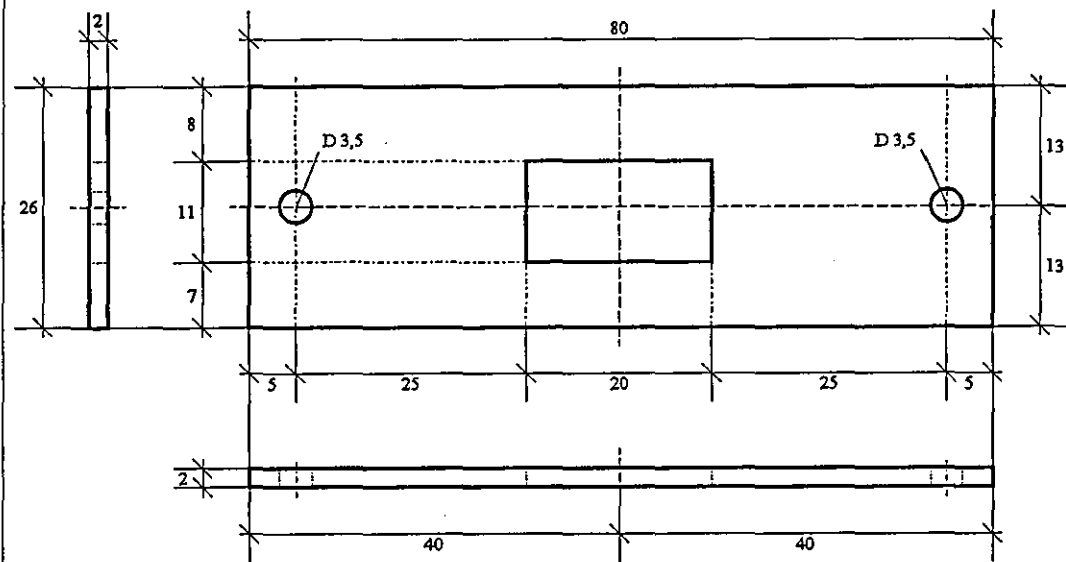
CONTENTS	PAGE #
1. Assembly schematic	N1
2. Parts list	N2
3. Blue prints	
N/1 Front plate	N3
N/2 Back plate	N4
N/3 Cover plate	N5
N/4 Side plate	N6



Part-No.:	Title: Assembly schematic of the shielding of the PSD circuit
Scale: Arbitrary	
Material:	
Date: October 1995	FHO-Fachhochschule Ostfriesland -Institut für Lasertechnik -
ENGR.: Dipl.-Ing. U. Samuels	

2. Parts list

<u>Part No.</u>	<u>Description</u>
1	Front plate
2	Back plate
3	Cover plate
4	Side plate



Part-No.: N/1

Scale:

Material: Aluminium

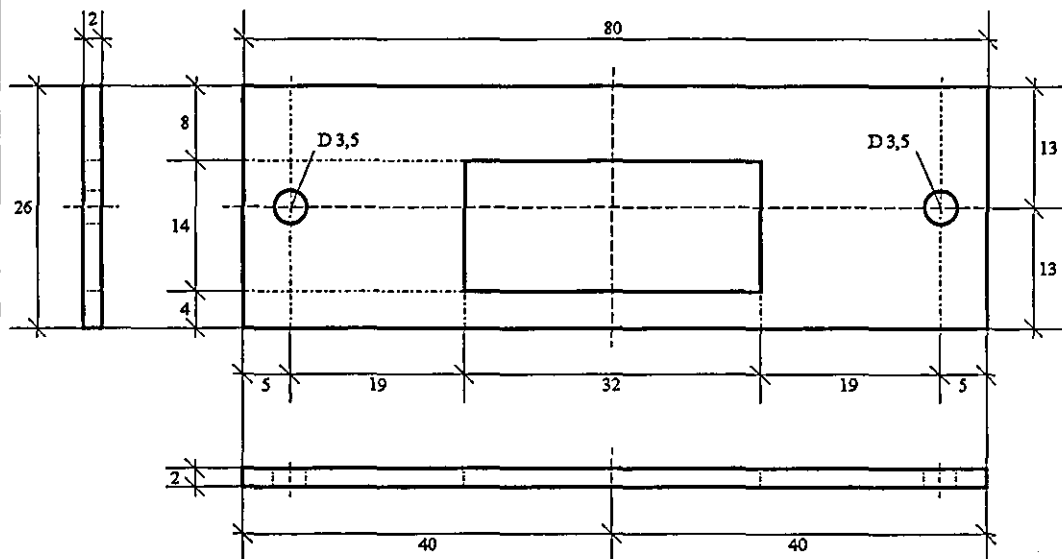
Date: October 1995

ENGR.: Dipl.-Ing. U. Samuels

Title:

Front plate

FHO-Fachhochschule Ostfriesland
-Institut für Lasertechnik -



Part-No.: N/2

Scale:

Material: Aluminium

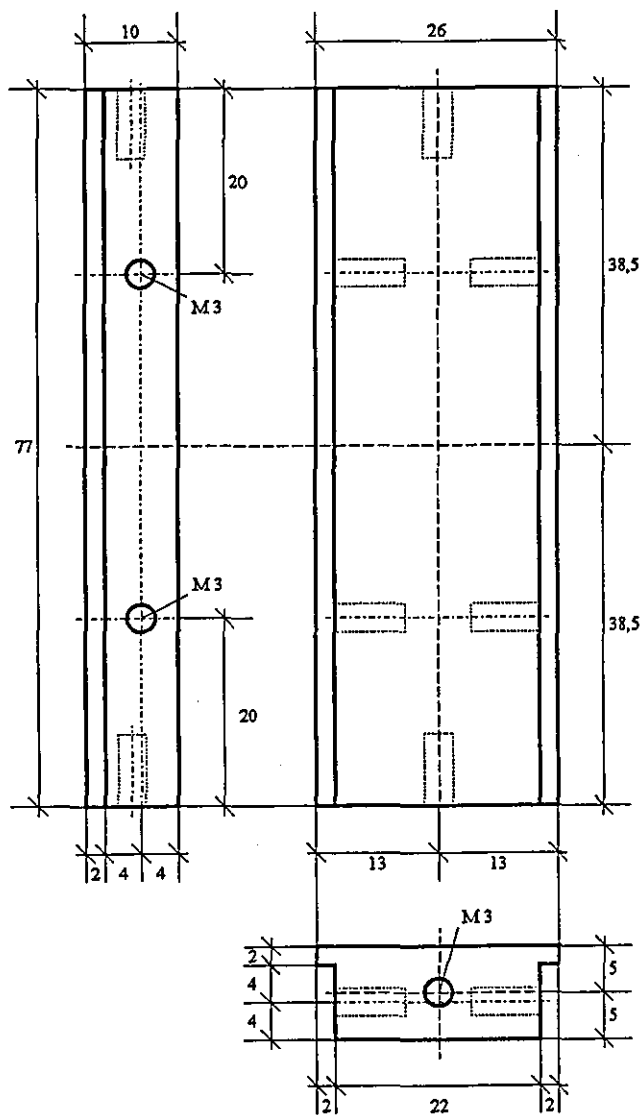
Date: October 1995

ENGR.: Dipl.-Ing. U. Samuels

Title:

Back plate

FHO-Fachhochschule Ostfriesland
-Institut für Lasertechnik -



Part-No.: N/4

Scale:

Material: Aluminium

Date: October 1995

ENGR.: Dipl.-Ing. U. Samuels

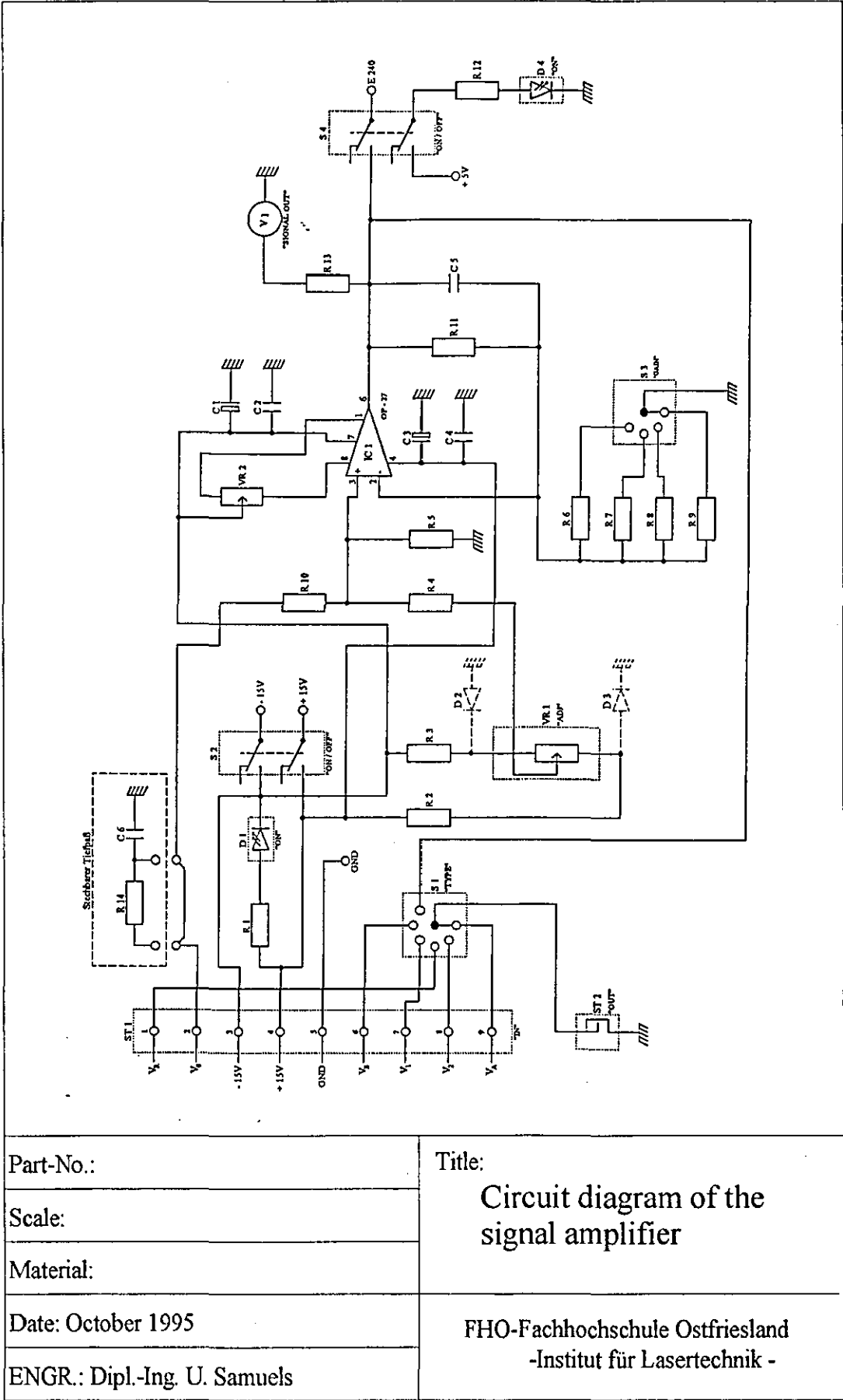
Title:

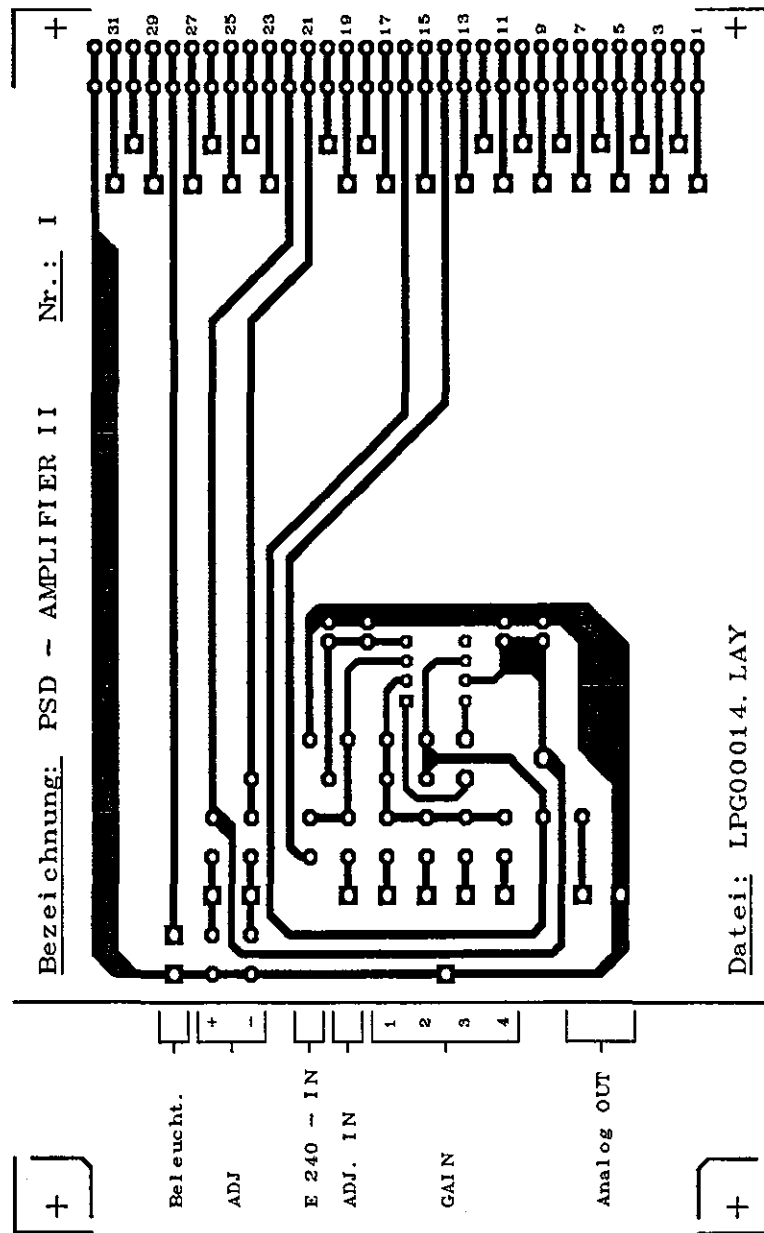
Side plate

FHO-Fachhochschule Ostfriesland
-Institut für Lasertechnik -

SIGNAL AMPLIFIER

CONTENTS	PAGE #
1. Circuit diagram	O1
2. PCB-Layout I	O2
3. PCB-Layout II	O3
4. Input terminal	O4
5. Parts list	O5





Part-No.:	Title: PCB of the signal amplifier
Scale:	
Material:	
Date: October 1995	FHO-Fachhochschule Ostfriesland -Institut für Lasertechnik -
ENGR.: Dipl.-Ing. U. Samuels	

4. Input terminal

Pin #	Description	-
1	Bias voltage input (V_R)	
2	Analog divider input (V_0)	V_B / V_A (at $V_A > 0$)
3	- V (- 15V)	
4	+ V (+ 15V)	
5	GND	
6	Difference signal input (V_B)	$V_1 - V_2$
7	Head amplifier input (V_1)	
8	Head amplifier input (V_2)	
9	Sum signal input (V_A)	$V_1 + V_2$

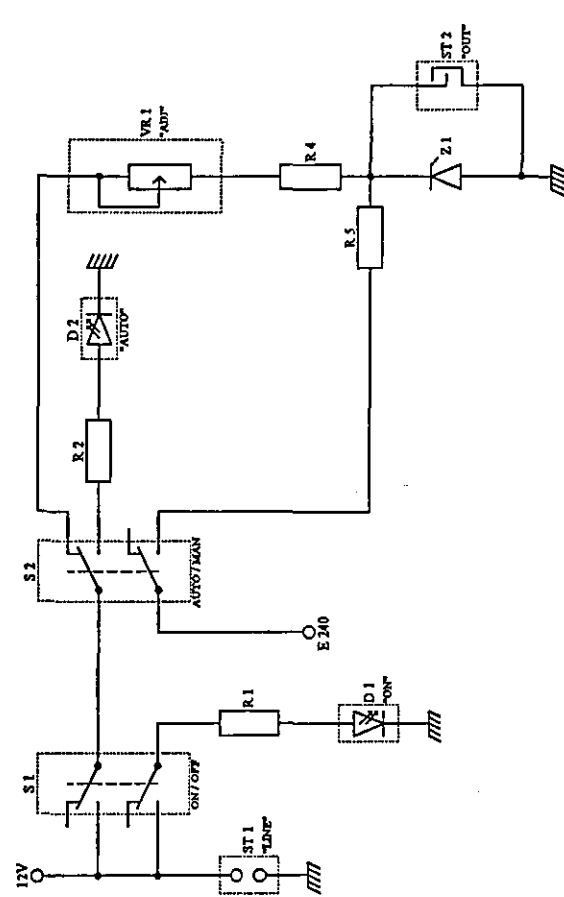
Table O1: Signal amplifier → Input terminal (Sub-D)

2. Parts list

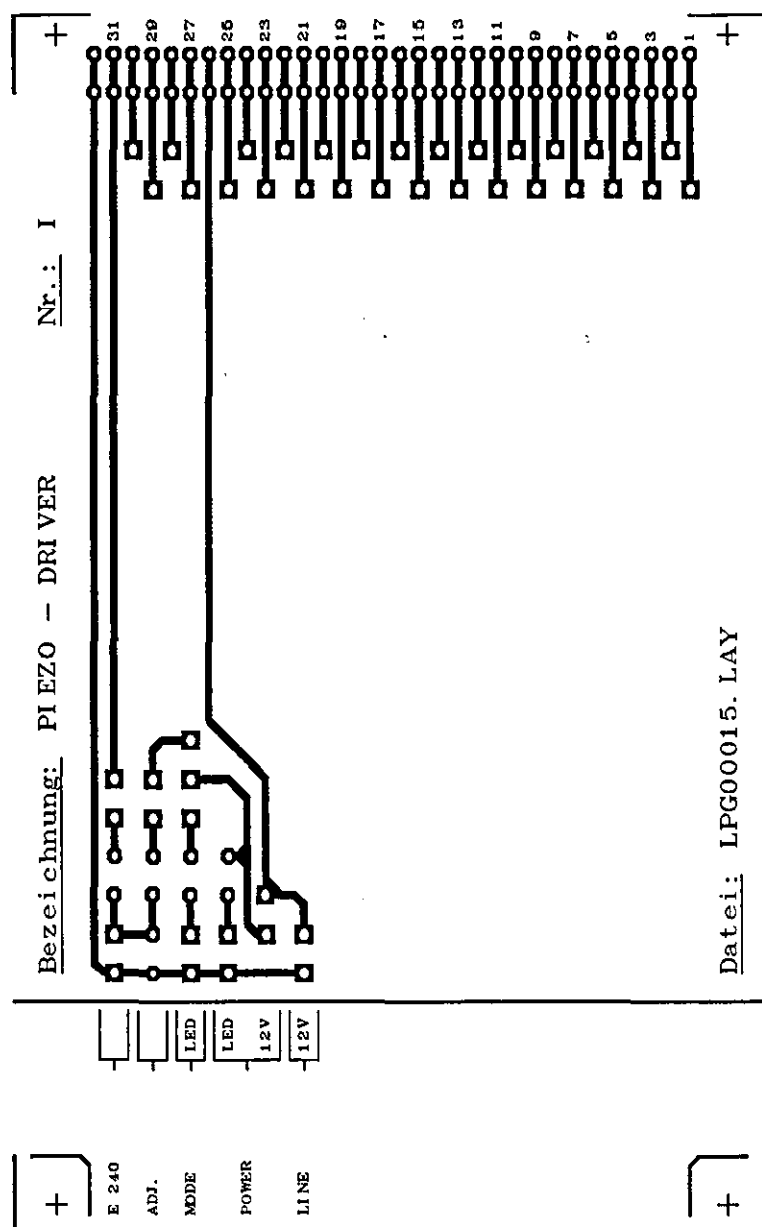
<u>Part No.</u>	<u>Description</u>
C1	10 μ F Elco 25V
C2	100nF Ceramic
C3	10 μ F Elco 25V
C4	100nF Ceramic
C5	10pF Ceramic
C6	10pf Ceramic
D1	LED red
D2	1N4178
D3	1N4178
D4	LED red
IC1	OP-27CN
R1	1k Ω
R2	47k Ω
R3	47k Ω
R4	10k Ω
R5	10k Ω
R6	0 Ω
R7	10k Ω
R8	40k Ω
R9	90k Ω
R10	10k Ω
R11	10k Ω
R12	270k Ω
R13	47k Ω
R14	47k Ω
S1	Step switch 6
S2	Snap switch 2xUM
S3	Step switch 4
S4	Snap swich 2xUM
ST1	Sub-D 9
ST2	BNC
V1	Voltmeter $\pm 50\mu$ A
VR1	5k Ω by 10 steps
VR2	19k Ω

PIEZO DRIVER

CONTENTS	PAGE #
1. Circuit diagram	P1
2. PCB-Layout	P2
3. Parts list	P3



Part-No.:	Title: Circuit diagram of the piezo driver
Scale:	
Material:	
Date: October 1995	FHO-Fachhochschule Ostfriesland -Institut für Lasertechnik -
ENGR.: Dipl.-Ing. U. Samuels	



Part-No.:	Title: PCB of the piezo driver
Scale:	
Material:	
Date: October 1995	FHO-Fachhochschule Ostfriesland -Institut für Lasertechnik -
ENGR.: Dipl.-Ing. U. Samuels	

3. Parts list

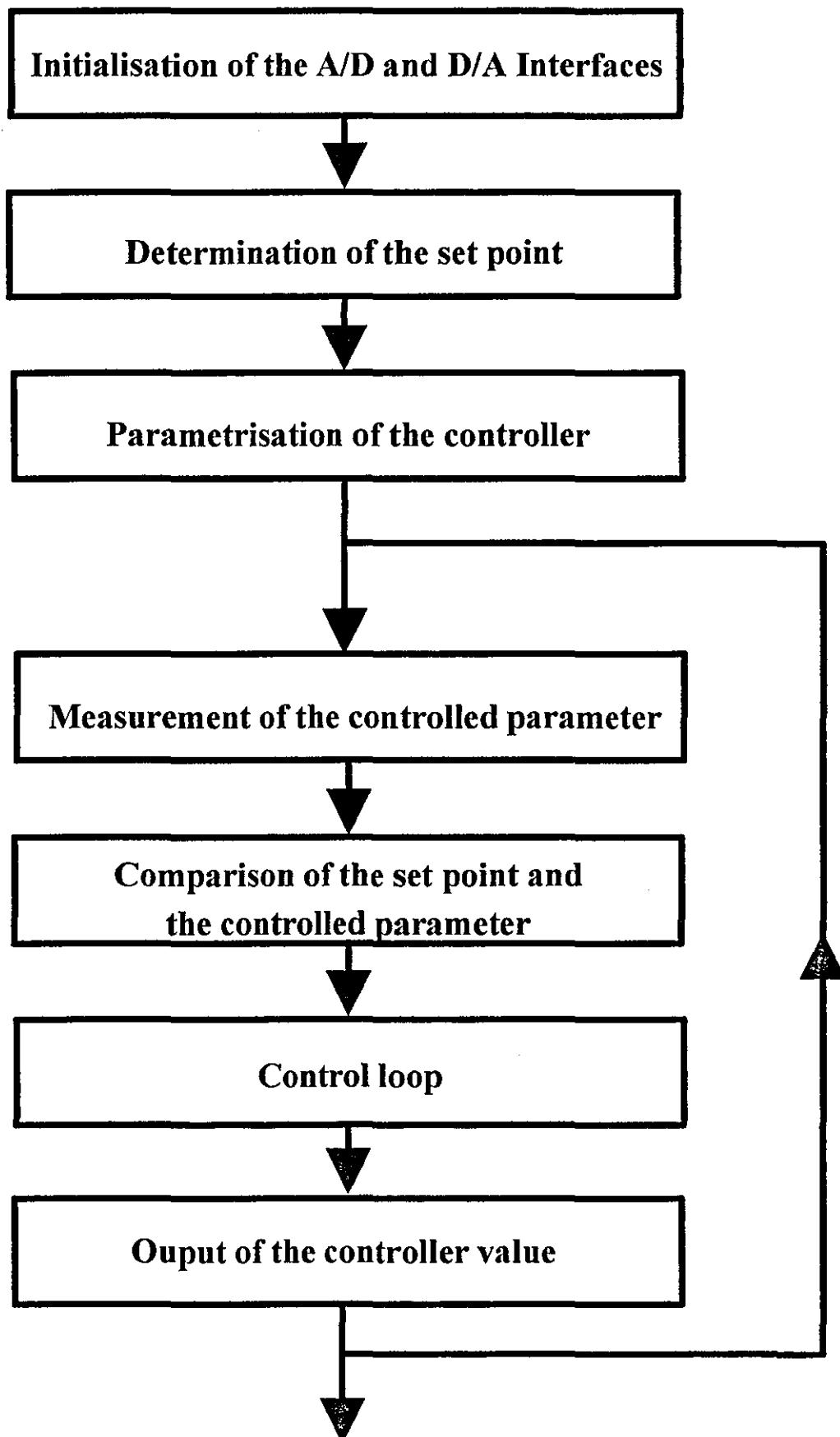
<u>Part No.</u>	<u>Description</u>
ST1	Jack socket
ST2	BNC
D1	LED red
D2	LED red
R1	1k Ω
R2	1k Ω
R4	120k Ω
R5	120k Ω
S1	Snap switch 2xUM
S2	Snap switch 2xUM
VR1	200k Ω
Z1	ZPD10

CONTROLLER PARAMETER TABLE

(Rules from Chien, Hrones, Reswik)

Recommended values for optimum controller adjustment				
Controller type	oscillating (short setting time)		creeping (without overshooting)	
	good disturbance behaviour at the input of the system to be controlled	good follow up characteristic	good disturbance behaviour at the input of the system to be controlled	good follow up characteristic
P	$K_P = 0.7 \tilde{K}$	$K_P = 0.7 \tilde{K}$	$K_P = 0.3 \tilde{K}$	$K_P = 0.3 \tilde{K}$
PI	$K_P = 0.7 \tilde{K}$ $T_n = 2.3 T_u$	$K_P = 0.6 \tilde{K}$ $T_n = T_g$	$K_P = 0.6 \tilde{K}$ $T_n = 4 T_u$	$K_P = 0.34 \tilde{K}$ $T_n = 1.2 T_g$
PID	$K_P = 1.2 \tilde{K}$ $T_n = 2 T_u$ $T_v = 0.42 T_u$	$K_P = 0.95 \tilde{K}$ $T_n = 1.35 T_g$ $T_v = 0.47 T_u$	$K_P = 0.95 \tilde{K}$ $T_n = 2.4 T_u$ $T_v = 0.42 T_u$	$K_P = 0.6 \tilde{K}$ $T_n = T_g$ $T_v = 0.5 T_u$

CONTROLLER PROGRAM FLOW CHART



CONTROLLER PROGRAM LISTING

CONTENTS	PAGE #
1. System requirements	S1
2. Description of the procedures and functions	S1
3. Description of the controller parameter	S2
4. Listing of the controller program	S3 - S7

1. System requirements

Computer:	Personal Computer with Intel 80386 processor
Interface:	D/A and A/D Converter DAQ-1212A (Physics instruments)
Compiler:	Turbo Pascal 6.0 from Borland
Tools:	Real-Time Graphics and measurement/control tools for Turbo Pascal 5.x, 6.x Version 2.0 from Quinn Curtis

2. Description of the procedures and functions

RTInitPIDStat:	Set a side pointer space on the heap for the number of PID loops you intend to control
RTFreePIDStat:	Frees the memory allocated for PID loops from the system heap
RTsetPIDParameters:	needs to be called for every PID loop in the system to establish the various constants associated with the PID calculation
RTCalcPID:	calculate the PID output value for the given PID loop

3. Description of the controller parameter

loopnum:	PID loop number
ptype:	PID type parameter, 0=position algorithm, 1 = velocity algorithm
setpnt:	PID setpoint value
steadystat:	approximate stead state value for output
prop:	PID-proportional control constant
integ:	PID-integral mode gain constant
deriv:	PID-derivative mode gain constant
lowclmp:	low clamping value for output. When output values are clamped, the summation of the error term is also halted to provide for anti-reset windup.
highclmp:	high clamping value for output. When output values are clamped, the summation of the error term is also halted to provide for anti-reset windup.
rateclmp:	rate of change clamp for output, measured in units/minute. If there is a large change in the setpoint, then the rate clamp parameter will prevent the PID output value from large step changes. Instead it will ramp up to the new value at the rate rateclmp.
sampleper:	sample period for the PID updates in units minutes/sample
filterconst:	the value for the measured variable can be automatically filtered if it is noisy. A filter value of 0.0 means that no filtering takes place. As the value increase toward 1.0 the filtering effect becomes more and more pronounced.

4. Listing of the controller program

 $\{ \$N+, E+ \}$

PROGRAM Controller adjustment; {digital controller}

```
uses crt,dos,rtpid,rtstdhdr;
```

```
const
DAQ12ADDR           = $320;
DAQ_Command         = DAQ12ADDR +3;
DAQ_LSB             = DAQ12ADDR +4;
DAQ_MSB             = DAQ12ADDR +5;
DAQ_LOAD            = DAQ12ADDR +6;
A2D_DATA            = DAQ12ADDR;
TTL_OUTPUT          = DAQ12ADDR+7;
```

```

var
x,I,loopnum, ptype,wert           : Integer;
Bitmuster                         : String;
TTL_In                           : Word;
DACOut                           : longint;
setpnt,steadystat,prop,integ,deriv,filterconst,
highclmp,lowclmp,ratclmp,sampleper,pidoutput : RealType;
Istwert                           : Real;

```

```
(*****)
```

```
(*      Procedures and functions      *)
```

```
(*****)
```

```
PROCEDURE Init DAQ; { Stores the D/A Value in register}
```

```

var x : real;
BEGIN
    PortW[$323] := $0;           {Select channel}
    PortW[$324] := $FF;         {LSB}
    PortW[$325] := $07;         {MSB}
    x := PortW[$326];           {in Register to out register}
END;

```

PROCEDURE Setchanel_2;	{initialisation of A/D channel 2}
BEGIN	
PortW[\$321] := \$c2;	{Channel 2, range +10 V}
PortW[\$322] := \$70;	{Magnification 1}
END;	

```

FUNCTION Analog_ein_1 : word;           {Input of A/D channel 2]
var index, a:integer;
  BEGIN
    index := 0;
    PortW[$32a] := 1;                   {set of 15 bit status register=1}
    a := PortW[$32c];                   {start}
    REPEAT
      delay(10);
    UNTIL (portw[$32f] and ($8000) <> 0); {status register 15. bit = 1}
    Analog_ein_1 := Portw[$320] and $0fff; {assignment}
    Portw[$32a] := 0;                   {set of 15. bit status register=0}
  END;

```

```

PROCEDURE Analog_Aus_1 (value : integer); {output of control value output }
                                           {at out1 pin 26}
  BEGIN
    PORT[DAQ_Command] := $0;
    PORT[DAQ_LSB] := value AND $07FF;
    PORT[DAQ_MSB] := value SHR 8;
    PORT[DAQ_LOAD] := 1;
  END;

```

```

PROCEDURE Analog_Aus_2 (value : integer); {Step at channel 2}
  BEGIN
    PORT[DAQ_Command] := $1;
    PORT[DAQ_LSB] := value AND $07FF;
    PORT[DAQ_MSB] := value SHR 8;
    PORT[DAQ_LOAD] := 1;
  END;

```

```

Procedure Inischleife;                  {center position of the piezo translator}
  Begin
    DACOut:=3052;
    Analog_Aus_1(DACOut);               {Output}
    Delay(3000);
  End;

```



```
(*****)  
(*                               MAIN                               *)  
(*****)
```

BEGIN

{Initialisation of the A/D and D/A interface}

clrscr;

Setchannel_2;

Init_DAQ;

RTInitPIDStat(32);

loopnum:=0;

ptype:=0;

steadystate:=5.0;

prop:=2.8;

integ:=3.8;

deriv:=0;

highclmp:=10;

lowclmp:=0;

rateclmp:=1000.0;

sampleper:=0.005;

filterconst:=0.1;

RTFreePIDStat;

Inischleife;

repeat

{Endless loop}

Begin

{Positive step}

{Determination of the setpoint}

I := Analog_Ein_1;	{I:=controlled parameter}
Istwert:=I*0.002442;	{Scaling to volt range}
DACOut:=2047+I DIV 2;	
Analog_Aus_1(DACOut);	
setpnt:=Istwert+0.5;	{Set point calculation}

{Parametrisation of the controller}

```

For loopnum:= 1 to 32 do
begin
  RTSetPIDParameters(loopnum, 0, setpnt, steadystate, prop, integ,
    deriv, lowclmp, highclmp, rateclmp,
    sampleper,filterconst);
end;

```

{Output of the trigger signal}

DACOut:=DACOut+100;	
Analog_Aus_1(DACOut);	{ 2047 = 0V to 4095 = 10V}

{Controller loop}

```

For loopnum:= 1 to 31 do
begin
  I := Analog_Ein_1;           {Measurement of the controlled parameter}
  Istwert:=I*0.002442;         {Scaling to the volt range}
  PIDOutput:= RTCalcPID(loopnum, Istwert, Setpnt); {call of the controller}
  DACOut:= 2047+ROUND(PIDOutput*202); {Offset +controller output}
  Analog_Aus_2(DACOut);        {Output of the signal}
End;

```

{Negative step}

{Determination of the setpoint}

I := Analog_Ein_1;	{I:= controlled parameter}
Istwert:=I*0.002442;	{Scaling to volt rang}}
DACOut:=2047+I DIV 2;	
Analog_Aus_1(DACOut);	{ 2047 = 0V bis 4095 = 10V}
setpnt:=Istwert-0.5;	{Setpoint calculation}

{Parametrisation of the controller}

```

For loopnum:= 1 to 32 do
begin
  RTSetPIDParameters(loopnum, 0, setpnt, steadystat, prop, integ,
    deriv, lowclmp, highclmp, rateclmp,
    sampleper,filterconst);
end;

```

{Output of the trigger signal}

```

DACOut:=DACOut-100;
Analog_Aus_1(DACOut); { 2047 = 0V bis 4095 = 10V}

```

{Controller loop}

```

For loopnum:= 1 to 31 do
begin
  I := Analog_Ein_1;           {Measurement of the controlled parameter}
  Istwert:=I*0.002442;         {Scaling to the volt range}
  PIDOutput:= RTCalcPID(loopnum, Istwert, Setpnt); {Call of the controller}
  DACOut:= 2047+ROUND(PIDOutput*202); {offset+controller output}
  Analog_Aus_2(DACOut);        {Output of the signal}
End;

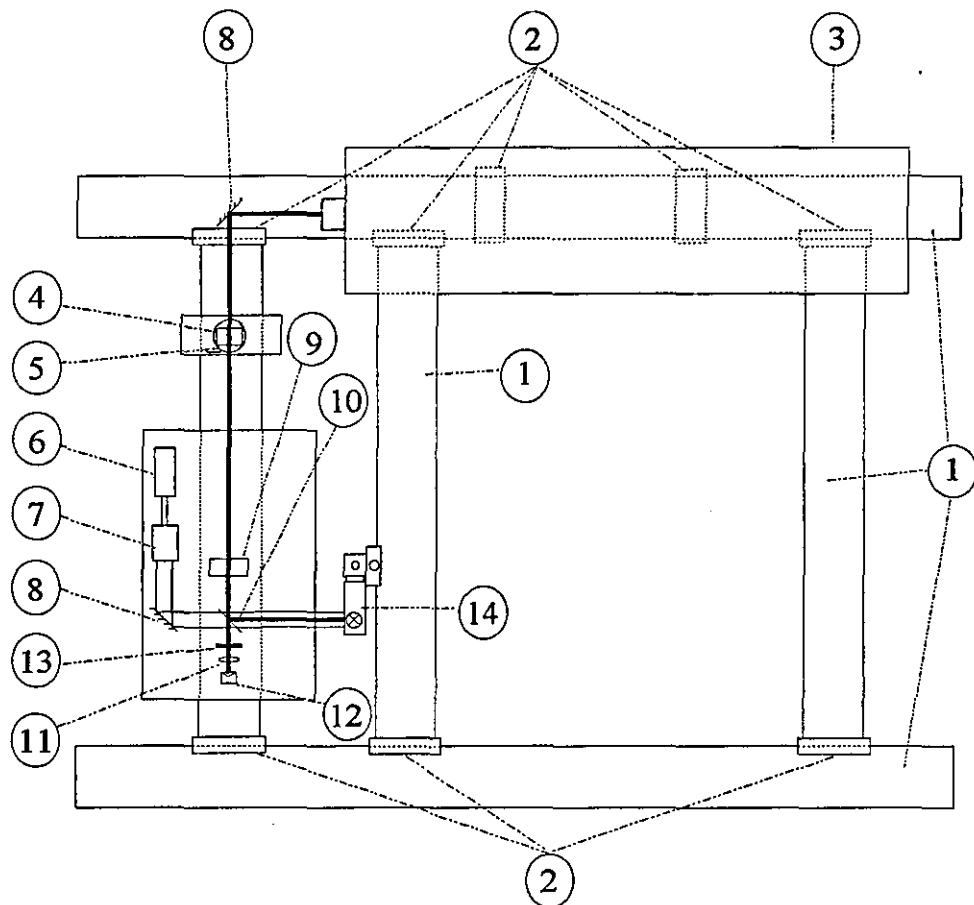
```

until keypressed;

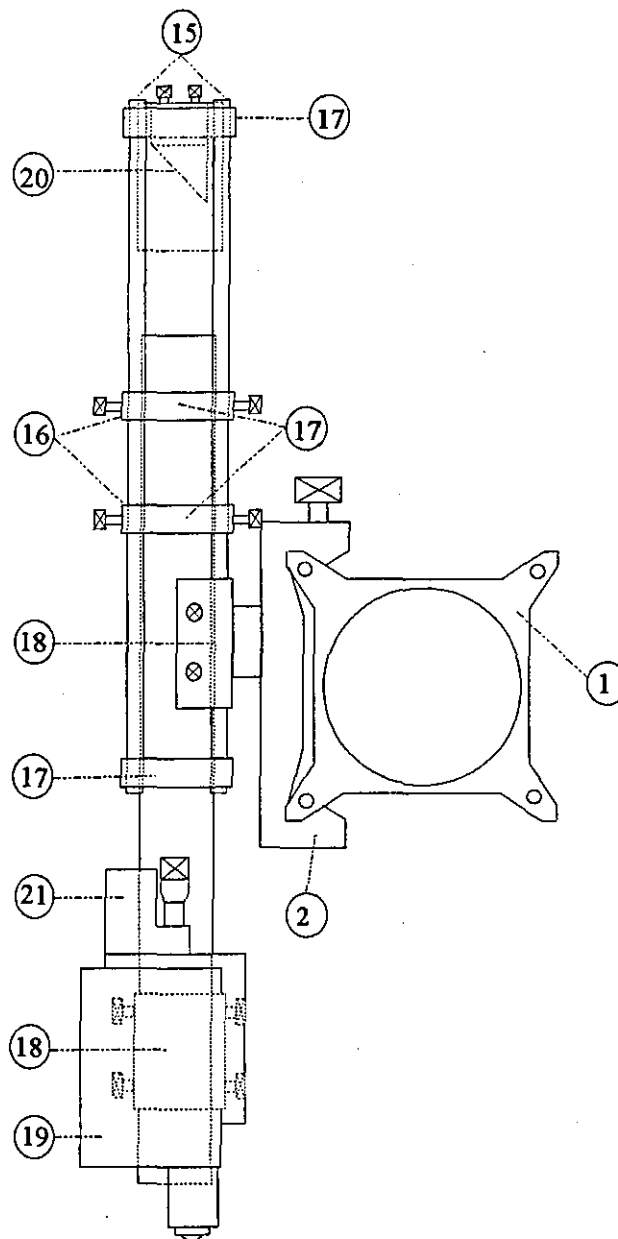
END.

OPTICAL CONSTRUCTION OF THE LPG

CONTENTS	PAGE #
1. X,Y plane of the LPG	T1
2. Z axis of the LPG	T2
3. Parts list	T3



Part-No.:	Title: X,Y plane of the LPG
Scale: Arbitrary	
Material:	
Date: October 1995	FHO-Fachhochschule Ostfriesland -Institut für Lasertechnik -
ENGR.: Dipl.-Ing. U. Samuels	



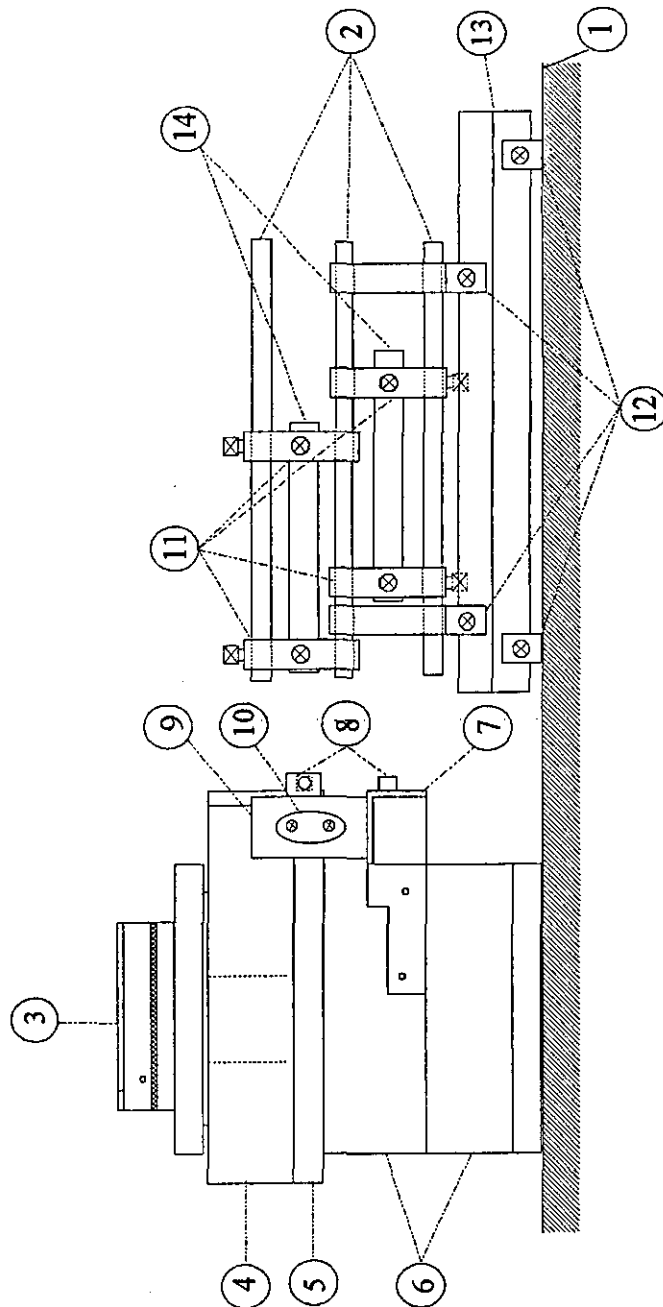
Part-No.:	Title: Z-axis of the LPG
Scale: Arbitrary	
Material:	
Date: October 1995	FHO-Fachhochschule Ostfriesland -Institut für Lasertechnik -
ENGR.: Dipl.-Ing. U. Samuels	

3. Parts list

<u>Part No.</u>	<u>Description</u>
1	X95 profile
2	X95 carriage
3	He-Cd laser
4	Micro rotation stage
5	AOM
6	Semiconductor laser
7	Telescope
8	Mirror
9	nd filter
10	Beam splitter
11	Mount with lens $f=20\text{mm}$
12	Photo detector
13	Beam stop
14	Z-axis
15	Precision rods
16	X25 carriage (small)
17	Mount
18	X25 carriage (large)
19	Autofocus sensor
20	Tilt mirror
21	Piezo translator

CONSTRUCTION OF THE LPG POSITIONING SYSTEM

CONTENTS	PAGE #
1. Side view	U1
2. Top view	U2
3. Parts list	U3



Part-No.:

Scale: Arbitrary

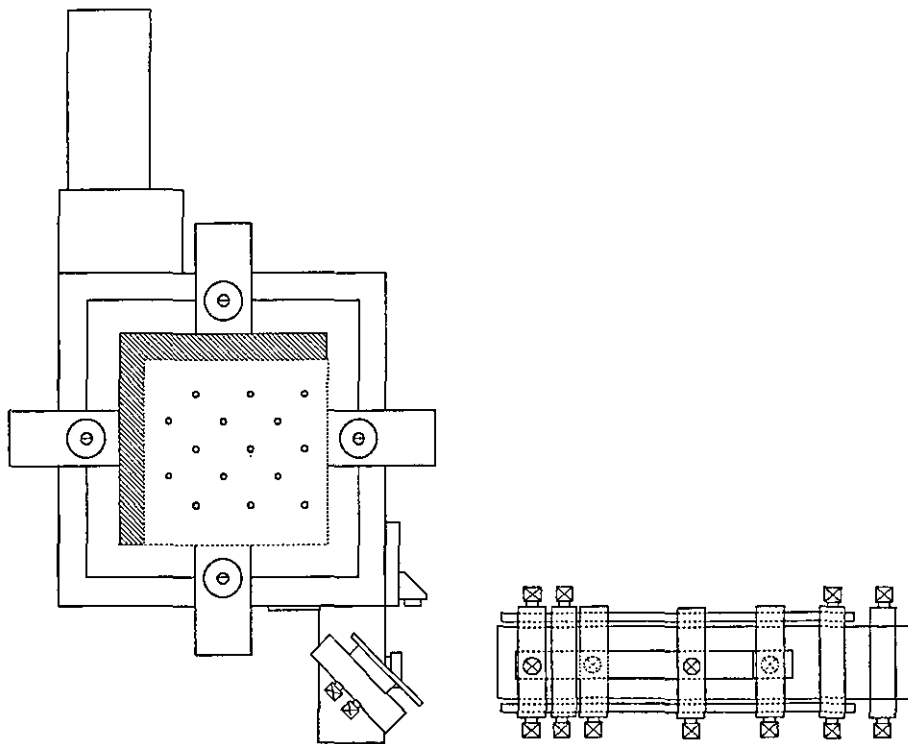
Material:

Date: October 1995

ENGR.: Dipl.-Ing. U. Samuels

Title:

Side view of the
positioning systemFHO-Fachhochschule Ostfriesland
-Institut für Lasertechnik -



Part-No.:	Title: Top view of the positioning system
Scale: Arbitrary	
Material:	
Date: October 1995	FHO-Fachhochschule Ostfriesland -Institut für Lasertechnik -
ENGR.: Dipl.-Ing. U. Samuels	

3. Parts list

<u>Part No.</u>	<u>Description</u>
1	Bread board
2	Precision rods
3	Substrate holder
4	Rotary stage
5	Adapter
6	Linear axis
7	Mounting board
8	Retro reflector
9	Mount
10	Tilt mirror
11	x,y mini stage
12	X25 carriage
13	X25 profile
14	Interferometer head

PHOTOGRAPHS

PHOTO	PAGE #
1. Laser pattern generator	V1
2. Laser pattern generator	V2
3. Beam guiding system	V2
4. Beam guiding system (detail)	V3
5. Beam guiding system (detail)	V3
6. X,Y and rotary table	V4
7. Interferometer head for X,Y positioning table control	V4
8. Optimised processing head (front view)	V5
9. Optimised processing head (side view)	V5
10. Shielded PSD analysing circuit	V6

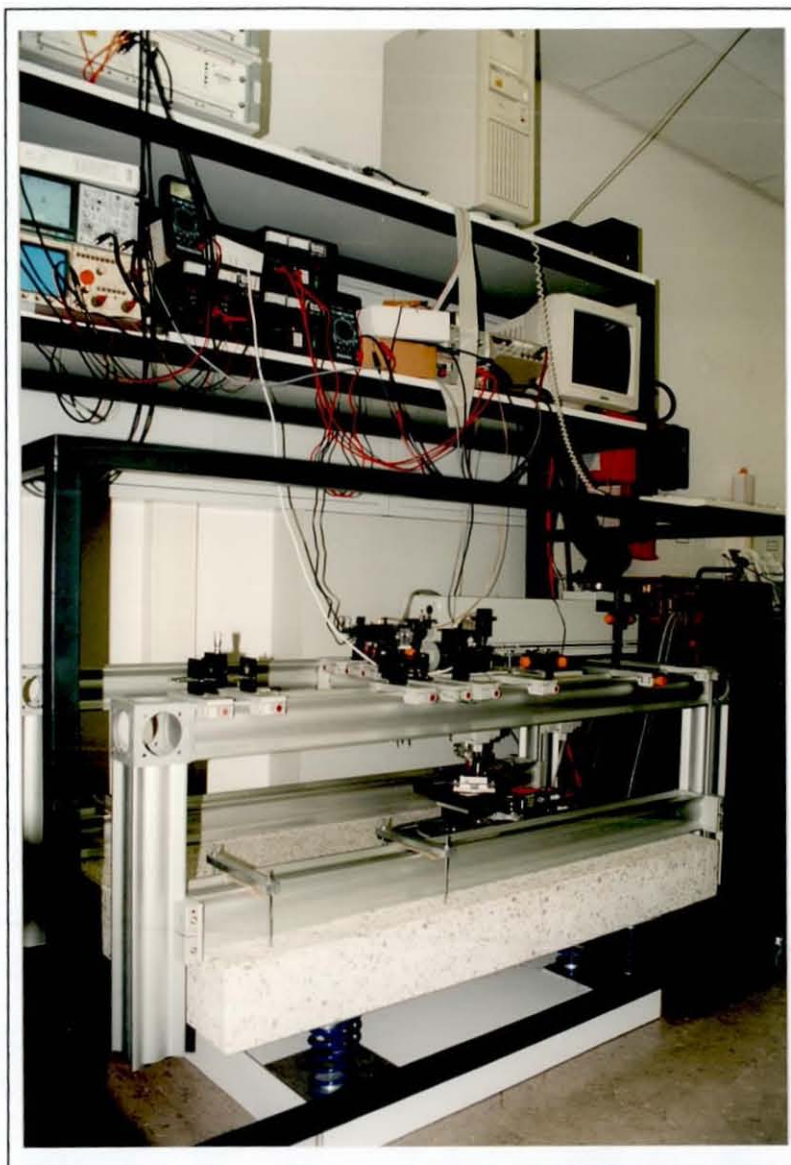


Photo 1: Laser pattern generator

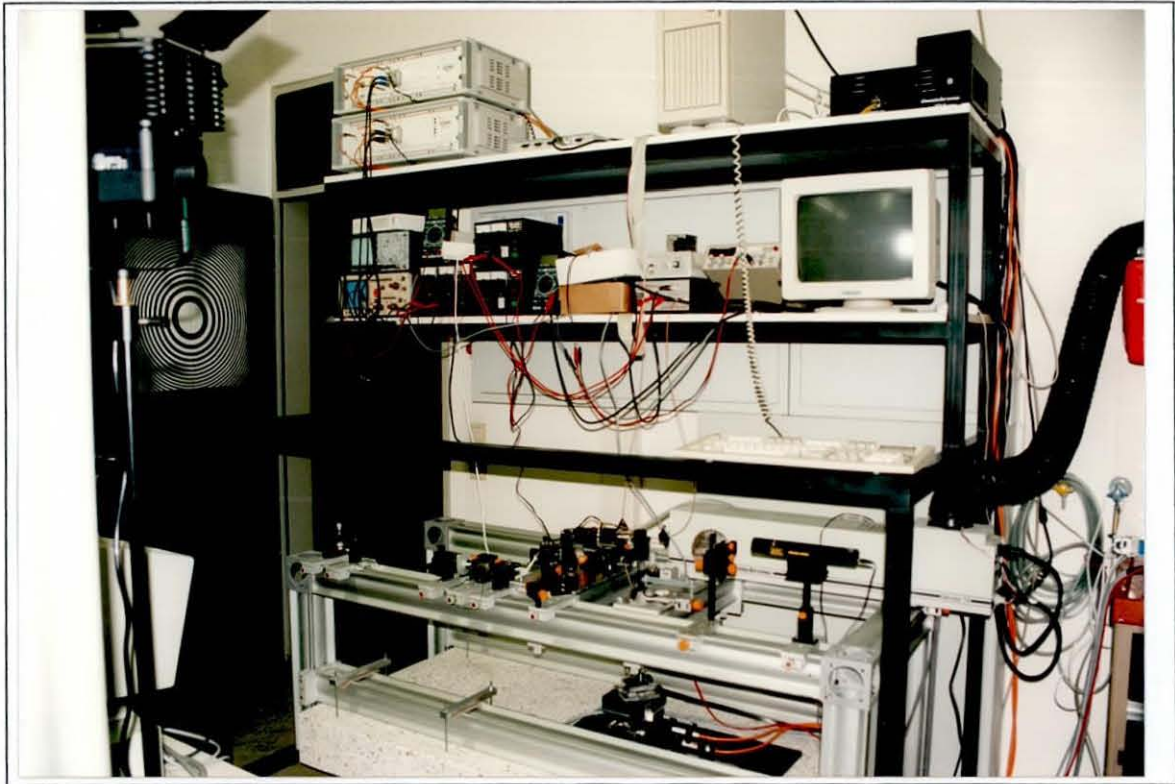


Photo 2: Laser pattern generator

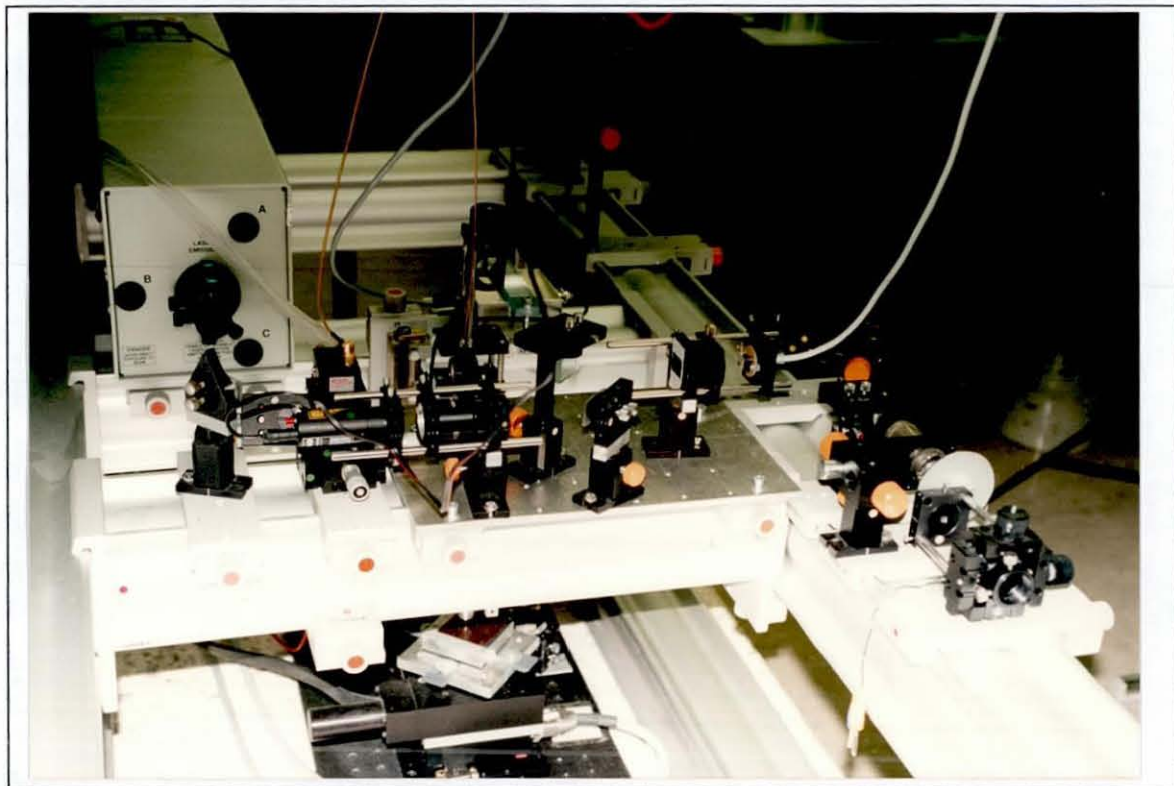


Photo 3: Beam guiding system

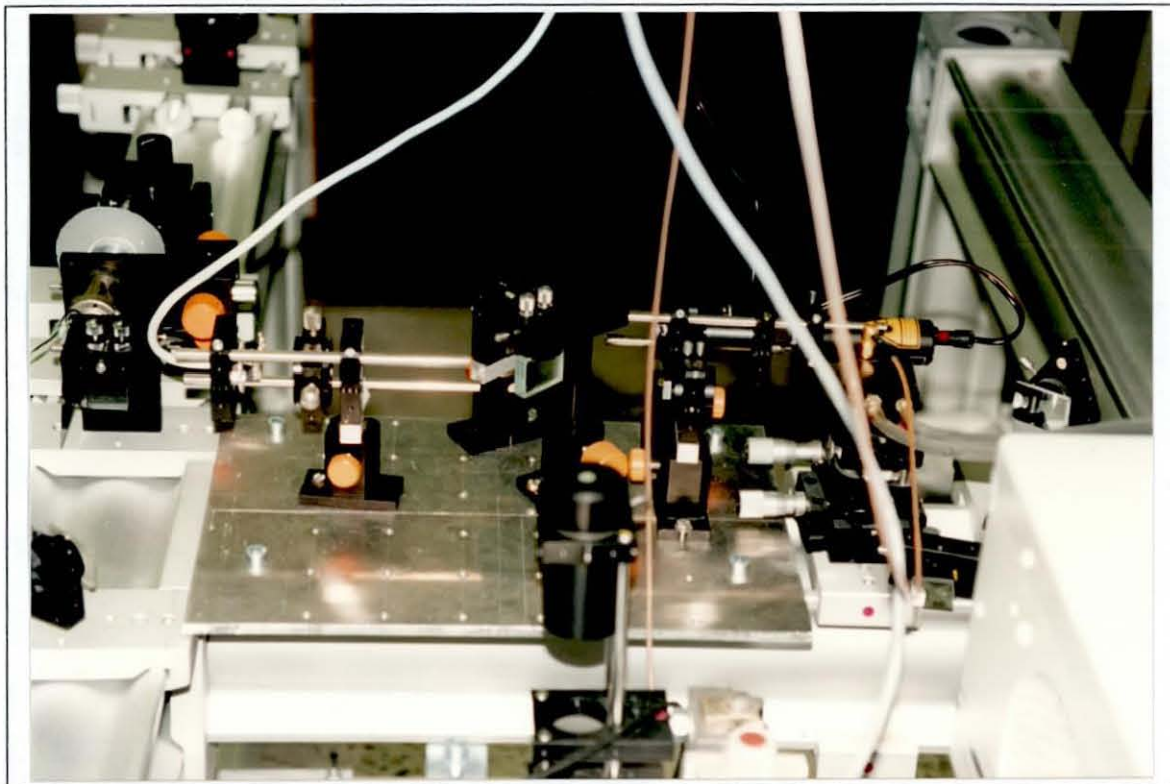


Photo 4: Beam guiding system (detail)

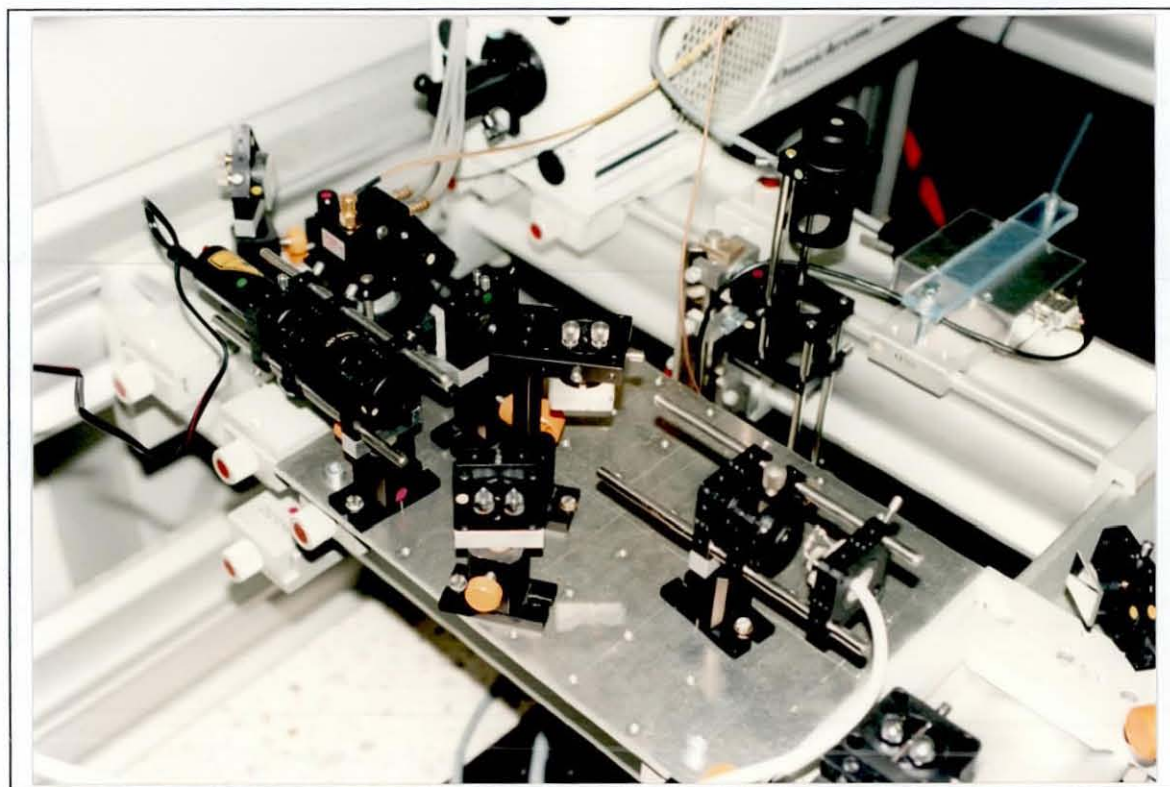


Photo 5: Beam guiding system (detail)

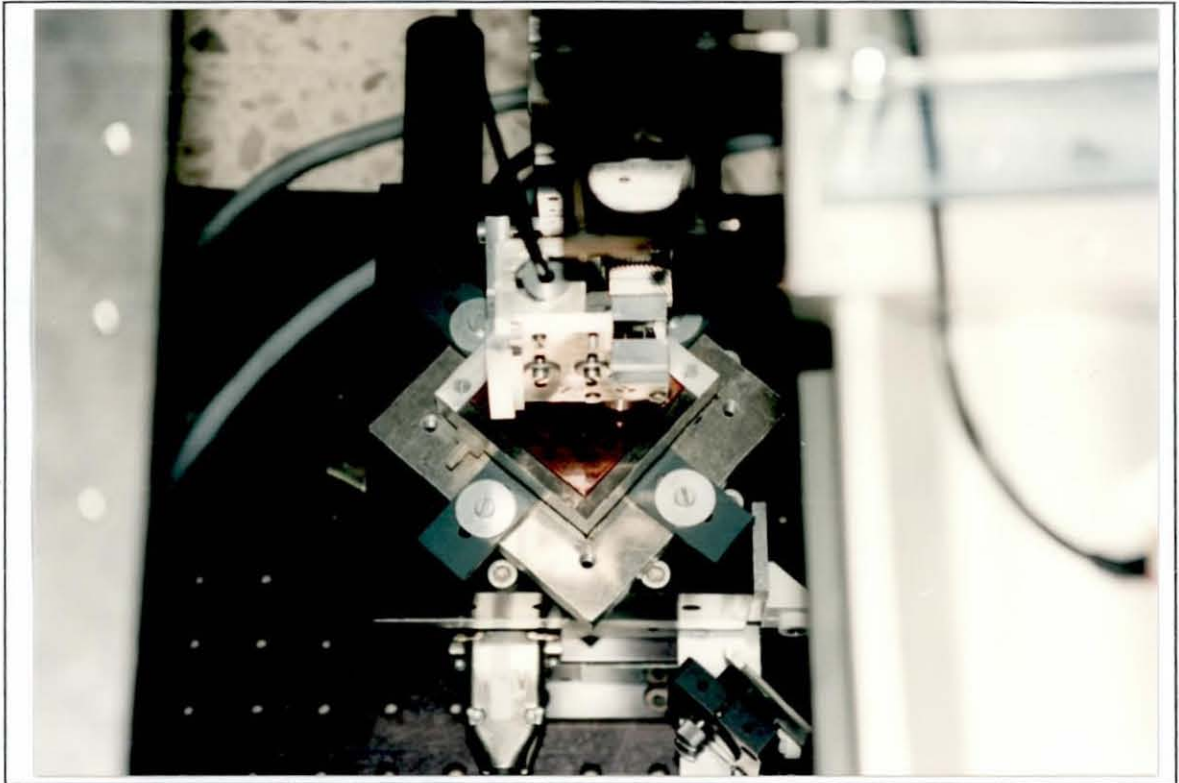


Photo 6: X, Y and rotary table

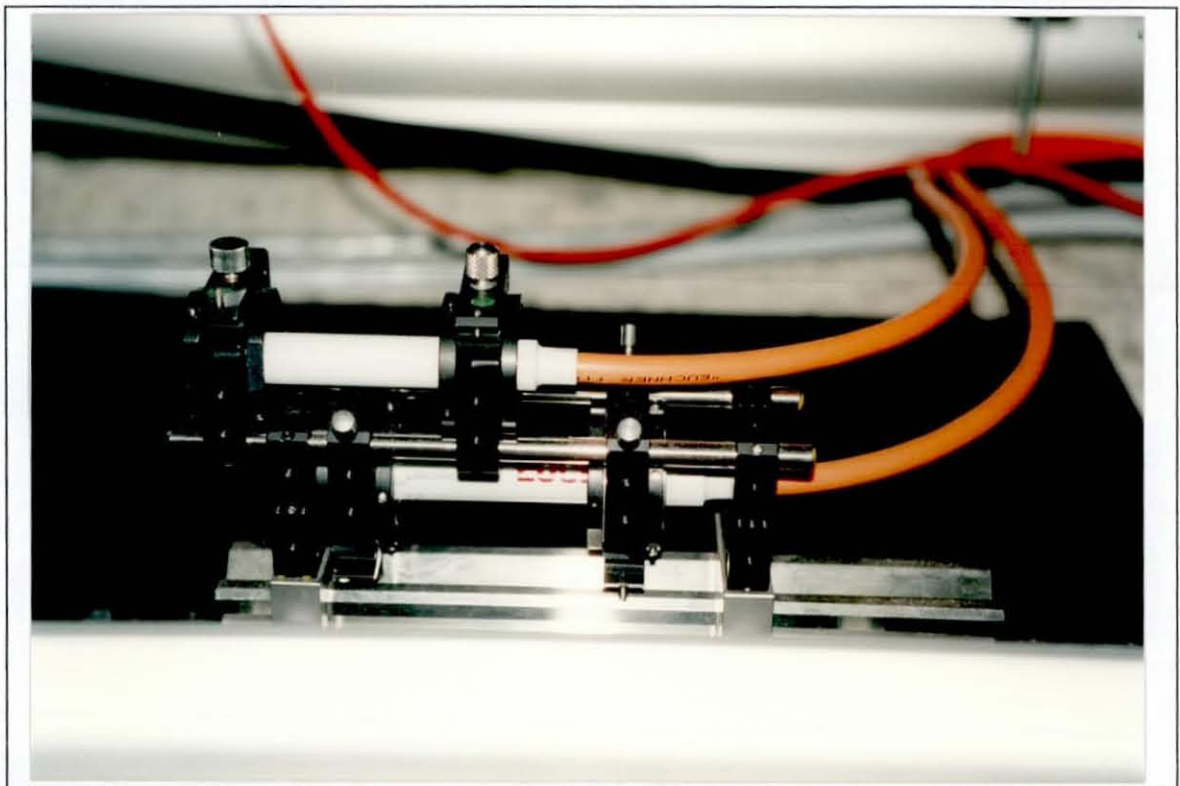


Photo 7: Interferometer head for X,Y positioning table control

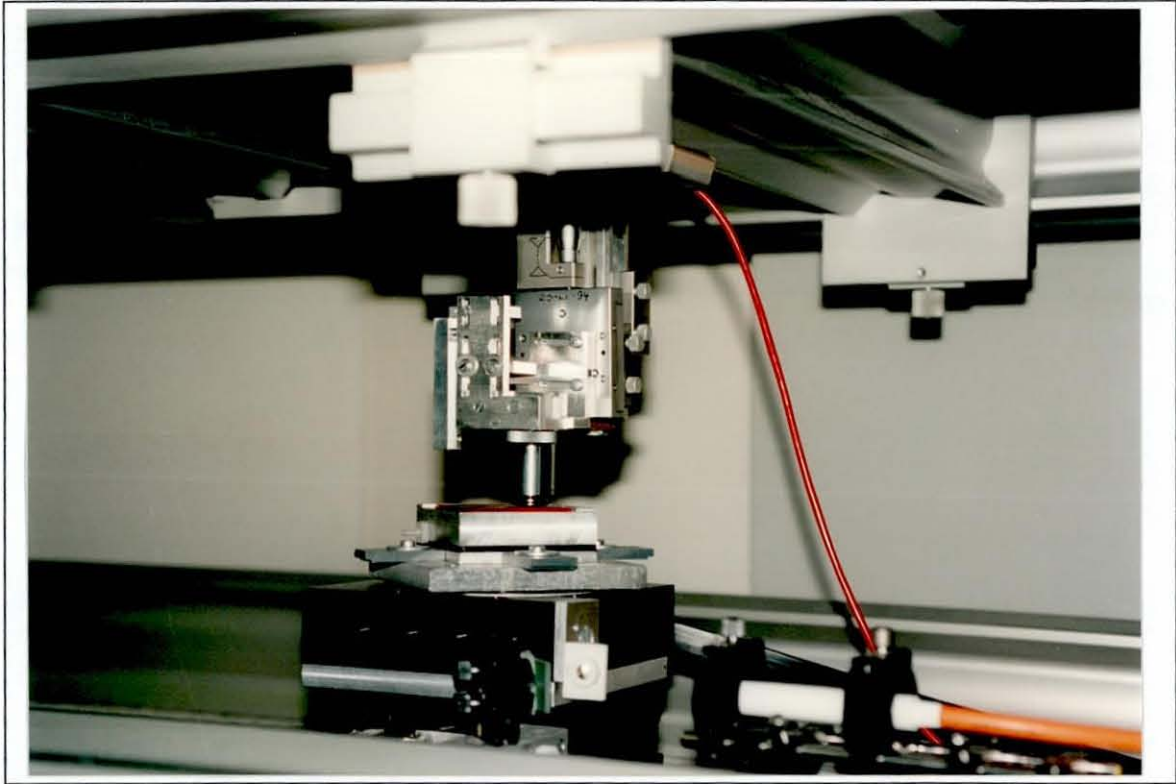


Photo 8: Optimised processing head (front view)

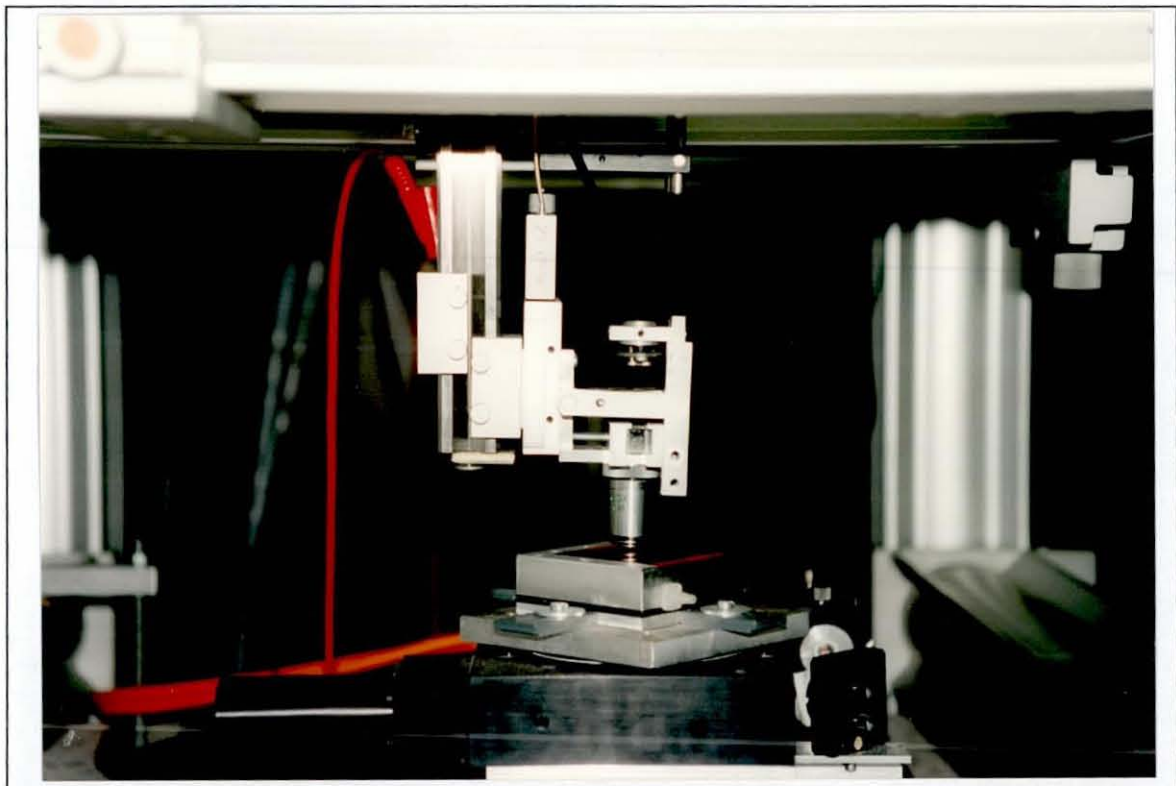


Photo 9: Optimised processing head (side view)

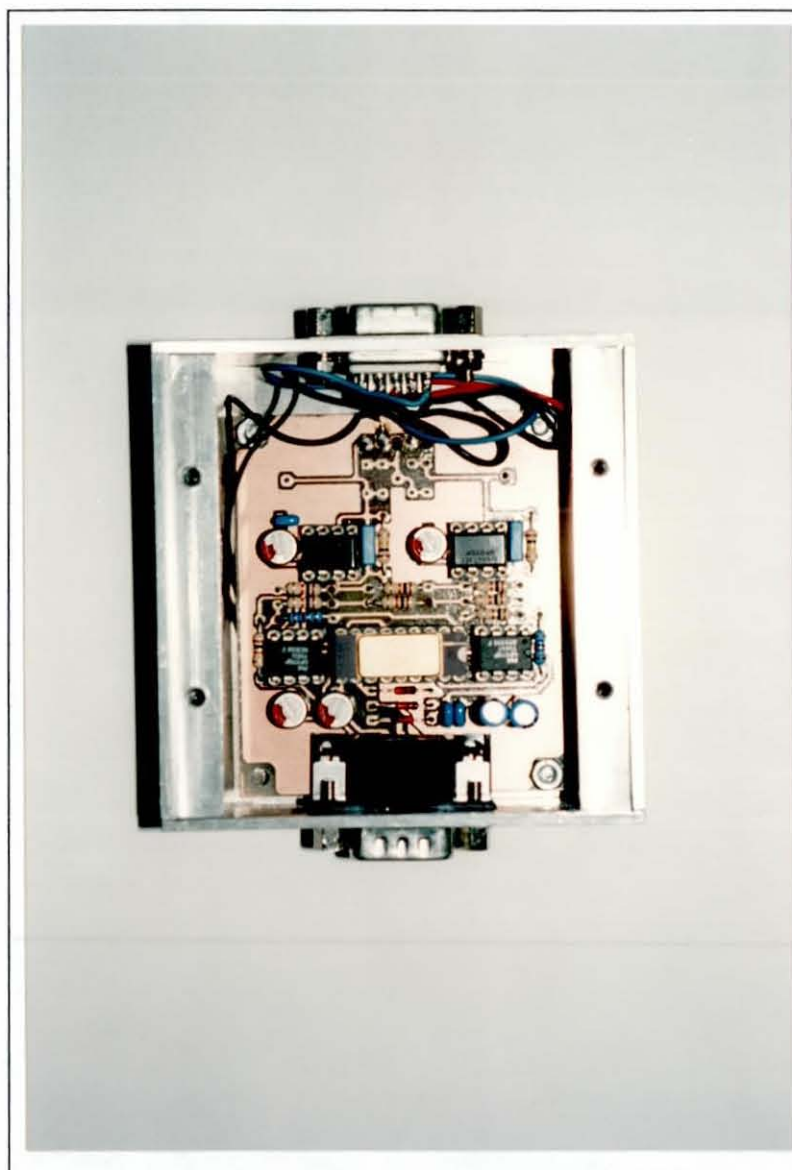


Photo 10: Shielded PSD analysing circuit

PUBLICATIONS

CONTENTS	PAGE #
1. List of publications	W1
2. Fiber optical sensor for absolute measurement of rotation angles	W2-W12
3. Measurement of absolute torsional angle by combining fiber optics distance sensors with gravity deformed cantilevers	W13-W16
4. Precise wavelength tuning of a dye laser using an active diffractive optical element	W17-W32
5. Automated surface measurement via laser tomography	W33-W40

1. List of publications

1. Kreitlow, H., Samuels, U., Fiber optical sensor for absolute measurement of rotation angles, Proceedings of Interometric fiber sensing on the SPIE conference Interferometry '94, Warsaw, 1994
2. Kreitlow, H., Samuels, U., Tiase, L., Boer, K., Schlaf, M., Measuring absolute torsional angles by combining fiber-optics distance sensors with gravity deformed cantilevers, Proceedings of the Laser 95
3. Samuels, U., Kreitlow, H., Wright, S.C., Budzinski, Ch., Tiziani, H.J., Precise wavelength tuning of a dye laser using an active diffractive optical element. Submitted for the publication in Optics&Laser Technolgy
4. Samuels, U., Parkin, R., Kreitlow, H., Automated surface measurement via laser tomography, IEE Colloquium „Innovations in manufacturing control through mechatronics“, Newport, 1995

Fiber optical sensor for
absolute measurement of rotation angles

H. Kreitlow and U. Samuels

Fachhochschule Ostfriesland
Fachbereich Naturwissenschaftliche Technik
Constantiaplatz 4, 26723 Emden, Germany

ABSTRACT

A fiber optical sensor (FOS) for sensitive measurements of absolute angles has been developed. The sensor principle is based on the well defined angular dependence of the bending of a cantilever under the influence of its own weight. The cantilever bending is measured via a non-contact and high resolution method using two fiber optical sensors. These sensors are oriented perpendicular to each other and fixed opposite to the cantilever so that they are rotated synchronously during every angular movement. The current values of the rotation angle, the angular velocity, and the angular acceleration are determined in an analysing and data processing unit and visualised on the computer monitor.

This high precision absolute rotation-angle sensor has the advantages of being compact, insensitive to external influences such as electromagnetic fields, humidity, atmospheric density fluctuations, and nuclear radiation and is therefore applicable in nearly every kind of angular measurement problem and in unfavorable environmental conditions.

1. CANTILEVER THEORY

The cantilever with length l , width b , and height h is clamped at one end for bending under its own weight. Figure 1 describes the geometry and the coordinate system used, where q is the load per unit length caused by the density of the cantilever material.

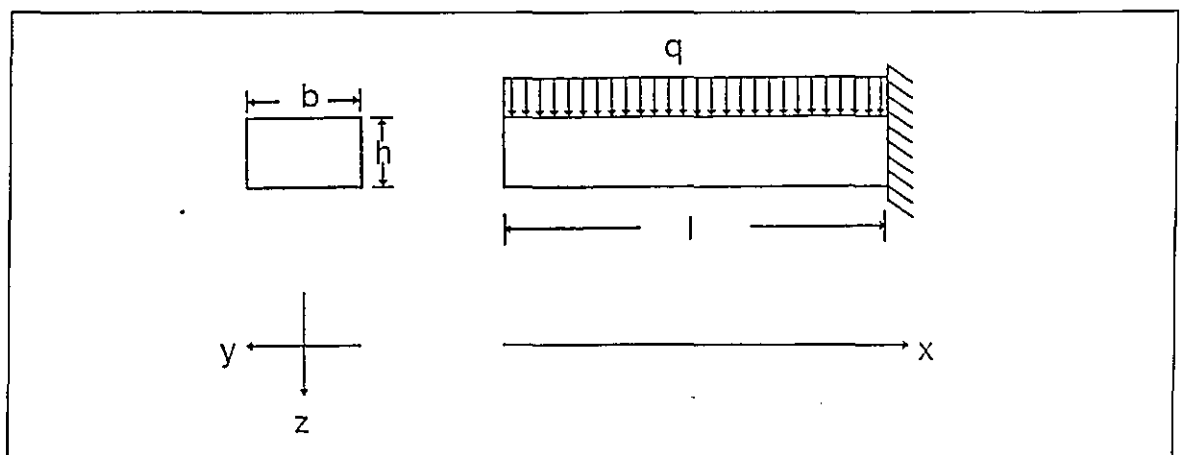


Figure 1: Cantilever model

The displacement $W(x)$ of the free end depends on the shear force and is defined by equation (1) where I is the moment of inertia and E is the module of elasticity. The product of E and I is called the rigidity.

$$W(x) = \frac{q \cdot l^4}{8 \cdot E \cdot I} * \left[1 - \frac{4}{3} * \frac{x}{l} + \frac{1}{3} * \frac{x^4}{l^4} \right] \quad (1)$$

The derivative $dW(x)/dx$ of equation (1) is necessary for the calculation of the slope (surface tangent) of the cantilever at point x which affects the angle between the incident and reflected light beams and has, therefore, to be taken into account for further considerations concerning the FOS-bending sensor described in chapter 2.

$$\frac{dW(x)}{dx} = \frac{q \cdot l^4}{8 \cdot E \cdot I} * \left[-\frac{4}{3} * \frac{1}{l} + \frac{4}{3} * \frac{x^3}{l^4} \right] = \tan(\beta) \quad (2)$$

Figure 2 illustrates the characteristic bending curve of the cantilever as well as the surface tangent at the point of maximum deflection f .

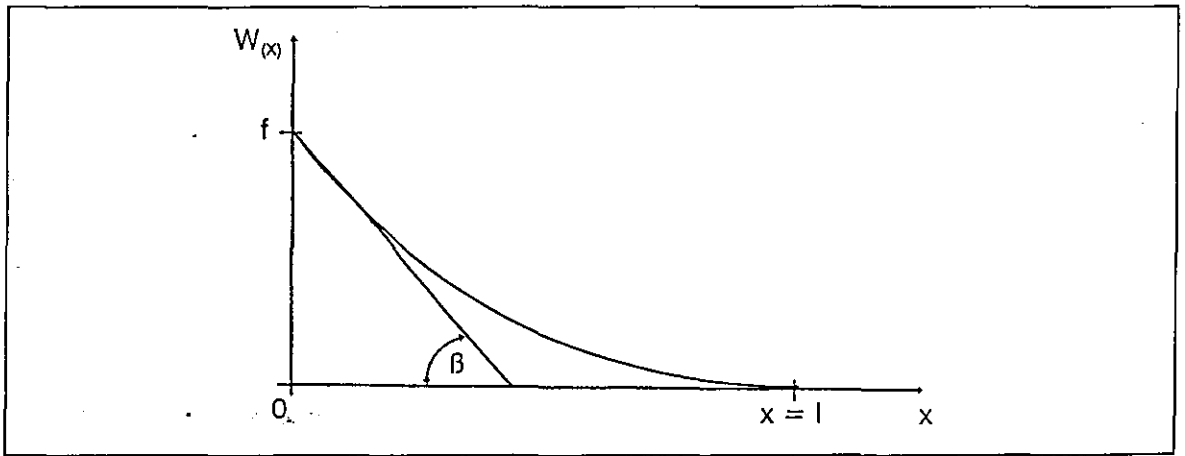


Figure 2: Cantilever deflection W as a function of x

The maximum deflection $f(y)$ and $f(z)$ at point $x=0$ in the two directions of the principle axes of the cantilever y and z , (see figure 1) depending on its angular orientation α with respect to the vertical can be obtained by rotation of the employed coordinate system by α .

$$f(y) = W(0) * \sin(\alpha) \quad (3)$$

$$f(z) = W(0) * \cos(\alpha) \quad (4)$$

Using cantilevers with square cross section ($b=h$) and isotropic material the moment of inertia I is equal in both directions y and z .

$$I(y) = I(z) = \frac{h^4}{12} \quad (5)$$

The load per unit length (q) is given by

$$q = \frac{F}{l} = \delta * b * h * g = \delta * h^2 * g \quad (6)$$

and, therefore, the deflection along the two principle axes at the point $x=0$ of maximum deflection is given by equations (7) and (8) where δ is the density of the cantilever material and g is the acceleration due to gravity at the Earth's surface.

$$f(y) = \frac{3 * \delta * g * l^4}{2 * E * h^2} * \sin(\alpha) \quad (7)$$

$$f(z) = \frac{3 * \delta * g * l^4}{2 * E * h^2} * \cos(\alpha) \quad (8)$$

Using this result, the cantilever as one part of the whole sensor can be optimized with respect to the FOS as the second important part of the rotation angle sensor.

2. FIBER OPTICAL SENSOR (FOS)

A wide variety of physical quantities can be measured using fiber optical sensors.² By means of a FOS, the mechanical bending of a cantilever as depends on its orientation compared to the vertical can be measured, to give the absolute rotation angle.

For measuring the cantilever deflection with highest possible sensitivity, a fiber optical sensor based on the principle of external light intensity modulation was employed as described in earlier work: the light from a light source (guided to the cantilever surface by the sending fiber) is reflected and scattered back from the cantilever surface into the coaxial receiving fibers for opto-electronic conversion by a photodiode.²

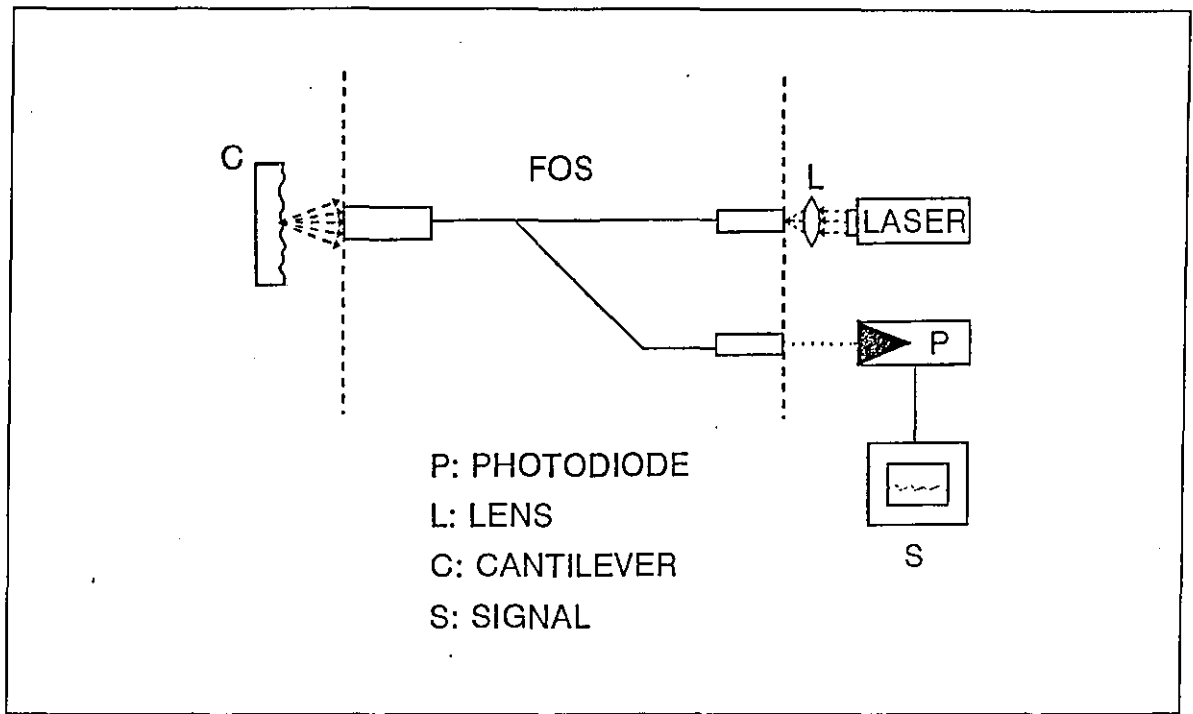


Figure 3: Principle of the fiber optical sensor (FOS)

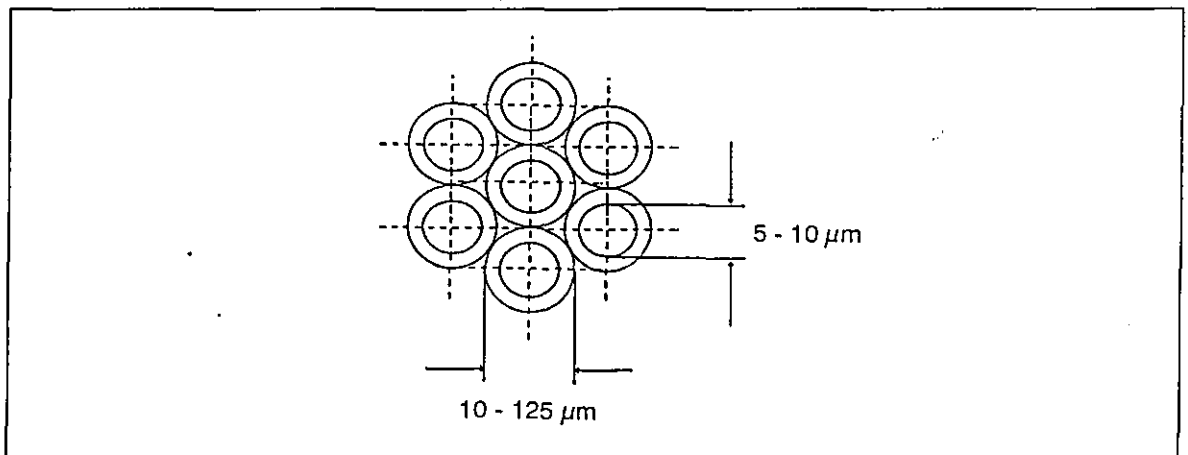


Figure 4: Cross-section of the FOS measuring head with the central (sending) fiber and the coaxial receiving fibers

The voltage output signal of the FOS is a function of the distance from and orientation of a reflecting and scattering surface at the points of light contact as shown in figure 5.

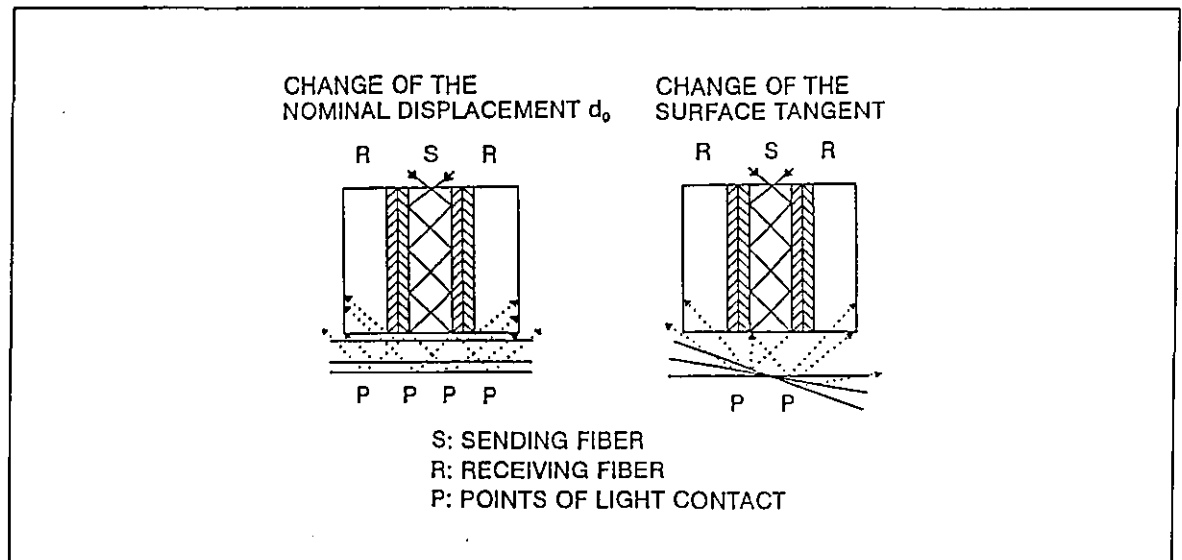


Figure 5: Input of the reflected light in the fiber optical sensor depending on the distance and the orientation of the reflecting and scattering surface

3. MEASUREMENT PRINCIPLE

With regards to sensor construction, the smallest measurable parameter changes and the measurement range are the major demands. In this development the rotation angle sensor has to work over the full-angle (360 degrees) with a resolution as high as possible. For this reason, the cantilever has to have a maximum angular-dependent bending amplitude. According to equations (7) and (8), the deflection of the cantilever is nearly linear at some ranges of both deflection curves with the additional advantage that these are also the high slope parts required for sensitive measurements (see figure 6).

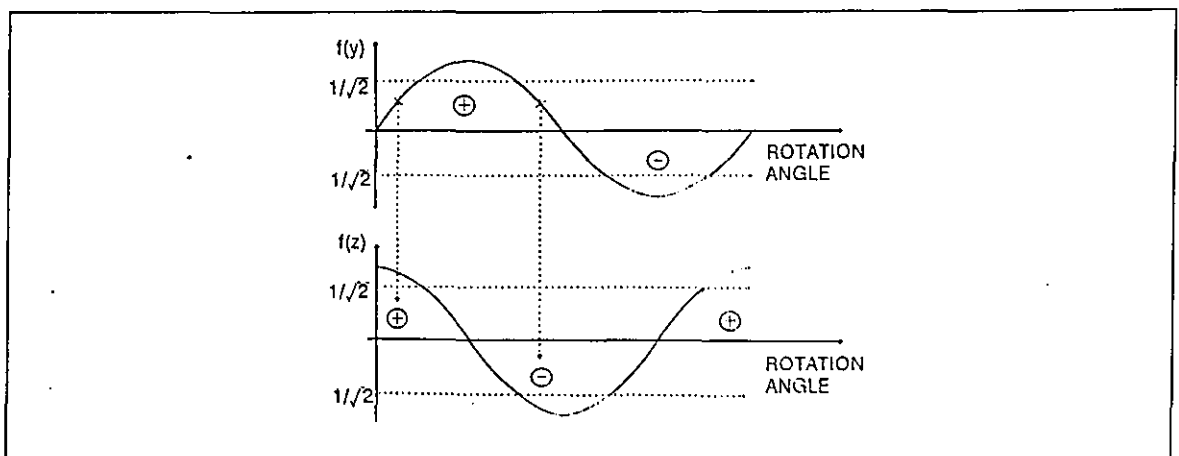


Figure 6: Bending of the cantilever as a function of the rotation angle

Using a cantilever with square cross section, the deflection curves $f(y)$ and $f(z)$ have equal amplitudes. Since the sine function bending characteristic is nearly linear in a range from 0 degree up to 45 degrees while the cosine function showing the bending of the orthogonal component delivers a nearly linear bending in the range from 45 degrees up to 90 degrees, these two curves should be used alternatively for linear rotation angle determination. Following from the behaviour of the sine- and cosine function, this method of angle determination is also applicable for angles between 90 and 360 degrees. Since the above mentioned ranges have also the characteristic of the highest slope, that is, within the deflection range between 0 and $1/\sqrt{2}$ of the maximum signal value, the angle measurement is also performed with highest sensitivity. In order to eliminate the ambiguity in the angle determination (each amplitude of both signals can be obtained by two different angles) an additional piece of information is required. Figure 6 shows the principle of angle determination where, at a given time, the bold lines in one of the curves can be used for angle determination and the other curve for elimination of the ambiguity by examining the sign which indicates the quadrant of the analysed signal. Usable maximum deflection amplitudes are limited by the linear output signal of the FOS in combination with the cantilever bending. The range of the linear portion of the characteristic curve of the FOS depends on the diameter of the receiving fibers and their distance from the sending fiber, as shown in figure 5.

4. ANALYSING AND DATA PROCESSING UNIT

For the determination of the rotation-angle value, a special system for analysing and evaluating the two FOS signals is required. To this end, a computer in combination with an interface to the sensor can be used. The analogue output signals of the sensor have to be transformed for the computer using an A/D converter with an appropriate number of characteristic bits for the signal representation influencing the obtainable quantisation accuracy. As described in chapter 3, only signals up to $1/\sqrt{2}$ of the maximum amplitude in the linear regions have to be analysed. The maximum quantisation error is caused at the point of $1/\sqrt{2}$ of the maximum amplitude and can be calculated depending on the number of A/D converter bits and can be compared with the value at the point of maximum amplitude.

MAXIMUM QUANTISATION ERROR/DEGREES		
BITS	$A=A_{(max)}$	$A=1/\sqrt{2} \cdot A_{(max)}$
8	7.16	0.629
10	3.58	0.158
12	2.53	0.04
14	1.79	$9.89 \cdot 10^{-3}$
16	1.27	$2.47 \cdot 10^{-3}$
18	0.90	$6.18 \cdot 10^{-4}$
20	0.63	$1.55 \cdot 10^{-4}$
22	0.45	$3.86 \cdot 10^{-5}$
24	0.32	$9.66 \cdot 10^{-6}$

Table 1: Maximum quantisation error as a function of A/D converter bits

The A/D converted signal value can be used in an algorithm for comparison of the signal values with:

- those in a look-up table or
- computer calculated sine and cosine functions incrementing the argument or
- a numerical approximation of the linear signal portions

to determine the current rotation angle. The computer program can be used to visualize the current angular value or the value over a longer period. Furthermore, the angular velocity and angular acceleration can be calculated and also presented on the computer monitor. By means of the D/A converter, all angular and angular dependent values can be used as control data for further applications.

5. EXPERIMENTAL OPTIMIZATION OF THE SENSOR

Optimization of the sensor was performed in two stages: optimization of the FOS and the resulting adaptation of the cantilever. The FOS was comprised of the following components:

- a semi-conductor laser as the light source
- a sending-fiber
- six receiving-fibers
- an opto-electronic signal converter (photodiode)
- a DC power supply (12V)

The sending and receiving fibers were of polymethylmethacrylate (PMMA) with a diameter of $50\mu\text{m}$. The output signal of the FOS for a given geometry (fiber diameter and separation between the fibers), is dependent upon the distance between the FOS and the surface of the cantilever (which is the sum of the nominal distance d_0 and the rotation-dependent deflection $W(\alpha)$) as well as the inclination of the surface tangent of the cantilever as a result of the bending at the position of measurement with respect to the FOS axis (see figures 5 and 7). Analysis of the characteristics of the output signal in relation to the above geometrical parameters allows one to choose the most linear operating region, thus optimizing the sensor for high precision rotation angle measurements. For this reason, two experiments were performed, in which a systematic study of the effect of the two parameters d_0 and W on the output signal were recorded. In order to ensure the reproducibility of the measurements, cantilevers with similar surface microstructures were used in all of the experiments.

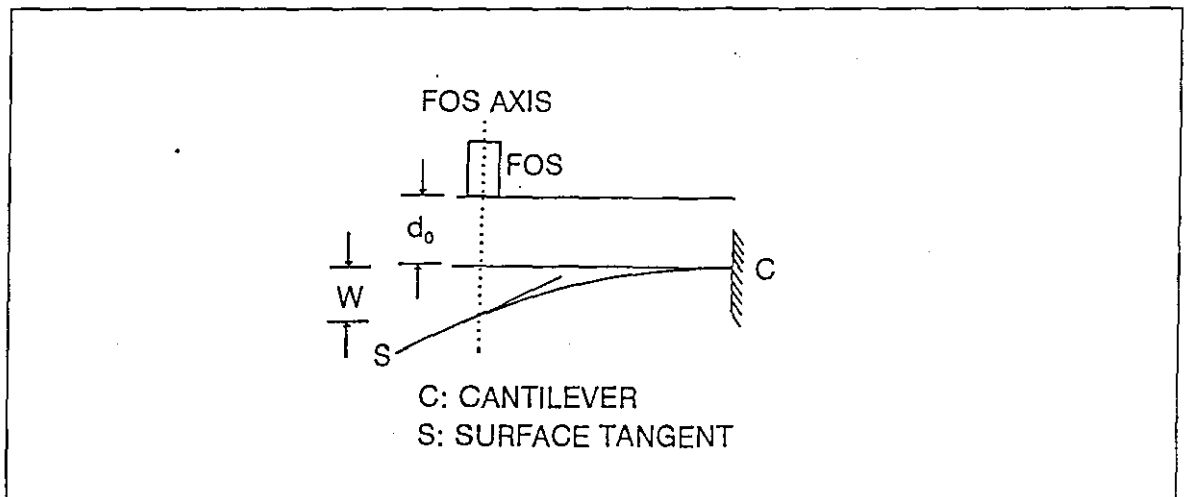


Figure 7: Geometrical parameters affecting the amplitude of the measured signal

In the first experiment, the dependence of the output of the FOS on the nominal displacement, d_0 , was determined by displacing the FOS in a well defined manner with a micrometer screw relative to the cantilever surface, which was oriented perpendicular to the FOS, and measuring the resulting reflected and scattered laser light collected by the receiving fibers.

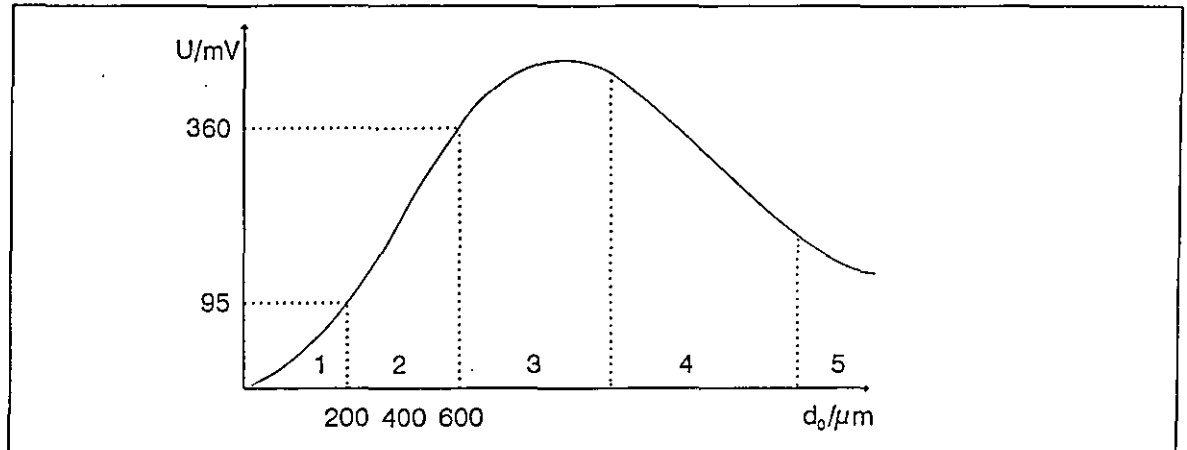


Figure 8: Output, S , of the FOS versus nominal displacement, d_0 , from the reflecting and scattering cantilever surface

d_0 : nominal displacement between cantilever surface and FOS

U : output signal from the FOS

1,3 and 5: non-linear signal regions

2 and 4: linear signal regions

Regions 2 and 4 are both characterized by a linear dependence of the signal on displacement, with the difference that region 2 ($200\mu\text{m} < d_0 < 600\mu\text{m}$) is more suitable for high-precision measurements of the deflection of the cantilever owing to its greater slope ($0.66\text{ mV}/\mu\text{m}$), resulting in a sensitivity of 10nm .

A second experiment was necessary to determine the influence of the cantilever deflection, W , on the output signal. For various values of d_0 within the linear region 2 (as determined above), the cantilever was deformed via a second micrometer screw and the output signal as a function of this well defined deflection recorded. The linear working range of the system was then defined as the smaller of the two ranges of linearity about the nominal displacement of the cantilever (that is, displacements due to deflection towards or away from the FOS). From Figure 9, one sees that the largest linear working range for deflections is $70\mu\text{m}$ when d_0 is set to $400\mu\text{m}$, that is, with d_0 set to the middle of the linear range from the first experiment (see figure 8).

Figure 10 shows that for a cantilever deflection of $70\mu\text{m}$ in both directions, a linear signal is obtained with a total signal variation of $\Delta U = 400\text{mV}$. In comparison to figure 8, the reduction of the linear working range and the increase in sensitivity to $2.82\text{ mV}/\mu\text{m}$ are a result of the inclination of the surface tangent of the cantilever with respect to the FOS during deflection. This results in an increased sensitivity of the measurement system.

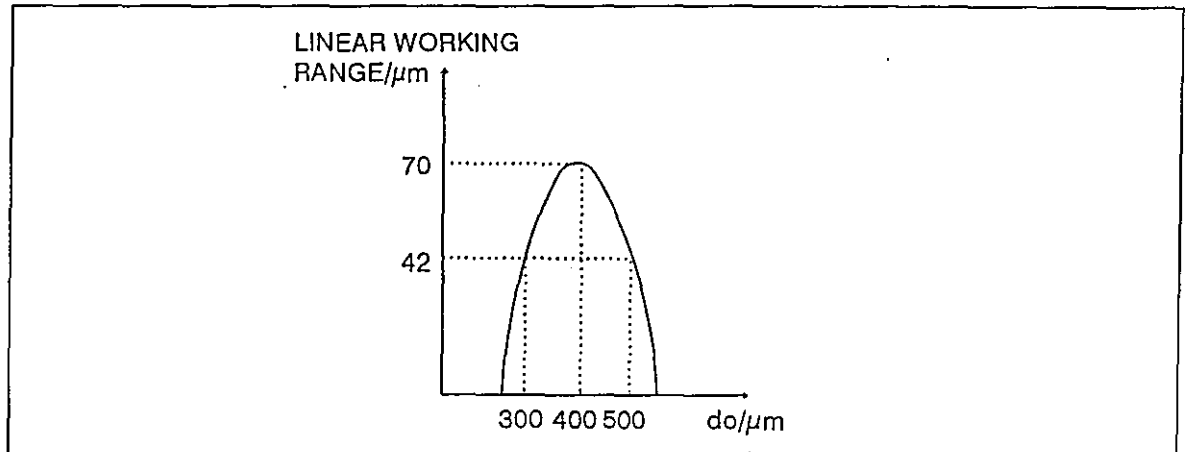


Figure 9: Linear working range of the FOS as a function of the nominal displacement, d_0 , between the FOS and the cantilever surface

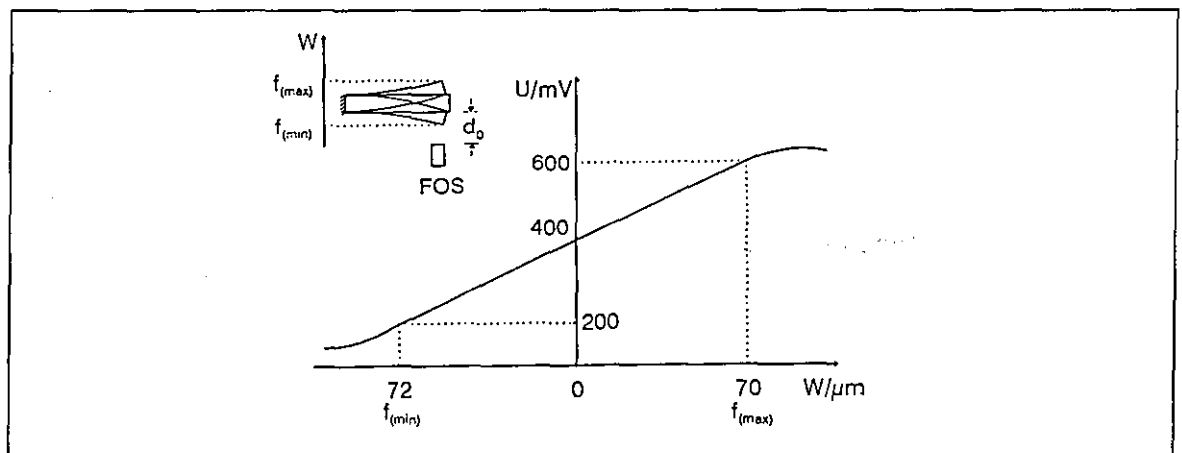


Figure 10: Dependence of the output signal from the FOS on the cantilever deflection, W , for a nominal displacement, d_0 , of $400\mu\text{m}$

Through use of equations (7) and (8), various combinations of parameters may be found, allowing optimal design of the cantilever using the full linear working range determined above. The following parameters were chosen:

MATERIAL:	BRASS (RED)
E:	98GPa
δ :	8.8Kg/dm
l:	0.15m
h=b:	3.1mm

Table 2: Cantilever parameters

6. MEASUREMENT CHARACTERISTICS OF THE ROTATION ANGLE SENSOR

To determine the measurement characteristics of the rotation angle sensor described in chapter 5 (see figure 11), a computer controlled apparatus was developed employing a high-precision rotation stage with a resolution of 1/1000 degree to rotate the cantilever about the horizontal axis.

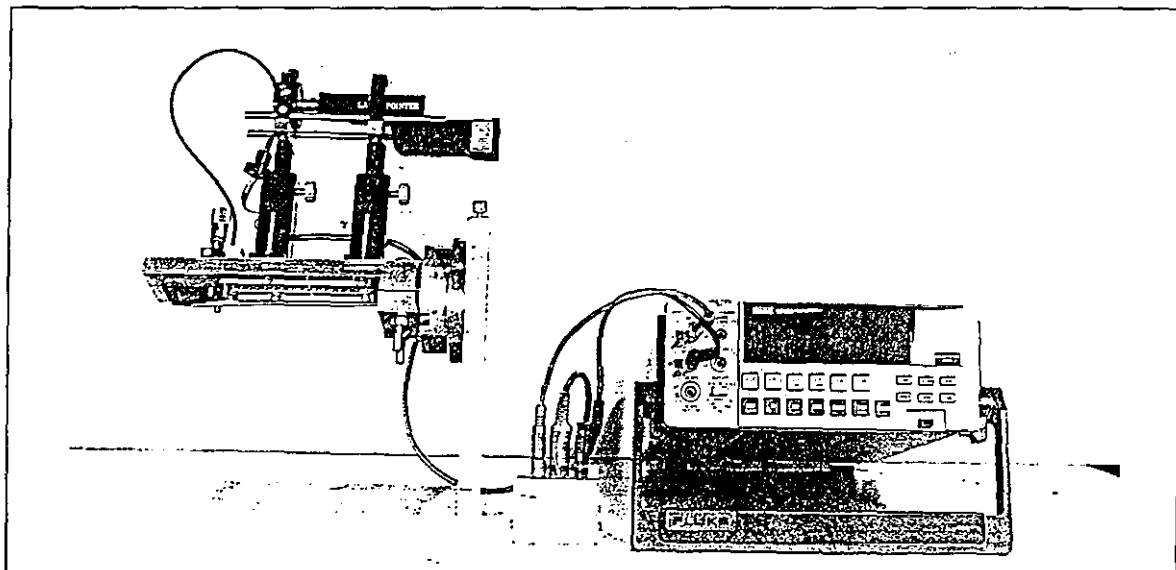


Figure 11: Rotation angle sensor construction

The dependence of the measured FOS-signal on the rotation angle, α , is confirming the theoretical description given by equations (7) and (8). The experiments result a signal of more than $7\mu\text{V}$ per rotary motion step of 1/1000 degree. In order to unambiguously determine the true rotation angle from these FOS-signals, a data processing unit was developed based on a PC with an integrated A/D and D/A converter, as described in chapter 4.

The current value of the rotation angle (which was updated every $10\mu\text{s}$ by polling the interface), the angular velocity, the angular acceleration as well as their development in time are displayed on the computer monitor with a measurement period of 30s (see figure 12).

These values are also made available at the output port of the D/A converter for systems control applications. The data processing algorithm developed, uses only the nearly-linear regions of the FOS-signals (sine and cosine functions) for the determination of the rotation angle, as described in chapter 3. In this manner, the sensitivity was increased and a minimal digitization error could be obtained, since only the signal values up to $1/\sqrt{2}$ of the maximum signal amplitude were used for the computation. The current value of the rotation angle is determined by the software by comparing the signals of the FOS with computer-generated sine and cosine functions, whose arguments could be incremented in steps of 1/1000 degrees. Due to the high resolution of the FOS developed, the optimization of the cantilever and the intelligent data processing algorithm using only signal regions of highest sensitivity which results in minimal digitization error during the A/D conversion, this rotation angle sensor delivers high-precision signals, whose precision is limited only by the characteristics of the digital conversion. For this reason, the A/D conversion card should be chosen to have the highest possible digital resolution. In order to isolate the system against undesirable external influences, the whole sensor was integrated into an enclosure.

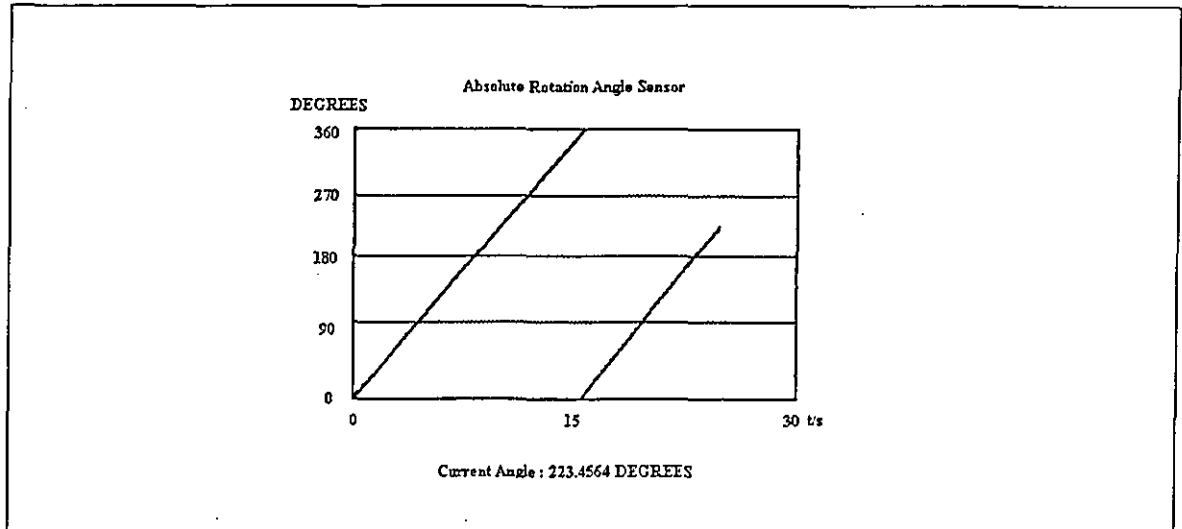


Figure 12: Monitor display of the rotation angle sensor signal

7. AREAS OF APPLICATION

The rotation-angle sensor can be used in a wide range of applications where highly precise information on angular orientation is required. Compared to other rotation-angle sensors such as code-discs and incremental counters, this sensor has the advantage of measuring absolute angles. Furthermore, the use of light as the information carrier as well as fiber optics ensures that this sensor is insensitive to environmental influences such as electromagnetic fields, humidity, and atmospheric density fluctuations. Using fiber optical links, long distances between the rotation-angle sensor and the analysing and data processing unit do not restrict the application of the sensor because of the small attenuation of the light in the fiber. The choice of a cantilever material with a small temperature expansion coefficient makes this sensor suitable for high temperature applications, since quartz or sapphire based fiber optics can be used up to 1000°C without influencing the measurements. Furthermore, this sensor is also useful in regions with up to 100 Krad nuclear radiation where electronic signals cannot be used.

8. REFERENCES

1. Szabó, I., "Einführung in die Technische Mechanik", Berlin, Springer-Verlag, 1966
2. Kreitlow, H., "Faseroptische Sensoren" in Pfeifer, T., et. al., "Optoelektronische Verfahren zur Messung geometrischer Größen in der Fertigungstechnik", Ehningen, expert-verlag, 1993

Measurement of absolute rotation angle by combining fiber-optics distance sensors with gravity deformed cantilevers

H. Kreitlow, U. Samuels, L. Tiase, K. Boer, M. Schlaf
 Fachhochschule Ostfriesland
 Fachbereich Naturwissenschaftliche Technik
 Institut für Lasertechnik
 Constantiaplatz 4, D-26723 Emden

ABSTRACT

The principle of a fiber optical sensor (FOS) for sensitive measurements of absolute angles has been investigated. The sensor principle is based on the well defined angular dependence of the bending of a cantilever under the influence of its own weight. The cantilever bending is measured via a non-contact and high resolution method using two fiber optical sensors. These sensors are oriented perpendicular to each other and fixed opposite to the cantilever so that they are rotated synchronously during every angular movement. The current values of the rotation angle are determined in an analysing and data processing unit and visualised on the computer monitor.

This high precision absolute rotation angle sensor has the advantages of being compact, insensitive to external influences such as humidity, atmospheric density fluctuations, electromagnetic fields, and nuclear radiation and is therefore applicable in nearly every kind of angular measurement problem and in unfavorable environmental conditions.

1. CANTILEVER

The cantilever with length l , width b , and height h is clamped at one end for bending under its own weight (see figure 1).

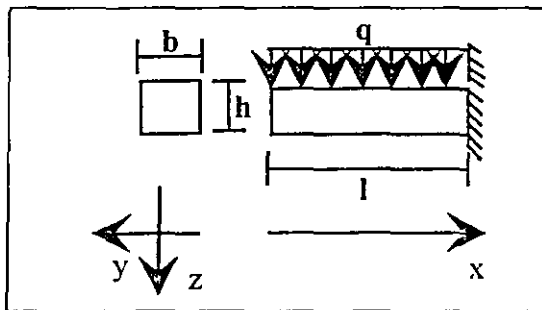


Figure 1: Cantilever model

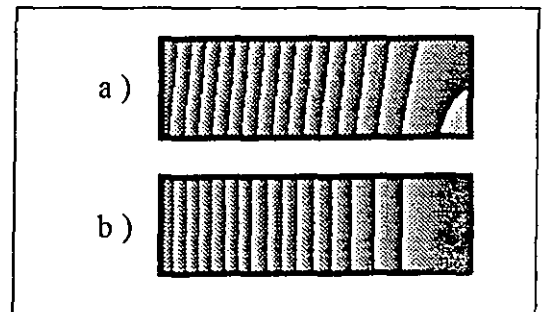


Figure 2: Fringe pattern simulation for cantilever optimization by holographic interferometry:
 a.) torsion; b.) ideal adjustment

The angular dependent deflection of a cantilever with square cross section ($b=h$) and isotropic material along the two principle axes at the point of maximum deflection is given by equations (1) and (2) where ρ is the density of the cantilever material, g is the acceleration due to gravity at the Earth's surface, and E is the module of elasticity.

$$f_y(\alpha) = \frac{3\rho g l^4}{2Eh^2} \sin(\alpha) \quad (1)$$

$$f_z(\alpha) = \frac{3\rho g l^4}{2Eh^2} \cos(\alpha) \quad (2)$$

Using this result, the cantilever as one part of the whole sensor can be optimized theoretically with respect to the FOS as the second important part of the rotation angle sensor. Experimental optimization of the cantilever was performed by holographic interferometry supported by a computer programme for holographic fringe pattern simulation (see figure 2).

2. FIBER OPTICAL SENSOR (FOS)

By means of a FOS, the mechanical bending of a cantilever as depends on its orientation compared to the vertical can be measured, to give the absolute rotation angle. For measuring the cantilever deflection with highest possible sensitivity, fiber optical sensors based on the principle of external light intensity modulation is employed as described: the light from a light source (guided to the cantilever surface by the sending fiber) is reflected and scattered back from the cantilever surface into the coaxial receiving fibers for opto-electronic conversion by a photodiode [1,2], see figures 3, 4, 5.

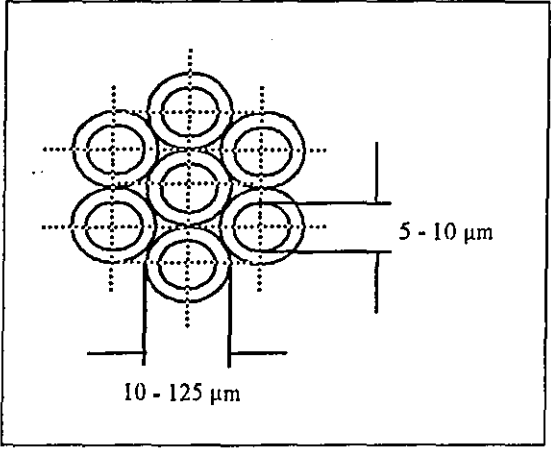
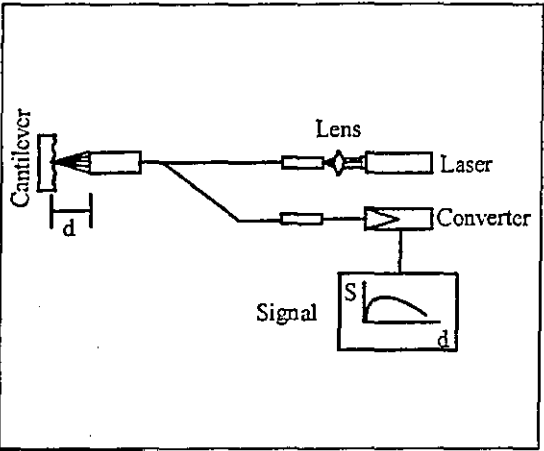


Figure 3: Principle of the fiber optical sensor (FOS) Figure 4: Cross-section of the FOS measuring head with the central (sending) fiber and the coaxial (receiving) fibers

The voltage output signal of the FOS is a function of the distance from and orientation of a reflecting and scattering surface at the points of light contact as shown in figure 5 and 6.

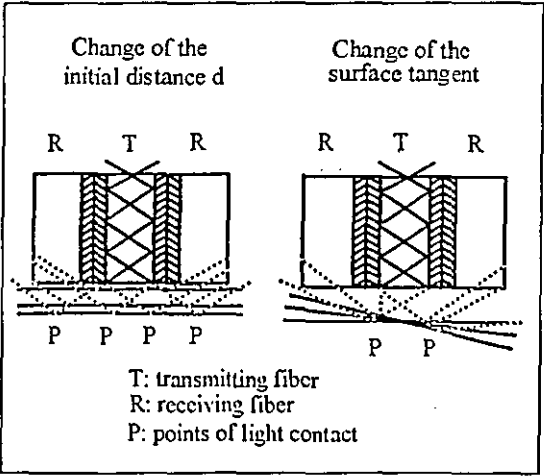


Figure 5: Input of the reflected light in the fiber optical sensor depending on the distance and the orientation of the reflecting and scattering surface

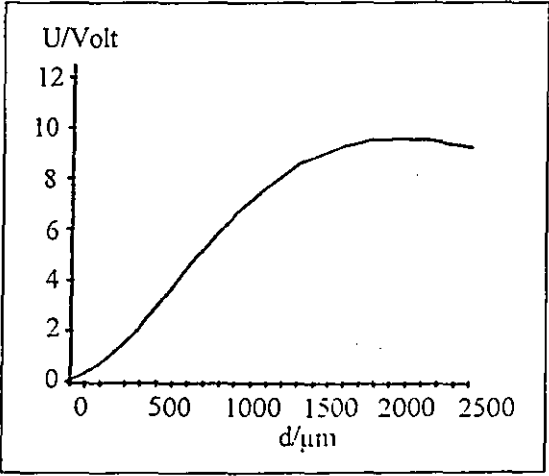


Figure 6: Output U of the FOS as a function of the nominal displacement d

3. COMBINATION OF FOS AND CANTILEVER

With regards to sensor construction, the smallest measureable parameter changes and the measurement range are the major demands. In this development the rotation angle sensor has to work over the full-angle (360 degrees) with a resolution as high as possible. For this reason, the cantilever has to have a maximum angular-dependent bending amplitude. According to equations (1) and (2), the deflection of the cantilever is nearly linear at some ranges of both deflection curves with the additional advantage that these are also the high slope parts required for sensitive measurements. Using a cantilever with square cross section, the deflection curves $f_y(\alpha)$ and $f_z(\alpha)$ have equal amplitudes. Since the sine function bending characteristic is nearly linear in a range from 0 degree up to 45 degrees while the cosine function showing the bending of the orthogonal component delivers a nearly linear bending in the range from 45 degrees up to 90 degrees, these two curves should be used alternatively for linear rotation angle determination. Following from the behaviour of the sine and cosine function, this method of angle determination is also applicable for angles between 90 and 360 degrees. Since the above mentioned ranges have also the characteristic of the highest slope, that is, within the deflection range between 0 and $1/\sqrt{2}$ of the maximum signal value, the angle measurement is also performed with highest sensitivity. In order to eliminate the ambiguity in the angle determination (each amplitude of both signals can be obtained by two different angles) an additional piece of information is required.

Through use of equations (1) and (2), various combinations of parameters may be found, allowing optimal design of the cantilever using the full linear working range determined above. The following parameters were chosen:

material:	Ceramtec [®]
E:	360kN/mm ²
ρ :	3.8Kg/dm ³
l:	50mm
h:	0.1mm
b:	5mm

Table 1: Cantilever parameters

4. SENSOR DESIGN

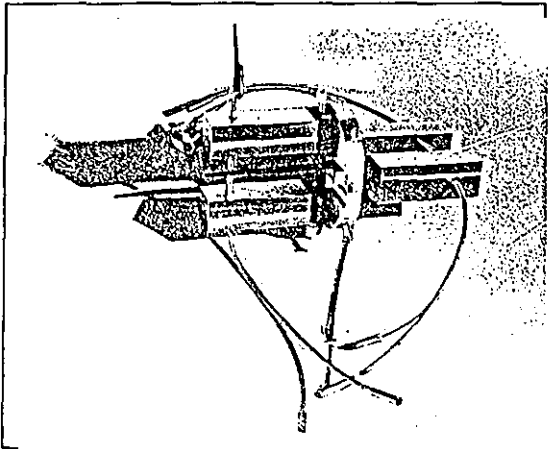


Figure 7: Design of the full angle sensor

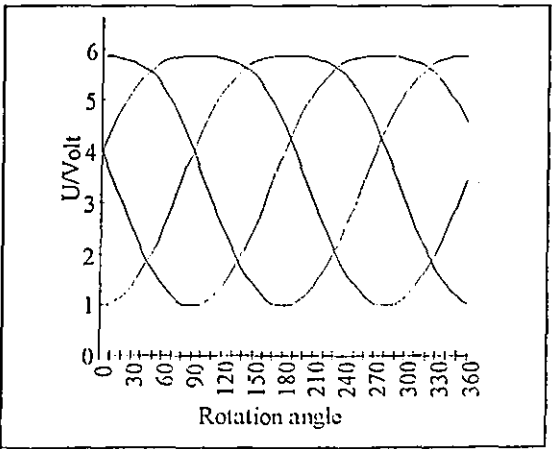


Figure 8: Output signal of the full angle sensor

For the measurement of absolute rotation angles with a measurement range of 360 degrees, a sensor was developed which is based on two cantilevers which are fixed perpendicular to each other in

combination with four FOS which are rotated synchronously with the cantilever. Figure 7 shows a picture of the full-angle sensor. The output signal of the four FOS as a function of the rotation angle is sketched in figure 8.

For special applications a miniaturized sensor for a measurement range of 180 degrees based on one FOS has been developed (see figure 9). The output signal of this sensor is shown in figure 10.

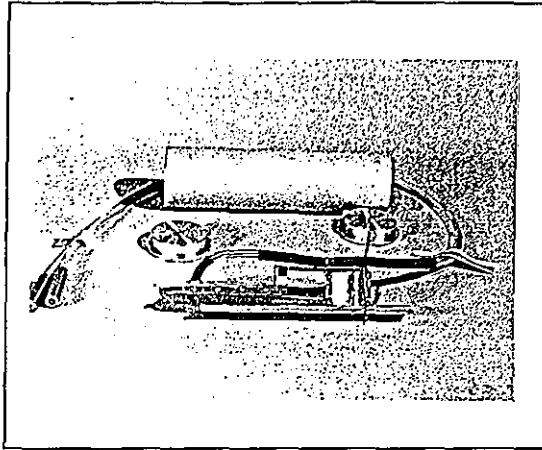


Figure 9: Miniaturized sensor design

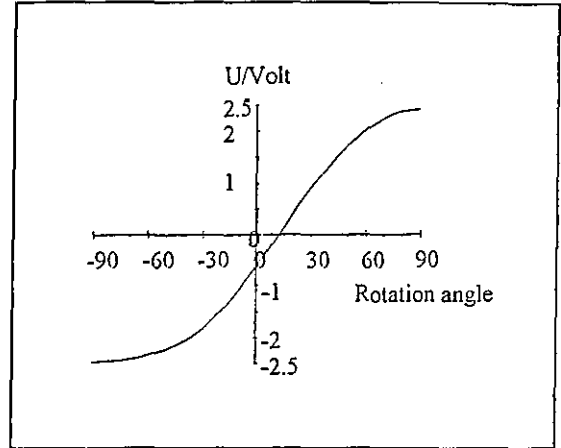


Figure 10: Output signal of the miniaturized sensor

5. RESULTS

The characteristics of the sensor developments are summarized in the following table

- measurement range: 360 degrees
- resolution : 1/1000 degree
- no measurement influence due to:
 - humidity
 - high temperature
 - electromagnetic fields
 - nuclear radiation < 100krad
- flexible signal guiding by modular fiber system
- noise minimized electronics for signal conversion and analysing
- measurement of angular acceleration and angular velocity by computer signal evaluation
- miniaturized sensor for measurement range: 180 degrees

REFERENCES

1. Kreitlow, H., "Faseroptische Sensoren" in Pfeifer, T., et. al., "Optoelektronische Verfahren zur Messung geometrischer Größen in der Fertigungstechnik", Ehningen, expert-verlag, 1993
2. Kreitlow, H., Samuels, U., "Fiber optical sensor for absolute measurement of rotation angles", presented on the SPIE Conference "Interferometry '94", Warsaw, 1994

Precise Wavelength Tuning of a Dye Laser using an Active Diffractive Optical Element

U. Samuels, H. Kreitlow, S. C. Wright
Fachhochschule Ostfriesland, Institut für Lasertechnik, Emden, Germany

Ch. Budzinski, H. J. Tiziani
Universität Stuttgart, Institut für Technische Optik, Stuttgart, Germany

Abstract

In this work, an active, reflecting diffraction grating was developed and characterised. A grating was holographically imposed onto the surface of a ceramic which could be deformed via the transverse, inverse piezoelectric effect, thus allowing active fine tuning of the grating constant. The tuning characteristics of this novel optical element were studied and the results compared to the linear theory of the piezoelectric effect. To demonstrate its applicability, the grating was installed in a dye laser and used to effect precise tuning of the output wavelength of the laser within a range of 220 pm. The possibility of quasi-static to high frequency operation of the system will allow this element to find use in a wide variety of applications.

1. Principles of Operation

The principles to be described in this work have been suggested previously^{1,2,3}. An area or volume change as a result of a uniform elastic deformation of a plane grating substrate (eg, piezoelectric ceramic), results in a change in the line spacing and the profile of the surface structure of a straight, equidistant groove system (classical plane grating).

From the grating equation

$$k\lambda = g(\sin \alpha + \sin \beta) \quad [1]$$

it follows that for a given optical geometry (ie, angles of incidence, α , and diffraction, β), the corresponding wavelength is dependent upon the grating constant

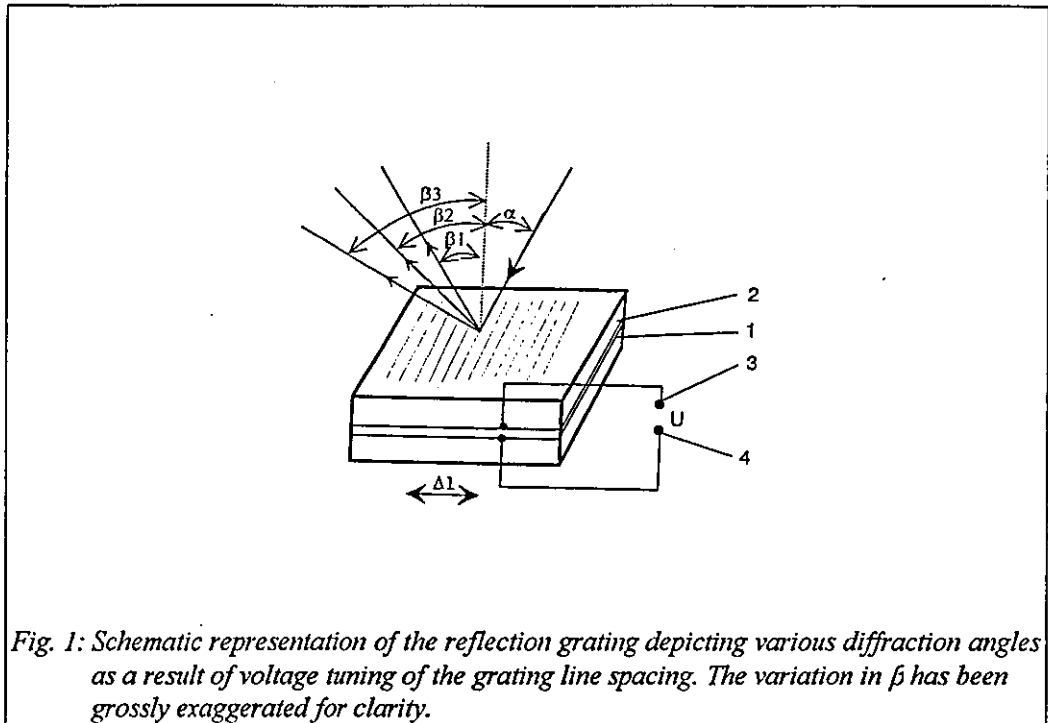
$$\frac{d\lambda}{dg} = \frac{1}{k}(\sin \alpha + \sin \beta) \quad [2]$$

whereby g is the grating constant and k the diffraction order.

From the linearity of the grating equation [1] also follows the direct relationship between the relative expansion of the grating substrate along the direction of dispersion and the relative variation of the wavelength into a given diffraction angle

$$\frac{dl}{l} = \frac{dg}{g} = \frac{d\lambda}{\lambda} \quad [3]$$

By use of a plane, polished piezoelectric ceramic grating substrate (1 in Figure 1) onto which a diffracting structure (2) and electrodes covering the major surfaces (3,4) have been imposed, it is possible to use the transverse, inverse piezoelectric effect to vary the grating line spacing via an imposed electric voltage as depicted.

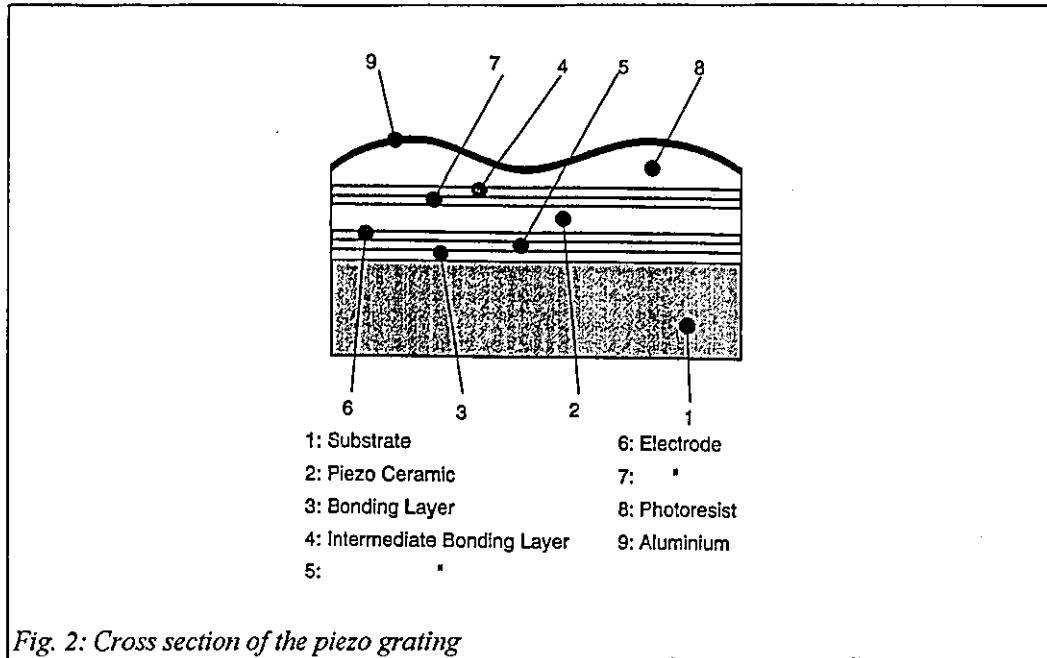


Substrate materials by which a length change may be caused via other effects (eg, electrostrictive or magnetostrictive materials) are also suitable for this purpose. The suitability of materials is, however, somewhat restricted in that it must be possible to polish the surface to optical quality. Regarding the choice of piezoelectric material, all ferroelectrics with a non-negligible transverse coefficient in their deformation matrix may also be considered suitable. In addition to the industrially produced solid solutions, in which certain characteristics may be especially cultivated, most natural substances also show piezoelectric and/or ferroelectric qualities. An important example is quartz which, owing to its high transparency in the visible and near ultraviolet spectral regions, is particularly interesting. However, the piezoelectric strain constant of quartz is small, thus limiting its use to very specialized applications.

2. Manufacture of the Grating

Figure 2 shows a detailed cross section of the piezo grating with its glass substrate (1), piezo ceramic (2) and the various bonding layers (3 to 5). In this work, the ceramic PK51 from the company Marco in Hermsdorf, Germany was chosen. This lead-zirconate-titanate ceramic (PZT) sample was 50 mm long, 20 mm wide and 1 mm thick. The upper surface of the ceramic was coated and polished to optical quality followed by deposition of electrodes (6) and (7) onto the upper and lower surfaces. Photoresist (8) was then brought onto the optically polished surface and formed to a sine grating with a grating constant of $g = 0.476 \mu\text{m}$ (2100 lines per mm) through holographic exposure in a laser interferometer. The surface of the grating was

then coated with a highly reflective aluminum layer in order to achieve a high diffraction efficiency in first order. Following electrical contacting, the piezo ceramic was polarized.



3. Tuning Characteristics of the Active Diffraction Grating

The principle of operation of piezo-ceramic actuators is based on the deformation of the piezoelectric material under the influence of an applied electric field (reciprocal piezoelectric effect). A positive (negative) voltage with respect to the direction of polarization results in an expansion (contraction) of the material in this direction and a contraction (expansion) in the perpendicular direction. Depending on the material employed and, thus, its piezoelectric strain constants, relative expansions of 0.15% may be attained. In the linear approximation, within the region of validity of Hooke's law, the relative change in length may be calculated as:

$$\frac{\Delta l}{l} = d_{ij}E = d_{ij} \frac{U}{h} \quad [4]$$

- l: undeformed length of the piezo-ceramic
- Δl : change of length of the piezo-ceramic
- h: distance between the electrodes
- d_{ij} : relevant piezoelectric strain constant
- E: electric field strength
- U: applied electric voltage

Linear expansion and contraction as described by equation [4] (deformation proportional to the applied field strength and to the undeformed length of the element), is valid only for small applied voltages with electric field strengths less than 50 V/mm. Above this value, deviations from linear behaviour and hysteresis are readily observed. For the material employed here the

range of applicable electric field strengths is limited by electrical breakdown of the material to about 2 kV/mm in the direction of polarization of the ceramic and to about 1/3 of this value for the opposite poling of the voltage source in order to avoid repolarization of the ceramic. The manufacturers specifications for the piezoelectric strain constants, valid for small electric field strengths, were given as⁴:

$$\begin{aligned} d_{31} &= -1.7 \cdot 10^{-10} \text{mV}^{-1} & (\text{deformation perpendicular to the electric field}) \\ d_{33} &= 4.5 \cdot 10^{-10} \text{mV}^{-1} & (\text{deformation parallel to the electric field}) \end{aligned}$$

Using the apparatus depicted in Figure 3, the validity of the linear deformation approximation for small signals and the non-linear response for larger signals was investigated.

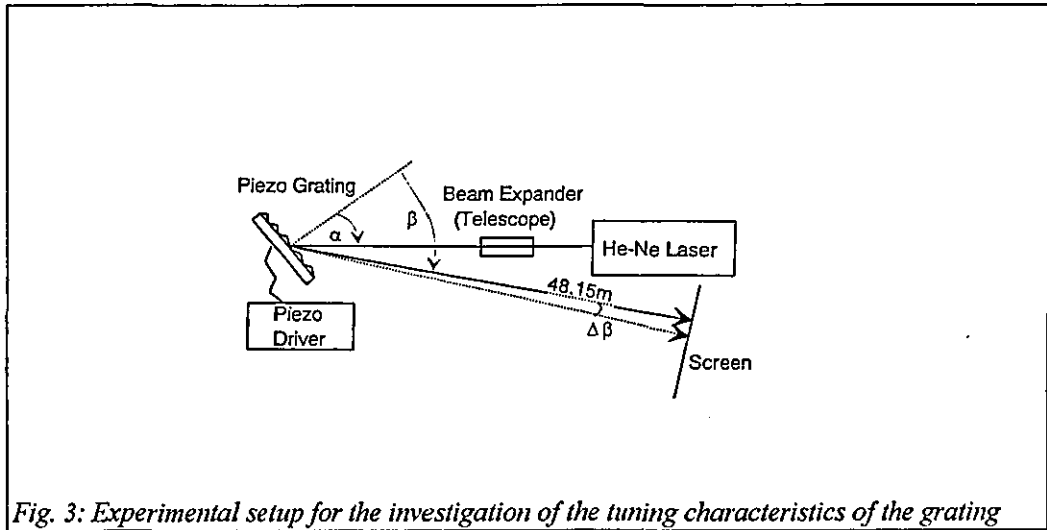


Fig. 3: Experimental setup for the investigation of the tuning characteristics of the grating

The He-Ne laser beam ($\lambda = 632.8 \text{ nm}$) was arranged to fall on the grating with an angle of incidence near the autocollimation angle which is calculated as $\alpha = \beta = 41.6^\circ$ for this case. The change in the diffraction angle in first order as a result of tuning the grating with an applied voltage was determined by measuring the displacement of the beam at a great distance (48.15 m). To ensure a high precision during these measurements of extremely small angles (the largest angle measured was 1.2 mrad), the laser beam was expanded with a telescope to reduce the beam divergence over the long path length.

From the known geometry, the diffraction angles were determined as a function of the applied voltage and the corresponding grating constants calculated. The results of this experiment are depicted in Figure 4 along with the calculated variation of the grating constant under the linear approximation from equations [3] and [4]:

$$g = g_0 \left(1 + d_{31} \frac{U}{h} \right) \quad [5]$$

using the strain constant specified above and $g_0 = \frac{1}{2100 \text{ mm}^{-1}}$.

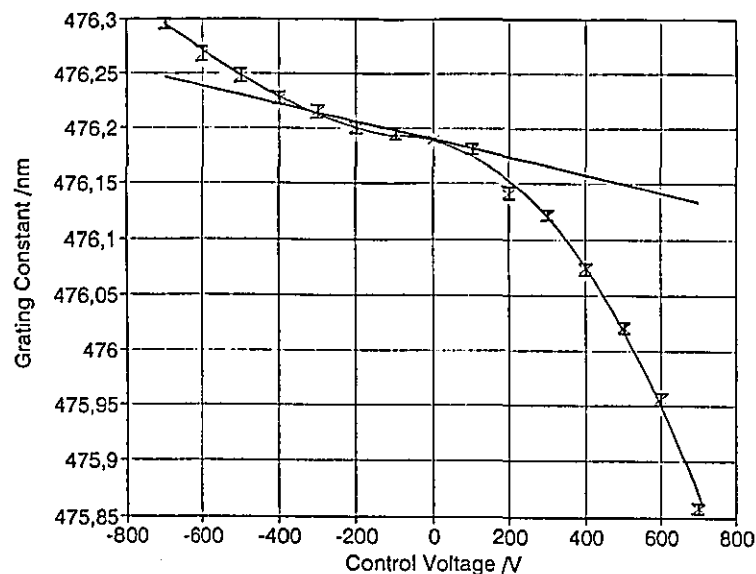


Fig. 4: Theoretically and experimentally determined grating constants as a function of the applied voltage. The curve drawn through the experimental data is to guide the readers eye only and is not intended to represent any particular functional dependance.

With the voltage applied in the polarization direction ($U > 0$ V), agreement with the linear theory was observed up to values of roughly 100 V, whereas for larger voltages, a strong deviation from linearity was found. With the opposite polarity ($U < 0$ V), the observed dependence was found to be approximately linear down to -300 V followed by a lesser deviation from non-linearity than was the case for positive voltages. At a voltage of -700 V, the measured change in the grating constant was 105 ± 4 pm, roughly 100% larger than the value expected from the linear theory.

A computer simulation was performed to test the insensitivity of the results with respect to small deviations from the assumed angle of incidence, which was found to indeed be the case for the geometry chosen with the beam incident near the autocollimation angle.

4. Fine Tuning of Dye Lasers

Many applications of tunable lasers require extremely precise tuning of the laser wavelength to within 1 pm or less and / or stabilization of the laser in the resonant mode. These requirements are difficult, if not impossible, to satisfy with mechanical actuators. The piezo grating described here is predestined for such applications, as fast wavelength tuning with a resolution less than 1 pm may be readily realised.

4.1 Design of the Dye Laser

Figure 5 shows the design of the dye laser used in this work, which was a modified FL 2000 system from Lambda Physik. Rhodamine 6G dye was chosen (tuning range 570 - 610 nm) which was continually recirculated through the cuvette via a pump system. The active diffraction grating was arranged with the high reflecting mirror in a Littmann / Metcalf (grazing incidence) configuration. This design has the advantage over the original Littrow configuration of this dye laser (in which the beam is diffracted directly back into the resonator without the use of a separate high reflector mirror), that the beam expander is obviated, resulting in a system which is simpler to adjust while using less expensive components. Furthermore, since the grating acts twice per pass, the dispersion is effectively increased, resulting in a narrowing of the wavelength bandwidth. The piezo grating was supported on a cardanic mount to allow coarse mechanical tuning to the desired centre wavelength. A Xe-Cl excimer laser was used as the pump source.

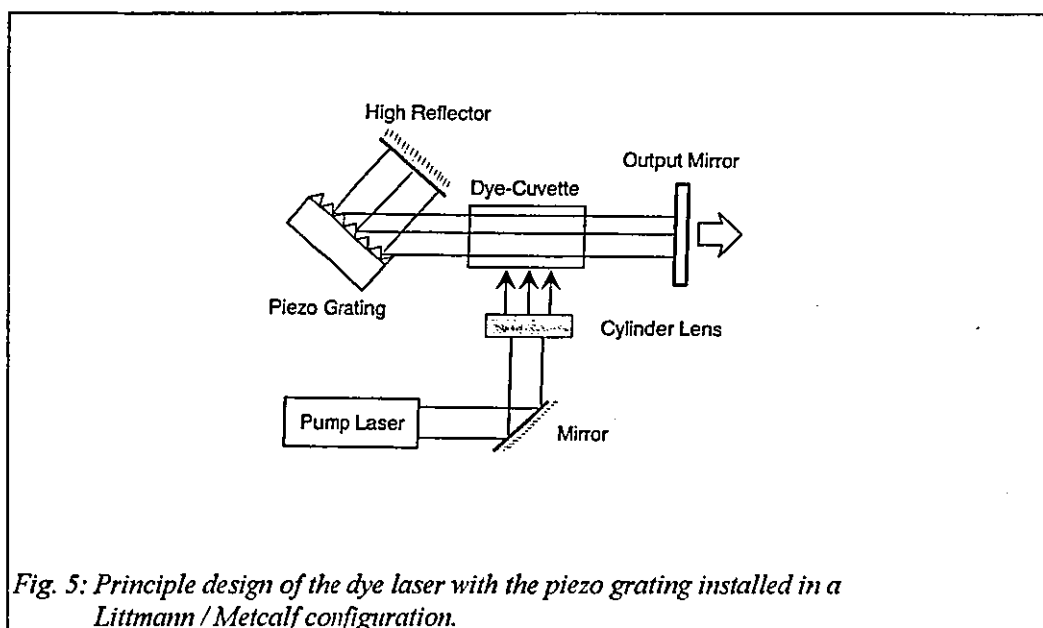


Fig. 5: Principle design of the dye laser with the piezo grating installed in a Littmann / Metcalf configuration.

4.2 Tuning Characteristics of the Dye Laser

For the purpose of tuning the dye laser, the control voltage was poled opposite to the polarisation direction of the piezo ceramic. The tuning characteristic of the dye laser according to the linear approximation to the transverse piezoelectric effect is obtained from equations [3] and [4] since variation of the grating constant, g , results in a variation in the wavelength of the light resonant within the laser cavity. Thus, the theoretical tunability of the dye laser is given by:

$$\frac{d\lambda}{dU} = d_{31} \frac{\lambda_0}{h} \quad [6]$$

For the chosen wavelength of 595.3 nm, a tuning sensitivity of 0.10 pm / V is predicted for small signals.

In order to demonstrate the size of the effect to be expected from the linear theory, values of the absolute wavelength change in first order are tabulated below for various pertinent wavelengths, using the parameters and typical voltages relevant for the present work.

λ / nm	$\Delta\lambda$ / pm (U = -50 V)	$\Delta\lambda$ / pm (U = -700 V)
308	2.6	37
595	5.1	71
800	6.8	96

Table 1: Tuning ranges for various pertinent wavelengths and voltages

Following application of the control voltage, the piezo substrate is, in addition to the transverse effect described above, also expected to contract along the direction of polarisation due to the longitudinal inverse piezoelectric effect. This results in a change of the length of the resonator which will, in principle, also result in a change in the wavelength of the light emitted from a given longitudinal mode. The change in thickness, Δh , of the substrate is determined by equation [4]. Specifically:

$$\frac{\Delta h}{h} = d_{33} E \quad [7]$$

Considering the geometrical details of the laser, as given in Figure 6, this results in a change in the length, ΔL , of the resonator as follows:

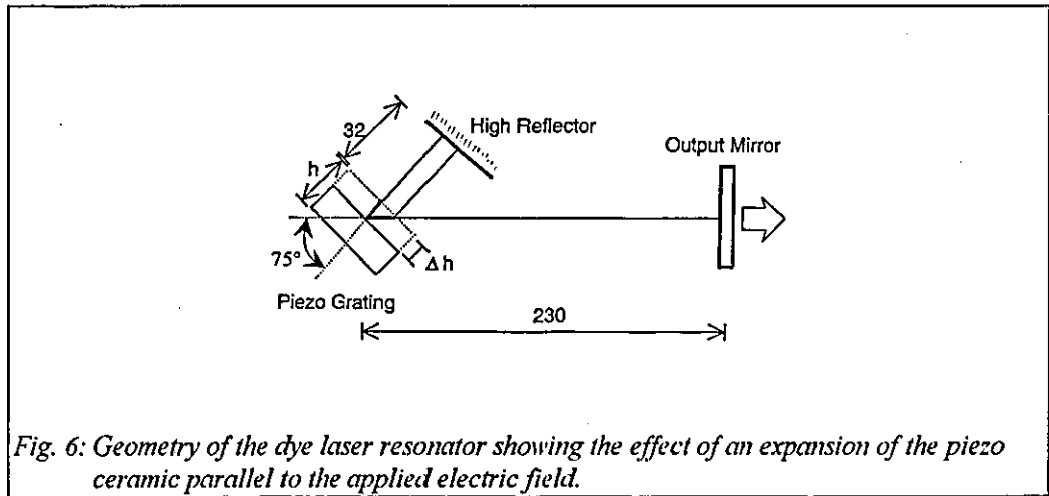


Fig. 6: Geometry of the dye laser resonator showing the effect of an expansion of the piezo ceramic parallel to the applied electric field.

$$\Delta L = \Delta h \frac{[1 + \cos(\alpha + \beta)]}{\cos \alpha} \quad [8]$$

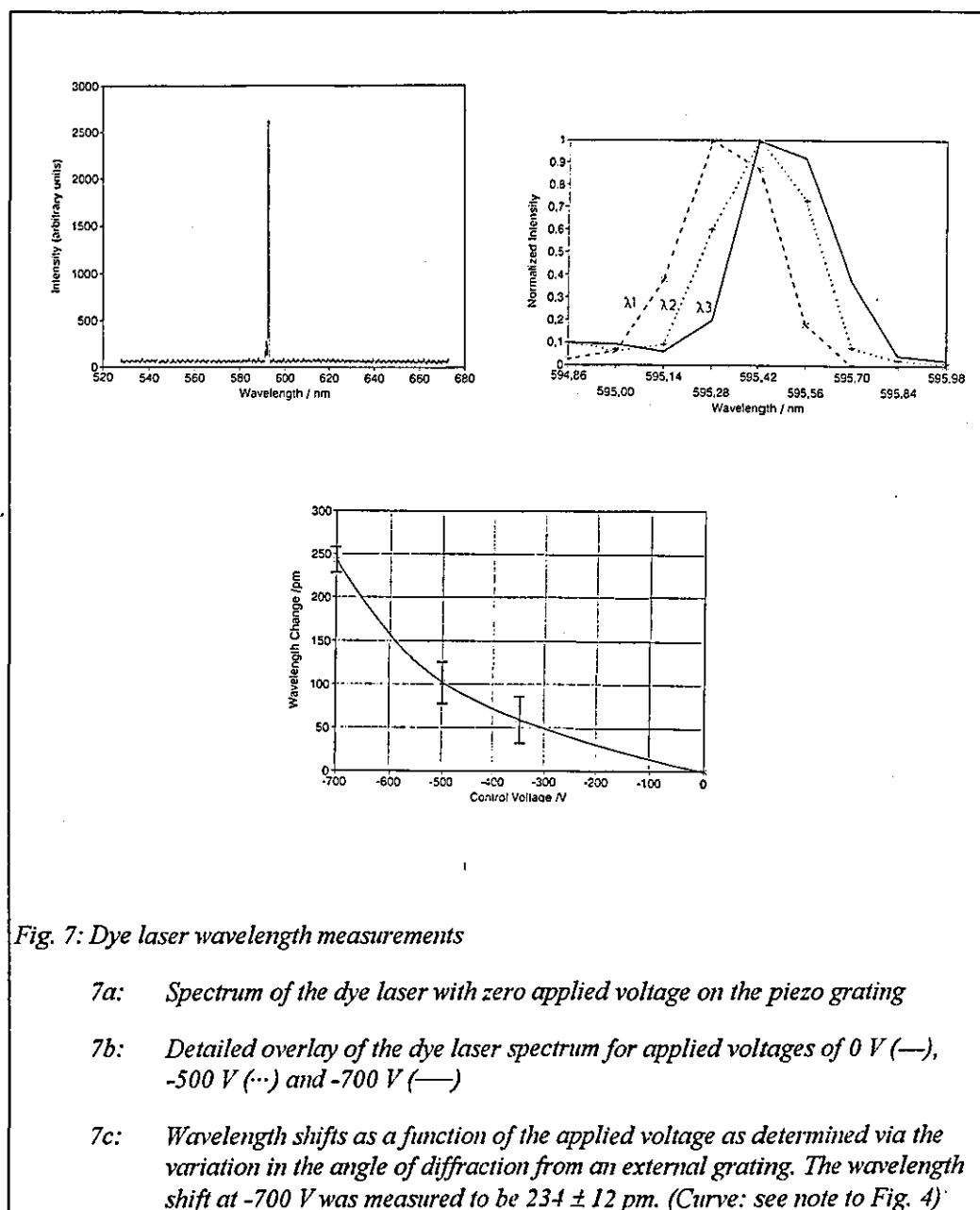
The tuning sensitivity due to this effect is, thus, given by

$$\begin{aligned} \frac{d\lambda}{dU} &= \frac{dL}{dU} \frac{\lambda}{L} = \frac{dh}{dU} \frac{\lambda}{L} \frac{[1 + \cos(\alpha + \beta)]}{\cos\alpha} \\ &= d_{33} \frac{\lambda}{L} \frac{[1 + \cos(\alpha + \beta)]}{\cos\alpha} \end{aligned} \quad [9]$$

Thus, for the geometry employed here, this effect leads to a 4% contribution to the tuning of the laser wavelength (4 fm/V) as compared to the contribution due to the variation of the grating constant and may, therefore, be neglected. Only for very grazing incidence configurations will this effect come into play, contributing 10% at $\alpha = 85^\circ$ and still only 50% at $\alpha = 89^\circ$.

4.3 Measurements of the Wavelength Tunability

The unshifted wavelength was measured and rough measurements of the wavelength shift for tuning voltages $U < -500$ V were made using a commercial spectrometer fitted with a diode array detector (see Figures 7a and 7b). These measurements were overly limited by the resolution of the spectrometer (1 pixel $\hat{=}$ 140 pm) and so can give only an estimate of the order of magnitude of the wavelength shifts to be expected. Measurements of the wavelength shift were also made by measuring the changes in the diffraction angle of the dye laser beam allowed to fall onto an external grating (1200 lines per mm) in an arrangement similar to that depicted in Figure 3. These results are displayed in Figure 7c.



A more accurate and detailed analysis was undertaken by recording the characteristic ring pattern generated by a Fabry-Perot etalon (FPE) for each wavelength as a function of the voltage applied to the piezo grating.

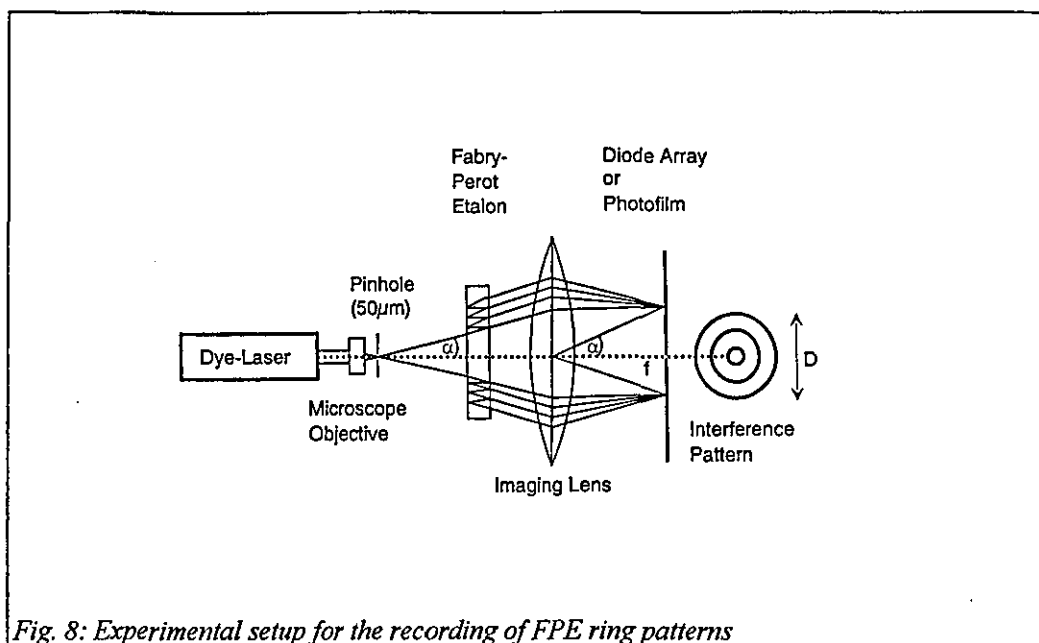
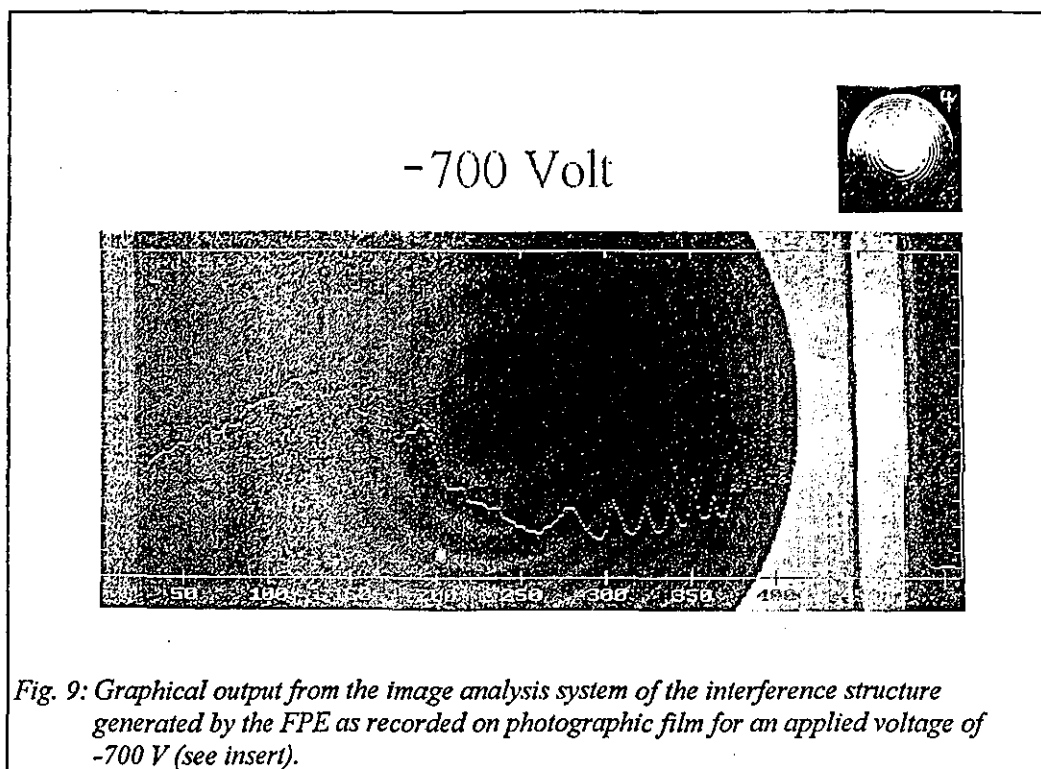


Fig. 8: Experimental setup for the recording of FPE ring patterns

Recordings of the interference rings were made alternatively on photographic film and with a photodiode array in the focal plane of the lens for applied voltages from 0 to -700 V in steps of 100 V. As an example, Figure 9 shows a typical interference pattern as recorded photographically for an applied voltage of -700 V. Through use of a CCD camera and a computer based image analysis system, the contrast of the photographs was increased and the equivalent of a densitometric analysis was made along one diameter of each by assigning each pixel to one of 256 grey scales. These results were graphically overlayed onto the photographs and the ring diameters were then determined by measuring the distances between the corresponding optical density maxima.



In Figure 10, the intensity distributions as a function of the distance from the centre of the pattern of interference fringes, as recorded with the photodiode array, are displayed for the various voltages applied. The intensity maxima of the different interference orders wander toward the centre of the pattern for decreasing voltages (that is, for increasing absolute values of the voltage, as a negative polarity was employed here).

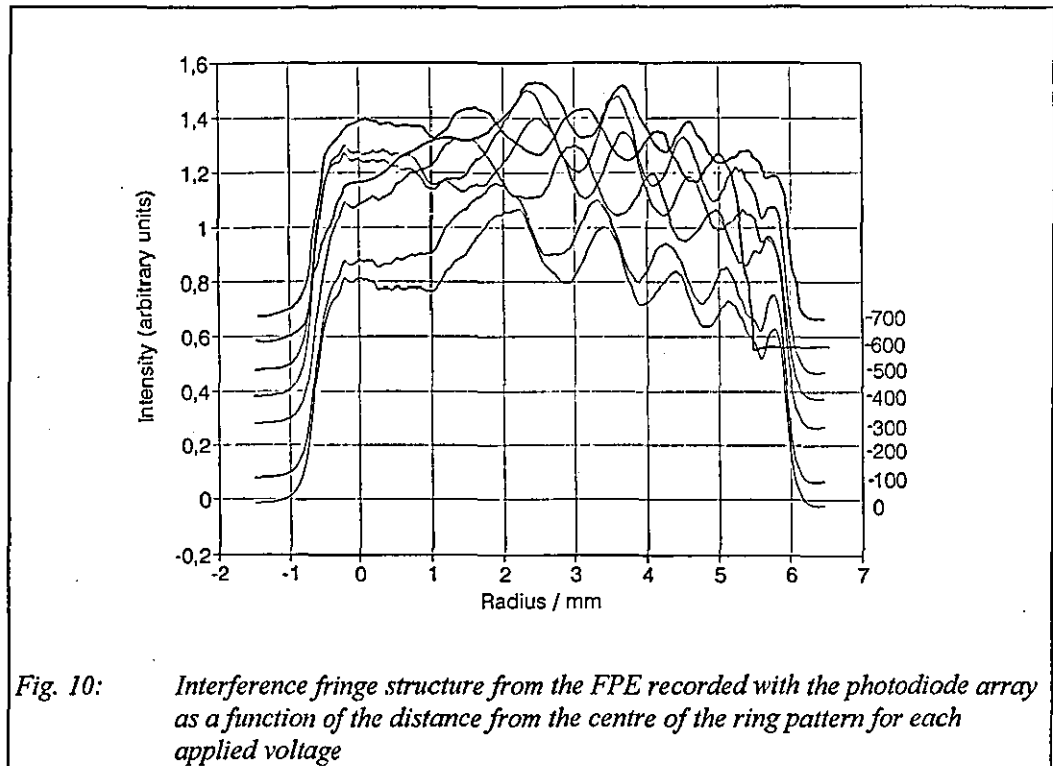


Fig. 10: Interference fringe structure from the FPE recorded with the photodiode array as a function of the distance from the centre of the ring pattern for each applied voltage

The analysis of the interference patterns involved use of two methods as detailed below.

1. Under the approximation of paraxial geometry, one obtains for the diameter D_p of a ring of given interference order in the focal plane of the imaging lens (see Fig. 9):

$$\lambda = \frac{d}{4pnf^2} D_p^2(U_j) = k D_p^2(U_j) \quad [10]$$

whereby n is the index of refraction of the FPE (1.5 for BK7 glass at 595 nm), d its thickness (0.9 mm), f_2 is the focal length of the imaging lens (600 mm) and p is the ring number, counted from the centre of the interference pattern. Since the images used for the analysis were not the original photographs, a magnification factor would have to be taken into account. Thus, the factor k (including the unknown magnification factor) was determined through the measurement of a single ring diameter for the known absolute wavelength as determined through the measurements with the spectrometer. It then follows that:

$$\Delta\lambda = k [D_p^2(U_j) - D_p^2(U_k)] \quad [11]$$

2. A procedure analogous to method 1 was employed, with the ring systems scaled according to the free spectral range of the FPE used, which for $\Delta\lambda \ll \lambda$ and $\alpha \ll 1$ is given by:

$$\Delta\lambda = \frac{\lambda^2}{2nd} \quad [12]$$

Although these methods are, in principle, equivalent, they involve measurements of different parameters which is useful as a means of control of the results. Both methods were used for the analyses of the photographic and diode array measurements and gave equivalent results within the limits of experimental error. For an unshifted wavelength of 595.2 nm and an applied voltage of -700 V, wavelength shifts of 210 ± 6 and 220 ± 6 pm were obtained from the photographic and diode array recordings respectively. The complete set of results are displayed graphically in Figure 11.

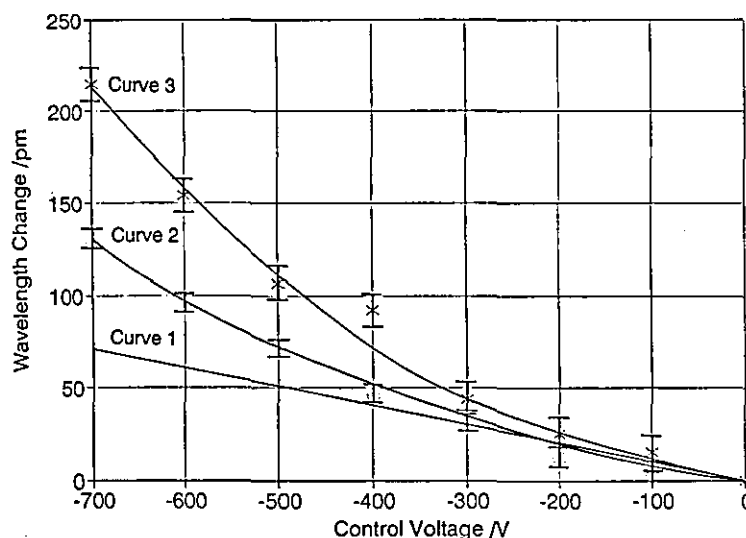


Fig. 11: Wavelength shift of the dye laser as a function of the voltage applied to the piezo grating:

Curve 1: linear theory according to equation [6]

Curve 2: calculated wavelength shifts, as expected from the experimentally determined grating constant data displayed in Figure 4

Curve 3: average of the data obtained from the FPE measurements using photographic film and the diode array. (Curve: see note to Fig.4)

In the region from 0 to -300 V, all measurements, including those using the external grating (see Figure 7c) gave results in good agreement with the linear theory (curve 1 of Figure 11). For larger applied voltages, the wavelength shifts calculated using the data from the measurements of the variation of the grating constant, diverge from the linear theory (compare with the equivalent results displayed in Figure 4). The results of the measurements employing the FPE (curve 3 of Figure 11) show the same characteristic dependence as displayed in Figure 7c and give an averaged value of 215 ± 9 pm for the wavelength shift at an unshifted wavelength of 598.2 nm and applied voltage of -700 V.

4.4 Determination of the Output Energy Stability of the Dye Laser During Wavelength Tuning

In order to determine the stability of the energy of the laser output during wavelength tuning, the pulse energy was measured using a fast photodiode and continually averaged over roughly 100 pulses using a boxcar averager since the shot-to-shot stability of this particular laser was quite poor. The results of this measurement are displayed in Figure 12, whereby each of the regions shown correspond to the results of one minute of measurement data during which time the applied voltage was held constant at the values indicated.

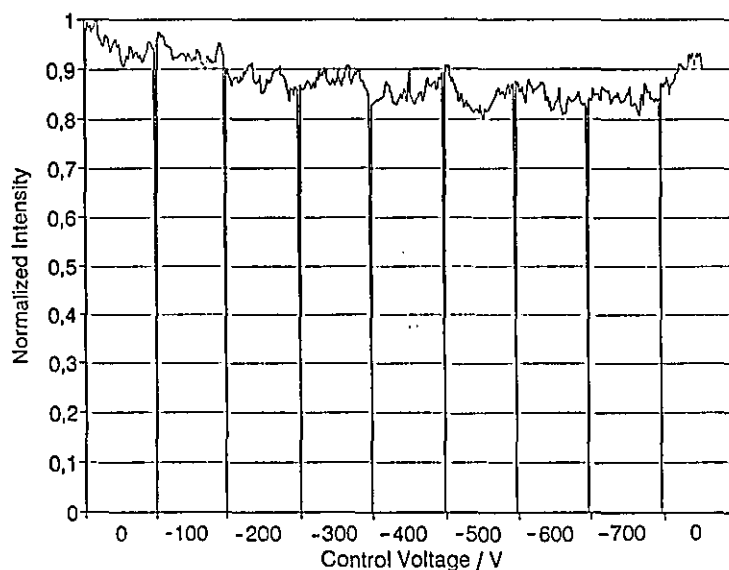


Fig. 12: Normalized pulse energy of the dye laser as a function of the applied voltage (each discrete voltage (0 V, -100 V, ..., -700 V) was held constant for a period of 1 minute during the regions indicated).

Despite the large fluctuations in output energy, the results indicate a definite trend towards decreasing energy with decreasing applied voltage. Thus, at an applied voltage of -700 V, the output energy was reduced to 85% of the starting value. The fact that the output energy did not return to the original value following removal of the applied voltage (last region in Figure 12) is an indication of hysteresis in the piezo-ceramic⁴. Similar indications of hysteresis were observed during the measurements of the grating constant. The energy fluctuations within each region of Figure 12 are, for the most part, due to fluctuations in the energy and beam quality of the excimer pump laser used.

5. Applications of the Active Diffraction Grating

The active diffraction grating described here is suitable for very sensitive tuning of laser wavelengths and diffraction angles, suggesting its use in a wide range of applications:

- fine tuning and stabilization of narrow bandwidth lasers (eg, dye and diode lasers), also in connection with coarse tuning (eg, by mechanically turning the piezo grating)
- distance measurements
- heterodyne measurement techniques
- two-wavelength contour measurements of large objects
- differential spectroscopy (eg, DIAL)
- atomic absorption spectroscopy
- doppler free spectroscopy
- optical switches

6. Conclusions

An active, diffracting optical element was manufactured and its optical characteristics and function were investigated both theoretically and experimentally. This active diffraction grating was installed in a dye laser and used for precise tuning of the output wavelength. At a wavelength of ca. 600 nm, a wavelength shift of 215 ± 9 pm was recorded for an applied control voltage of -700 V.

7. References

1. U. Samuels, H. Kreitlow, St. Wild, Ch. Budzinski, H.J. Tiziani, *Feindurchstimmung von Farbstofflasern mit einem aktiven diffraktiven optischen Element*, Conference of the German Society for Applied Optics (*Deutsche Gesellschaft für angewandte Optik, DGaO*), Berchtesgaden, 1994
2. G. Fenske, *Steuerbares Beugungsgitter*, DD279077 A1 WPG02B/3244294, 1990
3. S. Mory, G. Fenske, *Beitr. Opt. Quantenel.* 14, 148 (1989)
4. Data sheets, Marco Systemanalyse und Entwicklung GmbH, Hermsdorf, Germany

AUTOMATED SURFACE MEASUREMENT VIA LASER TOMOGRAPHY

U.Samuels, R. Parkin, H. Kreitlow*

Loughborough University of Technology, Mechanical Engineering Department,
Ashby Road, Loughborough, LE 11 3 TU, England

* Fachhochschule Ostfriesland, Forschungsschwerpunkt Lasertechnik
Constantiaplatz 4, 26723 Emden, Germany

1. Introduction

Increasingly high demands in quality assurance during the manufacture of high precision components e.g. in the automotive, aerospace, optical and bearing industries, require continuous improvements in measurement techniques. The measurement of roundness as well as shape measurement of technical components, for example turbine blades, are typical examples in quality measurements. All of the roundness measurement systems presented can be classified by use of combination in table 1.

Principle	Movement		Sensor		
	Sensor	Object	Contact	Signal	Dimension
1	Stationary	Rotating	Yes	Incremental	One
2	Rotating	Stationary	No	Absolute	Multi

Table 1: Classification of measurement principles for roundness measurement

For rotating objects, e.g. rotating spindles, special demands for the roundness of the object (static case) and the correct rotation concentricity exist. For this extended investigation range an automatic laser tomography measurement system for the investigation of the static and dynamic behaviour of axially symmetric rotating objects has been developed. According to table 1 the object movement system is based on a rotating table. The measurement principle of the stationary sensor is based on an optimised autofocus sensor which delivers absolute distance signals in a non-contact manner. By use of this one-dimensional measurement principle during an object rotation, cross sections of the object shape in one plane are obtained

while the complete object shape can be achieved as a result of the combination of several such cross sections which can advantageously be described in cylindrical coordinates.

The use of the non-contact measurement principle enables the investigation of ultra soft and ultra hard materials which are difficult to investigate with contacting measuring systems. The large dynamic range of the sensor as a result of the elimination of all moving sensor parts can be used for the investigations of dynamic behaviour.

2. Principle of the distance sensor

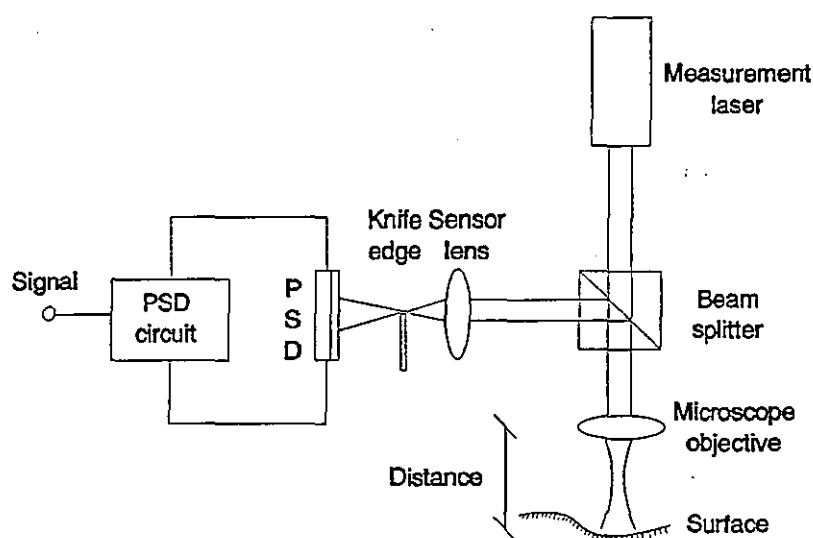


Figure 1: Principle of the autofocus sensor [1]

For the determination of distance signals the autofocus sensor shown in fig.1 has been developed. Opposite to the measurement surface the beam of the measurement laser is strongly focussed by a microscope objective. The reflection from the measurement surface is separated from the beam line using a beam splitter cube and then manipulated by a sensor lens and a knife edge. Following the registration of the laser light by means of a position sensitive detector (PSD) a signal conditioning circuit provides the distance dependent signal to the signal analysing unit. In contrast to other autofocus sensors this sensor has no moving parts so that the dynamic range is only restricted by the electronic characteristic and is therefore comparably large.

The output signal S of the sensor can nearly described by equation (1):

$$S \approx S_0 + K\Delta Z \quad (1)$$

Where S_0 means the initial signal and $K\Delta Z$ the change of the output signal as a function of the measured distance. Equation (1) shows that a nearly linear relationship between the measurement value and the sensor signal is achieved. Varying the sensitivity constant K according to equation (2) the measurement sensitivity and the measurement range of the sensor can be tuned in relatively large ranges, where largest measurement ranges of $100\mu\text{m}$ and highest resolutions of 200nm were achieved.

$$K = 4w \frac{(f_1 l_2 - f_1 f_2 - l_1 l_2 + l_1 f_2 - l_2 f_2)}{f_1^2 f_2} \quad (2)$$

In equation (2) l_1 means the distance between the microscope objective and the sensor lens, l_2 the distance between the sensor lens and the light detector, f_1 the focal length of the microscope objective, f_2 the focal length of the sensor lens and w the beam waist of the measurement laser.

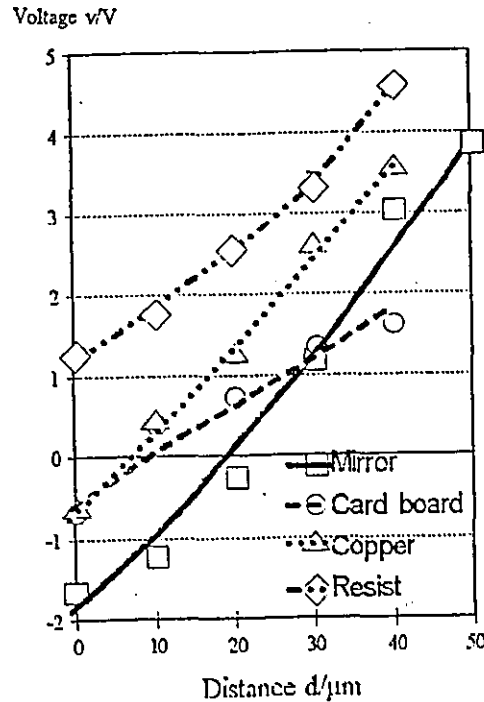


Figure 2: Measurement characteristics of the distance sensor

Figure 2 shows four typical measurement curves that were determined for four different surfaces materials using the same sensor with equal alignment. One can see that different surfaces deliver slightly varying measurement curves all having a linear working characteristic in a large working range. For this reason the sensor has to be calibrated to any new surface. These surfaces have to be homogenous and therefore no contamination (by e.g. oxidation or oil) is permitted.

3. Automated measurement system

For the automated measurement the pulse width adjustment of the motor for precise rotation of the object, the signal pick-up via a analogue/digital converter as well as the allocation of the measured value to the corresponding angle using an encoder signal, is performed by a computer, equipped with special interfaces. On the same computer the subsequent analysing and storage as well as the visualisation of the measured evaluated data is performed.

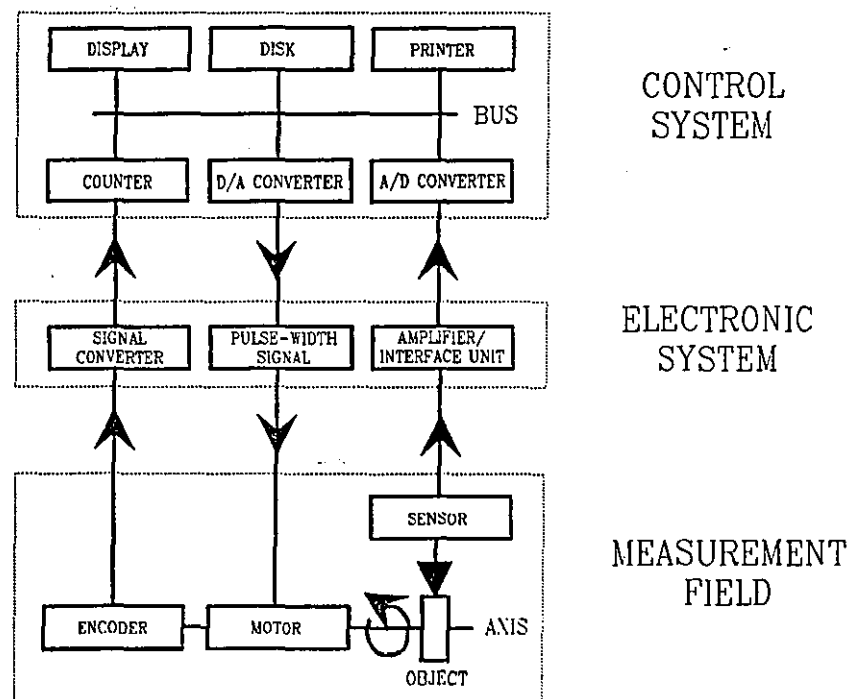


Figure 3: Principle construction of the automated system for roundness measurement

4. Measurement examples

The roundness of a precise and very slow rotating axis (quasi static investigation) was measured with by means of the autofocus sensor. The sensitivity of $112\text{mV}/\mu\text{m}$ in a linear measurement range of nearly $50\mu\text{m}$ was tuned according to equation (1) so that a positioning resolution of 200nm was achieved. Figure 4 shows a hard copy of an oscilloscope screen for one period of the measurement signal for one object turn which represents a plane referenced illustration of the shell surface. With the above mentioned measurement sensitivity of $112\text{mV}/\mu\text{m}$ the signal of 0.53V indicates a R_t (Roughness Total) value of $4.73\mu\text{m}$. The reproducibility of the measurement was determined by the comparison of several measurement curves for the same turn of the axis.

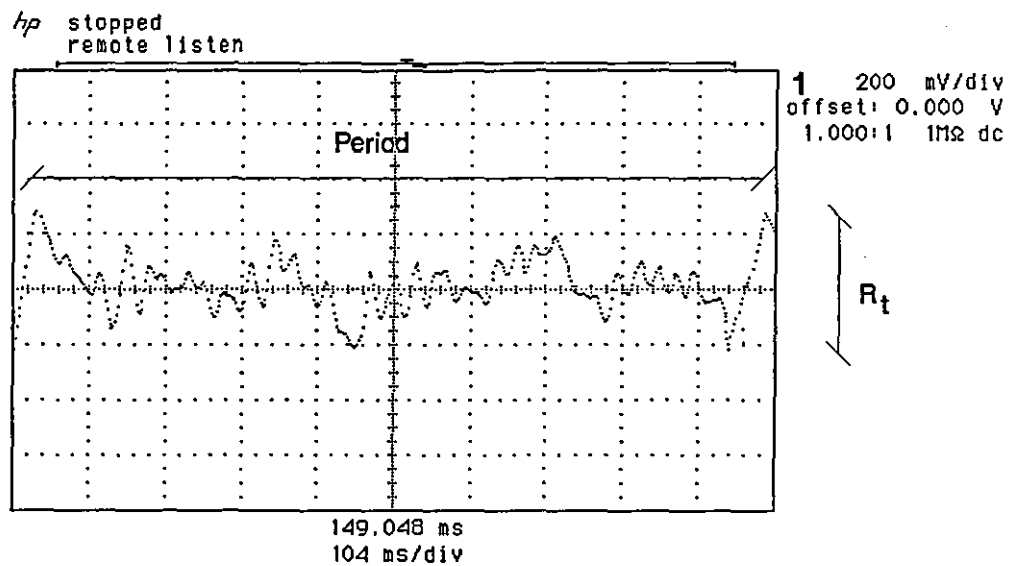


Figure 4: Example of the roundness measurement using the tomography system

In addition to the measurement of the roundness in a second example the application of the tomography system for dynamic concentricity of the axis has been demonstrated. A low pass filtering of the sensor signal, tuned in accordance to the rotation speed, cares for the reverse clipping of the influence on the sensor signal so that the signal is only a function of the waviness and the radial runout of the axis.

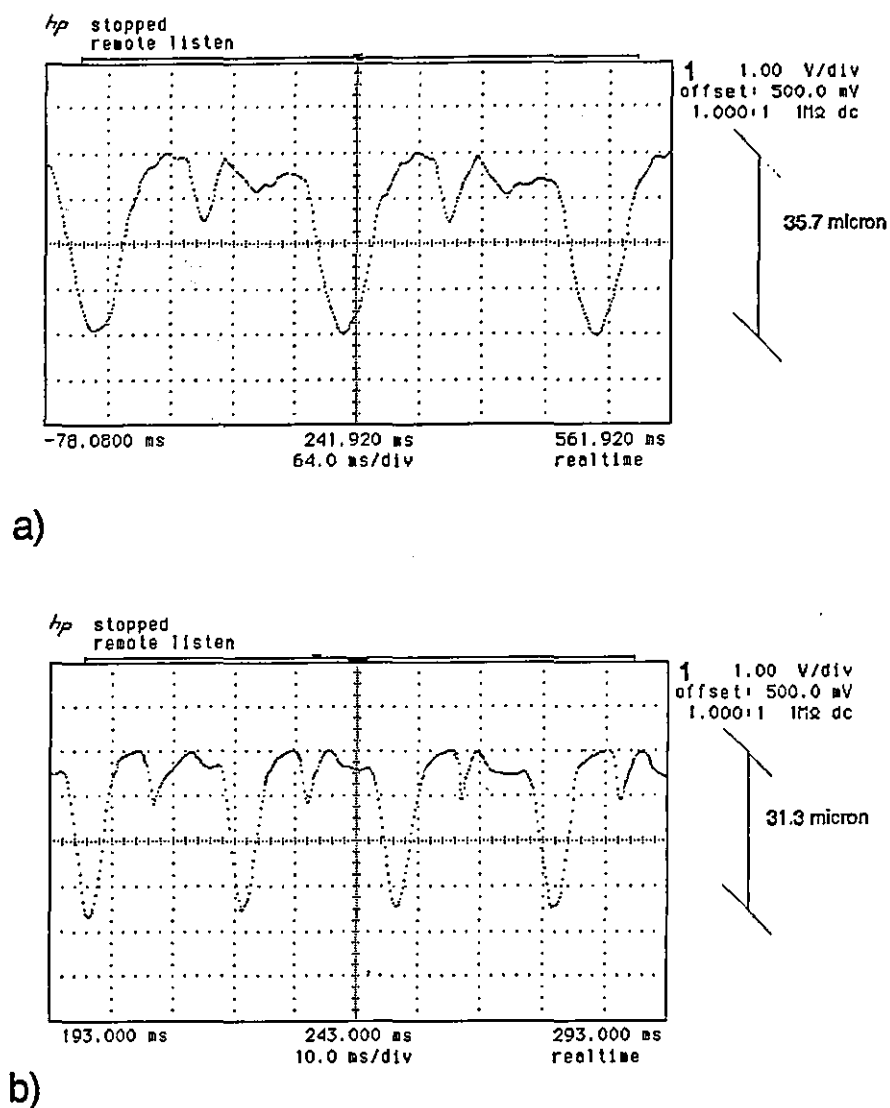


Figure 5: Examples for dynamic concentricity measurement using the tomography system

For the above mentioned sensitivity of the sensor curve a) shows a peak to peak movement of $35.7\mu\text{m}$ for rotation speeds of 240rpm and in curve b) a peak to peak movement of $31.3\mu\text{m}$ for rotation speeds of 2400rpm. The period of the shown signals is equal to the period of one spindle turn. The reproducibility has been determined by the observation of numerous periods. It can be shown that different values of rotation speed cause different deviations from the concentricity.

5. Optimised measurement system

Every measurement requires the presence of a reference. For the special case of the determination of roundness deviation compared to a circle the reference is in general a high precision bearing that allows the rotation of the measurement object relative to a distance sensor [2][3]. The distance sensor measures the profile during one object turn leading directly to the deviation between object shape and ideal circle shape. Since every rotation deviation of the bearing influences the measurement result this procedure is restricted to relatively precise movements between the distance sensor and the object. Therefore this measurement procedure can only be used for the determination of circle shape deviations that are large compared to the radial runout of the spindle in use. Further problems are observed concerning large objects that are difficult to handle. In these cases the use of the 3 point method is preferred [4][5]. By combination of two three point measurement systems to a four point system [6] and a suitable angle adjustment between supporting/node/bearer points and the sensor [7] the measurement accuracy can be further improved. To preserve the advantages of the non contact measurement technique for dynamic investigations and/or the measurement of sensitive objects in a 3 or 4 point method the reference determination has to be performed in a non contact manner as well. The tunability of the autofocus sensor according to equation (2) makes this sensor also applicable for this task. For the investigation at a high rotation speed also a fast signal analysing and evaluation is required. For most accurate and flexibel signal evaluations the fourier transform can be applied where the measured signal is decomposed into its spectrum. Based on geometrical relations of the mechanical measurement system, consisting of the sensor and the supporting points the transfer function of the spectrum of the measured signal to the desired roundness deviation can be determined.

6. Conclusion

A laser tomograph as an automated measurement system based on an autofocus sensor has been presented, which allows the shape measurement of rotationally symmetrical objects. By use of the autofocus sensor working without any moving part in a non contact manner the measurement of ultra hard and ultra soft objects in static and dynamic applications can be performed. The system can be used e.g. in quality assurance of precisely manufactured objects and roll bearings as well as in rapid prototyping.

7. References

- [1] Samuels, U.: Focal position controlled processing head for a laser pattern generator (LPG) for flexible microstructuring, MPhil Thesis, Loughborough University of Technology, November 1995
- [2] Moore, D.: Design consideration in multiprobe roundness measurement, J.Phys.E:Sci. Instr., 1989, Vol.22
- [3] Stevens, D.M.: An investigation into the use of a wide range interferometric transducer for roundness measurement, MPhil Thesis, CNAA, Leicester Polytechnic, August 1989
- [4] Mitsui, K.: Development of a new measurement method for spindle rotation accuracy by three points method, Proceedings of the 23rd conference on machine tool design and research MTDR, 1982
- [5] Westkämper, Michel, S, Gente, A., Lange, D.: Prozeßnahe Rundheitsmeßtechnik mit 3-Punkte Meßsystem, Research description on the Interkama, Düsseldorf, 1995
- [6] Zhang, G.X., Wang, R.K.: Four point of roundness and spindle error measurements, Annals of the CIRP, Vol. 42/1, 1993
- [7] Steger, A.: Über die Möglichkeiten und Grenzen der Dreipunktmessung zur Bestimmung der Formabweichung vom Kreis. Dissertation TH Karl-Marx-Stadt, 1976

